Final Report on Department of Energy Grant DE-FG26-05NT42544

Entitled

Chemical Kinetics in Support of Syngas Turbine Combustion

Author: Frederick L. Dryer

December 2007

Project Title:	**Chemical Kinetics in Support of Syngas Turbine Combustion**
Grant No:	DE-FG26-05NT42544
Agency:	National Energy Technology Laboratory Department of Energy
Program:	
DOE Project Manager:	Rondle Harp, Project Manager Power Systems Projects Division U.S. Department of Energy National Energy Technology Laboratory P.O. Box880 Mail stop E063610 Collins Ferry Road Morgantown, WV. 26507-0880 Phone: (304)285-5436 Fax: (304)285-4403 email: rondle.harp@netl.doe.gov
Amount:	$49,999
Project Period:	08/01/05-07/31/06, with no cost extension to 07/31/07
Reporting Period:	Final Report
Principal Investigator:	Prof. Frederick L. Dryer
Contact Address:	D-329-D Engineering Quadrangle Mechanical and Aerospace Engineering Department Princeton University, Princeton, NJ 08544-5263 609-258-5206, 609-258-6109 (fax) fldryer@princeton.edu
Students:	(i) Kenneth Kroenlein

DISCLAIMER

Executive Summary

This document is the final report on an overall program formulated to extend our prior work in developing and validating kinetic models for the CO/hydrogen/oxygen reaction by carefully analyzing the individual and interactive behavior of specific elementary and subsets of elementary reactions at conditions of interest to syngas combustion in gas turbines. A summary of the tasks performed under this work are:

1. Determine experimentally the third body efficiencies in $H+O_2+M = HO_2+M$ (R1) for CO_2 and H_2O.
2. Using published literature data and the results in this program, further develop the present H_2/O_2/diluent and $CO/H_2/O_2$/diluent mechanisms for dilution with CO_2, H_2O and N_2 through comparisons with new experimental validation targets for H_2-CO-O_2-N_2 reaction kinetics in the presence of significant diluent fractions of CO_2 and/or H_2O, at high pressures. (task amplified to especially address ignition delay issues, see below).
3. Analyze and demonstrate issues related to NOx interactions with syngas combustion chemistry (task amplified to include interactions of iron pentacarbonyl with syngas combustion chemistry, see below).
4. Publish results, including updated syngas kinetic model.

Results are summarized in this document and its appendices. Three archival papers which contain a majority of the research results have appeared. Those results not published elsewhere are highlighted here, and will appear as part of future publications. Portions of the work appearing in the above publications were also supported in part by the Department of Energy under Grant No. DE-FG02-86ER-13503.

As a result of and during the research under the present contract, we became aware of other reported results that revealed substantial differences between experimental characterizations of ignition delays for syngas mixtures and ignition delay predictions based upon homogenous kinetic modeling. We adjusted emphasis of Task 2 to understand the source of these noted disparities because of their key importance to developing lean premixed combustion technologies of syngas turbine applications. In performing Task 3, we also suggest for the first time the very significant effect that metal carbonyls may have on syngas combustion properties. This work is fully detailed in Appendix C. The work on metal carbonyl effects is entirely computational in nature. Pursuit of experimental verification of these interactions was beyond the scope of the present work.

Results over this Progress Period

Approach

The present research further extended our prior work in developing and validating kinetic models for the CO/hydrogen/oxygen principally studied under Department of Energy Grant No. DE-FG02-86ER-13503, by providing additional experimental data using a Variable Pressure Flow Reactor (VPFR) on the collisional efficiencies of water and carbon dioxide in the reaction $H+O_2+M = HO_2 + M$ (R1) by carefully analyzing the individual and interactive behavior of specific elementary and subsets of elementary reactions at the conditions of interest, and by extending computational model comparisons with data obtained in this program and those appearing in the literature since 2004 to further test and refine the model at conditions relevant to gas turbine applications. Additionally, syngas contaminant species such as small hydrocarbons (e.g., methane) and other combustion gas components (e.g. NO_x) have been identified and it is suspected that these contaminants may affect syngas chemistry in gas turbine applications, particularly in mixing regions of entering fuel and air. These contaminants can have significant influence on some of the kinetic behavior. The initial research plan was to investigate only the effects of small local amounts of NO_x on ignition kinetics of $CO/H_2/O_2$ mixtures, but for reasons elaborated upon below, we also investigated the contaminant effects of iron pentacarbonyl more generally. Only computational research on the effects of this contaminant was performed.

Summary of Results and Discussion

Task 1. This task is reported in detail here, since the work has not been archivally published as of issuance of this report. The objective of this task was to experimentally determine the third body collision efficiency of CO_2 in the low-pressure rate of reaction $H+O_2(+M) = HO_2(+M)$ (R1). To achieve this goal, we made use of the approach demonstrated by Mueller et al. (1998). At temperatures below the explosion limit of the H_2/O_2 system, reaction (R1) efficiently converts H atoms to HO_2 radicals; as temperature increases, however, (R1) competes with $H+O_2 = O+OH$ (R2). Studies of the low-pressure rate of (R1) at practical combustion temperatures become complicated because of this competition. However, at high pressure conditions and at temperatures below the explosion limit the effective rate of (R1), $k_{1,eff}$, is much larger than that of (R2) (i.e. $k_{1,eff} >> k_2$), and the addition of small amounts of nitrogen oxides can be used to provide an alternate consumption route for HO_2 radicals through reactions (R13) and (R14) below:

$$NO+HO_2 = NO_2+OH \qquad \text{(R13)}$$
$$NO_2+H = NO+OH \qquad \text{(R14)}$$

Reactions (R13) and (R14) form a catalytic cycle which rapidly consumes H_2 and greatly simplifies the kinetic behavior of the perturbed H_2/O_2 system (Ashmore and Tyler, 1962).

In the present study, flow reactor experiments of the H_2/O_2 system were performed at pressures of 12.5 atm and initial temperatures of approximately 810 K. At these conditions, the flux of H and O atoms through the branching reaction (R2) is very small and the consumption of both H_2 and O_2 as well as the relative concentrations of NO and NO_2 depend, almost entirely, on k_1 and

k_{14}. Since k_{14} is considered to be well-characterized (Ko and Fontijn, 1991; Su et al., 2002), measurements of O_2 and NO_2 profiles can be used to estimate the low-pressure rate constant of (R1), $k_{1,0}$. This is evident by performing a steady-state analysis of HO_2 and NO_2 concentrations, using the reactions above, which yields:

$$[NO_2] = \frac{k_{1,\text{eff}}}{k_{14}}[O_2] \qquad (1)$$

Experimental efforts were first aimed at reproducing data reported by Mueller et al. (1998) to ascertain experimental reproducibility as well as the value reported by Mueller et al. for $k_{1,0}$ with N_2 as the main diluent. Dilute mixtures of $H_2/O_2/NO/N_2$ (approximately 3% molar concentration of reactants) were used which ensure a small temperature rise (~50 K) so that $k_{1,0}$ can be considered a constant rather than temperature dependent in the modeling efforts. In order to study the effect of CO_2 on $k_{1,0}$ $H_2/O_2/CO_2/NO/N_2$ mixtures were used. Due to experimental limitations, only experiments containing about an 8% (molar) concentration of CO_2 could be performed. Before embarking in these $H_2/O_2/CO_2/NO/N_2$ experiments, some numerical work was carried out to investigate the feasibility of the data obtained from such experiments in the determination of the third body efficiency of CO_2. These are summarized below.

First, due to the presence of CO_2 in the system, it is expected that the effective rate of (R1) will increase. Following the relationship shown in Eqn. 1 (and knowing that at low initial NO concentration all the NO converts to NO_2) to obtain a comparable H_2 consumption rate as in the "baseline" experiments without CO_2, the initial concentration of NO has to be increased. Figure 1 shows the ratio of the initial NO concentration needed for the CO_2 experiments to that of the baseline case as a function of CO_2 content. The relationship shown in Fig. 1 is linear and can help guide the selection of the initial conditions for the $H_2/O_2/CO_2/NO/N_2$ experiments.

Second, numerical tests were performed on a series of cases to determine whether the third body efficiency of CO_2 could be recovered by considering expected experimental measurements. Four cases were studied and summarized in Table 1: a baseline case without CO_2 and three cases with 10% CO_2 dilution and various efficiency values. For all cases with CO_2 as one of the dilutants, the initial NO concentration followed the relationship shown in Fig. 1. All mixtures treated lean hydrogen-oxygen systems (1% H_2/2% O_2, ϕ=0.25) at initial pressure and temperature of 12.5 atm and 808 K, respectively. Each of the four cases was modeled as a constant pressure, adiabatic system using SENKIN (Lutz et al., 1987) and the kinetic model of Li et al. (2007) with NO_x chemistry adopted from Mueller et al. (1999). From the modeling results, the computed NO_2 and O_2 concentrations were used to calculate $k_{1,\text{eff}}$ using Eqn. 1 and $k_{1,0}$ was obtained from Troe relationships (Gilbert et al., 1983) using the high-

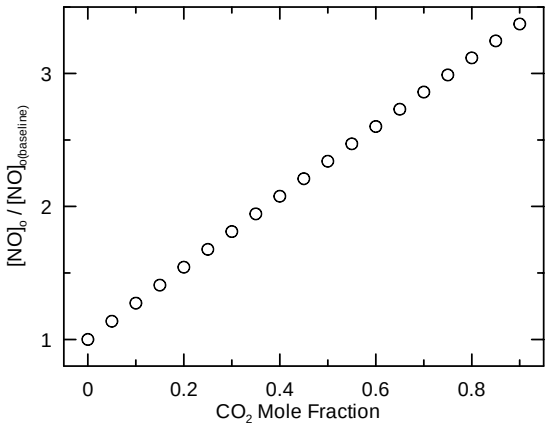

Figure 1. Initial NO concentration needed in a 1% H_2/2% O_2/$NO/N_2/CO_2$ mixture at 12.5 atm and 810 K as a function of CO_2 content, related to the concentration for a mixture without CO_2. The collision efficiency of CO_2 is assumed to be 3.8.

pressure limit and centering parameters of Li et al. (2007) for (R1). These values are shown in Fig. 2 for all cases over an extent of reaction from 20% to 80% when considering the H_2 profile. Averaging over this extent of reaction and assuming that CO_2 is the only major collider in reaction (R1) the following relationship can be established:

$$\left[X_{CO2}\varepsilon_{CO2} + \left(1 - X_{CO2}\right)\right]k_{1,0\,N2} = k_{1,0\,CO2} \qquad (2)$$

Therefore,

$$\varepsilon_{CO2} = \frac{k_{1,0\,CO2} \Big/ k_{1,0\,N2} - \left(1 - X_{CO2}\right)}{X_{CO2}} \qquad (3)$$

Where $k_{1,0\,N2}$ is the low pressure rate for the baseline case, $k_{1,0\,CO2}$ is the low pressure rate for the cases with CO_2, ε_{CO2} is the third body efficiency of CO_2, and X_{CO2} is the molar concentration of CO_2 in the mixture. Table 1 shows the results when applying Eqn. 3 to the average of the data shown in Fig. 2. The efficiency values obtained using this approach closely approximate (within 2% or better) the initial values used in the modeling, see Table 1.

Table 1. Initial conditions and results of numerical tests

	$[NO]_o$ (ppm)	$k_{1,eff}$ (Eqn. 1) $cm^3/mole/s$	$k_{1,0}$ $cm^6/mole^2/s$	ε_{CO2} (Eqn. 3)
Baseline	135	7.360×10^{11}	4.317×10^{15}	---
Case 1 10% CO_2 $\varepsilon_{CO2} = 1.9$	145	8.009×10^{11}	4.693×10^{15}	1.87
Case 2 10% CO_2 $\varepsilon_{CO2} = 3.8$	170	9.379×10^{11}	5.515×10^{15}	3.78
Case 3 10% CO_2 $\varepsilon_{CO2} = 7.6$	220	1.211×10^{12}	7.168×10^{15}	7.61

Given the validity of the method described above, the analysis of the experimental results shown in the next section will make use of Eqns. 1 and 3 to determine the third body efficiency of CO_2.

Experimental Results

Results for the baseline case, without CO_2, are shown in Fig. 3. From these results, considering the NO_2 and O_2 experimental profiles along with Eqn. 1 an average for $k_{1,eff}$ = 7.14×10^{11} cm^3/mole/s is obtained. The high pressure limit rate of (R1) used in this study is 1.475×10^{12} $T^{0.6}$ with F_c=0.8 (Li et al., 2007). Using these values the low pressure rate of (R1) is computed to be $k_{1,0}$ = 4.15×10^{15} $cm^6/mol^2/s$ for N_2 as the third body in the reaction. This value is in very good agreement (within 5%) with the low pressure rate reported by Mueller et al. (1998) of 4.03×10^{15} $cm^6/mol^2/s$ and demonstrates good experimental repeatability. The modeling results shown in Fig. 3 use the model of Li et al. (2007) with the NO_x kinetic subset of Mueller et al. (1999) where $k_{1,0}$ is treated as a constant and set to the value calculated from experimental data.

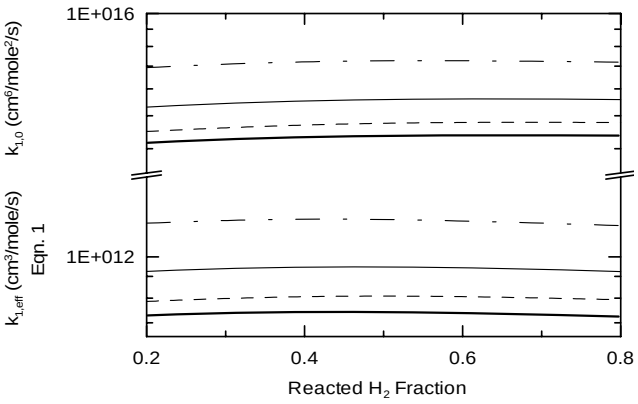

Figure 2. Computed values for $k_{1,eff}$ and $k_{1,0}$ from the NO and O_2 concentration profiles for each of the cases listed in Table 1. Bold solid line: baseline case; dashed line: case 1; solid line: case 2; dash-dot line: case 3 (see Table 1). Values are plotted as a function of the extent of H_2 reacted.

As mentioned above, only a maximum CO_2 concentration of approximately 8% could be achieved in the experiments where CO_2 was used as a third body. The initial conditions were similar as in the baseline case except for a higher initial NO concentration to account for the expected increase in the effective rate of (R1) as explained above. The results from these experiments are shown in Fig. 4. Again, making use of Eqn. 1 along with measured profiles for NO_2 and O_2 an effective rate of $k_{1,eff}$ = 7.97×10^{11} cm^3/mole/s can be calculated. This value corresponds to a low pressure rate of $k_{1,0}$ = 4.80×10^{15} $cm^6/mol^2/s$.

Using the low pressure rate values obtained above for (R1) with N_2 and N_2+CO_2 as third bodies, one can employ Eqn. 3 to calculate the third body efficiency of CO_2. Our results indicate a third body efficiency of $\varepsilon_{CO2} \approx 3.0$ which is approximately 20% lower than that commonly used in chemical kinetic models (i.e. ε_{CO2} = 3.8). One should note, however, that the low pressure rate values obtained in this study have uncertainties of ±30% (Mueller et al., 1998) and that both $k_{1,0}$ rates computed for the cases shown in Figs. 3 and 4 lie within this uncertainty range, making the reported value for ε_{CO2} not accurate. In order to obtain a better estimate of ε_{CO2}, experiments with CO_2 as the carrier gas (rather than N_2) are necessary as it is expected that the value of $k_{1,0}$ in this case will be approximately 3 times that for N_2 as the third body. Such tests are prohibitive in

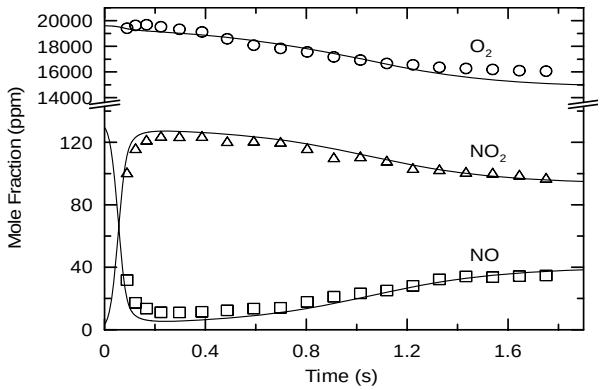

Figure 3. Species profiles for a 0.98% H_2/1.96% O_2/133 ppm NO/N_2 mixture at 12.5 atm and 808 K. Symbols show experimental data and lines are modeling results with $k_{1,0}$ = 4.15×10^{15} $cm^6/mol^2/s$. Modeling results have been shifted by -0.1 s.

the present flow reactor venue as CO_2 can damage the flow heating system.

Task 2 Prior to this contract, we developed and presented as part of efforts on modeling ethanol oxidation (Li, 2004; Li, 2004a) a comprehensively tested model of C_1 oxidation kinetics (Li et al., 2005; Li et al., 2006). New experimental data along with data published in the literature were used to hierarchically develop an updated mechanism for $CO/H_2O/H_2/O_2$, CH_2O, and CH_3OH oxidation. Important modifications included recent revisions for the hydrogen-oxygen sub-mechanism (Li et al., 2004b) we developed earlier (Yetter et al., 1991; Kim et al., 1995; Mueller, et al., 1999; Mueller et al., 2000), an updated sub-mechanism for methanol reactions (Held and Dryer, 1998), and kinetic/thermochemical parameter modifications, based upon recently published kinetic and thermodynamic information. The most important updates in this work were: updated descriptions for the reaction $H + O_2 + M = HO_2 + M$, (R1); particularly in terms of the efficiencies of important collision partners (Michael et al., 2002); an improved kinetic correlation for the reaction $H + O_2 = OH + O$ (R2) at temperatures near and below the hydrogen-oxygen second explosion limit conditions; a modified rate correlation for $H + OH + M = H_2O + M$ (R3); and updated thermodynamic parameters, particularly for the heat of formation of OH. In terms of extending earlier work on the $CO/H_2/O_2$ reaction system (Mueller et al. 2000), we recommended new rate constant correlations for $CO + OH = CO_2 + H$ (R4), $HCO + M = H + CO + M$ (R5), and $HCO + O_2 = HO_2 + CO$ (R6), motivated by a new identification of the temperatures over which these rate constants most affect laminar flame speed predictions (Zhao et al., 2005). The C_1/O_2 mechanism so developed compared favorably against a wide range of experimental conditions for laminar premixed flame speed, shock tube ignition delay, and flow reactor species time history data at each level of hierarchical development. This model was first made available on the web in late 2004, a paper detailing the development and validation of the model is presently in review (Li et al., submitted), and the work served as a motivation for the present research. In Mueller et al. (2000), we discussed several of the issues inclusive of 1) the importance of uncertainties and non-Arrhenius behavior of the rate correlations for $HO_2 + OH = H_2O + O_2$ (R7), $HO_2 + H = OH + OH$ (R8), $HO_2 + H = H_2 + O_2$ (R9), and $HO_2 + H_2 = H_2O_2 + H$ (R10) at high pressures and temperatures near 1,000 K; the importance of the pressure fall-off of $CO + O + M = CO_2 + M$ (R11) at high pressures, and that recommended rates for the reaction $CO + HO_2 = CO_2 + OH$ (R12) based upon other work in our laboratory (Zarubiak, 1997) appeared to be too large. As revised, the C_1 model discussed above performed extremely well against the experimental database on reaction systems available at the time, including as a sub-mechanism for oxidation of formaldehyde, methanol, and dimethyl ether. However, the data validations did not include results specific to the chemistry of syngas mixtures at pressures and conditions that were encompassed those conditions expected in syngas gas turbine combustion applications. New data recently appearing in rapid compression machine and shock tube studies (Sivaramakrishnan et al., 2005; Mittal and Sung, 2006; Mittal et al., 2006) suggested the effects

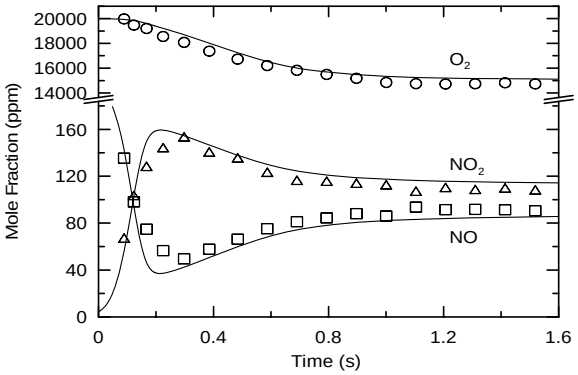

Figure 4. Species profiles for a 0.99% H_2/2% O_2/7.86% CO_2/200 ppm NO/N_2 mixture at 12.5 atm and 808 K. Symbols show experimental data and lines are modeling results with $k_{1,0} = 4.80\times10^{15}$ $cm^6/mol^2/s$. Modeling results have been shifted by -0.21 s.

of the above uncertainties were more apparent in experimental observations in these venues at very high pressures.

In order to further clarify the relative importance of specific elementary reactions on the chemical kinetic ignition of $CO/H_2/O_2/N_2$ mixtures at high pressure, we applied a computational singular perturbation (CSP) analysis approach we have recently demonstrated (Kazakov et al., 2006) as well as elementary sensitivity analyses. Unlike prior implementations of CSP methodology, the present formulation includes temperature as one of the state variables so that factors controlling ignition can be unambiguously determined. As developed (Kazakov et al., 2006), the methodology was applicable to the analysis of systems that can be modeled as constant volume processes (e.g. shock tubes). However, given recent experimental data obtained in Rapid Compression Machines (RCM) (Mittal and Sung, 2006) and for the purposes of this report, the initially developed technique was further modified to accommodate systems with volume changes as a function of time. Incorporating a volume change as a function of time is the method used by Sung and co-workers to account for non adiabatic compression in RCM experiments.

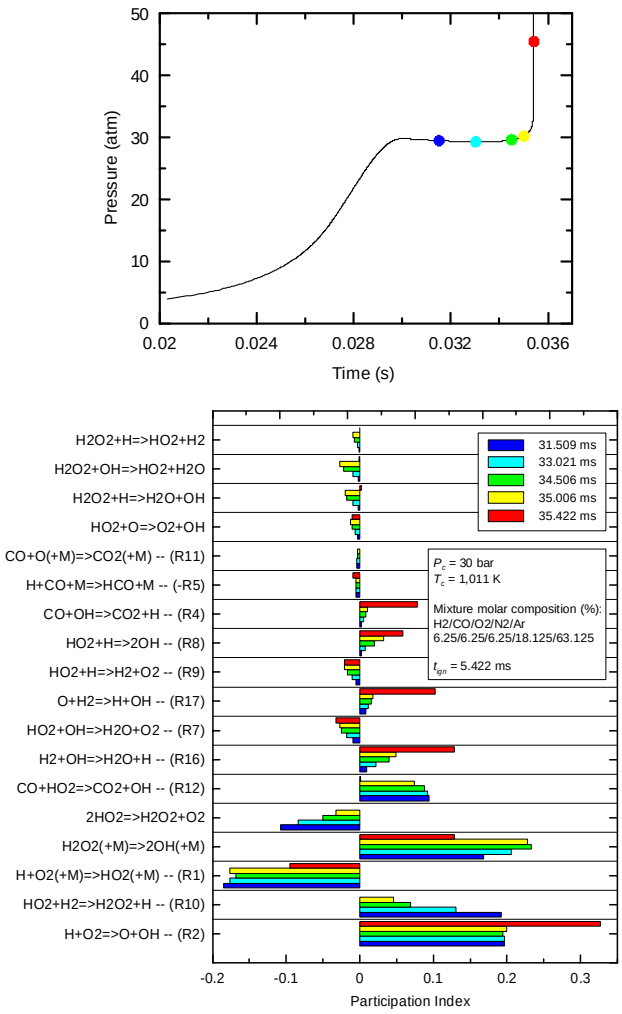

Figure 5. Reactions participating in the thermal evolution of a $H_2/CO/N_2/Ar$ kinetic system under Rapid Compression Machine (RCM) conditions (Mittal et al., 2006), obtained from CSP analysis. Analyses were performed after the compression stroke as shown by the top figure.

Figure 5 shows the relative importance of reactions most significantly affecting the heat release rate (reaction temperature) under the RCM conditions of Mittal et al. (2006) at specific reaction times after the end of the compression stroke. What is clearly apparent is that the reactions $CO + O + M = CO_2 + M$ (R11) and $CO + HO_2 = CO_2 + H$ (R12) are only important in the chemical induction period. After chemical ignition occurs, these reactions no longer contribute significantly to the rate of heat release. On the other hand reactions such as $HO_2 + OH = H_2O + O_2$ (R7), $HO_2 + H = 2OH$, (R8), $H_2 + OH = H_2O + H$ (R16), and $H_2 + O = H + OH$ (R17) are significant in describing the heat release rate. A sensitivity analysis which separately considers the sensitivity of the extent of reaction to the various reactions prior to and after ignition occurs confirms the above findings for the importance of reactions (R11) and (R12). This indicates that HO_2 and H_2O_2 chemistry becomes important under the RCM conditions considered here as these intermediate species rapidly build up during the induction period, more

so than H or OH. Once ignition occurs, OH reactions become more dominant as evidenced by Figure 5 (e.g. CO+OH (R4) becomes one of the primary reactions at ignition as opposed to CO+HO_2 (R12) during the induction period). We find some effect of modifying the reaction rate for reaction (R7) from the former measurement of Hippler *et al.* (1995) used in the C_1 mechanism to the more recent determination of Kappel *et al.* (2002), but there is little effect on any observable other than the chemical induction time.

Sivaramakrishnan *et al*. (2006) have also studied H_2/CO oxidation in a shock tube at much higher pressures, (exceeding 200 atm) and somewhat higher temperatures (> 1,100 K) for highly dilute H_2/CO/O_2/Ar mixtures. CSP analysis was applied to a representative case, as shown in Figure 6. Figure 6b shows that under these high-pressure and high-temperature conditions, and for the highly dilute mixtures studied, there is not a well defined ignition delay. There is, however, an obvious induction period. Similar to the RCM analysis above, CSP was performed during this induction period and the results are shown in Figure 6c. The identified reactions participating in the evolution of the system are essentially different from those shown in Figure 5 for the RCM case. It is important to note that those reactions identified during the heat release/ignition stage in Figure 5 (e.g. R7, R16, and R17) appear as the main participating reactions in Figure 6 with (R12) having a reduced impact. Therefore, the present CSP analysis shows that for highly dilute mixtures at sufficiently high pressures and temperatures reaction (R7) needs to be considered in order to properly describe the H_2/CO kinetic system whereas under more moderate pressures and temperatures reaction (R12) needs to be taken into account in predictions where

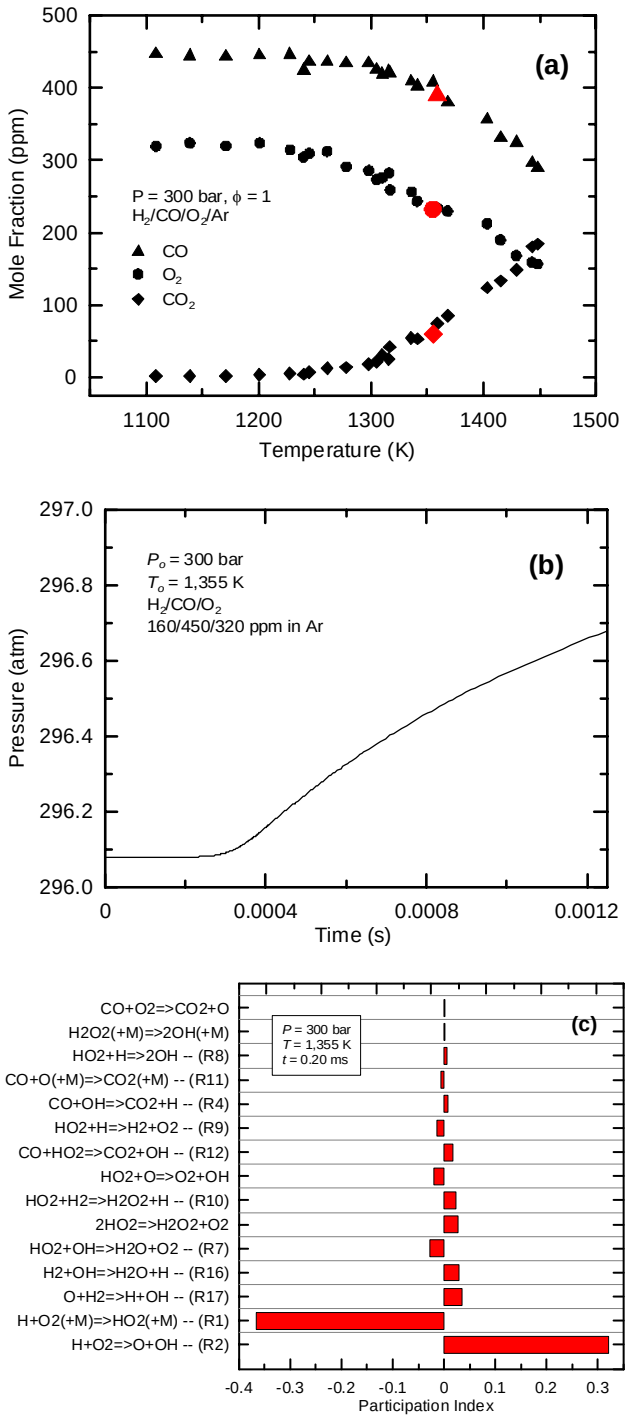

Figure 6. H_2/CO oxidation in a high pressure shock tube. (a) Experimental data of Sivaramakrishnan *et al*.; (b) temperature profile and (c) CSP analysis during the induction period in (b) for the conditions chosen in (a) (red symbols).

chemical induction processes are to be expected to be important. It is further noted that a similar analysis under the pressure/temperature conditions shown Figure 6 using higher reactant concentrations (as those shown in Figure 5) identifies the same relative importance of reactions shown in Figure 5; dilution, thus, plays a role in the relative importance of specific reactions for these different investigations. Figures 5 and 6 show that reactions (R12) and (R7) appear to have, separately, a distinct impact in these systems. At pressures and temperatures similar to those in the work of Sivaramakrishnan *et al*. (2006), the current C_1 model predictions are unchanged by a variations of as much as a factor of five in the rate of reaction (R12). In contrast, changes in reaction (R7) yield little effect in RCM modeling. Finally, it should be noted that the very high participation index of $H + O_2 + M = HO_2 + M$ (R1) results in a significant influence of the third body effects on both induction and post induction kinetics.

Update on $CO+HO_2$ Reaction Rate Correlation

In Chaos and Dryer (2008), we discuss in detail recent updating in the rate correlation information for reaction (R12). Mittal et al. (2006) investigated the ignition of $H_2/CO/O_2/N_2/Ar$ mixtures in a RCM at pressure and temperature ranges of 15-50 bar and 950-1100 K, respectively. They noted that the reproduction of their experimental data required rate values for $CO+HO_2=CO_2+OH$ (R12) that were up to a factor of four smaller than those used in current H_2/CO models (Davis et al., 2005; Li et al., 2007). In a follow-up study to their RCM measurements, Mittal et al. (2007) used Monte Carlo and "Morris-one-at-a-time" uncertainty analyses in evaluating predictions based upon the model of Davis et al. (2005). The results pointed to a rate value for (R12) that could be up to a factor of ten lower with respect to that of Baulch et al. (1973), consistent with the findings of Mittal et al. (2006).

Prior to this research, (R12) had not received as much attention theoretically as other reactions in the H_2/CO system. As reviewed by You et al. (2007), the few theoretical studies available (Allen et al., 1996; Sun et al., 2007) did not adequately treat critical geometries as well as hindered internal rotations in the *trans*-HOOC•O adduct through which (R12) proceeds. Furthermore, the complexity of the potential energy surface due to the *trans*- and *cis*- conformers and their mutual isomerization were not considered. Consequently, You et al. (2007) performed an improved theoretical treatment of (R12) and showed that this reaction is pressure independent for conditions relevant to combustion applications with a temperature dependence of:

$$k_{R12}\left(\mathrm{cm^3/mol/s}\right) = 1.6\times10^5 T^{2.18}\exp\left(\frac{-9030}{T}\right) \qquad (4)$$

S.J. Klippenstein employed transition state theory and a two barrier model to produce the correlation recommended in Mittal et al. (2007). Adopting the rate expression for (R12) derived by You et al. (2007) into the model of Li et al. (2007) considerably improves its predictions of RCM ignition delay at high pressures. It should be stated again, however, that reaction (R12) is only important during the chemical induction period, principally through its impact on the initial build-up of HO_2. After chemical ignition occurs, which is associated with the decomposition of hydrogen peroxide and transition to chemical branching through (R2), reaction (R12) no longer contributes significantly to the system behavior (i.e. the rate of heat release). Subsequent to ignition and at all pressures, the system dramatically shifts to one dominated by reactions involving the OH radical. As a result, in combustion applications where radical back-mixing or heterogeneous processes result in chemical reaction initiation, reaction (R12) does not significantly impact predictions.

Update on $HO_2 + OH = H_2O + O_2$ Reaction Rate Correlation

Reaction (R7) carries significant importance in the HO_x cycle of atmospheric chemistry and has been extensively studied at low temperatures (e.g. see database evaluations such as http://kinetics.nist.gov). Recent high temperature measurements (Hippler et al. 1995; Kappel et al., 2002) show that (R7) exhibits an uncommon and highly non-Arrhenius behavior, indicative of the formation of an activated complex. There is an unusually narrow and deep minimum in the rate at about 1000-1200 K with a rapid increase below and above the minimum. The lack of experimental data at intermediate temperatures (400-900 K) makes finding an expression that accurately captures the observed temperature dependence challenging.

In order to predict their high pressure experimental data (up to 450 atm), Sivaramakrishnan et al. (2007) recently proposed a new parameterization for (R7). Sivaramakrishnan et al. (2007) fitted experimental data from a number of studies (DeMore, 1982; Goodings and Hayhurst, 1988; Hippler et al., 1995; Hippler and Troe, 1992; Kappel et al., 2002; Keyser, 1988; Li et al., 1980; Peters and Mahnen, 1973). The fit gives larger weight to the data of Hippler et al. (1995) rather than to the more recent, and arguably more reliable, measurements of Kappel et al. (2002). While the proposed rate expression appears to considerably improve H_2/CO oxidation predictions of the high pressure experiments (Sivaramakrishnan et al., 2007), we note that the rate predictions increase for T > 1400 K, quickly reaching values that exceed the collision limit.

We suggest that (R7) is better represented by a correlation that reaches a limiting value at high temperatures, similar to the observations of Hippler et al. (1995) for the reaction $H_2O_2+OH=HO_2+H_2O$ (R18). In Chaos and Dryer (2008), we report two new least-squares analyses of available experimental data to obtain rate expressions constrained by a high temperature limiting value (Goodings and Hayhurst, 1988; Srinivisan et al., 2006), one using the measurements of Hippler et al. (1995), who measured a rate minimum near 1240 K, and a second using the data of Kappel et al. (2002), who located the rate minimum near 1010 K. We found that reasonable predictions of the high pressure oxidation data of Sivaramakrishnan et al. (2007) can only be obtained using values of the rate for (R7) predicted by the correlation developed using the Hippler et al. (1995) results:

$$k_{R7}\left(\mathrm{cm^3/mol/s}\right) = 1.467\times10^{11}T^{0.73}\exp\left(\frac{587}{T}\right) + 1.105\times10^{37}T^{-6.35}\exp\left(\frac{-13297}{T}\right) - 8.976\times10^{163}T^{-42.44}\exp\left(\frac{-54377}{T}\right) \quad (5)$$

Using the Li et al. (2007) CSP analyses applied to the conditions of Sivaramakrishnan et al. (2007), we note above that (R7) is only important during chemical induction at all pressures. As the reacting system evolves, (R8) becomes much more important than (R7) in determining the overall rate of reaction since it is the major direct source of OH at high pressures for reacting with CO through (R4). The correlation proposed by Sivaramakrishnan et al. (2007) as well as that developed by Chaos and Dryer (2008) above essentially lowers the rate of (R7) over the temperature range of interest, therefore slowing a termination path for both HO_2 and OH. Thus, hydroxyl radical formation (relative to HO_2 formation) is greatly diminished.

While lowering the rate of (R7) below the value used in Li et al. (2007) leads to marked improvement in emulating the data at pressures of approximately 250 atm, only moderate

improvements result at higher pressures. At higher pressures, reaction (R7) strongly competes with $HO_2 + H = OH + OH$ (R8) for HO_2 radicals. The flux of HO_2 to form H_2O_2, (R10), becomes considerably larger than through reaction (R7), and at high temperatures, H_2O_2 decomposes rapidly to yield OH, (R19), removing the significance of reaction (R7). As a result, our detailed analyses (Chaos and Dryer, 2008) suggest that the study of Sivaramakrishnan et al. (2007) only supports the likelihood of a lower rate for reaction (R7) over $1200 < T < 1400$ K consistent with the measurements of Hippler et al. (1995), and that suitable fits of the syngas oxidation data can be obtained with modification of other reactions within their uncertainty bounds.

Syngas Ignition Characteristics

In a Short Communication published during this research, Petersen et al. (2007) reported new data on ignition delay for syngas-air mixtures in a high pressure shock tube and a flow reactor. These new data were summarized in an Arrhenius-type plot along with other recently published data from the rapid compression studies of Walton et al. (2007) and from an earlier high pressure flow reactor study described in an Electric Power Research Institute report (Peschke et al., 1985), all normalized to conditions of 20 atm pressure. Petersen et al. noted that at temperatures lower than about 1050 K, experimental observations of syngas ignition delay, determined by various criteria, begin to substantially depart from homogeneous gas phase predictions utilizing any of the recently published H_2/CO detailed kinetic models. The authors emphasized that the disparity was evident in all of the different types of experiments and could not be attributed to differences in criteria used to determine the ignition delay. the authors stated that the disagreement between experiment and model "may not be surprising, since few data have existed at the temperature and pressure ranges of the present study to which the (previously) published models could be calibrated."

In a Short Communication appearing as Appendix B in this report, and elaborated upon further in a full length paper appearing as Appendix C, we support their conclusion that the noted departures of the experimental observations of syngas ignition delay measurements from homogenous gas phase kinetic predictions at temperatures lower than about 1050 K are real and that the reported measurements impose limitations on gas turbine designs for lean premixing of syngas compositions with air. In contrast, however, our analyses indicate that the principle source(s) of disagreement are not homogenous kinetic model inadequacies, but interpretations of the data as representing pure homogenous chemical kinetic observations. We argue that 1) the principal underlying sources of the disparities noted for syngas ignition delays predictions in Petersen et al have been evident in many hydrogen oxidation studies since the 1960's; 2) the disparities between measured and predicted syngas ignition delays are mostly a result of the failure of homogeneous gas phase predictions to capture perturbations of chemical induction processes in the mild ignition regime by one or more phenomena.

Experiments and analyses of hydrogen-oxygen ignition delay measurements in the "mild" ignition regime show high sensitivity to perturbations by the presence of contaminants in the reactants or on experimental surfaces, compressible fluid dynamic effects, inhomogeneous mixing, and catalysis from particles or surface materials. In any combination, these perturbations can lead to repeatable reductions of the predicted chemical induction time scales in the mild ignition regime by as much as several orders of magnitude. The reactions $CO+HO_2 =$

CO_2+OH and CO+O+M = CO_2+M also modify syngas chemical induction times from those observed for hydrogen/oxygen systems, but these modifications are small in comparison to those produced by the perturbation sources listed above. Finally, as a result of the fact that these sources of perturbations, in any combination, produce within a factor of ten or less the same reduction in chemical induction times in all of the venues discussed in Petersen et al. (2007), we show that a simple zero-dimensional representation of their effects as homogenous catalytic processes that promote H_2O_2 production and decomposition to hydroxyl radicals provides reasonable engineering estimates of the perturbed ignition delay in the mild ignition regime, without modification of homogenous ignition delay predictions at other conditions. Detailed discussions of these points appear in Appendices B and C of this report and are not repeated here.

Task 3 The effect of NO_x on ignition under back-mixing conditions in gas turbines has not been studied previously, and this was one of the originating tasks of the present research. Generation of syngas (through coal gasification, for example) for gas turbine applications can lead to the presence of small hydrocarbons (e.g., methane) and other combustion gas components (e.g. NO_x) in these systems, particularly in mixing regions of entering fuel and air. Prior work (e.g., Ashmore and Tyler, 1962; Mueller et al., 1998, 1999) the presence of small quantities of NO_x can drastically modify the relative influence of HO_2 chemistry at conditions near the extended second explosion limit of the H_2/O_2 system. NO_x provides an alternate consumption route for HO_2 radicals via NO+HO_2=NO_2+OH (R13). The NO_2 so formed can then react with H atoms via NO_2+H=NO+OH (R14) to give back NO and thereby reactions (R13) and (R14) establish a catalytic cycle which consumes H_2 at temperatures well below the explosion limits of the unperturbed system. This coupling results in two very important effects. In the temperature range where this catalytic cycle is active, small amounts of NO_x significantly affect the overall chemical reaction rate, principally through substantial reductions in the chemical induction time leading to establishing critical branching. At very low NO_x concentrations (sub-ppm), essentially all the NO is oxidized to NO_2 without significant consequence. However, increasing the NO_x concentration beyond a threshold value (which is very low) leads to sufficient NO_2 concentrations that enable reaction (R14) to compete effectively with reaction (R2) for H atoms. In this case, not only is the extended second explosion limit behavior modified, but the overall rate of reaction (defined by the fuel concentration reacted over the characteristic reaction time) is significantly altered. At higher concentrations of NO_x, the reaction NO+OH=HONO (R15) rapidly comes to partial equilibrium, and the addition of further amounts of NO leads to chemical inhibition by removal of OH radicals.

In work detailed in Appendix C, we found that there is a non-linear effect in terms of the amount of added NO, and further that the effect is also a function of both reaction temperature and pressure. Addition of an appropriate amount of NO causes the overall activation energy of the oxidation reaction of syngas to be nearly the same above and below the explosion limit condition. The difference in overall oxidation rate above and below the explosion limit eventually is decreased (due to the increased rate of reactions involving HO_2), and the explosion limit becomes described by essentially the same overall temperature dependence. It is this function that is most important in defining the engineering parameters over which mixing can be accomplished without flashback or pre-ignition in gas turbine systems. Detailed analyses appear in Appendix C.

A contaminant not initially considered in the proposed research has been considered that is likely much more significant in its effects on combustion than NOx; iron pentacarbonyl. Williams and Shaddix (2007) have recently reported observing wall deposits formed when operating a swirl-stabilized combustor running on simulated syngas-air mixtures. The deposits were analyzed and found to be composed mostly of iron oxides and, to a lesser extent, nickel oxides. It was concluded that the source of the metal contaminants was the CO used. For laboratory combustion experiments, many researchers use CO stored in high pressure carbon-steel cylinders. CO can readily react at high pressure with metals present in steel to form carbonyls; especially iron pentacarbonyl, $Fe(CO)_5$. It appears that industry is aware as well that carbonyls are present in syngas, likely produced in the contact of carbon-monoxide-rich streams with hot metal surfaces. Metallic compounds are known to have strong flame inhibition effects (Lask and Wagner, 1960; Reinelt and Linteris, 1996; Rumminger and Linteris, 2000, 2002; Rumminger et al., 1999; Vanpee and Shirodkar, 1978). When present in premixed flames, iron pentacarbonyl can reduce the burning velocity considerably (Lask and Wagner, 1960; Reinelt and Linteris, 1996; Rumminger and Linteris, 2000). Of relevance to the present discussion is the work of Rumminger and Linteris (2000) who studied stoichiometric $H_2/CO/O_2/N_2$ premixed flames with hydrogen contents of up to 1.5%. It was shown that reductions in burning velocity of 30% were attained for $Fe(CO)_5$ concentrations on the order of 150 ppm as a result of a catalytic inhibition cycle that removes H and O atoms. At higher iron pentacarbonyl loadings, it was observed that the inhibition effectiveness decreased due to saturation of the catalytic cycle, and perhaps particle condensation (Rumminger and Linteris, 2000).

The above discussions led us to further analyze recent measurements of syngas laminar burning velocities at both atmospheric and elevated pressures. As detailed in Appendix C, we used a submechanisms developed by Rumminger et al (1999) for $FeCO_5$ interactions in flames combined with the Li et al C_1 mechanism to study the effects of iron pentacarbonyl in various combustion configurations at pressures and temperatures found in gas turbines. We numerically show that $Fe(CO)_5$ has a very noticeable effect on rich flames. A sensitivity analysis of burning velocity on kinetic rates showed that iron containing species become important at rich conditions. A chemical flux analysis revealed that hydrogen atoms are removed through reactions involving iron oxide and hydroxide species (i.e. the cycle $FeO \rightarrow Fe(OH)_2 \rightarrow FeOH \rightarrow FeO$). The "O-atom" cycle (Rumminger and Linteris, 2000) involving the path $Fe \rightarrow FeO_2 \rightarrow FeO \rightarrow Fe$ is not active since the present flames have considerable amounts of hydrogen. We also noted that iron oxide hydroxide – FeO(OH) – was also an important species as it interacts with the main H-atom cycle (not noted in prior work).

We also investigated numerically the effects of $Fe(CO)_5$ on counterflow diffusion flame ignition (Fotache et al., 2000) as well as homogeneous ignition delay (Dean et al., 1978) of H_2/CO systems, again assuming 200 ppm $Fe(CO)_5$ concentration in the CO source. No substantial differences were found between predictions with or without iron pentacarbonyl in the fuel source for the counterflow configuration with carbonyl present in the fuel. However, adding 100 ppm $Fe(CO)_5$ to the air side significantly increased the modeled ignition temperature.

Oxidation of carbon monoxide in shock tubes has been shown to be accelerated in the presence of chromium, nickel, and iron carbonyls (Izod et al., 1972; Matsuda, 1972a; Matsuda, 1972b). Under conditions similar to the shock tube study of Petersen et al. (2007), we found that a CO

source contaminated by 200 ppm of $Fe(CO)_5$ an overall mixture concentration of iron pentacarbonyl of approximately 10 ppm was obtained. Over a temperature range of 850-2000 K, computations showed moderate ignition delay reductions on the order of 3% to 30%. At higher $Fe(CO)_5$ loadings, the radical scavenging cycles described above will reduce radical concentrations leading to ignition delay inhibition (Linteris, 2007).

In summary we conclude that carbon monoxide sources used in research and syngas products should be carefully scrutinized in terms of metallic impurities. The presence of these impurities under syngas generation from coal gasification and its downstream purification will be intimately tied to the process design and material construction Thus, the commercial implications of metal carbonyl contamination are unknown, but deserve attention. For research purposes, carbonyl-free carbon monoxide sources supplied in pressurized aluminum cylinders with brass fittings should be used. The above discussion supports the need for further experimental investigation of carbonyl effects, especially on burning rate measurements of syngas mixtures to be used for model validation.

Task 4 The results of this work have been published as materials in three separate archival publications:

Chaos, M. and Dryer, F.L. (2008). Syngas Combustion Kinetics and Applications, in Special Issue: *Syngas Combustion* (V. Yang and T. Lieuwen, eds.) *Combustion Sci. Tech.* In Press.

Dryer, F.L. and Chaos, M. (2008), Ignition of Syngas/air and Hydrogen/air Mixtures at Low Temperatures and High Pressures: Experimental Data interpretation and Kinetic Modeling Implications, *Combust. Flame* 152, 293-299.

Li, J. Zhao, Z., Kazakov, A., Chaos, M. and Dryer, F.L. (2007) A Comprehensive Kinetic Mechanism for CO, CH_2O, CH_3OH Combustion, *Int. J. Chem. Kin.* 39, 109-136.

The only work conducted under this contract presently not in the published archival literature is that work summarized in the above materials as Task 1. This work will be part of future publication based upon additional experimental developments which would require construction of a new flow reactor that can operate exclusively with water vapor or carbon dioxide as the carrier gas. This experimental need was identified as a result of the present work and is beyond the scope and resources available in the present grant.

Reactions
Referenced in this Report

$H + O_2 + M = HO_2 + M$	(R1)	$CO + O + M = CO_2 + M$	(R11)
$H + O_2 = OH + O$	(R2)	$CO + HO_2 = CO_2 + OH$	(R12)
$H + OH + M = H_2O + M$	(R3)	$NO + HO_2 = HO + OH$	(R13)
$CO + OH = CO_2 + H$	(R4)	$NO_2 + H = NO + OH$	(R14)
$HCO + M = H + CO + M$	(R5)	$NO + OH = HONO$	(R15)
$HCO + O_2 = HO_2 + CO$	(R6)	$H_2 + OH = H_2O + H$	(R16)
$HO_2 + OH = H_2O + O_2$	(R7)	$H_2 + O = OH + O$	(R17)
$HO_2 + H = OH + OH$	(R8)	$H_2O_2 + OH = HO_2 + H_2O$	(R18)
$HO_2 + H = H_2 + O_2$	(R9)	$H_2O_2 + M = OH + OH + M$	(R19)
$HO_2 + OH = H_2O_2 + H$	(R10)		

References

Allen, T.L., Fink, W.H., and Volman, D.H. (1996) Theoretical Studies of the Mechanism of the Gas Phase Reaction of the Hydroperoxo Radical with Carbon Monoxide to Form Hydroxyl Radical and Carbon Dioxide. *J. Phys. Chem.*, 100, 5299-5302.

Ashmore, P.G. and Tyler, B.J. (1962) Reaction of hydrogen atoms with nitrogen dioxide. *Trans. Farad. Soc.*, 58, 1108-1116.

Ashman, P. J. and Haynes, B. S. (1998). Rate coefficient of $H+O_2+M \rightarrow HO_2+M$ ($M=H_2O$, N_2, Ar, CO_2), *27th Symp. (Int.) on Combust.*, The Combustion Institute. P185

Baulch, D.L., Drysdale, D.D., Duxbury, J., and Grant, S. (1973) *Evaluated Kinetic Data for High Temperature Reactions*. Vol. 3, Butterworths, London.

Bromly, J. H., Barnes, F. J., Nelson, P. F., and Haynes, B. S. (1995). Kinetics and modeling of the H_2-O_2-NO_X system, *Int. J. Chem. Kin.*, 27, 1165 (1995).

Chaos, M. and Dryer, F.L. (2008). Syngas Combustion Kinetics and Applications, in Special Issue: *Syngas Combustion* (V. Yang and T. Lieuwen, eds.) *Combustion Sci. Tech.* In Press.

Davis, S.G., Joshi, A.V., Wang, H., and Egolfopoulos, F. (2005) An Optimized Kinetic Model of H_2/CO Combustion. *Proc. Combust. Inst.*, 30, 1283-1292.

Demore, W.B. (1979) Reaction of HO_2 with O_3 and the Effect of Water Vapor on HO_2 Kinetics. *J. Phys. Chem.*, 83, 1113-1118.

DeMore, W.B. (1982) Rate Constant and Possible Pressure Dependence of the Reaction Hydroxyl + Hydroperoxo. *J. Phys. Chem.*, 86, 121-126.EPRI report

Dryer, F.L. and Chaos, M. (2008), Ignition of Syngas/air and Hydrogen/air Mixtures at Low Temperatures and High Pressures: Experimental Data interpretation and Kinetic Modeling Implications, *Combust. Flame* 152, 293-299.

Fotache, C.G., Kreutz, T.G., Zhu, D.L., and Law, C.K. (1997) Ignition of counterflowing methane versus heated air under reduced and elevated pressures. *Combust. Flame*, 108, 442-470.

Fotache, C.G., Tan, Y., Sung, C.J., and Law, C.K. (2000) Ignition of CO/H2/N2 versus Heated Air in Counterflow: Experimental and Modeling Results. *Combust. Flame*, 120, 417–426.

Gilbert, R.G., Luther, K., and Troe, J. (1983) Theory of thermal unimolecular reactions in the fall-off range. 2. Weak collision rate constants. *Ber. Bunsenges. Phys. Chem.*, 87, 169-177.

Goodings, J.M. and Hayhurst, A.N. (1988) Heat Release and Radical Recombination in Premixed Fuel-Lean Flames of $H_2 + O_2 + N_2$ - Rate Constants for $H + OH + M \rightarrow H_2O + M$ And $HO_2 + OH \rightarrow H_2O + O_2$. *J. Chem. Soc. Faraday Trans. 2*, 84, 745-762

Held T.J. and Dryer, F.L. (1998) Comprehensive mechanism for methanol oxidation. *Int. J. Chem. Kinet.*, 30, 805-830.

Hippler, H., Troe, J., and Willner, J. (1990) Shock wave study of the reaction $HO_2 + HO_2 = H_2O_2 + O_2$: Confirmation of a rate constant minimum near 700 K. *J. Chem. Phys.*, 93, 1755-1760.

Hippler, H. and Troe, J. (1992) Rate Constants of the Reaction HO + H_2O_2 → HO_2 + H_2O at T ≥ 1000 K. *Chem. Phys. Lett.*, 192, 333-337.

Hippler, H., Neunaber, H., and Troe, J. (1995) Shock wave studies of the reactions HO + H_2O_2 = H_2O + HO_2 and HO + HO_2 = H_2O + O_2 between 930 and 1680 K. *J. Chem. Phys.*, 103, 3510-3516.

Kappel, C-H, Luther, K. and Troe, J. (2002) Shock wave study of the unimolecular dissociation of H_2O_2 in its falloff range and of its secondary reactions. *Phys. Chem. Chem. Phys.*, 4, 4392-4398.

Kazakov, A., Chaos, M., Zhao, Z. and Dryer, F.L. (2006) Computational singular perturbation analysis of two-stage ignition of large hydrocarbons. *J. Phys. Chem. A.* 110, 7003-7009.

Keyser, L.F. (1988) Kinetics of the Reaction OH + HO_2 → H_2O + O_2 From 254 K to 382 K. *J. Phys. Chem.*, 92, 1193-1200.

Kim, T.J., Yetter, R.A., and Dryer, F.L. (1994) New results on moist CO oxidation. High pressure, high temperature experiments and comprehensive kinetic modeling. *Proc. Combust. Inst.*, 25, 759-766.

Ko, T. and Fontijn, A. (1991) High-temperature photochemistry kinetics study of the reaction H + NO_2 → OH + NO from 296 K to 760 K. *J. Phys. Chem.*, 95, 3984-3987.

Lask, G. and Wagner, H.Gg. (1960) Influence of Additives on the Velocity of Laminar Flames. *Proc. Combust. Inst.*, 8, 432-438.

Lewis, B. and von Elbe, G. (1987). *Combustion, Flames, and Explosions of Gases* (3rd ed) Academic Press, Inc., Orlando, FL.

Li, J. (2004) Ph.D. Thesis, Department of Mechanical and Aerospace Engineering, Princeton University, Princeton, NJ.

Li, J., Kazakov, A., and Dryer, F.L. (2004a). Experimental and numerical studies of ethanol decomposition reactions. *J. Phys. Chem. A*, 108, 7671-7680.

Li, J., Zhao, Z., Kazakov, A., and Dryer, F.L. (2004b). An updated comprehensive kinetic model of hydrogen combustion. *Int. J. Chem. Kinet.*, 36, 566-575.

Li, J., Kazakov, A., and Dryer, F.L. (2005). Chemical kinetics of ethanol oxidation, 2nd European Combustion Workshop, Louvain-la-Neuve, Belgium, April 3-6. Poster R15-019.

Li, J., Zhao, Z., Kazakov, A., Chaos, M., Dryer, F.L., and Scire, J.J. Jr. (2007) A comprehensive kinetic mechanism for CO, CH_2O, CH_3OH combustion. *Int. J. Chem. Kinet.*, 39, 109-136.

Lutz, A.E., Kee, R.J., and Miller, J.A. (1987) *SENKIN: a Fortran program for predicting homogeneous gas phase chemical kinetics with sensitivity analysis*, Report SAND87-8248, Sandia National Laboratories, Albuquerque, NM.

Michael, J.V., Su, M.C., Sutherland, J.W., Carroll, J.J., and Wagner, A.F. (2002) Rate constants for H + O_2 + M = HO_2 + M in seven bath gases. *J. Phys. Chem. A.*, 106, 5297-5313.

Mittal G. and Sung, C-J. (2006). A rapid compression machine for chemical kinetics studies at elevated pressures and temperatures. *Combust. Sci. Tech.* 38, 516-529 (2006).

Mittal, G., Sung, C.J., and Yetter, R.A. (2006) Autoignition of H_2/CO at Elevated Pressures in a Rapid Compression Machine. *Int. J. Chem. Kinet.*, 38, 516–529.

Mittal, G., Sung, C.J., Fairweather, M., Tomlin, A.S., Griffiths, J.F., and Hughes, K.J. (2007) Significance of the HO_2+CO Reaction during the Combustion of CO+H_2 Mixtures at High Pressures. *Proc. Combust. Inst.*, 31, 419-428.

Mueller, M.A., Yetter, R.A., and Dryer, F.L. (1998) Measurement of the rate constant for $H+O_2+M = HO_2+M$ (M = N_2, Ar) using kinetic modeling of the high-pressure $H_2/O_2/NO_x$ reaction. *Proc. Combust. Inst.*, 27, 177 184.

Mueller, M.A., Yetter, R.A., and Dryer, F.L. (1999) Flow reactor studies and kinetic modeling of the $H_2/O_2/NO_x$ and $CO/H_2O/O_2/NO_x$ reactions. *Int. J. Chem. Kinet*., 31, 705-724.

Mueller, M.A., Yetter, R.A., and Dryer, F.L. (2000) Kinetic modeling of the $CO/H_2O/O_2/NO/SO_2$ system: Implications for high-pressure fall-off in the $SO_2+O(+M) = SO_3(+M)$ reaction. *Int. J. Chem. Kinet.*, 32, 317-339.

Peeters, J. and Mahnen, G. (1973) Reaction Mechanisms and Rate Constants of Elementary Steps in Methane-Oxygen Flames. *Proc. Combust. Inst.*, 14, 133-146.

Peschke, W.T. and Spadaccini, L.J. (1985) Determination of Autoignition and Flame Speed Characteristics of Coal Gases having Medium Heating Values. Electric Power Research Institute, Report EPRI AP-4291.

Petersen, E.L., Kalitan, D.M., Barrett, A.B., Reehal, S.C., Mertens, J.D., Beerer, D.J., Hack, R.L., and McDonell, V.G. (2007) *Combust. Flame*, 1-2, 244-247.

Reinelt, D. and Linteris, G.T. (1996) Experimental Study of the Inhibition of Premixed and Diffusion Flames by Iron Pentacarbonyl. *Proc. Combust. Inst.*, 26, 1421-1428.

Rumminger, M.D. and Linteris, G.T. (2000) Inhibition of Premixed Carbon Monoxide-Hydrogen-Oxygen-Nitrogen Flames by Iron Pentacarbonyl. *Combust. Flame*, 120, 451-464.

Rumminger, M.D. and Linteris, G.T. (2002) The Role of Particles in the Inhibition of Counterflow Diffusion Flames by Iron Pentacarbonyl. *Combust. Flame*, 128, 145-164.

Rumminger, M.D., Reinelt, D., Babushok, V., and Linteris, G.T. (1999) Numerical Study of the Inhibition of Premixed and DiffusionFlames by Iron Pentacarbonyl. *Combust. Flame*, 116, 207-219.

Sivaramakrishnan, R., Comandini, A., Tranter, R.S., Brezinsky, K., Davis, S. G. and Wang, H. (2007) Combustion of CO/H_2 mixtures at elevated pressures. *Proc. Combust. Inst.* , 31, 429-438.

Srinivasan, N. K., Su, M.-C., Sutherland, J.W., Michael, J.V., and Ruscic, B. (2006) Reflected shock tube studies of high-temperature rate constants for $OH+NO_2 = HO_2+NO$ and $OH + HO_2 = H_2O + O_2$. *J. Phys. Chem. A*, 110, 6602-6607.

Su, M.-C., Kumaran, S.S., Lim, K.P., Michael, J.V., Wagner, A.F., Harding, L.B., and Fang, D.-C. (2002) Rate constants, $1100 \leq T \leq 2000$ K, for $H + NO_2 \rightarrow OH + NO$ using two shock tube techniques: comparison of theory to experiment. *J. Phys. Chem. A*, 106, 8261-8270.

Sun, H., Yang, S. I., Jomaas, G., and Law. C. K. (2007) High pressure laminar flame speeds and kinetic modeling of carbon monoxide/hydrogen flames. *Proc. Combust. Inst.*, 31, 439-446.

Vanpee, M. and Shirodkar, P.P. (1978) Study of Flame Inhibition by Metal Compounds. *Proc. Combust. Inst.*, 17, 787-795.

Walton, S.M., He, X., Zigler B. T., and Wooldridge, M.S. (2007) An experimental investigation of the ignition properties of hydrogen and carbon monoxide mixtures for syngas turbine applications. *Proc. Combust. Inst.*, 31, 3147-3154.

Williams, T.C. and Shaddix, C.R. (2007) Contamination of Carbon Monoxide with Metal Carbonyls: Implications for Combustion Research. *Combust. Sci. Tech.*, 175, 1225-1230.

Yetter, R.A., Dryer, F.L., and Rabitz, H. (1991) A comprehensive reaction mechanism for carbon monoxide/hydrogen/oxygen kinetics. *Combust. Sci. Tech.* 79, 129-140.

You, X. Goos, E. Sung, C.-J., and Wang, H. (2006) Reaction kinetics of $CO+HO_2$ = products: ab-initio study and master equation modeling. 31st International Symposium on Combustion, Heidelberg, Germany, August 6-11. Poster 2C-22.

You, X., Wang, H., Goos, E., Sung, C.J., and Klippenstein, S.J. (2007) Reaction Kinetics of $CO + HO_2 \rightarrow$ Products: Ab Initio Transition State Theory Study with Master Equation Modeling. *J. Phys. Chem. A*, 111, 4031-4042.

Zarubiak, D.C.Z., (1997). M.S. Thesis, Department of Mechanical and Aerospace Engineering, Princeton University, Princeton, NJ.

Zhao, Z., Li, J., Kazakov, A., and Dryer, F.L. (2005) Temperature-dependent feature sensitivity analysis for combustion modeling. *Int. J. Chem. Kinet*., 37, 282-295.

Zheng X.L. and Law, C.K. (2004) Ignition of premixed hydrogen/air by heated counterflow under reduced and elevated pressures. *Combust. Flame*, 136, 168-179.

Classified/Sensitive Data

None

Cost Status

Contract fully expended and closed

Technology Transfer Activities

We continue to discuss findings and results with personnel in the industry (e.g. Siemens, Gas Turbine Combustion Technology, Orlando, FL) and other gas turbine manufacturers.

Publications

Li, J., Zhao, Z., Kazakov, A., Chaos, M., Dryer, F.L., and Scire, J.J. Jr. (2007) A comprehensive kinetic mechanism for CO, CH_2O, CH_3OH combustion. *Int. J. Chem. Kinet.*, **39**, 109-136. Attached as Appendix A.

Dryer, F.L. and Chaos, M. (2008), Ignition of Syngas/air and Hydrogen/air Mixtures at Low Temperatures and High Pressures: Experimental Data interpretation and Kinetic Modeling Implications, *Combust. Flame* 152, 293-299. Attached as Appendix B

Chaos, M. and Dryer, F.L. (2008). Syngas Combustion Kinetics and Applications, in Special Issue: *Syngas Combustion* (V. Yang and T. Lieuwen, eds.) *Combustion Sci. Tech.* In Press. Attached as Appendix C

Appendices

Appendix A

Published in:
International Journal of Chemical Kinetics, vol. 39, iss. 3, 2007, pp. 109-136.

A Comprehensive Kinetic Mechanism for CO, CH_2O, CH_3OH Combustion

Juan Li, Zhenwei Zhao, Andrei Kazakov, Marcos Chaos, Frederick L. Dryer

Department of Mechanical and Aerospace Engineering
Princeton University
Princeton, NJ 08544
USA

James J. Scire, Jr.

Advanced Fuel Research, Inc.
East Hartford, CT 06108
USA

Corresponding Author: Prof. Frederick L. Dryer
Department of Mechanical and Aerospace Engineering
Princeton University
Princeton, New Jersey 08544-5263
Phone: (609)-258-5206
Fax: (609)-258-1939
E-Mail: fldryer@princeton.edu

A Comprehensive Kinetic Mechanism for CO, CH_2O, CH_3OH Combustion

Juan Li[1], Zhenwei Zhao, Andrei Kazakov[2], Marcos Chaos, Frederick L. Dryer[3]
Department of Mechanical and Aerospace Engineering
Princeton University, Princeton, NJ 08544

James J. Scire, Jr.
Advanced Fuel Research, Inc.
East Hartford, CT 06108

Abstract

New experimental profiles of stable species concentrations are reported for formaldehyde oxidation in a variable pressure flow reactor at initial temperatures of 850-950 K and at constant pressures ranging from 1.5 to 6.0 atm. These data, along with other data published in the literature and a previous comprehensive chemical kinetic model for methanol oxidation are used to hierarchically develop an updated mechanism for $CO/H_2O/H_2/O_2$, CH_2O, and CH_3OH oxidation. Important modifications include recent revisions for the hydrogen-oxygen sub-mechanism [1], an updated sub-mechanism for methanol reactions, and kinetic and thermochemical parameter modifications based upon recently published information. New rate constant correlations are recommended for CO+OH = CO_2+H (R23) and HCO+M = H+CO+M (R24), motivated by a new identification of the temperatures over which these rate constants most affect laminar flame speed predictions [2]. The new weighted least squares fit of literature experimental data for (R23) yields $k_{23}=2.23\times10^5 T^{1.89}\exp(583/T)$ cm^3/mole/s and reflects significantly lower rate constant values at low and intermediate temperatures in comparison to another recently recommended correlation and theoretical predictions. The weighted least squares fit of literature results for (R24) yields $k_{24}=4.75\times10^{11}T^{0.66}\exp(-7485/T)$ cm^3/mole/s, which predicts values within uncertainties of both prior and new [3, 4] measurements. Use of either of the data correlations reported in [3, 4] for this reaction significantly degrade laminar flame speed predictions for oxygenated fuels as well as for other hydrocarbons.

The present C_1/O_2 mechanism compares favorably against a wide range of experimental conditions for laminar premixed flame speed, shock tube ignition delay, and flow reactor species time history data at each level of hierarchical development. Very good agreement of the model predictions with all of the experimental measurements is demonstrated.

---

[1] Presently at: Praxair, Inc., Tonawanda, NY 14221.
[2] Presently at: Thermodynamics Research Center, NIST, Boulder, CO 80305.
[3] Corresponding author. *Fax*: (609) 258-6109. *Email*: fldryer@princeton.edu

Introduction

The hierarchical nature of hydrocarbon oxidation kinetics and the importance of small molecule and radical kinetics in controlling the oxidation of larger carbon number species are well-established notions [5, 6]. The hydrogen-oxygen kinetic sub-mechanism [6] controls the most reactive radical pool composition of H, OH, O, and HO_2 that attack the primary fuel. Carbon monoxide is a major intermediate species and its conversion to CO_2 is responsible for a significant fraction of the exothermicity accompanying hydrocarbon oxidation. It has been shown (e.g. [6, 7]) that nearly all carbon atoms bonded to one another, to hydrogen atoms, or hydroxyl groups are converted to CO through formaldehyde (CH_2O) and/or formyl radicals (HCO). Formyl radicals are a major source of H atoms and HO_2 radicals in larger carbon number hydrocarbon combustion.

Methanol (CH_3OH), the simplest alcohol, converts to CO through CH_2O reactions, and introduces additional species, particularly CH_2, CH_3, CH_3O and CH_2OH [8]. Over almost all conditions of practical interest, methanol combustion produces CH_3 in such minor concentrations that no C_2 hydrocarbon species are formed and, hence, no sooting occurs. The collection of kinetic phenomena involved in hydrogen/oxygen, carbon monoxide, formaldehyde, and methanol are therefore representative of the small radical pool interactions that couple with methyl radical and higher carbon number species and radicals in hydrocarbon combustion systems.

Detailed mechanisms for H_2, CO, CH_2O, and CH_3OH combustion are also individually of practical importance. Hydrogen kinetic properties have long been of interest in terms of safety, given the major use of hydrogen in chemical synthesis and fuel refining. The proposed transition to a hydrogen energy economy further emphasizes the need to understand hydrogen safety issues [e.g. 9, 10] as well as hydrogen combustion under mild combustion conditions and with very high exhaust gas recirculation. Carbon monoxide and formaldehyde are primary pollutant species emitted from many combustion systems and are important in reforming chemistry to produce hydrogen from hydrocarbons, as well as in atmospheric chemistry, toxicity and carcinogen assessments and analyses. Methanol is a used oxygenate additive in gasoline, and is also an attractive alternative to traditional transportation fuels because of its non-sooting characteristics, its facile synthesis from a wide variety of feedstocks, and its possible interim role as a hydrogen carrier for fuel cell applications.

The combustion chemistry of each of the above species has been extensively studied previously. Experimental data exist in the literature from laminar flame, shock tube, flow reactor, and static reactor experiments, collectively covering wide ranges of initial temperature, pressure, and equivalence ratio. Our group has had a long involvement in studying these small molecule kinetics in flow reactors (Yetter et al. [11, 12]; Hochgreb and Dryer [13]; Kim et al. [14], Norton and Dryer [15], Held and Dryer [8, 16], Mueller et al. [17-21]). We have previously developed comprehensive mechanisms for CO [12], CH_2O [13] and CH_3OH [8], and our recent work on updating and developing a comprehensive mechanism for hydrogen-oxygen [1] that includes advances in chemical kinetic rate and thermochemical information as well as validation data sources points to the need to similarly revisit and update our prior work on carbon monoxide, formaldehyde, and methanol kinetics. While the flow reactor data we have previously published for hydrogen, carbon monoxide, and methanol systems each cover a very wide range of pressures, our prior work on formaldehyde oxidation was limited to atmospheric pressure studies [13]. In that work, chemical analyses were conducted using off-line gas chromatography, an analytical method with potentially higher uncertainties than can be achieved using the Fourier Transform Infrared on-line analytical methods available today. formaldehyde oxidation obtained in a variable pressure flow reactor at initial temperatures of 850-950 K and constant pressures ranging from 1.5 to 6.0 atm to expand the range of validation conditions. Moreover, new experiments in other venues, especially for CH_2O oxidation, have appeared in the literature in shock tubes [3, 22-24] and laminar premixed flames [25]. In addition, there have been some elementary kinetic publications further addressing the important reactions involved in the C_1 oxidation system (e.g. [3, 4, 26]).

Utilizing our recent work on hydrogen/oxygen kinetics [1], and updating the CO/O_2, CH_2O/O_2, and CH_3OH/O_2 mechanisms with more recent kinetic and thermochemical information, a comprehensive mechanism has been hierarchically developed [27] that satisfactorily reproduces new experimental targets as well as those utilized in the original mechanism studies appearing in Refs. 8, 12, and 13. This paper reports the key features of the updated mechanism, summarizes the comparisons of predictions with experimental targets as performed in [27], and augments these earlier comparison using the results with some additional, recently published, kinetic measurements and validation experimental data.

Experimental Methods

The new experiments on formaldehyde oxidation reported here were conducted in the Princeton Variable Pressure Flow Reactor (VPFR) [28]. Detailed information on the VPFR instrumentation and experimental methodology can be found in other publications [29], and only a brief description is given here.

Carrier gas (N_2 in this study) is heated by a pair of electrical resistance heaters and directed into a reactor duct. Oxygen is also introduced at the duct entrance. The carrier gas/oxygen mixture flows around a baffle plate into a gap serving as the entrance to a diffuser. The vaporized fuel (trioxane with water in this study) flows into the center tube of a fuel injector, and injects radially outward into the gap where it rapidly mixes with the carrier gas and oxygen. The reacting mixture exits the diffuser into a constant area test section. Near the exit of the test section, a sampling probe is positioned on the reactor centerline to continuously extract and convectively quench a small percentage of the flow. At the same axial location, the local reaction gas temperature is measured with a type R thermocouple accurate to ±3 K.

The sample gas flows via heated Teflon lines to analytical equipment including a Fourier transform infrared spectrometer (FTIR), an electrochemical O_2 analyzer, and a pair of non-dispersive infrared analyzers for CO and CO_2. Other stable species of interest (e.g. CH_2O, H_2O) are measured continuously on-line using FTIR spectrometry. The measurement uncertainties for the data reported here are: O_2 - ±2%; CO - ±2%; CO_2 - ±2%; CH_2O - ±3%; H_2O - ±6% of reading.

The distance between the point of fuel injection and the sampling position is varied by moving the fuel vapor injector probe (with attached mixer/diffuser assembly) relative to the fixed sampling location. Mean axial velocity measurements along the centerline of the reactor are used to correlate distance with residence time. By this means, profiles of stable species versus residence time can be determined experimentally. The uncertainty in the residence time is approximately 5%.

In the present experiments, formaldehyde monomer was generated through the decomposition of 1,3,5-trioxane. Hochgreb and Dryer [13] also employed this technique in their atmospheric pressure flow reactor (APFR) experiments. Trioxane decomposition proceeds by the concerted rupture of the three C-O bonds to form three formaldehyde molecules [13, 30]. Using gas chromatography, it was experimentally verified that CH_2O is the only product of

trioxane decomposition, and trioxane decomposition is much faster than the subsequent reaction of formaldehyde at flow reactor conditions. For modeling purposes, one mole of trioxane reactant could therefore be replaced by three moles of formaldehyde.

In earlier work, [13, 30], trioxane was melted and delivered as a liquid to the evaporator of a prior atmospheric pressure flow reactor. A similar methodology would have required a complex modification of the present reactor and a different approach to deliver trioxane to the reactor was utilized. At 18°C, the solubility of trioxane in water is 17.2 g/100 ml [31]. Trioxane was dissolved in distilled water, and the unheated solution was volumetrically metered to a liquid vaporizer system located within the VPFR pressure shell and at the immediate entrance to the fuel vapor injector probe. The metered liquid flow was gas-blast atomized using heated nitrogen, and the nitrogen, water vapor, and trioxane vapor mixture was then injected into the reactor at the mixing location with hot carrier gas. It was verified that the decomposition rate of trioxane at the conditions of the reported experiments led to immediate formation of monomer during the injection and mixing process, well upstream of the radially uniform reaction region where the reported data were obtained. Due to heat addition limitations for the hot nitrogen used to vaporize the liquid reactant flow and the solubility limit of trioxane in water, the maximum initial CH_2O mole fraction investigated was limited to 500 ppm. Other than this limitation, the use of water to deliver the trioxane did not significantly affect the experiments, as the amount of water added was included in the kinetic modeling comparisons.

A series of moist formaldehyde oxidation experiments were conducted in the VPFR at initial temperatures of 850-950 K and in the pressure range 1.5-6.0 atm. For all of the experiments, the total carbon and oxygen balances experimentally determined at each residence time were within 4% of the specified input. The nearly identical total carbon and oxygen concentrations at each sampling location not only provide verification of the experimental measurements, but also imply that any other carbon- or oxygen-containing stable species present were only in negligible quantities. Although formic acid has been observed using these same diagnostics in VPFR experiments on methanol [8] and dimethyl ether [32] oxidation, none was detected in the present experiments on formaldehyde oxidation. This is most likely the result of the very low fuel concentrations studied here, and that formic acid would be expected to be below detection limits.

Updated Kinetic Mechanisms for CO, CH_2O, and CH_3OH Combustion

We used a slightly modified version of the methanol mechanism published by Held and Dryer [8] as a starting point in developing the present mechanism[+]. In the course of the present work, a number of thermochemical parameters and rate constant correlations were modified to reflect more recent kinetic information. The revised H_2/O_2 sub-mechanism is discussed in detail and validated against a large set of hydrogen/oxygen targets in a separate publication [1] and this sub-mechanism is absorbed without further modifications in the present work. Revisions included the use of the heat of formation of OH recommended by Ruscic et al. [34], which is in very good agreement with recent experimental results [35]. For the current work, we utilized 3.0 kcal/mol as the standard heat of formation of HO_2 at 298.15 K [36]. Very recently Ruscic et al. [37] have updated this heat of formation to 2.94 ± 0.06 kcal/mole. This change makes no significant differences in the level of comparison of computations with the targets utilized in the present work and appears in the Chemkin data files available from the authors.

In addition to revising the components associated with the hydrogen-oxygen sub-mechanism, the following revisions were also adopted over the course of this work:

1. Thermochemical Data for CH_2OH

The thermochemical properties of CH_2OH, including enthalpy of formation, standard entropy, and heat capacity at different temperatures, were updated to those reported by Johnson and Hudgens [38]. The data of Johnson and Hudgens also agree well with another recent IUPAC evaluation by Ruscic et al. [39]. These thermodynamic properties were fitted with a 14 coefficient polynomial [40].

2. $CO + OH = CO_2 + H$ (R23)

This well studied reaction is of critical importance to combustion modeling because it is the main pathway to convert CO to CO_2, the oxidation of CO is responsible for a major fraction of the energy release derived in oxidation of hydrocarbons, and CO_2 dissociation important in determining adiabatic flame temperatures as a function of pressure. The reaction proceeds

[+] In verifying the published mechanism we found that the model reported in [8] resulted in calculated flame speeds that were much higher than those shown in the publication. Dr. Held [33] concurs that the flame speed calculations reported in the paper resulted from the slightly modified version of the reported mechanism, used as a basis in the current work.

through the formation of HOCO adducts and thus is pressure dependent, particularly at low temperatures [26, 41]. Under most practical combustion conditions, however, the reaction can be treated as pressure-independent.

The rate of oxidation of $H_2/CO/O_2$ and moist CO mixtures is very sensitive to reaction (R23) [12]. Moreover, laminar flame speed predictions of hydrocarbons are strongly influenced by this reaction [42, 43]. It is not surprising that targets such as shock tube ignition delay data or flow reactor data would constrain model parameters only over the particular range of temperature covered by the work. However, the temperature range over which laminar flame speed predictions are most sensitive to a particular elementary reaction has typically not been considered.

Recently, Zhao et al. [2] introduced a methodology to determine the temperature dependent sensitivity of premixed laminar flame speeds to elementary rate constant and transport properties. Analyses were conducted by locally perturbing the parameter with a Gaussian function profile. The center of the Gaussian profile was moved with an assigned temperature mean, and the sensitivity of the predicted flame speed was determined as a function of the perturbation assigned mean temperature. The analysis leads to the determination of a "temperature window" in which the predicted laminar flame speed is found to be most sensitive to perturbations in the particular parameter. The temperature sensitivity of laminar flames for hydrogen/carbon monoxide mixtures with respect to (R23) was used as an application demonstration. The predicted laminar flame speed was shown to be most sensitive to the specific rate of (R23) in the temperature range 300-1900 K (Fig. 1).

Recently, Yu [44], Troe [45], Zhu et al. [46], and Senosiain et al. [26] performed detailed RRKM calculations to model the temperature and pressure dependence of this reaction. Most of these correlations were primarily calibrated against high-temperature shock-tube data and predict higher rates than experimental measurements at low to intermediate temperatures, as shown in Fig. 2 (the only exception being the results of Zhu et al. [46] which underpredict the majority of experimental data at the temperatures of interest). These temperatures include the temperature sensitivity window for CO laminar flame speed to this reaction. If one assumes that the theoretical fits misrepresent the specific rate of this reaction by comparison with the (presumably) more accurate experimental data at these temperatures, one would expect CO/H_2 flame speeds to be over-predicted with the reaction models based on these rate parameters.

Indeed, as shown in Fig. 3, GRI-Mech 3.0 [47] which uses the values of Yu [44] over-predicts the experimentally-measured CO/H_2/air laminar flame speeds of McLean et al. [48].

Based upon the above considerations, we fit the entire body of experimentally measured rate constants available in literature [44, 49-54] by the method of weighted least squares to obtain a more representative correlation of the experimental measurements of this rate constant. The sum of weighted error squares,

$$\Psi = \sum_{i=1}^{N} \left(\frac{\log k_{\exp}(T_i) - \log k(T_i)}{\sigma_i} \right)^2 \qquad (1),$$

is minimized by taking the rate constant, k, as:

$$k_{23} = 10^{5.35\binom{-0.39}{+0.48}} T^{1.89\binom{+0.11}{-0.14}} \exp\left[583 \binom{+82}{-106} \Big/ T \right] \text{ cm}^3/\text{mole/s} \qquad (2).$$

In Eq. (1), $k_{\exp}$ is the rate constant measured experimentally at temperature T_i, and σ_i is the absolute error of $\log k_{\exp}$ at T_i. Equation (2) was used as the rate constant of reaction (R23) in this study. The values shown in parentheses in Eq. 2 are the 95% confidence intervals of the fitted parameters.

Figure 2 shows the comparison of this expression with literature results, including those of Lissianski et al. [54] which in the current study were recalculated based on the present thermochemical data and the rate constant of the reverse reaction of (R23) provided in the original paper [54]. The new correlation predicts specific rate constant values in close agreement with those obtained from the correlation of Yu et al. [55] (within 6% at 800-3500 K) derived by fitting their high temperature experimental measurements in a shock tube. In the temperature window of 800-2000 K, predictions from the new expression agree well (within 10%) with those of Troe [45] at 1 atm, while they are about 20% lower than the theoretical predictions of Yu [44] and Senosiain et al. [26] at 1 atm.

Very recently, and since the thesis research on this work [27], another theoretical treatment of reaction (R23) has appeared in the literature [56]. Joshi and Wang [56] have pointed out that consideration of both cis- and trans-isomeric forms of HOCO adduct as well as hindered rotation connecting the two (ignored in prior theoretical studies) leads to significant changes in the predicted thermal rate constant for reaction (R23). The resulting expression recommended by these authors is also plotted in Fig. 2. As can be seen, their result is

significantly lower at the intermediate temperatures of interest than the earlier theoretical predictions. Joshi and Wang have also indicated that "the treatment of the title reaction (R23) remains semi-empirical as more than one different model can satisfactory reproduce a wide range of data". The present empirical fit (Eq. 2) is approximately half-way between the theoretical results of Senosiain et al. [26] and the new results of Joshi and Wang [56].

3. HCO + M = H + CO + M (R24) and HCO + O_2 = HO_2 + CO (R25)

Both the unimolecular decomposition and abstraction reactions of formyl radicals are the main pathways to generate CO during the high temperature combustion of hydrocarbons. Because the H atom in HCO is very weakly bound, the dissociation reaction (R24) competes strongly with the H-abstraction reactions from HCO by H, OH, and O_2. Timonen et al. [57, 58] directly measured the rate constant of reaction (R24) and (R25) in a heated tubular reactor below 832 and 713 K, respectively. More recently, Friedrichs et al. [3] detected HCO in a shock tube for the first time by using frequency-modulated (FM) spectroscopy. Based on a reaction mechanism primarily derived from GRI-Mech 3.0 [47], the rate constant of reaction (R24) was estimated by fitting the experimental HCO profiles at 835-1230 K [3]. The work of Friedrichs et al. [3] infers that the rate of (R24) is about two times lower than the measurements of Timonen et al. [57]. DeSain et al. [4] also studied reaction (R25) at 296-673 K experimentally, and reported a temperature-independent rate constant, which is about two times lower than that of Timonen et al. [58] at 1000 K.

In a flow reactor study of $CH_2O/NO/O_2$, Glarborg et al. [59] adopted the expressions of Friedrichs et al. [3] and DeSain et al. [4] for reactions (R24) and (R25), respectively, in a revised kinetic mechanism, which predicted their flow reactor measurements reasonably well. Incorporating these expressions within the present mechanism also results in as good agreement with the flow reactor experiments of Ref. 13 as achieved using the recommendations of Timonen et al. [57, 58]. Closer inspection, however, reveals that the ratio k_{24}/k_{25} for the new correlations is almost the same as that used previously, and that the CH_2O/O_2 system predictions under flow reactor conditions are sensitive to this ratio, rather than to the absolute magnitudes of the individual specific rate constants [13]. On the other hand, premixed laminar flame speeds of hydrocarbons, particularly those of simple oxygenates such as formaldehyde and methanol, are very sensitive to the absolute rates of (R24) and (R25) (e.g. [8]). Using the recommendations of

Refs. 3 and 4 yields substantially different flame speed predictions from those obtained with the correlations of Timonen et al. [57, 58]. Attempting to compensate for these discrepancies by combinatorial modifications of other elementary rate constants degrades the quality of predictions against other experimental targets.

Figure 3 compares the experimental flame speeds of CO/H_2/air mixtures [48] with model predictions of GRI-Mech-3.0 [47] and with the predictions of a "modified" GRI-Mech-3.0 in which the rate coefficient correlations for reactions (R24) and (R25) are replaced by the recommendations of Friedrichs et al. [3] and DeSain et al. [4], respectively. The overall uncertainty of the experimental flame speeds was reported to be ± 3% [48]. Obviously, the predictions of the modified mechanism are significantly degraded in comparison to those using the original mechanism and depart substantially from the experiments, particularly at fuel rich equivalence ratios. Similar behavior was observed for the laminar flame speeds of other hydrocarbon/air mixtures, particularly those for CH_3OH/air and C_2H_5OH/air mixtures. In further demonstration of the novel method of temperature-dependent sensitivity analysis, Zhao et al. [2] showed that 1300-2000 K and 1200-1900 K are the temperature windows where hydrocarbon laminar flame speed predictions are most sensitive to reaction (R24) and (R25), respectively (Fig. 1). These temperature ranges are well above the range of conditions of both the recent measurements of Refs. 3 and 4, and the earlier measurements of Timonen et al. [57, 58]. Extrapolation of the rate constant correlations recommended in [3, 4] yield substantially lower values for the rate constants within these temperature ranges than extrapolation of those recommended in [57, 58]. As a result of these analyses, the correlations recommended previously by Timonen et al. [57] and those in Refs. 3 and 4 were not adopted in this study even though the reported rate measurements [3, 4] appear to have smaller estimated uncertainties than the previous measurements [57, 58]. Instead, we again applied a weighted least squares fitting to all experimental data available in the literature for k_{24} [3, 22, 57, 60-73], to yield a new rate correlation,

$$k_{24} = 10^{11.68\binom{-4.86}{+3.74}} T^{0.66\binom{+1.42}{-1.15}} \exp\left[-7485\binom{+2360}{-1380}\Big/T\right] \text{ cm}^3\text{/mole/s} \qquad (3).$$

Figure 4 compares this new correlation with literature data and the previous correlations. In the range of 1500-2000 K, the prediction of Eq. (3) agrees with the data correlation of Timonen et al. [57] within 30%, and is about 2~3 times higher than the correlation recommended by Friedrichs

et al. [3]. Over 500-1300 K where the rate coefficient of (R24) was measured by Friedrichs et al. [3], Timonen et al. [57], Krasnoperov et al. [72], and Hippler et al. [73] the current correlation predicts values almost equidistant from the measurements reported by Timonen et al. [57] and Friedrichs et al. [3].

It should be noted that the correlation shown in Eq. (3) was obtained by fitting low pressure limit data. Timonen et al. [57] concluded, based on resonance theory, that significant deviations from the low pressure limit would occur at (high) pressures beyond the scope of practical combustion processes and reaction (R24) may be regarded as being in the low pressure limit for most combustion applications. Recently, the pressure dependence of the rate constant of reaction (R24) has been measured by Krasnoperov et al. [72], and Hippler et al. [73] and the data show a somewhat unusual pressure fall-off behavior. Based on their measurements and an isolated resonance model with variable resonance lifetimes, Hippler et al. [73] challenged the conclusions drawn by Timonen et al. [57] and indicated that deviations from the low pressure limit may occur even below atmospheric pressure; Krasnoperov [74], however, has questioned the experimental method and analyses performed by Hippler et al. [73] when obtaining low pressure data (see refs. 74 and 75 for full details). Figure 5 plots the pressure dependent measurements of Krasnoperov et al. [72], and Hippler et al. [73] and compares them against the low pressure data of Friedrichs et al. [3] and Timonen et al. [57] as well as Eq. (3). It is clearly seen that, even though fall-off behavior is observed, the deviation from the low-pressure limit data is only significant at temperatures below 580 K; calculated values (using Eq. 3) are within a factor of 2-3 of the measured high pressure data below this temperature. At lower temperatures and in any applications related to combustion, the reaction of HCO with HO_2 will be far more important than (R24). Therefore for combustion modeling the use of a low pressure limit rate constant for reaction (R24) causes no significant differences in model predictions. Regardless of this result, more studies of the fall-off behavior of (R24) are warranted.

Because there are few specific experimental rate constant measurements at high temperatures for (R25), (e.g. see NIST kinetics database; http://kinetics.nist.gov) the recommendation of Timonen et al. [58] was retained [93]. Given the fact that the new rate expression for (R24) (Eq. 3) does not deviate considerably from the recommendation of Timonen et al. [57] over the temperature range relevant to flow reactor studies, retaining this rate coefficient does not significantly alter the k_{24}/k_{25} ratio which, as mentioned above, is important

for the CH_2O system at flow reactor conditions. More recently, Colberg and Friedrichs [76] published new measurements for the rate of reaction (R25) at both room temperature and in the temperature range of 739 – 1108 K. Implementing this newly proposed rate (k_{25} (295 K) = 3.55×10^{12}; k_{25} (739–1108 K) = 3.70×10^{13} exp(–1563/T) cm^3-mole^{-1}-s^{-1}) in the present mechanism has little impact on the quality of its predictions against targets discussed in the sections below. Under flow reactor conditions, this rate differs by no more than 20 % from the recommendation of Timonen et al. [58], assuring a reasonable k_{24}/k_{25} ratio. At higher temperatures (T > 1500 K), however, the new rate correlation yields values approximately twice those recommended in Ref. 58 and results in some differences in the modeling of laminar flame speeds (see Fig. 1). Laminar flame speed predictions are changed by approximately 10%, slightly more than typical uncertainties in modern measurements reported in the literature. On the basis of these results and considering that the new expression of Colberg and Friedrichs [76] has not been validated at higher temperatures, we continue to use the recommendation of Ref. 58 in the model reported here.

4. CH_2O Related Reactions

In addition to the modifications in specific rate constant correlations for reactions (R23), (R24), and (R25), other important reactions for the CH_2O/O_2 system were reviewed, and the rate constants were updated to those appearing in more recent publications. These reactions include,

$$CH_2O + M = H + HCO + M \quad \text{(R34)}$$

$$CH_2O + M = H_2 + CO + M \quad \text{(R35)}$$

$$CH_2O + H = HCO + H_2 \quad \text{(R36)}$$

$$CH_2O + HO_2 = HCO + H_2O_2 \quad \text{(R40)}$$

$$CH_2OH + HCO = CH_2O + CH_2O \quad \text{(R60)}$$

Formaldehyde oxidation is very sensitive to the abstraction reactions (R36) and (R40) under flow reactor conditions, and to the unimolecular decomposition reactions (R34) and (R35) in shock tube studies, as demonstrated earlier [13]. Eiteneer et al. [23] studied the ignition of CH_2O/O_2/Ar mixtures behind reflected shock waves and developed an expression for the rate constant of reaction (R40) by fitting their data and literature results. This new expression yields rates in close agreement with those used by Hochgreb and Dryer [13] at intermediate temperatures (within 7% at 1000 K), while the predicted rate constant is about two times higher

at 500 K and 2000 K. In the current study, the rate correlation for (R40) suggested by Eiteneer et al. [23] was adopted.

Irdam et al. [77] performed formaldehyde pyrolysis experiments and transition state theory calculations for reaction (R36). The recommended rate coefficient, adopted in the present study, was later found to be in excellent agreement with the direct measurements of Friedrichs et al. [78]. In a shock tube study of CH_2O thermal decomposition, Friedrichs et al. [24] measured the species time history profiles of CH_2O and HCO and conducted RRKM calculations for reactions (R34) and (R35). The authors also presented a new value for the rate constant of reaction (R60), which becomes important for mixtures with high concentrations of CH_2O. The recommendations of Friedrichs et al. [24] for reactions (R34), (R35), and (R60) were used in the current mechanism. In addition, the rate coefficient of reaction,

$$CH_2OH + HCO = CH_3OH + CO \qquad \text{(R59)}$$

which competes with reaction (R60), was modified to 1×10^{13} cm^3-mol^{-1}-s^{-1} thus keeping the branching ratio, k_{60}/k_{59}, the same as in the original mechanism [8].

Furthermore, in an effort to include in the present model the most up-to-date rate information for the systems treated in this study, the very recent measurements of the addition of OH and O_2 to formaldehyde (reactions R38 and R39, respectively) have been adopted from the studies of Vasudevan et al. [79, 80]. The recommended rate constants [79, 80] are within a factor of 2 of those suggested by Tsang and Hampson [81].

5. CH_3OH Related Reactions

As in the case of formaldehyde, the methanol oxidation system is very sensitive to fuel abstraction and decomposition reactions [8]. There are several publications on the kinetics of these reactions that have appeared after the work of Held and Dryer [8]. In GRI-Mech 3.0 [47], the decomposition reactions of methanol were investigated using RRKM theory and results were then fitted to several sets of experimental data published from 1984 to 1994. The obtained rate constants were expressed in Troe form [82] for the temperature and pressure dependence of the decomposition reactions. Koike et al. [83] have estimated the rate constant of the major decomposition reaction of methanol,

$$CH_3OH (+ M) = CH_3 + OH (+ M) \qquad \text{(R72)}$$

from shock tube experiments of CH_3OH pyrolysis at 0.4-0.82 atm and 1400-2500 K. Under these conditions, the estimated rate constant is in reasonable agreement (about 50%) with that provided in GRI-Mech 3.0. In a more recent study, Krasnoperov and Michael [84] have reported the experimental recombination rates of CH_3 and OH at conditions close to high-pressure limit that are lower than the high-pressure reverse rate of (R72) used by GRI-Mech. While detailed multi-channel simulations of this system that would attempt to reconcile these new data are clearly warranted for future studies, the GRI-Mech 3.0 [47] rate constants for methanol decomposition reactions were adopted in the current study. There are two pathways for methanol abstraction reactions due to the two distinct sites of H atoms in CH_3OH molecules. Jimenez et al. [85] experimentally derived the total rate constants of the abstraction reaction,

$$CH_3OH + OH \rightarrow \text{products}$$

at 235-360 K. The total rate constants agree within 20% with those of Bott and Cohen [86], which were used in the original mechanism [8] and retained in the present work.

Results and Discussion

The revised C_1/O_2 mechanism as described above consists of 84 reversible elementary reactions among 18 species and the thermochemical data listed in Table I and II, respectively. Reverse rate constants are computed from the forward rate constants and the equilibrium constants. The first 31 reactions listed in Table I can be used as the comprehensive kinetic model for CO combustion, and it predicts the same behavior of $CO/H_2/O_2$ systems as that found using the entire C_1 oxidation mechanism. The absence of potential C_2 sub-mechanism elements as well as CH_2 (singlet and triplet states) reactions on CO, CH_2O, and CH_3OH oxidation predictions for the targets investigated here was tested by incorporating a C_2H_X (X = 1 – 6) reaction subset primarily taken from Wang et al. [112] and comparing predictions with the original mechanism. Negligible differences were found for all of the cases studied here. For example, the compiled C_2 mechanism predicts less than 1% higher CH_3OH/air flame speeds than the present C_1 model.

The current C_1/O_2 mechanism has been compared against a wide range of experimental results, including laminar flame speeds, shock tube ignition delay data, and species profiles measured in flow reactor, shock tube, and burner-stabilized flame studies. The SENKIN code [113] was used to simulate experimental conditions in shock tubes and flow reactors assuming adiabatic systems under constant volume and constant pressure, respectively. The PREMIX code [114] was used for flame calculations. We used the standard CHEMKIN transport package [115] with Soret effects and multi-component diffusion included. To assure a fully converged flame speed prediction, a minimum of 1000 grid points was imposed in the PREMIX calculations. Tables III, IV, and V list the experiments that the current $CO/H_2/O_2$, CH_2O/O_2, and CH_3OH/O_2 mechanism has been compared against.

Representative results for these comparisons are shown in Figs. 6 – 26. The performance of each of the hierarchical sub-mechanisms involving carbon is discussed below.

1. $CO/H_2/O_2$ Mechanism Predictions

Comparisons in Figs. 6 and 7 show that the predictions of the current CO oxidation mechanism are in good agreement with the premixed laminar flame speed measurements for $CO/H_2/O_2/N_2$ mixtures at atmospheric pressure. Predictions also compare very well with shock tube ignition delay data, as demonstrated in Figs. 8 and 9. The predicted ignition delay times presented in these figures were defined as the time required for CO_2 [116] or OH [117] concentration to reach a specified value, similar to the criteria used in the experimental work. Figures 10 and 11 show the time history of major species under flow reactor conditions. Predictions using the current mechanism agree very well with all of the experimental target information.

Sensitivity analyses were performed based on the present CO oxidation mechanism for three representative cases: the laminar premixed flame speed at equivalence ratio of 5.0 [48], the mass fraction of CO in a VPFR case at 3.5 atm [118], and the ignition delay time under the shock tube conditions of Dean et al. [116]. The most sensitive reactions along with their sensitivity coefficients are shown in Fig. 12. The normalized sensitivity coefficient of a reaction is defined as $\frac{\partial \ln Y}{\partial \ln k}$, $\frac{\partial \ln s}{\partial \ln k}$, and $\frac{\partial \ln \tau}{\partial \ln k}$ for the disappearance of a species Y in a flow reactor, for laminar flame speed, and for ignition delay time, respectively, where k is the rate constant of the reaction, Y the mass fraction of a species, s the laminar flame speed, and τ the ignition delay time. In addition to those reactions within the H_2/O_2 sub-mechanism (which govern the radical pool), $CO/H_2/O_2$ combustion is most sensitive to the chain propagation reaction (R23) and to the chain termination reaction,

$$CO + O (+M) = CO_2 (+M) \qquad (R20)$$

The potential use of mixtures of hydrogen and carbon monoxide (syngas) in combined cycle gas turbine combustion at high pressures is stimulating new interest in the behavior of these sub-mechanisms at high pressures. Very recently, new experiments involving carbon monoxide and carbon monoxide-hydrogen mixtures in rapid compression machines (RCM) [119], and high pressure shock tubes [120] have begun to appear that represent targets significantly beyond the parameter ranges of previously available validation data sources. Mittal et. al [119]

used an early release of the present mechanism and reported discrepancies between simulations and their RCM ignition results and attributed these to the importance of HO_2/H_2O_2 chemistry under high pressures.

In light of these results and in order to further clarify the relative importance of specific elementary reactions on the chemical kinetic ignition of $CO/H_2/O_2/N_2$ mixtures at high pressure, we applied a computational singular perturbation (CSP) analysis approach we have recently demonstrated [121] as well as elementary sensitivity analyses. Unlike prior implementations of CSP methodology, the present formulation includes temperature as one of the state variables so that factors controlling ignition can be unambiguously determined. As developed [121], the methodology is applicable to the analysis of systems that can be modeled as constant volume processes (e.g. shock tubes). However, given recent experimental RCM data [119], the initially developed technique was further modified to accommodate systems with volume changes as a function of time. Incorporating a volume change as a function of time is the method used by Sung and co-workers [119, 122] to account for non adiabatic compression in RCM experiments. The importance of individual reactions within the CSP methodology used here is described in terms of participation index (see [121] for details).

Figure 13 shows the relative importance (expressed in terms of a participation index, see [121]) of reactions most significantly affecting the heat release rate (reaction temperature) under the RCM conditions of Mittal et. al. [119] at specific reaction times after the end of the compression stroke. What is clearly apparent is that the reactions $CO+O+M = CO_2+M$ (R20) and $CO+HO_2 = CO_2+OH$ (R22) are only important during the chemical induction period. After chemical ignition occurs, these reactions no longer contribute significantly to the rate of heat release. On the other hand reactions such as $HO_2+OH = H_2O+O_2$ (R13), $HO_2+H = 2OH$ (R11), $H_2+OH = H_2O+H$ (R3), and $H_2+O = H+OH$ (R2) are significant in describing the heat release rate. A sensitivity analysis which separately considers the sensitivity of the extent of reaction to the various reactions prior to and after ignition occurs confirms the above findings for the importance of reactions (R20) and (R22). This indicates that HO_2 and H_2O_2 chemistry becomes important under the RCM conditions considered here, consistent with the conclusions of Mittal et al. [119], as these intermediate species rapidly build up during the induction period, more so than H or OH. Once ignition occurs, OH reactions become more dominant as evidenced by Fig.

13 (e.g. CO+OH (R23) becomes one of the primary reactions at ignition as opposed to CO+HO_2 (R22) during the induction period).

Sivaramakrishnan et al. [120] have also studied H_2/CO oxidation in a shock tube at much higher pressures (exceeding 200 atm) and somewhat higher temperatures (> 1,100 K) for highly dilute H_2/CO/O_2/Ar mixtures. CSP analysis was applied to a representative case, as shown in Fig. 14. Figure 14b shows that under these high-pressure and high-temperature conditions, and for the highly dilute mixtures studied, there is not a well defined ignition delay in the pressure history. There is, however, an obvious induction period. Similar to the RCM analysis above, CSP was performed during this induction period and the results are shown in Fig. 14c. The identified reactions participating in the evolution of the system are essentially different from those shown in Fig. 13 for the RCM case. It is important to note from Fig. 14c that reaction (R22), even though present in the initial evolution stages, quickly loses importance, more so than in the case shown in Fig. 13 with reaction (R13) becoming much more dominant as the system evolves. Therefore, the present CSP analysis shows that for highly dilute mixtures at sufficiently high pressures and temperatures, reaction (R13) needs to be considered in order to properly describe the H_2/CO kinetic system whereas under more moderate pressures and reaction temperatures (R22) needs to be taken into account in predictions where chemical induction processes are to be expected to be important. It is further noted that a similar analysis under the pressure/temperature conditions shown Fig. 14 using higher reactant concentrations (as those shown in Fig. 13) identifies the same relative importance of reactions shown in Fig. 13; dilution, thus, plays a role in the relative importance of specific reactions for these different investigations.

Figures 13 and 14 show that reactions (R13) and (R22) appear to have, separately, a distinct impact in these systems. At pressures and temperatures similar to those in the work of Sivaramakrishnan et al. [120], the current C_1 model predictions are unchanged by a variations of as much as a factor of five in the rate of reaction (R22). In contrast, changes in reaction (R13) yield little effect in RCM modeling. Reaction (R22) has been shown to have a strong sensitivity in RCM studies [119], and as shown here it is expected to have little effect on any observable other than the chemical induction time. Reactions (R13) and (R22) are the subject of new studies that have recently appeared in the literature [123, 124] and which suggest [124] a much lower rate for (R22) than that presently employed. Implementing the recommendations for (R13) [123] and (R22) [124] in the present model yields very good agreement with data

presented in those studies. Large uncertainties still exist, however, in both reactions (R13) and (R22) (e.g. see the work of Kappel et al. [125] for the highly nonlinear behavior of R13). Therefore, we acknowledge that further insights into elementary HO_2/H_2O_2 kinetics (and, especially, investigations of the rates of R13 and R22) are warranted to properly model experimental data in these high pressure venues [119, 120, 123, 124] using the present mechanism. We have retained the current rate expressions for these reactions since the present mechanism performs satisfactorily under a wide pressure and temperature range for a variety of fuel systems. Finally, it should be noted that the very high participation index of $H+O_2+M = HO_2+M$ (R9) (see Figs. 13 and 14) results in a significant influence of third body effects on both induction and post induction kinetics.

2. CH_2O/O_2 Mechanism

Comparisons of the current CH_2O/O_2 mechanism with representative formaldehyde experiments are shown in Figs. 15 to 20. Formaldehyde readily polymerizes at ambient conditions. In the experiments, pure formaldehyde was generated by heating either paraformaldehyde [22] or trioxane [23] to more than 100°C. Figure 15 shows the comparison of predictions with formaldehyde pyrolysis and oxidation measurements in a shock tube [23], including the time when CO concentration reaches 0.25 and 0.5 times its maximum value (Figs. 15a and 15b), and the profiles of CO concentration normalized by its maximum (Figs. 15c and 15d). The agreement of the current model predictions and the experimental data are excellent. Figure 16 shows the time history of CH_2O concentration under the shock tube conditions of Hidaka et al. [22]. Buxton and Simpson [126] measured the production rates of CO during high temperature formaldehyde pyrolysis experiments in a shock tube. The present CH_2O/O_2 mechanism reproduces the production rates very well as illustrated in Fig. 17.

To the best of our knowledge, the only published experimental study that reported profile data for formaldehyde flames is the low pressure work by Vandooren et al. [127], who investigated the structure of a lean CH_2O/O_2 flame using molecular beam sampling coupled with mass spectrometric analysis. Unfortunately, experimental uncertainties are quite large. For example, the error limits in HCO and HO_2 concentrations were reported as ±25% [127], and the carbon and hydrogen balances from the experimental profiles disagree with the quoted initial inputs by ±10% and ±20%, respectively [13]. The experimental flame temperature profile was

used as input in the present PREMIX calculations. Species profiles predicted by the current updated CH_2O mechanism are in reasonable agreement with the experimental measurements, as shown in Fig. 18. Additional experimental flame studies would be useful for mechanism verification and/or modification.

Predictions using the current mechanism were also compared with the atmospheric pressure flow reactor studies from Ref. 13. As shown in Fig. 19, the predictions are in excellent agreement with the measured profiles of stable species concentrations. The comparison in Fig. 20 demonstrates that the present mechanism reproduces the new VPFR experimental measurements reported here very well. Tabulation of the initial conditions and results for the measurements shown in Fig. 20 are supplied as a supplemental file.

Figure 21 illustrates the most sensitive reactions for formaldehyde oxidation in a flow reactor [13] and for formaldehyde pyrolysis under the shock tube conditions of Hidaka et al. [22]. For both cases, the sensitivity coefficient of a reaction is defined as $\frac{\partial \ln Y}{\partial \ln k}$, where k is the rate constant of the reaction, and Y is the mass fraction of CH_2O. The calculation results are reported for conditions when 50% of the initial CH_2O concentration has been consumed under constant pressure and constant volume assumption for the flow reactor and shock tube cases, respectively. Formaldehyde oxidation in the flow reactor is very sensitive to the abstraction reaction with HO_2, and to the two competitive HCO reactions (R24) and (R25). The sensitivity coefficients of these two reactions are almost equal but of opposite sign. Consequently, CH_2O oxidation in the flow reactor is not sensitive to the absolute rate constant of either reaction but rather to the ratio k_{24}/k_{25}, as explained above. Formaldehyde pyrolysis is very sensitive to the fuel decomposition reactions (R34) and (R35) and to the abstraction reaction (R36) where the H atom mainly comes from the HCO dissociation, i.e. reaction (R24). A majority of HCO is generated from reaction (R36). Species flux analysis reveals that the formaldehyde pyrolysis can be represented by the following five reactions,

$$HCO + M = H + CO + M \qquad \text{(R24)}$$

$$HCO + H = H_2 + CO \qquad \text{(R26)}$$

$$CH_2O + M = H + HCO + M \qquad \text{(R34)}$$

$$CH_2O + M = H_2 + CO + M \qquad \text{(R35)}$$

$$CH_2O + H = HCO + H_2 \qquad \text{(R36)}$$

3. *CH_3OH/O_2 Mechanism*

Predictions using the present oxidation mechanism have been compared with the experimental targets utilized in the developing the mechanism of Held and Dryer [8]. The model performance over a wide array of experimental conditions was found to be better than that of the original mechanism, especially for ignition delay and premixed flame cases. Representative comparisons are shown in Figs. 22 to 25.

Comparisons in Figs. 22 and 23 demonstrate that the predictions are in good agreement with the species time history measurements in flow reactors [29, 128, 129]. Predictions also compare well with shock tube ignition delay data, as shown in Fig. 24. In the shock tube study of Bowman [130], the ignition delay time, τ, was approximated by the time at which the product of CO and O concentrations reached its maximum. The ignition delay time calculated using the original methanol mechanism, which is systematically shorter than the experimental observations especially at low temperatures, is also presented in Fig. 24. Prediction comparisons with laminar premixed flame speeds at three different initial temperatures also demonstrate good agreement with experimental data [131] and noticeable improvement over comparisons generated using the original mechanism (Fig. 25).

Sensitivity analysis was performed using the present CH_3OH/O_2 mechanism for three representative situations: the mass fraction time history of CH_3OH in a VPFR case at 2.5 atm [29], the ignition delay time under shock tube conditions of Bowman [130], and the laminar flame speed of CH_3OH/air mixture at ϕ = 1.1 [131]. The most sensitive reactions found are shown in Fig. 26 along with their sensitivity coefficients. As can be seen, HO_2 and H_2O_2 have critical influence on the overall reaction rate under flow reactor conditions. The fuel concentration is most sensitive to the abstraction reaction with HO_2,

$$CH_3OH + HO_2 = CH_2OH + H_2O_2 \qquad \text{(R82)}$$

although this reaction does not significantly contribute directly to the fuel destruction. Hydrogen peroxide (H_2O_2), is mainly formed via reaction (R82) and

$$2HO_2 = H_2O_2 + O_2 \qquad \text{(R14)}$$

Once formed, hydrogen peroxide primarily undergoes thermal decomposition,

$$H_2O_2 (+M) = 2OH \qquad \text{(R15)}$$

accounting for more than 90% of the total OH production. Flux analysis shows that more than 70% of the fuel is consumed by abstraction reactions with OH,

$$CH_3OH + OH = CH_3O + H_2O \quad \text{(R78)}$$

$$CH_3OH + OH = CH_2OH + H_2O \quad \text{(R79)}$$

to which the CH_3OH/O_2 system also exhibits large sensitivity. In addition to the fuel abstraction reactions with HO_2, OH, and H, the ignition delay time is also very sensitive to the fuel dissociation reaction (R72). For the laminar premixed flame case, H atom has a critical influence on the flame speed because H atom plays an important role in radical pool buildup and has large diffusivity. As can be seen from Fig. 26, the flame speed is mainly sensitive to the chain branching reaction,

$$H + O_2 = O + OH \quad \text{(R1)}$$

and to the formyl radical decomposition reaction,

$$HCO + M = H + CO + M \quad \text{(R24)}$$

which was found through reaction flux analysis to be the main source of H atoms in the system [8], along with

$$CO + OH = CO_2 + H. \quad \text{(R23)}$$

Conclusions

The detailed CH_3OH oxidation mechanism of Held and Dryer [8] has been updated using recently published rate constants and thermochemical data for OH, HO_2, and CH_2OH to yield a new, comprehensive C_1 kinetic mechanism. The mechanism was developed in a hierarchical manner, which included substantial validation of sub-mechanism components through comparisons of predictions against experiments involving H_2, CO, and CH_2O as the initial fuel. Modifications to rate correlations for reactions (R23) and (R24), which are responsible for the formation of CO_2 and CO, were extensively investigated, and new rate correlations for reactions (R23) and (R24) were developed based upon weighted least square fits of available experimental measurements. The new correlations significantly improve reproductions of experimental results over temperature ranges of most significance in modeling premixed laminar flame speeds.

Predictions using the present C_1 mechanism were compared against a wide range of experimental conditions (300-3000 K, 0.15-9.6 atm, ϕ = 0.4-6.1 for CO oxidation; 300-2150 K, 0.03-12.0 atm, ϕ = 0.005 ~ pyrolysis for CH_2O; 300-2200 K, 1.0-20 atm, ϕ = 0.05-6.0 for

CH_3OH oxidation) found in laminar premixed flames, shock tubes, and flow reactors for CO, CH_2O, and CH_3OH combustion. Very good agreement of model predictions with the experimental measurements demonstrates that the updated C_1 mechanism is a comprehensive model for CO, CH_2O, and CH_3OH combustion. The current mechanism in an electronic form compatible with CHEMKIN is provided here as a supplemental file.

Acknowledgments

This work was supported by the Chemical Sciences, Geosciences and Biosciences Division, Office of Basic Energy Sciences, Office of Science, U.S. Department of Energy under Grant No. DE-FG02-86ER13503. The authors thank Mr. Paul Michniewicz for his assistance in performing the VPFR experiments. We also wish to thank Prof. C-J. Sung for an advance copy of he and his co-authors' manuscript [119] prior to publication.

Bibliography

1. Li, J.; Zhao. Z.; Kazakov, A.; Dryer, F.L. Int. J. Chem. Kinet. 2004, 36, 565.
2. Zhao, Z.; Li, J.; Kazakov, A.; Dryer, F.L. Int. J. Chem. Kinet. 2005, 37. 282.
3. Friedrichs, G.; Herbon, J.T.; Davidson, D.F.; Hanson, R.K. Phys. Chem. Chem. Phys. 2002, 4, 5778.
4. DeSain, J.D.; Jusinski, L.E.; Ho, A.D.;Taatjes, C.A. Chem. Phys. Lett. 2001, 347, 79.
5. Westbrook, C.K.; Dryer, F.L. Proc. Combust. Inst. 1981, 18, 749.
6. Westbrook, C.K; Dryer, F.L. Prog. Ener. Combust. Sci. 1984, 10, 1.
7. Glassman, I. Combustion; 3rd Edition, Academic Press, Inc. 1996.
8. Held, T.J.; Dryer, F.L. Int. J. Chem. Kinet. 1998, 30, 805.
9. Dryer, F.L.; Chaos, M.; Zhao, Z.; Stein, J.N.; Alpert, J.Y.; Homer, C. J. Combust. Sci. Tech. 2006 (in press).
10. Astbury, G.R.; Hawksworth, S.J. Proceedings of the International Conference on Hydrogen Safety, Pisa, Italy, 2005; also in Int. J. Hydrogen Energ. 2006 (in press).
11. Yetter, R.A.; Rabitz, H.; Dryer, F.L. Combust. Sci. Tech. 1991, 79, 129.
12. Yetter, R.A.; Dryer, F.L.; Rabitz, H. Combust. Sci. Tech. 1991, 79, 97
13. Hochgreb, S.; Dryer, F.L. Combust. Flame 1992, 91, 257.
14. Kim, T.J.; Yetter, R.A.; Dryer, F.L. Proc. Combust. Inst. 1994, 25, 759.
15. Norton, T.S.; Dryer, F.L. Int. J. Chem. Kinet. 1990, 22, 219.
16. Held, T.J.; Dryer, F.L. Proc. Combust. Inst. 1994, 25, 901.

17. Mueller, M.A. Ph.D. Thesis; Department of Mechanical and Aerospace Engineering, Princeton University, Princeton, NJ, 2000.
18. Mueller, M.A.; Yetter, R.A.; Dryer, F.L. Int. J. Chem. Kinet. 1999, 31, 113.
19. Mueller, M.A.; Yetter, R.A.; Dryer, F.L. Proc. Combust. Inst. 1998, 27, 177.
20. Mueller, M.A.; Kim, T.J.; Yetter, R.A.; Dryer, F.L. Int. J. Chem. Kinet. 1999, 31, 705.
21. Mueller, M.A.; Yetter, R.A.; Dryer, F.L. Int. J. Chem. Kinet. 2000, 32, 317.
22. Hidaka, Y.; Taniguchi, T.; Tanaka, H.; Kamesawa, T.; Inami, K.; Kawano, H. Combust. Flame 1993, 92, 365.
23. Eiteneer, B.; Yu, C.L.; Goldenberg, M.; Frenklach, M. J. Phys. Chem. A 1998, 102, 5196.
24. Friedrichs, G.; Davidson, D.F.; Hanson, R.K. Int. J. Chem. Kinet. 2004, 36, 157.
25. Huang, Y.; Sung, C.J.; Eng, J.A. Combust. Flame 2004, 139, 239.
26. Senosiain, J.P.; Musgrave, C.B.; Golden, D.M. Int. J. Chem. Kinet. 2003, 35, 464.
27. Li, J. Ph.D. Thesis; Department of Mechanical and Aerospace Engineering, Princeton University, Princeton, NJ, 2004.
28. Scire Jr., J..J. Ph.D. Thesis; Department of Mechanical and Aerospace Engineering, Princeton University, Princeton , NJ, 2002.
29. Held, T.J. Ph.D. Thesis; Department of Mechanical and Aerospace Engineering, Princeton University, Princeton, NJ, 1993.
30. Hochgreb, S.; Dryer, F.L. J. Phys. Chem. 1992, 96, 295.
31. Budavari, S.; O'Neil, M.J.; Smith, A.; Heckelman, P.E.; Kinneary, J.F. The Merck Index*;* Twelfth Edition, Merck Research Laboratories, 1996.
32. Fischer S.L.; Dryer, F.L.; Curran, H.J. Int. J. Chem. Kinet. 2000, 32, 713.
33. Held, T.J. Personal communication, 2004.
34. Ruscic, B.; Wagner, A.F.; Harding, L.B.; Asher, R.L.; Feller, D.; Dixon, D.A.; Peterson, K.A.; Song, Y.; Qian, X.; Ng, C.; Liu, J.; Chen, W.; Schwenke, D.W. J. Phys. Chem. A 2002, 106, 2727.
35. Herbon, J.T.; Hanson, R.K.; Golden, D.M.; Bowman, C.T. Proc. Combust. Inst. 2002, 29, 1201.
36. Hills, A.J.; Howard, C.J. J. Chem. Phys. 1984, 81, 4458.
37. Ruscic, B.; Pinzon, R.E.; Morton, M.L.; Srinivasan, N.K.; Su, M.-C.; Sutherland, J.W.; Michael, J.V. J. Phys. Chem. A, in press.

38. Johnson, R.D.; Hudgens, J.W. J. Phys. Chem. 1996, 100, 19874.
39. Ruscic, B.; Boggs, J.E.; Burcat, A.; Csaszar, A.G.; Demaison, J.; Janoschek, R.; Martin, J.M.L.; Morton, M.L.; Rossi, M.J.; Stanton, J.F.; Szalay, P.G.; Westmoreland, P.R.; Zabel, F.; Berces, T. J. Phys. Chem. Ref. Data 2005, 34, 573.
40. Gordon, S.; McBride, B.J., NASA SP-273, 1971.
41. Dryer, F.L. Ph.D. Thesis; Department of Mechanical and Aerospace Engineering, Princeton University, Princeton, NJ, 1972.
42. Warnatz, J., In "Combustion Chemistry", Gardiner, W.C., Jr., Ed., Springer-Verlag, New York, NY, 1984.
43. Miller, J.A.; Kee, R.J.; Westbrook, C.K. Annu. Rev. Phys. Chem. 1990, 41, 345.
44. Yu, C.L. Ph.D. thesis; Department of Materials Science and Engineering, Pennsylvania State University, PA, 1996.
45. Troe, J. Proc. Combust. Inst., 1998, 27, 167.
46. Zhu, R.S.; Diau, E.G.W.; Lin, M.C.; Mebel, A.M. J. Phys. Chem A 2001, 105, 11249.
47. Smith, G.P.; Golden, D.M.; Frenklach, M.; Moriarty, N.W.; Eiteneer, B.; Goldenberg, M.; Bowman, C.T.; Hanson, R.K.; Song, S.; Gardiner, Jr., W.C.; Lissianski, V.V.; Qin, Z. (1999). http://www.me.berkeley.edu/gri_mech/.
48. McLean, I.C.; Smith, D.B.; Taylor, S.C. Proc. Combust. Inst. 1994, 25, 749.
49. Ravishankara, A.R.; Thompson, R.L. Chem. Phys. Lett. 1983, 99, 377.
50. Wooldridge, M.S.; Hanson, R.K.; Bowman, C.T. Proc. Combust. Inst. 1994, 25, 741.
51. Wooldridge, M.S.; Hanson, R.K.; Bowman, C.T. Int. J. Chem. Kinet. 1996, 28, 361.
52. Westenberg, A.A.; deHaas, N. J. Chem. Phys. 1973, 58, 4061.
53. Vandooren, J.; Peeters, J.; Van Tiggelen, P.J. Proc. Combust. Inst. 1975, 15, 745.
54. Lissianski, V.; Yang, H.; Qin, Z.; Mueller, M.R.; Shin, K.S.; Gardiner Jr., W.C. Chem. Phys. Lett. 1995, 240, 57.
55. Yu, C.L.; Wang, C.; Frenklach, M. Eastern States Section of the Combustion Institute Technical Meeting, Ithaca, NY, 1991.
56. Joshi, A.V.; Wang, H. Int. J. Chem. Kinet. 2006, 38, 57.
57. Timonen, R.S.; Ratajczak, E.; Gutman, D. J. Phys. Chem. 1987, 91, 5325.
58. Timonen, R.S.; Ratajczak, E.; Gutman, D. J. Phys. Chem. 1988, 92, 651.

59. Glarborg, P.; Alzueta, M.U.; Kjargaard, K.; Dam-Johansen, K. Combust. Flame 2003, 132, 629.
60. Pearson, G.S. J. Phys. Chem. 1963, 67, 1686.
61. Schecker, H.G.; Jost, W. Ber. Bunsen-Ges. Phys. Chem. 1969, 73, 521.
62. Browne, W.G.; Porter, R.P.; Verlin, J.D.; Clark, A.H. Proc. Combust. Inst. 1969, 12, 1035.
63. Bowman, C.T. Combust. Sci. Technol. 1970, 2, 161.
64. Ahumada, J.J.; Michael, J.V.; Osborne, D.T. J. Chem. Phys.1972, 57, 3736.
65. Baldwin, R.R.; Jackson, D.; Melvin, A.; Rossiter, B.N. Int. J. Chem. Kinet. 1972, 4, 277.
66. Wang, H.Y.; Eyre, J.A.; Dorfman, L.M. J. Chem. Phys. 1973, 59, 5199.
67. Westbrook, C.K.; Creighton, J.; Lund, C.; Dryer, F.L. J. Phys. Chem. 1977, 81, 2542.
68. Campbell, I.M.; Handy, B.J. J. Chem. Soc. Faraday Trans. 2 1978, 74, 316.
69. Hochanadel, C.J.; Sworski, T.J.; Ogren, P.J. J. Phys. Chem. 1980, 84, 231.
70. Cherian, M.A.; Rhodes, P.; Simpson, R.J.; Dixon-Lewis, G. Proc. Combust. Inst., 1981, 18, 385.
71. Cribb, P.H.; Dove, J.E.; Yamazaki, S. Combust. Flame, 1992, 88, 169.
72. Krasnoperov, L.N.; Chesnokov, E.N.; Stark H.; Ravishankara A.R. J. Phys. Chem A 2004, 108, 11526.
73. Hippler, H.; Kastreva, N.; Striebel, F. Phys. Chem. Chem. Phys., 2004, 6, 3383.
74. Krasnoperov, L.N. Phys. Chem. Chem. Phys., 2005, 7, 2074.
75. Hippler, H.; Kastreva, N.; Striebel, F. Phys. Chem. Chem. Phys., 2005, 7, 2077.
76. Colberg, M.; Friedrichs, G. J. Phys. Chem. A 2006, 110, 160.
77. Irdam, E.A.; Kiefer, J.H.; Harding, L.B.; Wagner, A.F. Int. J. Chem. Kinet. 1993, 25, 285.
78. Friedrichs, G.; Davidson, D.F.; Hanson, R.K. Int. J. Chem. Kinet. 2002, 34, 374.
79. Vasudevan, V.; Davidson, D.F.; Hanson, R.K. Int. J. Chem. Kinet. 2005, 37, 98.
80. Vasudevan, V.; Davidson, D.F.; Hanson, R.K.; Bowman, C.T.; Golden, D.M. Proc. Combust. Inst. 31, in press.
81. Tsang, W.; Hampson, R.F. J. Phys. Chem. Ref. Data 1986, 15, 1087.
82. Gilbert, R.G.; Luther, K.; Troe, J. Ber. Bunsenges. Phys. Chem. 1983, 87, 169.
83. Koike, T; Kudo, M.; Maeda, I.; Yamada, H. Int. J. Chem. Kinet. 2000, 32, 1.
84. Krasnoperov, L.N.; Michael, J.V. J. Phys. Chem. A 2004, 108, 8317.
85. Jimenez, E.; Gilles, M.K.; Ravishankara, A.R. J. Photochem. Photobiol. A 2003, 157, 237.

86. Bott, J.F.; Cohen, N. Int. J. Chem. Kinet. 1991, 23, 1075.
87. Hessler, J.P. J. Phys. Chem. A 1998, 102, 4517.
88. Sutherland, J.W.; Michael, J.V.; Pirraglia, A.N.; Nesbitt, F.L.; Klemm R.B. Proc. Combust. Inst. 1986, 21, 929.
89. Michael, J.V.; Sutherland, J.W. J. Phys. Chem. 1988, 92, 3853.
90. Sutherland, J.W.; Patterson, P.M.; Klemm, R.B. Proc. Combust. Inst. 1990, 23, 51.
91. Cobos, C.J.; Hippler, H.; Troe, J. J. Phys. Chem. 1985, 89, 342.
92. Hippler, H.; Troe, J.; Willner, J., J. Chem. Phys. 1990, 93, 1755.
93. Brouwer, L.; Cobos, C.J.; Troe, J.; Dubal, H.R.; Crim, F.F. J. Chem. Phys. 1985, 86, 6171.
94. Michael, J.V.; Su, M.C.; Sutherland, J.W.; Carroll, J.J.; Wagner, A.F. J. Phys. Chem. A 2002, 106, 5297.
95. Baulch, D.L; Cobos, C.J.; Cox, R.A.; Esser, C.; Frank, P.; Just, Th.; Kerr, J.A.; Pilling, M.J.; Troe, J.; Walker, R.W.; Warnatz, J. J. Phys. Chem. Ref. Data 1992, 21, 411.
96. Hippler, H.; Troe, J. Chem. Phys. Lett. 1992, 192, 333.
97. Troe, J. J. Phys. Chem. 1975, 83, 114.
98. Westmoreland, P.R.; Howard, J.B.; Longwell, J.P.; Dean, A. M. AIChE J. 1986, 32, 1971.
99. Slagle, I.R.; Sarzynski, D.; Gutman, D. J. Phys. Chem. 1987, 91, 4375.
100. Scire, J.J.; Yetter, R.A.; Dryer, F.L. Int. J. Chem. Kinet. 2001, 33, 75.
101. Frenklach, M.; Wang, H.; Goldenberg, M.; Smith, G. P.; Golden, D. M.; Bowman, C. T.; Hanson, R. K.; Gardiner, W. C.; Lissianski, V. GRI Technical Report No. GRI-95/0058, 1995.
102. Schatz, G.C.; Wagner, A.F.; Dunning, T.H. J. Phys. Chem. 1984, 88, 221.
103. Klemm, R.B.; Tanzawa, T.; Skolnik, E.G.; Michael, J.V. Proc. Combust. Inst. 1981, 18, 785.
104. Felder, W.; Madronich, S. Combust. Sci. Tech. 1986, 50, 135.
105. Tsang, W. J. Phys. Chem. Ref. Data 1987, 16, 471.
106. Grotheer, H.H.; Riekert, G.; Walter, D.; Just, Th. J. Phys. Chem. 1988, 92, 4028.
107. Page, M.; Lin, M.C.; He, Y.; Choudhury, T.K. J. Phys. Chem. 1989, 93, 4404.
108. Wantuck, P.J.; Oldenborg, R.C.; Baughcum, S.L.; Winn, K.R. J. Phys. Chem. 1987, 91, 4653.
109. Cathonnet M.; Boettner, J.C.; James, H. J. Chim. Phys. 1982, 79, 475.

110. Kee, R.J.; Rupley, F.M.; Miller, J.A. Technical Report SAND87-8215B, Sandia National Laboratories, 1987.

111. Burcat, A., Technion Aerospace Engineering, Report #867, 2001.

112. Wang, H.; Laskin, A.; Djurisic, Z.M.; Law, C.K.; Davis, S.G.; Zhu, D.L. Eastern States Section of the Combustion Institute Fall Technical Meeting, 1999, 129, Raleigh, NC

113. Lutz, A.E.; Kee, R.J.; Miller, J.A. Technical Report SAND87-8248, Sandia National Laboratories, 1987.

114. Kee, R.J.; Grcar, J.F.; Smooke, M.D.; Miller, J.A., Technical Report SAND85-8240, Sandia National Laboratories, 1985.

115. Kee, R.J.; Dixon-Lewis, G.; Warnatz, J.; Coltrin, M.E.; Miller, J.A. Technical Report SAND86-8246, Sandia National Laboratories, 1986.

116. Dean, A.M.; Steiner, D.C.; Wang, E.E. Combust. Flame 1978, 32, 73.

117. Gardiner Jr., W.C.; McFarland, M.; Morinaga, K.; Takeyama, T.; Walker, B.F. J. Phys. Chem. 1971, 75, 1504.

118. Mueller, M.A.; Yetter, R.A.; Dryer, F.L. Int. J. Chem. Kinet. 1999, 31, 705.

119. Mittal G.; Sung, C-J.; Yetter R.A. Int. J. Chem. Kinet. 2006, 38, 516.

120. Sivaramakrishnan, R.; Comandini,A.; Tranter, R.S.; Brezinsky, K. 6th International Conference on Chemical Kinetics, Gaithersburg, MD. July 25-29, 2005.

121. Kazakov, A.; Chaos, M.; Zhao, Z.; Dryer, F.L. J. Phys. Chem. A. 2006, 110, 7003.

122. Mittal G.; Sung, C-J. Combust. Sci. Tech., in press.

123. Sivaramakrishnan, R.; Comandini,A.; Tranter, R.S.; Brezinsky, K; Davis, S.G.; Wang, H. Proc. Combust. Inst. 31, in press.

124. Mittal, G.; Sung, C.J.; Fairweather, M.; Tomlin, A.S.; Griffiths, J.F.; Hughes, K.J. Proc. Combust. Inst. 31, in press.

125. Kappel, C-H; Luther, K; Troe, J. Phys. Chem. Chem. Phys. 2002, 4, 4392.

126. Buxton, J.P.; and Simpson, C.J.S.M. Chem. Phys. Lett. 1986, 128, 577.

127. Vandooren, J.; Oldenhove de Guertechin, L.; Van Tiggelen, P.J. Combust. Flame 1986, 64, 127.

128. Aronowitz, D.; Santoro, R.J.; Dryer, F.L.; Glassman, I. Proc. Combust. Inst. 1979, 17, 633.

129. Norton, T.S.; Dryer, F.L. Combust. Sci. Tech. 1989, 63, 107.

130. Bowman, C.T. Combust. Flame 1975, 25, 343.
131. Egolfopoulos, F.N.; Du, D.X.; Law, C.K. Combust. Sci. Tech. 1992, 83, 33.
132. Dean, A.M.; Johnson, R.L.; Steiner, D.C. Combust. Flame 1980, 37, 41.

Table I - Detailed C_1/O_2 Reaction Mechanism. Units are cm^3-mol-sec-cal-K; $k = A\ T^n \exp(-E_a/RT)$.

#	Reaction		A	n	E_a	Reference
H_2/O_2 reactions						
1	$H+O_2 = O+OH$		3.55E+15	-0.40	1.66E+04	[87]
2	$O+H_2 = H+OH$		5.08E+04	2.70	6.29E+03	[88]
3	$H_2+OH = H_2O+H$		2.16E+08	1.50	3.43E+03	[89]
4	$O+H_2O = OH+OH$		2.97E+06	2.00	1.34E+04	[90]
5	$H_2+M = H+H+M$		4.58E+19	-1.40	1.04E+05	[81]
	$\varepsilon_{H2} = 2.5$, $\varepsilon_{H2O} = 12.0$, $\varepsilon_{CO} = 1.9$, $\varepsilon_{CO2} = 3.8$, $\varepsilon_{Ar} = 0.0$, $\varepsilon_{He} = 0.0$					
	$H_2+Ar = H+H+Ar$		5.84E+18	-1.10	1.04E+05	[81]
	$H_2+He = H+H+He$		5.84E+18	-1.10	1.04E+05	[81]
6	$O+O+M = O_2+M$		6.16E+15	-0.50	0.00	[81]
	$\varepsilon_{H2} = 2.5$, $\varepsilon_{H2O} = 12.0$, $\varepsilon_{CO} = 1.9$, $\varepsilon_{CO2} = 3.8$, $\varepsilon_{Ar} = 0.0$, $\varepsilon_{He} = 0.0$					
	$O+O+Ar = O_2+Ar$		1.89E+13	0.00	-1.79E+03	[81]
	$O+O+He = O_2+He$		1.89E+13	0.00	-1.79E+03	[81]
7	$O+H+M = OH+M$		4.71E+18	-1.00	0.00	[81]
	$\varepsilon_{H2} = 2.5$, $\varepsilon_{H2O} = 12.0$, $\varepsilon_{CO} = 1.9$, $\varepsilon_{CO2} = 3.8$, $\varepsilon_{Ar} = 0.75$, $\varepsilon_{He} = 0.75$					
8	$H+OH+M = H_2O+M$		3.80E+22	-2.00	0.00	[1]
	$\varepsilon_{H2} = 2.5$, $\varepsilon_{H2O} = 12.0$, $\varepsilon_{CO} = 1.9$, $\varepsilon_{CO2} = 3.8$, $\varepsilon_{Ar} = 0.38$, $\varepsilon_{He} = 0.38$					
9	$H+O_2 (+M) = HO_2 (+M)$	k_∞	1.48E+12	0.60	0.00	[91]
		k_0	6.37E+20	-1.72	5.25E+02	[71], M = N_2
	$\alpha = 0.8$, T*** = 1.0E-30, T* = 1.0E+30					
	$\varepsilon_{H2} = 2.0$, $\varepsilon_{H2O} = 11.0$, $\varepsilon_{CO} = 1.9$, $\varepsilon_{CO2} = 3.8$, $\varepsilon_{O2} = 0.78$					
	$H+O_2 (+M) = HO_2 (+M)$	k_∞	1.48E+12	0.60	0.00	[91]
		k_0	9.04E+19	-1.50	4.92E+02	[94], M = Ar or He
	$\alpha = 0.5$, T*** = 1.0E-30, T* = 1.0E+30					
	$\varepsilon_{H2} = 3.0$, $\varepsilon_{H2O} = 16.0$, $\varepsilon_{CO} = 2.7$, $\varepsilon_{CO2} = 5.4$, $\varepsilon_{O2} = 1.1$, $\varepsilon_{He} = 1.2$					
10	$HO_2+H = H_2+O_2$		1.66E+13	0.00	8.23E+02	[18]
11	$HO_2+H = OH+OH$		7.08E+13	0.00	2.95E+02	[18]
12	$HO_2+O = O_2+OH$		3.25E+13	0.00	0.00	[95]
13	$HO_2+OH = H_2O+O_2$		2.89E+13	0.00	-4.97E+02	[95]
14	$HO_2+HO_2 = H_2O_2+O_2$	Duplicate	4.20E+14	0.00	1.20E+04	[92]
	$HO_2+HO_2 = H_2O_2+O_2$	Duplicate	1.30E+11	0.00	-1.63E+03	
15	$H_2O_2 (+M) = OH+OH (+M)$	k_∞	2.95E+14	0.00	4.84E+04	[93]
		k_0	1.20E+17	0.00	4.55E+04	[42]
	$\alpha = 0.5$, T*** = 1.0E-30, T* = 1.0E+30					
	$\varepsilon_{H2} = 2.5$, $\varepsilon_{H2O} = 12.0$, $\varepsilon_{CO} = 1.9$, $\varepsilon_{CO2} = 3.8$, $\varepsilon_{Ar} = 0.64$, $\varepsilon_{He} = 0.64$					
16	$H_2O_2+H = H_2O+OH$		2.41E+13	0.00	3.97E+03	[81]
17	$H_2O_2+H = HO_2+H_2$		4.82E+13	0.00	7.95E+03	[81]

18	H_2O_2+O = OH+ HO_2		9.55E+06	2.00	3.97E+03	[81]
19	H_2O_2+OH = HO_2+ H_2O	Duplicate	1.00E+12	0.00	0.00	[96]
	H_2O_2+OH = HO_2+ H_2O	Duplicate	5.80E+14	0.00	9.56E+03	
	CO reactions					
20	CO+O (+M) = CO_2 (+M)	k_∞	1.80E+10	0.00	2.38E+03	[97]
		k_0	1.55E+24	-2.79	4.19E+03	[98]
	ε_{H2} = 2.5, ε_{H2O} = 12.0, ε_{CO} = 1.9, ε_{CO2} = 3.8, ε_{Ar} = 0.87					
21	CO+O_2 = CO_2+O		2.53E+12	0.00	4.77E+04	[81]
22	CO+HO_2 = CO_2+OH		3.01E+13	0.00	2.30E+04	[17]
23	CO+OH = CO_2+H		2.23E+05	1.90	-1.16E+03	This study
	HCO reactions					
24	HCO+M = H+CO+M		4.75E+11	0.70	1.49E+04	This study
	ε_{H2} = 2.5, ε_{H2O} = 6.0, ε_{CO} = 1.9, ε_{CO2} = 3.8					
25	HCO+ O_2 = CO+HO_2		7.58E+12	0.00	4.10E+02	[58]
26	HCO+H = CO+H_2		7.23E+13	0.00	0.00	[57]
27	HCO+O = CO+OH		3.02E+13	0.00	0.00	[81]
28	HCO+OH = CO+ H_2O		3.02E+13	0.00	0.00	[81]
29	HCO+O = CO_2+H		3.00E+13	0.00	0.00	[81]
30	HCO+HO_2 = CO_2+OH+H		3.00E+13	0.00	0.00	[81]
31	HCO+HCO = H_2+CO+CO		3.00E+12	0.00	0.00	[81]
32	HCO+CH_3 = CO+CH4		1.20E+14	0.00	0.00	[81]
33	HCO+HCO = CH_2O+CO		3.00E+13	0.00	0.00	[59]
	CH_2O reactions					
34	CH_2O+M = HCO+H+M		3.30E+39	-6.30	9.99E+04	[24]
	ε_{H2} = 2.5, ε_{H2O} = 12.0, ε_{CO} = 1.9, ε_{CO2} = 3.8, ε_{Ar} = 0.87					
35	CH_2O +M = CO+H_2+M		3.10E+45	-8.00	9.75E+04	[24]
	ε_{H2} = 2.5, ε_{H2O} = 12.0, ε_{CO} = 1.9, ε_{CO2} = 3.8, ε_{Ar} = 0.87					
36	CH_2O +H = HCO+ H_2		5.74E+07	1.90	2.75E+03	[77]
37	CH_2O +O = HCO+OH		1.81E+13	0.00	3.08E+03	[81]
38	CH_2O +OH = HCO+ H_2O		3.43E+09	1.20	-4.47E+02	[79]
39	CH_2O +O_2 = HCO+HO_2		1.23E+06	3.00	5.20E+04	[80]
40	CH_2O +HO_2 = HCO+ H_2O_2		4.11E+04	2.50	1.02E+04	[23]
41	CH_2O +CH_3 = HCO+CH_4		3.64E-06	5.40	9.98E+02	[32]
	CH_3 reactions					
42	CH_3+O = CH_2O+H		8.43E+13	0.00	0.00	[99]
43	CH_3+O_2 = CH_3O+O		1.99E+18	-1.60	2.92E+04	[81]
44	CH_3+O_2 = CH_2O+OH		3.74E+11	0.00	1.46E+04	[100]
45	CH_3+HO_2 = CH_3O+OH		2.41E+10	0.80	-2.33E+03	[27]
46	CH_3+H (+M) = CH_4 (+M)	k_∞	1.27E+16	-0.60	3.83E+02	[101]
		k_0	2.48E+33	-4.76	2.44E+03	[101]
	α = 0.783, T*** = 7.40E+01, T* = 2.94E+03, T** = 6.96E+03					

	ε_{H2} = 2.0, ε_{H2O} = 6.0, ε_{CO} = 1.5, ε_{CO2} = 2.0, ε_{Ar} = 0.7, ε_{CH4} = 2.0					
CH_4 reactions						
47	$CH_4+H = CH_3+H_2$		5.47E+07	2.00	1.12E+04	[102]
48	$CH_4+O = CH_3+OH$		3.15E+12	0.50	1.03E+04	[103]
49	$CH_4+OH = CH_3+ H_2O$		5.72E+06	2.00	2.64E+03	[104]
50	$CH_3+HO_2 = CH_4+O_2$		3.16E+12	0.00	0.00	[100]
51	$CH_4+HO_2 = CH_3+ H_2O_2$		1.81E+11	0.00	1.86E+04	[81]
CH_2OH reactions						
52	$CH_2OH+M = CH_2O+H+M$		1.00E+14	0.00	2.51E+04	[71]
53	$CH_2OH+H = CH_2O +H_2$		6.00E+12	0.00	0.00	[105]
54	$CH_2OH+H = CH_3+OH$		9.64E+13	0.00	0.00	[81]
55	$CH_2OH+O = CH_2O +OH$		4.20E+13	0.00	0.00	[105]
56	$CH_2OH+OH = CH_2O +H_2O$		2.40E+13	0.00	0.00	[105]
57	$CH_2OH+O_2 = CH_2O+HO_2$	Duplicate	2.41E+14	0.00	5.02E+03	[106]
	$CH_2OH+O_2 = CH_2O+HO_2$	Duplicate	1.51E+15	-1.00	0.00	
58	$CH_2OH+HO_2 = CH_2O +H_2O_2$		1.20E+13	0.00	0.00	[105]
59	$CH_2OH+HCO = CH_3OH+CO$		1.00E+13	0.00	0.00	See text
60	$CH_2OH+HCO = CH_2O + CH_2O$		1.50E+13	0.00	0.00	[24]
61	$2CH_2OH = CH_3OH+ CH_2O$		3.00E+12	0.00	0.00	[105]
62	$CH_2OH+CH_3O = CH_3OH+ CH_2O$		2.40E+13	0.00	0.00	[105]
CH_3O reactions						
63	$CH_3O+M = CH_2O+H+M$		8.30E+17	-1.20	1.55E+04	[107]
64	$CH_3O+H = CH_3+OH$		3.20E+13	0.00	0.00	[108]
65	$CH_3O+O = CH_2O+OH$		6.00E+12	0.00	0.00	[81]
66	$CH_3O+OH = CH_2O+H_2O$		1.80E+13	0.00	0.00	[81]
67	$CH_3O+O2 = CH_2O+HO_2$	Duplicate	9.03E+13	0.00	1.20E+04	[108]
	$CH_3O+O2 = CH_2O+HO_2$	Duplicate	2.20E+10	0.00	1.75E+03	
68	$CH_3O+HO_2 = CH_2O+H_2O_2$		3.00E+11	0.00	0.00	[81]
69	$CH_3O+CO = CH_3+CO_2$		1.60E+13	0.00	1.18E+04	[81]
70	$CH_3O+HCO = CH_3OH+CO$		9.00E+13	0.00	0.00	[81]
71	$2CH_3O = CH_3OH+CH_2O$		6.00E+13	0.00	0.00	[81]
CH_3OH reactions						
72	$OH+CH_3 (+M) = CH_3OH (+M)$	k_∞	2.79E+18	-1.40	1.33E+03	[47]
		k_0	4.00E+36	-5.92	3.14E+03	[47]
	α = 0.412, T*** = 1.95E+02, T* = 5.90E+03, T** = 6.39E+03					
	ε_{H2} = 2.0, ε_{H2O} = 6.0, ε_{CO} = 1.5, ε_{CO2} = 2.0, ε_{CH4} = 2.0					
73	$H+CH_2OH (+M) = CH_3OH (+M)$	k_∞	1.06E+12	0.50	8.60E+01	[47]
		k_0	4.36E+31	-4.65	5.08E+03	[47]
	α = 0.6, T*** = 1.00E+02, T* = 9.00E+04, T** = 1.00E+04					
	ε_{H2} = 2.0, ε_{H2O} = 6.0, ε_{CO} = 1.5, ε_{CO2} = 2.0, ε_{CH4} = 2.0,					
74	$H+CH_3O (+M) = CH_3OH (+M)$	k_∞	2.43E+12	0.50	5.00E+01	[47]

	k_0	4.66E+41	-7.44	1.41E+04	[47]
	α = 0.7, T*** = 1.00E+02, T* = 9.00E+04, T** = 1.00E+04				
	ε_{H2} = 2.0, ε_{H2O} = 6.0, ε_{CO} = 1.5, ε_{CO2} = 2.0, ε_{CH4} = 2.0				
75	$CH_3OH+H = CH_2OH+H_2$	3.20E+13	0.00	6.10E+03	[42]
76	$CH_3OH+H = CH_3O+H_2$	8.00E+12	0.00	6.10E+03	[42]
77	$CH_3OH+O = CH_2OH+OH$	3.88E+05	2.50	3.08E+03	[105]
78	$CH_3OH+OH = CH_3O+H_2O$	1.00E+06	2.10	4.97E+02	[86]
79	$CH_3OH+OH = CH_2OH+H_2O$	7.10E+06	1.80	-5.96E+02	[86]
80	$CH_3OH+O_2 = CH_2OH+HO_2$	2.05E+13	0.00	4.49E+04	[105]
81	$CH_3OH+HCO = CH_2OH+CH_2O$	9.64E+03	2.90	1.31E+04	[105]
82	$CH_3OH+HO_2 = CH_2OH+H_2O_2$	3.98E+13	0.00	1.94E+04	[109]
83	$CH_3OH+CH_3 = CH_2OH+CH_4$	3.19E+01	3.20	7.17E+03	[105]
84	$CH_3O+CH_3OH = CH_3OH+CH_2OH$	3.00E+11	0.00	4.06E+03	[105]

Table II - Thermochemical Data for Species Considered in the C_1/O_2 Mechanism. Units are cal/mol/K for $S_{(298)}$ and C_P, and kcal/mol for $\Delta H_{f\,(298)}$.

Species	$\Delta H_{f\,(298)}$	$S_{(298)}$	$C_{P\ 300K}$	$C_{P\ 500K}$	$C_{P\ 800K}$	$C_{P\ 1000K}$	$C_{P\ 1500K}$	$C_{P\ 2000K}$	Reference
Ar	0	36.98	4.97	4.97	4.97	4.97	4.97	4.97	[110]
CH_2O	-27.71	52.33	8.41	10.48	13.36	14.91	16.92	18.08	[110]
CH_2OH	-4.25	58.36	11.36	14.19	17.07	18.42	20.65	21.86	See text
CH_3	35.06	46.37	9.2	10.75	12.86	14.09	16.25	17.57	[111]
CH_3O	3.9	54.61	9.08	12.43	16.63	18.6	21.51	23.26	[110]
CH_3OH	-48.06	57.28	10.51	14.26	19.08	21.4	25.02	27.25	[110]
CH_4	-17.9	44.47	8.43	11.14	15	17.25	20.63	22.59	[110]
CO	-26.42	47.22	6.95	7.14	7.61	7.95	8.41	8.67	[110]
CO_2	-94.06	51.08	8.91	10.65	12.32	12.99	13.93	14.44	[110]
H	52.1	27.39	4.97	4.97	4.97	4.97	4.97	4.97	[110]
H_2	0	31.21	6.9	7	7.07	7.21	7.73	8.18	[110]
H_2O	-57.8	45.1	8	8.45	9.22	9.87	11.26	12.22	[110]
H_2O_2	-32.53	55.66	10.42	12.35	14.29	15.21	16.85	17.88	[110]
HCO	10.4	53.66	8.25	9.28	10.74	11.52	12.56	13.14	[110]
He	0	30.12	4.97	4.97	4.97	4.97	4.97	4.97	[110]
HO_2	3	54.76	8.35	9.47	10.77	11.38	12.48	13.32	See text
N_2	0	45.77	6.95	7.08	7.5	7.83	8.32	8.6	[110]
O	59.56	38.47	5.23	5.08	5.02	5	4.98	4.98	[110]
O_2	0	49.01	7.01	7.44	8.07	8.35	8.72	9.03	[110]
OH	8.9	43.91	7.16	7.05	7.15	7.34	7.87	8.28	See text

Table III - Literature Experiments Used for Validation of CO/O_2 Mechanism.

Method	Source	Mixture	T (K)	P (atm)	ϕ
Shock Tube	Gardiner et al. [117]	$CO/H_2/O_2/Ar$	1400– 2500	0.15 – 0.3	0.4
	Dean et al. [116]	$CO/H_2/O_2/Ar$	2000 – 2850	1.2 – 2.2	1.6 – 6.1
Laminar Premixed Flame	McLean et al. [48]	CO/H_2/air	298	1	0.5 – 6.0
	Huang et al. [25]	$CO/H_2/N_2$/air	298	1	0.7 – 1.4
Flow Reactor	Yetter et al. [12]	$CO/H_2O/O_2/N_2$	1033	1	0.44 – 1.44
	Kim et al. [14]	$CO/H_2O/O_2/N_2$	960 – 1200	1.0 – 9.6	0.33 – 2.1
	Mueller et al. [118]	CO/H_2O $/O_2/N_2$	1038	1.0 – 9.6	1.0

Table IV - Literature Experiments Used for Validation of CH_2O/O_2 Mechanism.

Method	Source	Mixture	T (K)	P (atm)	ϕ
Shock Tube	Dean et al. [132]	$CH_2O/O_2/Ar$	1935 – 2150	1.1 – 1.3	pyrolysis – 0.67
	Buxton and Simpson [126]	CH_2O/Ar	1750 – 2100	0.6 – 3.5	pyrolysis
	Hidaka et al. [22]	$CH_2O/O_2/Ar$	1240 – 1950	1.5 – 2.9	pyrolysis – 4.0
	Eiteneer et al. [23]	$CH_2O/O_2/Ar$	1440 – 2120	0.9 – 2.3	pyrolysis – 6.0
	Friedrichs et al. [3]	CH_2O/Ar	955 – 975	0.3 – 1.8	pyrolysis
Burner-Stabilized Flame	Vandooren et al. [127]	CH_2O/O_2	300	0.03	0.22
Flow Reactor	Hochgreb and Dryer [13]	CH_2O $/O_2/N_2$	945 – 1095	1	0.013– 1.74
	This study	CH_2O $/H_2O/O_2/N_2$	850 – 950	1.5 – 6.0	~ 0.005

Table V - Literature Experiments Used for Validation of CH_3OH/O_2 Mechanism.

Method	Source	Mixture	T (K)	P (atm)	ϕ
Shock Tube	Bowman [130]	$CH_3OH/O_2/CO/Ar$	1545 – 2180	1.2 – 4.7	0.375 – 6.0
Laminar Premixed Flame	Egolfopoulos et al. [131]	CH_3OH/air	318 – 368	1.0	0.5 – 2.0
Flow Reactor	Aronowitz et al. [128]	$CH_3OH/O_2/N_2$	1000 – 1010	1.0	0.05 – 1.6
	Norton and Dryer [129]	$CH_3OH/O_2/N_2$	1027 – 1034	1.0	0.6 – 1.6
	Held [29]	$CH_3OH/O_2/N_2$	750 – 1040	1.5 – 20.0	0.3 – 2.6

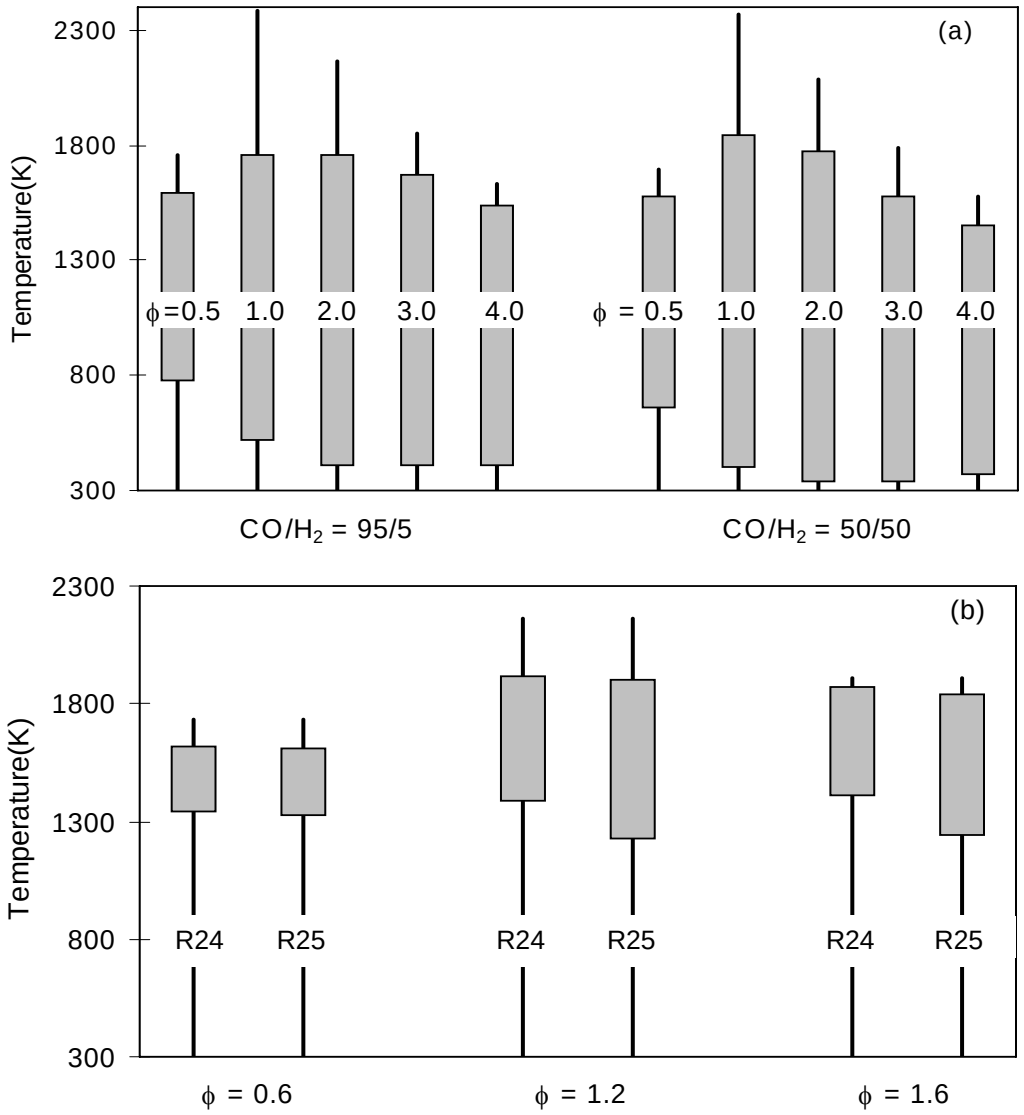

Figure 1 Sensitivity spectrum of reactions CO + OH = CO_2 + H, (R23), HCO + M = H + CO + M, (R24), and HCO + O_2 = HO_2 + CO, (R25), for a range of equivalence ratio predicted by the present C_1/O_2 kinetic mechanism. The figures are taken from Zhao et al. [2]. Figure (a) is the sensitivity spectrum of (R23) for ambient CO/H_2/air flames of two initial fuel compositions (95% CO + 5% H_2 and 50% CO + 50% H_2); (b) is that of (R24) and (R25) for ambient CH_3OH/air flames. Bars indicate the temperature range where the sensitivity is larger than 10% of the maximum value, and lines represent the temperature span for the specific flame.

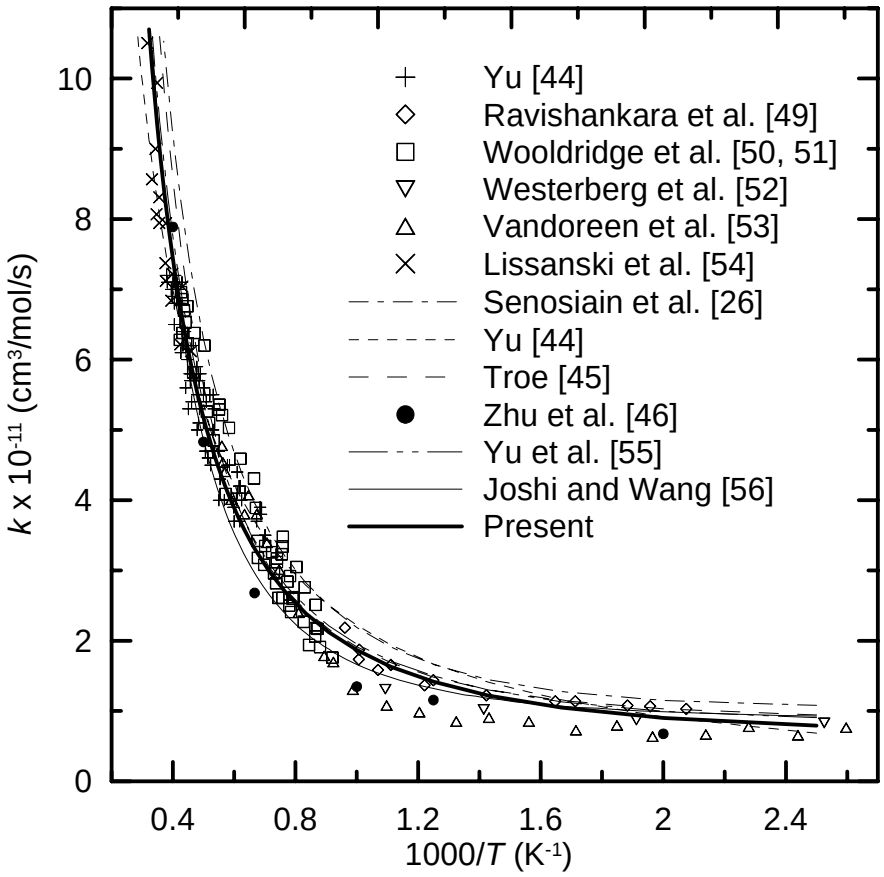

Figure 2 Rate constant of reaction CO + OH → CO_2 + H (R23). Symbols are experimental data (except for atmospheric pressure theoretical results of Zhu et al. [46]), lines are the recommendations of Yu [44], Troe [45], Yu et al. [55] at 1 atm, Senosiain et al. [26] at 1 atm, Joshi and Wang [56] at the low-pressure limit, and that used in the present C_1 mechanism (Eq. 2).

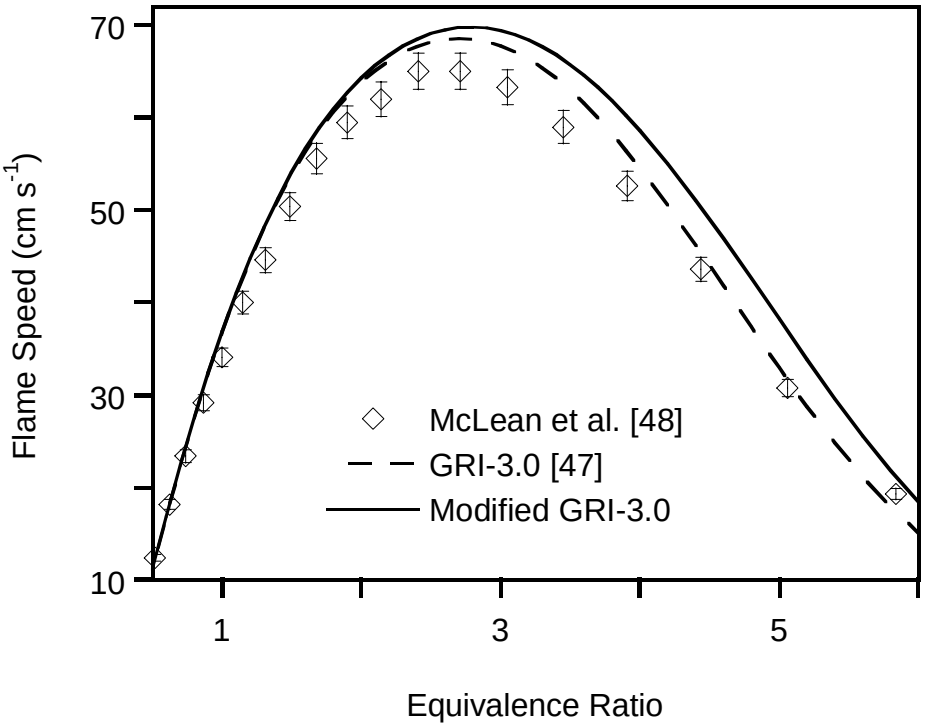

Figure 3 Laminar flame speed of CO/H_2/air mixtures at 298 K and 1 atm. The fuel composition is 95% CO and 5% H_2. Symbols – experimental data of McLean et al. [48]; dotted line – predictions of GRI-Mech 3.0 [47]; solid line – predictions of GRI-Mech 3.0 modified by replacing the rate coefficients of reaction (R24) and (R25) with the recommendations of Friedrichs et al. [3] and DeSain et al. [4], respectively.

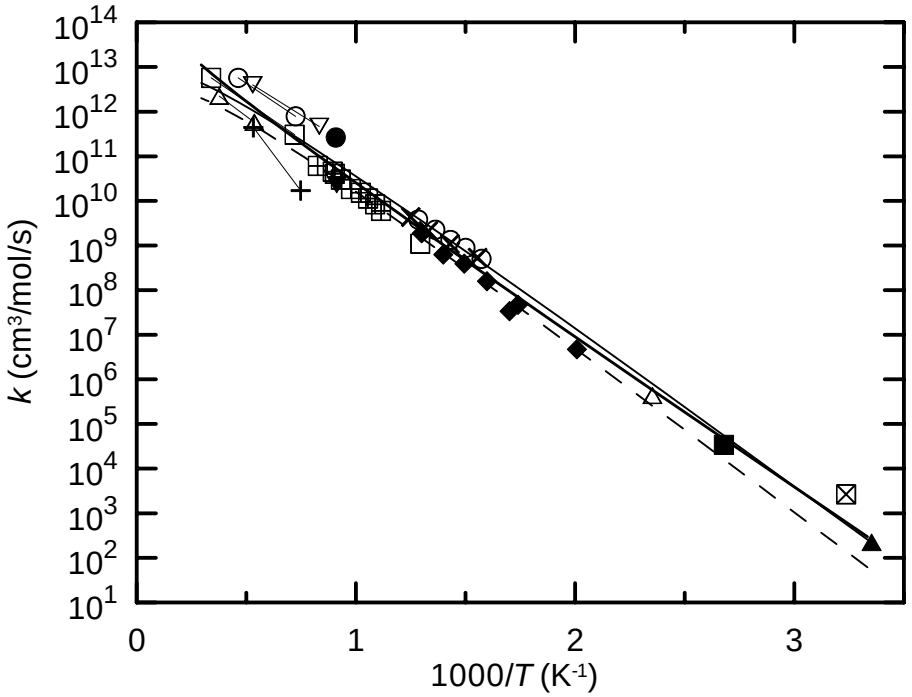

Figure 4 Rate constant of reaction HCO + M → H + CO + M (R24). Symbols and lines with symbols are literature results: Friedrichs et al. [3]; Hidaka et al. [22]: Timonen et al. [57]; Pearson et al. [60]; Schecker et al. [61]; Browne et al. [62]; Bowman [63]; Ahumada et al. [64]; Baldwin et al. [65]; Wang et al. [66]; Westbrook et al. [67]; Campbell et al. [68]; Hochnadel et al [69]; Cherian et al. [70]; Cribb et al [71]; Kraspanerov et al. [72]; Hippler et al. [73]. The dotted line is the recommendation of Timonen et al. [57], the dashed line is the recommendation of Friedrichs et al. [3], and the solid line represents the values used in the present model (Eq. 3).

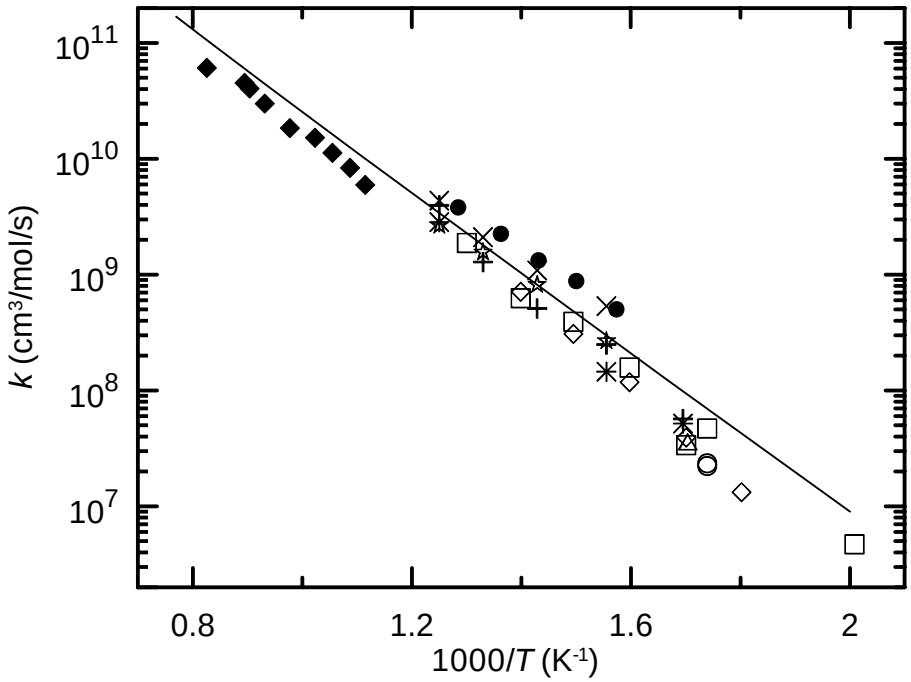

Figure 5 Pressure dependence of the rate constant of reaction (R24) as measured by Krasnoperov et al. [72] (☎ – 1 bar; 🖋 – 10 bar; 🖷 – 30 bar; 🖹 – 100 bar) and Hippler et al. [73] (🖬 – 1 bar; ✍ – 10 bar; ✌ – 30 bar; ✂ – 100 bar), the rate expression used in the present model (solid line) as well as the low pressure measurements of Friedrichs et al [3] and Timonen et al [57] (🕮 and 🖭, respectively) are also shown for comparison.

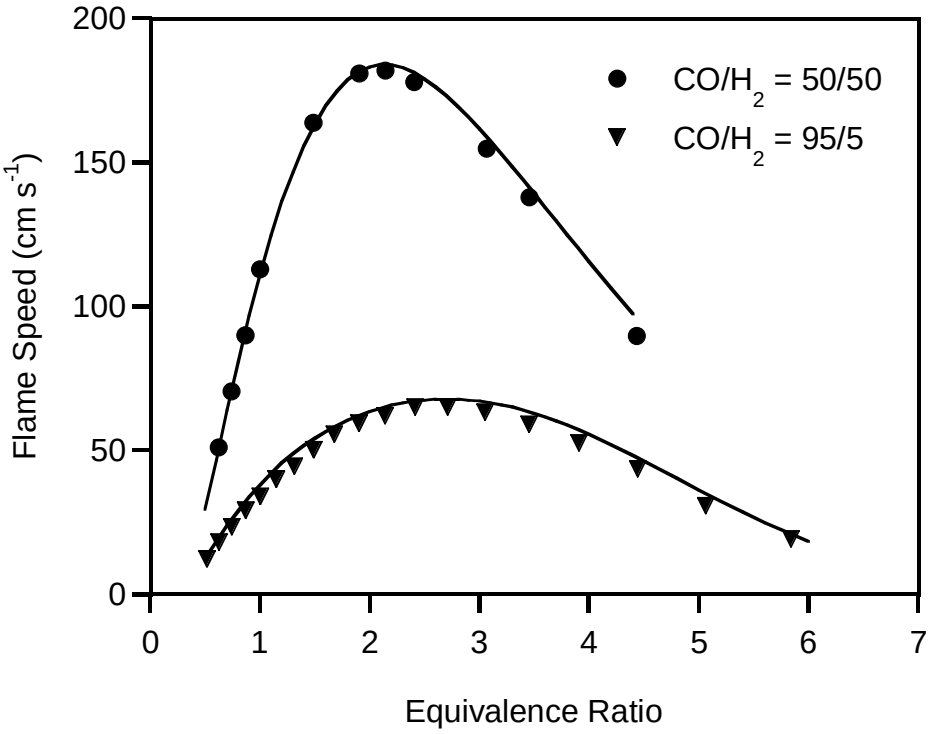

Figure 6 Laminar flame speeds of CO/H_2/air mixtures at 298 K and 1 atm for two fuel compositions (95% CO + 5% H_2 or 50% CO + 50% H_2). Symbols represent the experimental data [48], and lines are predictions of the present $CO/H_2/O_2$ mechanism.

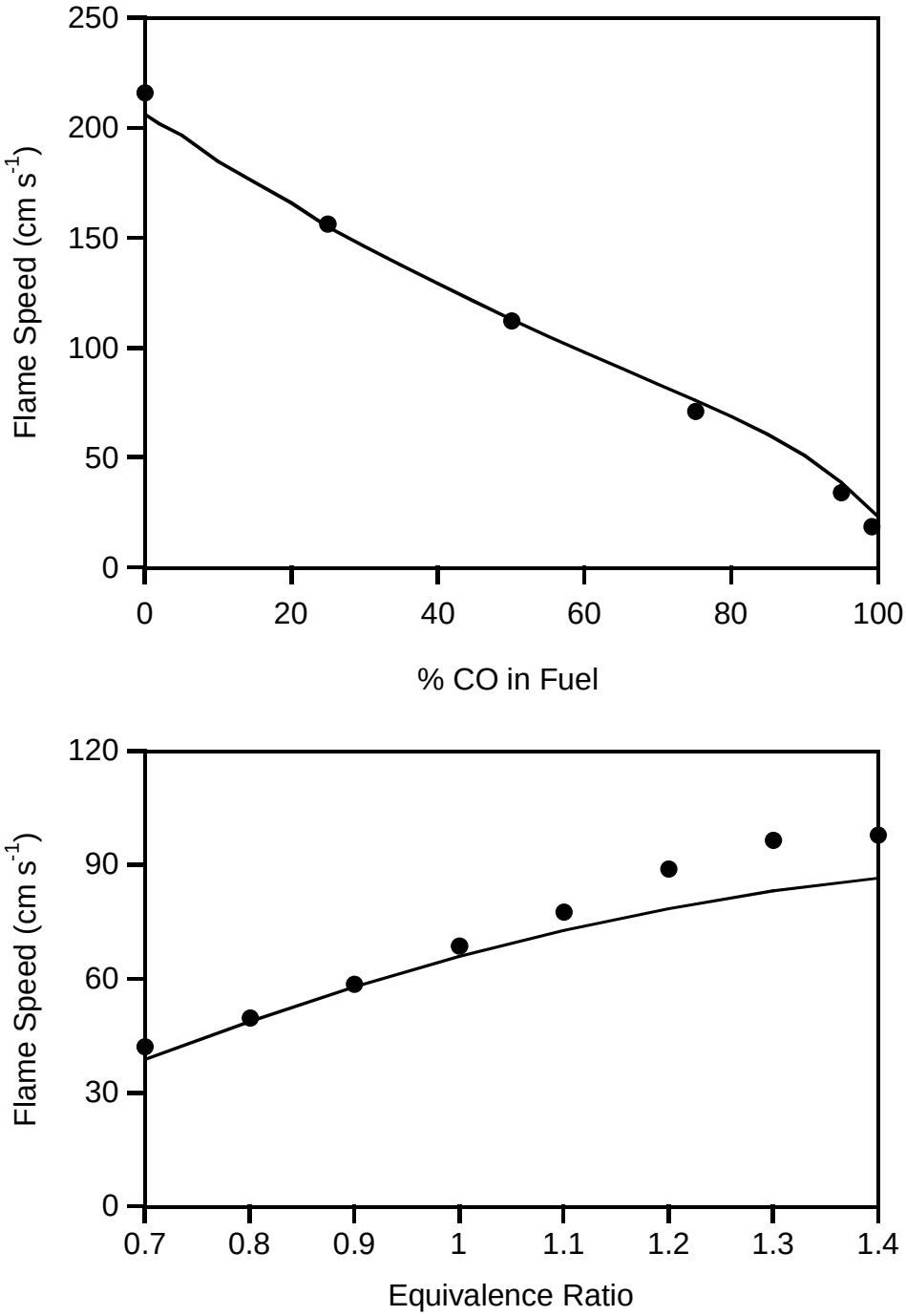

Figure 7 Laminar flame speeds for stoichiometric CO/H_2/air mixtures (top) and reformer gas/air mixtures (bottom) at 298 K and 1 atm. Composition of reformer gas is 28% H_2, 25% CO, and 47% N_2. Symbols represent the experimental data of McLean et al. [48] (top), and Huang et al. [25] (bottom). Lines are predictions of the present $CO/H_2/O_2$ mechanism.

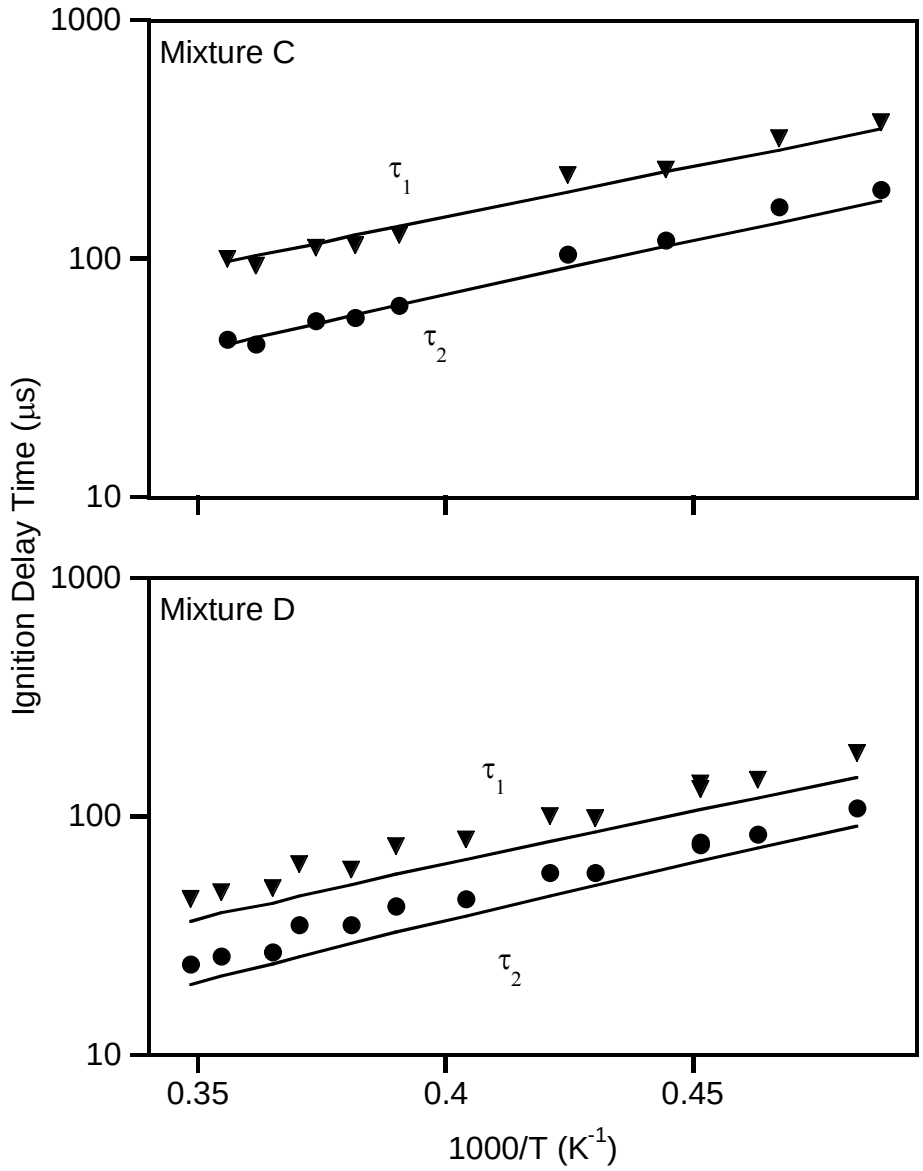

Figure 8 Ignition delay times of $CO/H_2/O_2/Ar$ mixtures. The composition of mixture C is 0.049% H_2, 1.01% O_2, 3.28% CO, and balance Ar. The composition of mixture D is 0.05% H_2, 1.00% O_2, 12.17% CO, and balance Ar. Ignition delay time τ_1 is defined as the time when $[CO_2]$ reaches 2.4×10^{16} molecule/cm^3 for mixture C and 3.0×10^{16} molecule/cm^3 for mixture D. Time τ_2 is defined as the time when $[CO_2]$ reaches 8.0×10^{15} molecule/cm^3 for mixture C and 1.0×10^{16} molecule/cm^3 for mixture D. Symbols represent the experimental data [116], and lines are predictions of the present $CO/H_2/O_2$ mechanism.

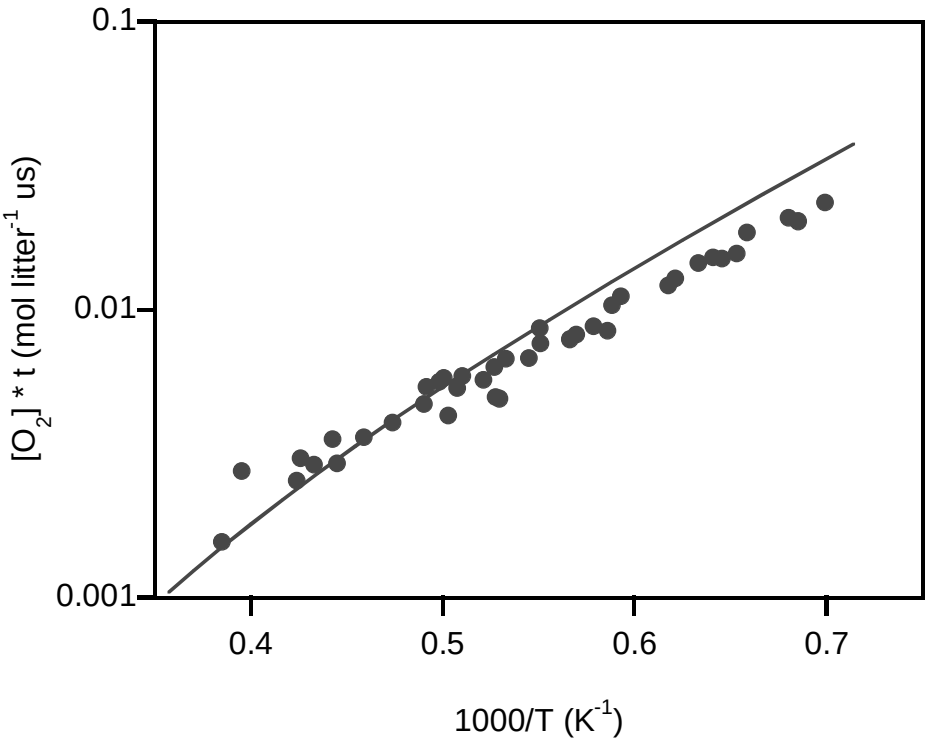

Figure 9 Induction times of $CO/H_2/O_2/Ar$ mixtures in a shock tube. Initial condition: CO = 3.0%, H_2 = 1.0%, O_2 = 5.0% with balance Ar at 0.15 ~ 0.3 atm. Symbols represent the experimental data of Gardiner et al. [117], and the solid line shows predictions of the present $CO/H_2/O_2$ mechanism.

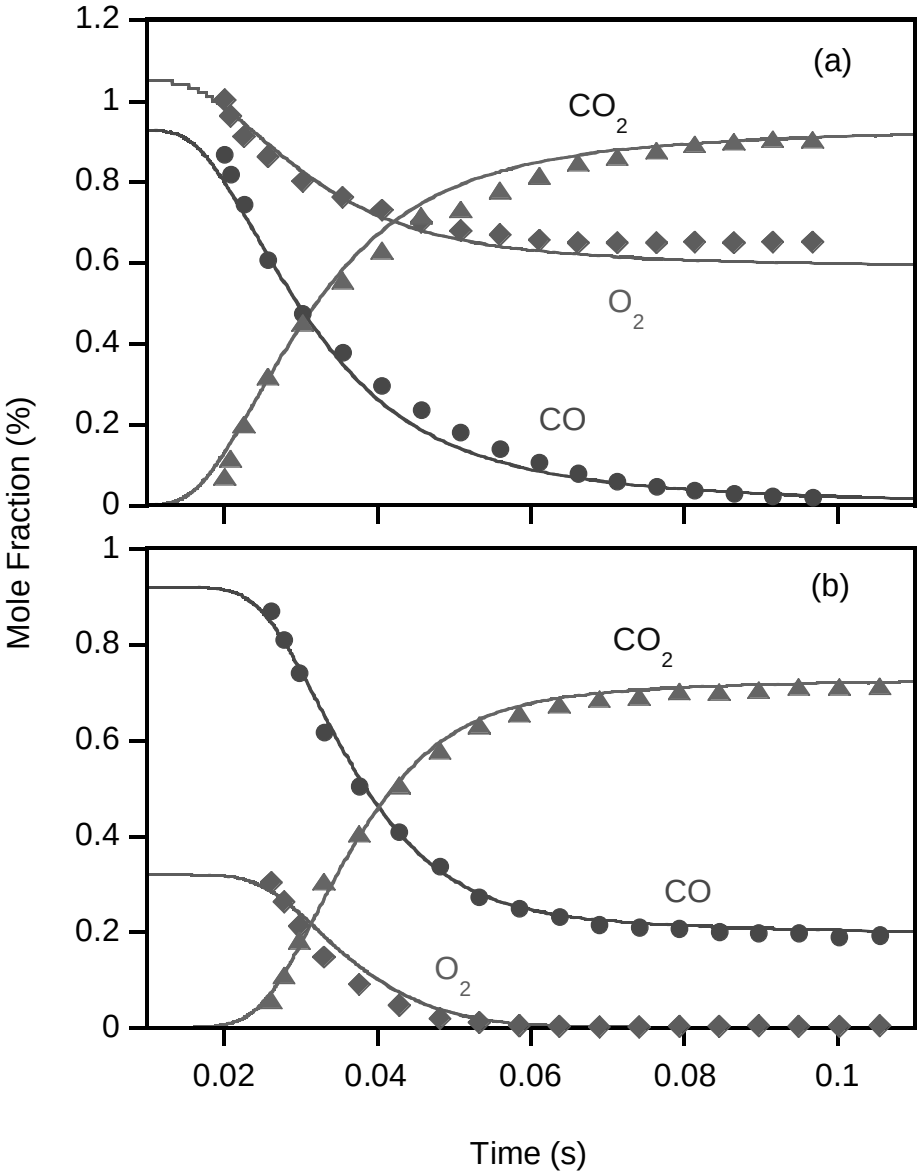

Figure 10 Reaction profiles of $CO/H_2O/O_2/N_2$ mixtures in an atmospheric pressure flow reactor. Initial condition: (a) CO = 0.93%, H_2O = 0.58%, O_2 = 1.05% with balance N_2 at 1033 K; (b) CO = 0.92%, H_2O = 0.59%, O_2 = 0.32% with balance N_2 at 1034 K. Symbols represent the experimental data of Yetter et al. [12], and lines are predictions of the present $CO/H_2/O_2$ mechanism. Model predictions are time shifted to match the 50% fuel consumption point.

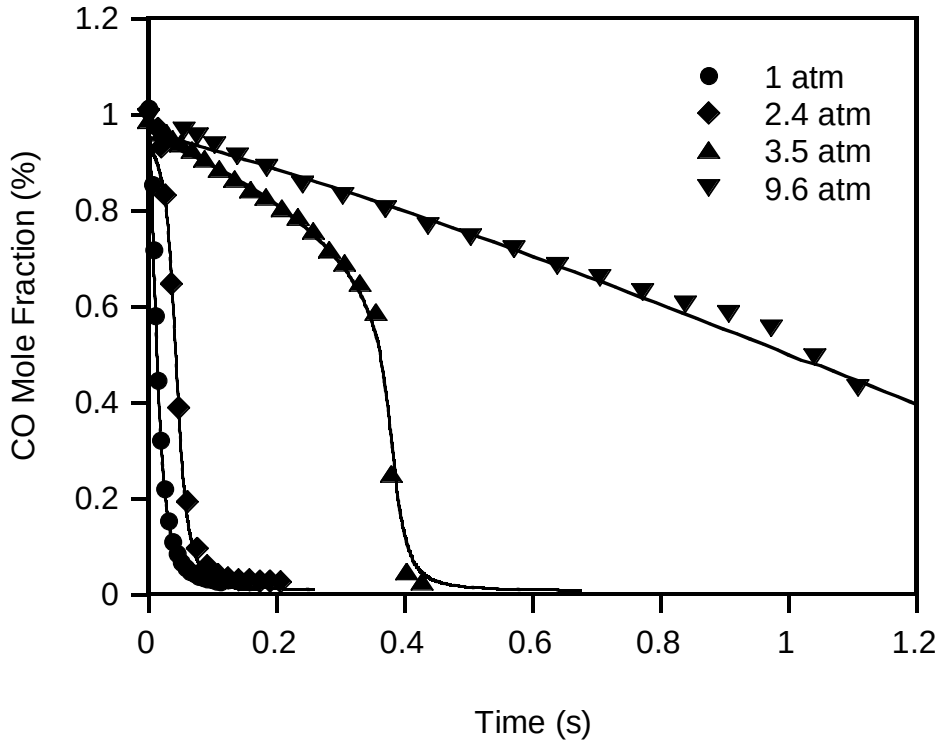

Figure 11 Reaction profiles of $CO/H_2O/O_2/N_2$ mixtures in a variable pressure flow reactor. Initial condition: CO = 1.01%, H_2O = 0.65%, O_2 = 0.52% with balance N_2 at 1038 K and 1.0 atm; CO = 1.01%, H_2O = 0.65%, O_2 = 0.50% with balance N_2 at 1038 K and 2.4 atm; CO = 0.99%, H_2O = 0.65%, O_2 = 0.49% with balance N_2 at 1038 K and 3.5 atm; CO = 0.99%, H_2O = 0.65%, O_2 = 0.49% with balance N_2 at 1040 K and 9.6 atm. Symbols represent the experimental data of Mueller et al. [20], and lines are predictions of the present $CO/H_2/O_2$ mechanism. Model predictions are time shifted to match the 50% fuel consumption point.

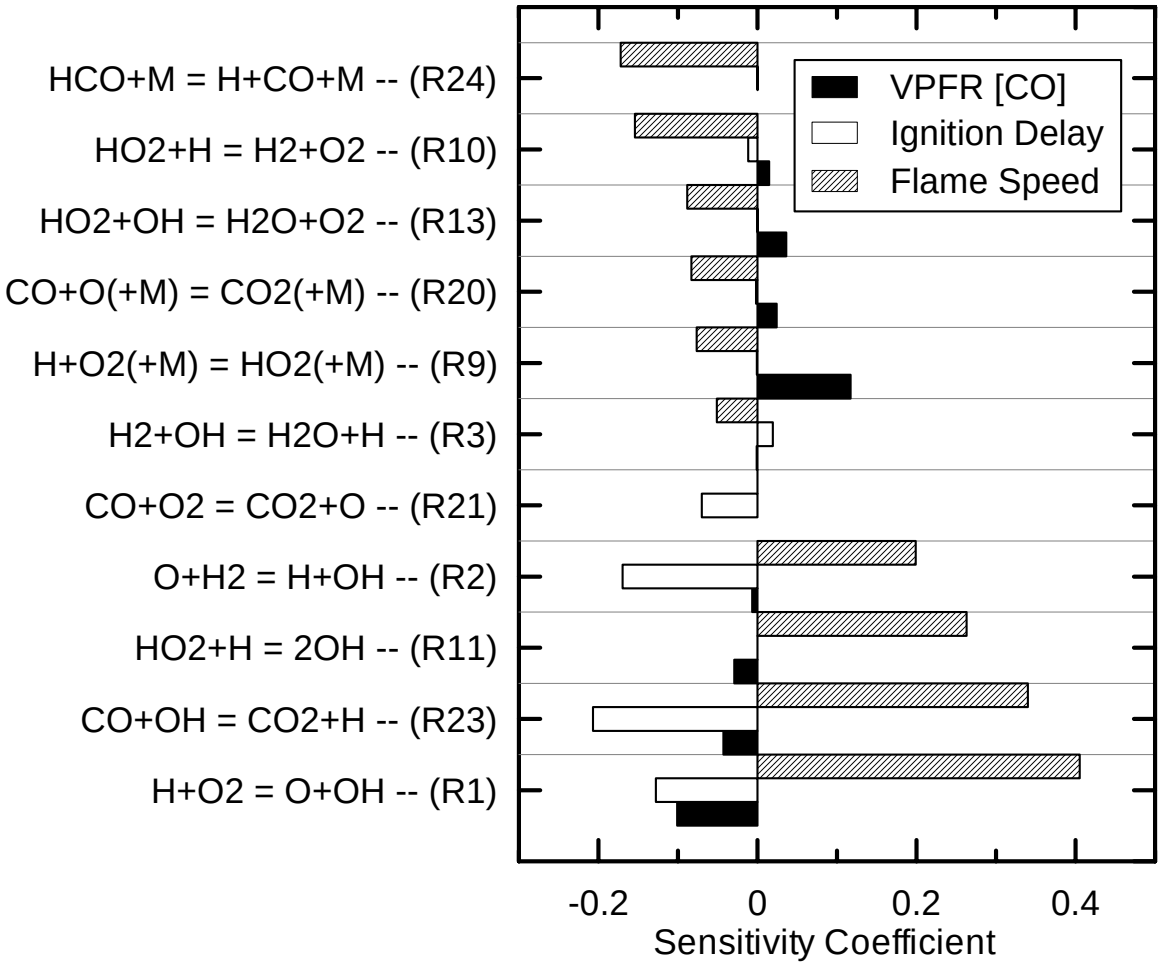

Figure 12 Sensitivity coefficients of reactions for flow reactor [20], laminar premixed flame [48], and shock tube [116] cases. Initial conditions: 0.99% CO, 0.49% O_2, 0.65% H_2O with balance N_2 at 3.5 atm and 1038 K [20]; 3.28% CO, 1.01% O_2, 0.049% H_2 with balance Ar at 1.41 atm and 2250 K [116]; 64.3% CO, 6.8% O_2, 3.4% H_2 with balance N_2 at 1.0 atm and 298 K [48]. The sensitivity coefficient for the flow reactor case is taken at the time when 50% CO has been consumed. The shock tube ignition delay time is defined as the time when CO_2 concentration reaches 8×10^{15} molecule/cm^3.

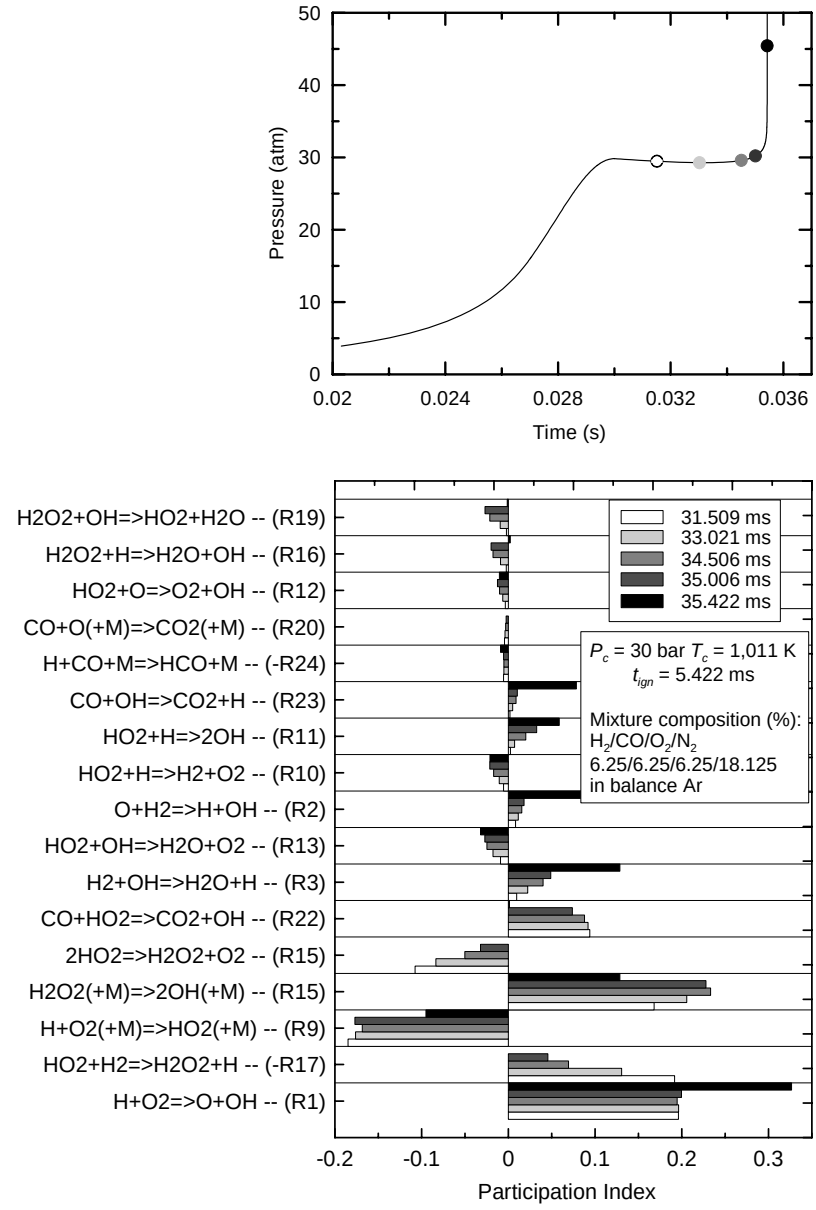

Figure 13 Reactions participating in the thermal evolution of a H_2/CO/N_2/Ar kinetic system under Rapid Compression Machine (RCM) conditions (Mittal et al., [119]), obtained from CSP analysis. Analyses were performed after the compression stroke at the selected points shown in the top figure.

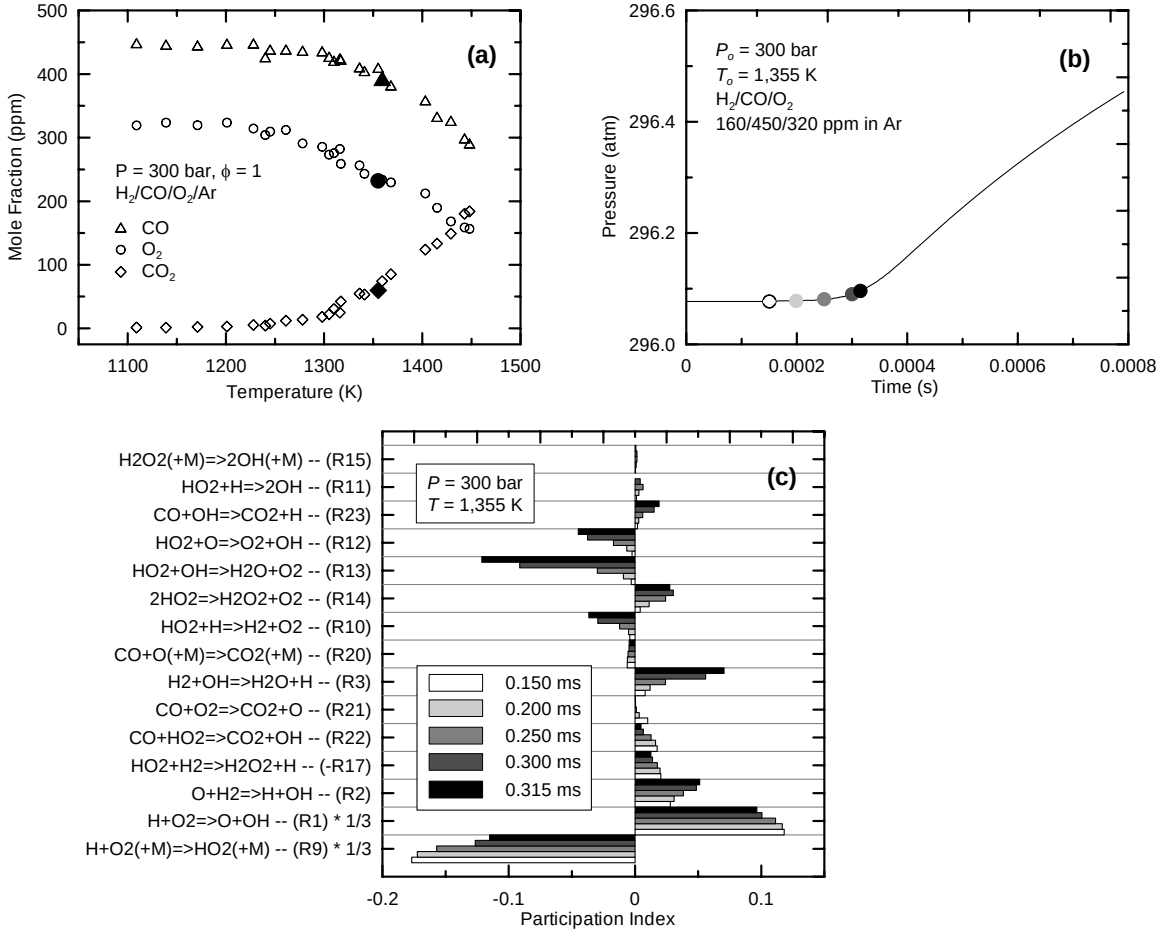

Figure 14 H_2/CO oxidation in a high pressure shock tube. (a) Experimental data of Sivaramakrishnan et al. [120]; (b) temperature profile and (c) CSP analysis during the induction period in (b) for the conditions chosen in (a) (filled symbols). Note that the participation indices of reactions (R1) and (R9) have been reduced by one third to better display the spectrum of other reactions involved in the system.

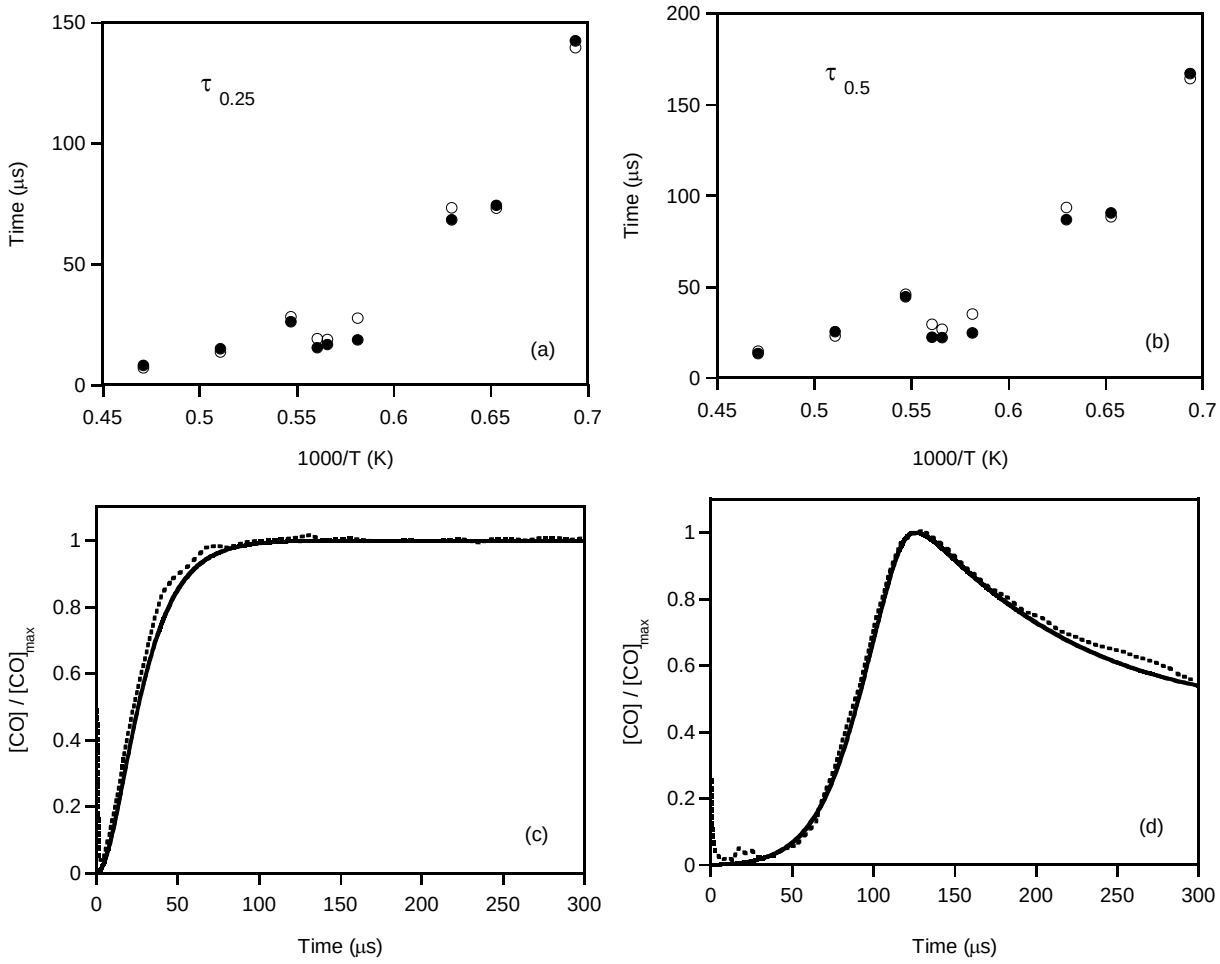

Figure 15 Ignition delay results for CH_2O/O_2/Ar mixture in a shock tube. In (a) and (b), initial conditions are for cases 10, 14, 24, 33, 47, 62, 70, 74, and 98 listed in Table 1 of Eiteneer et al. [23]. Initial conditions for (c) are 1.97% CH_2O with balance Ar at 1959 K and 1.27 atm; for (d) 1.5% CH_2O, 1.5% O_2 with balance Ar at 1532 K and 1.35 atm. $\tau_{0.25}$ and $\tau_{0.5}$ are the time when the CO concentration reaches 0.25 and 0.5 times its maximum value, respectively. Open symbols and dashed lines represent experimental data [23], solid symbols and solid lines represent predictions of the present CH_2O/O_2 mechanism.

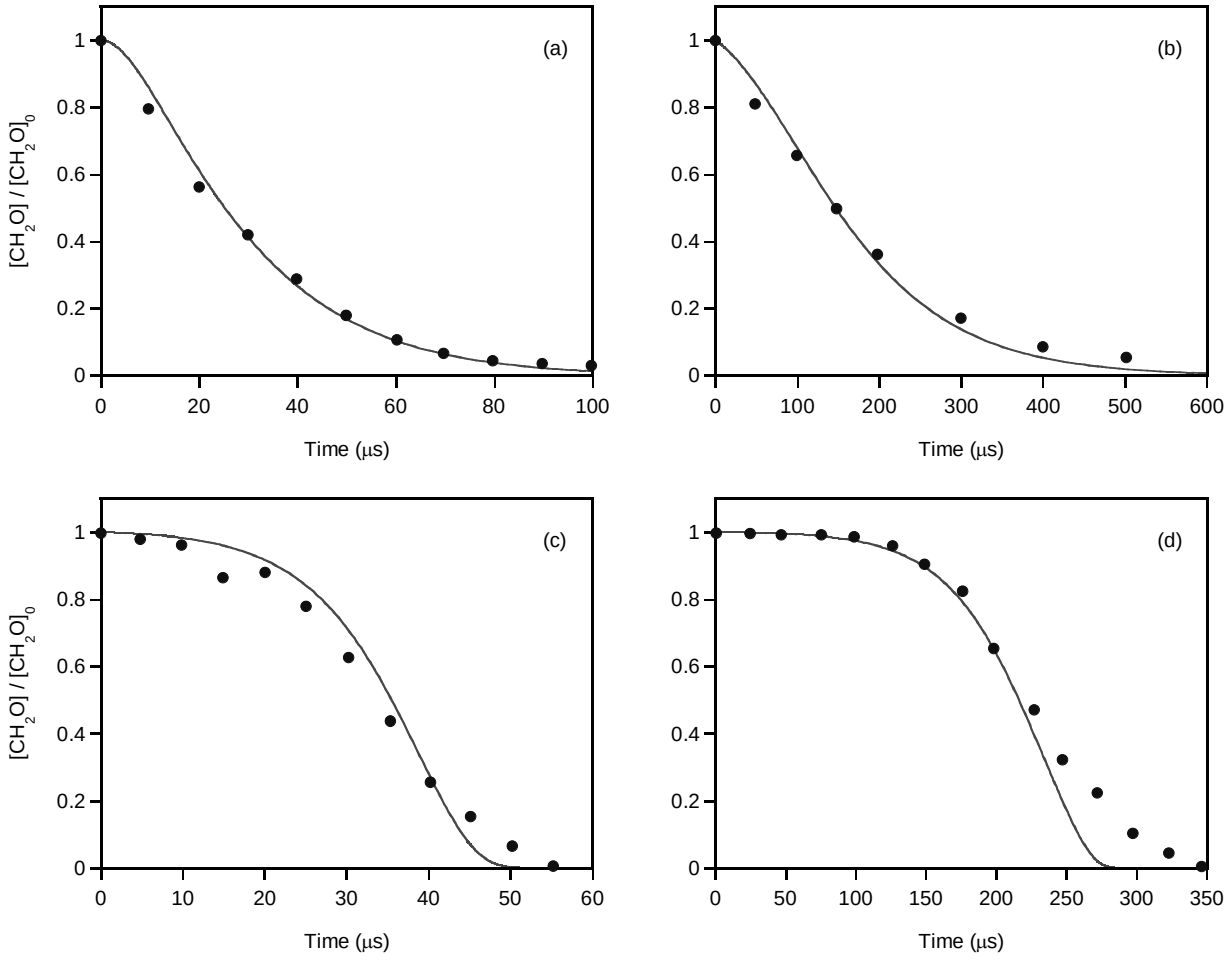

Figure 16 Normalized CH_2O concentration profiles for CH_2O/O_2/Ar mixtures in a shock tube. Initial conditions for (a) are 4.0% CH_2O with balance Ar at 1805 K and 2.81 atm; for (b) 0.01% CH_2O with balance Ar at 1907 K and 2.64 atm; for (c) 1.0% CH_2O, 4.0% O_2 with balance Ar at 1583 K and 2.16 atm; for (d) 1.0% CH_2O, 1.0% O_2 with balance Ar at 1414 K and 1.75 atm. Symbols represent experimental data of Hidaka et al. [22], and lines represent predictions of the present CH_2O/O_2 mechanism.

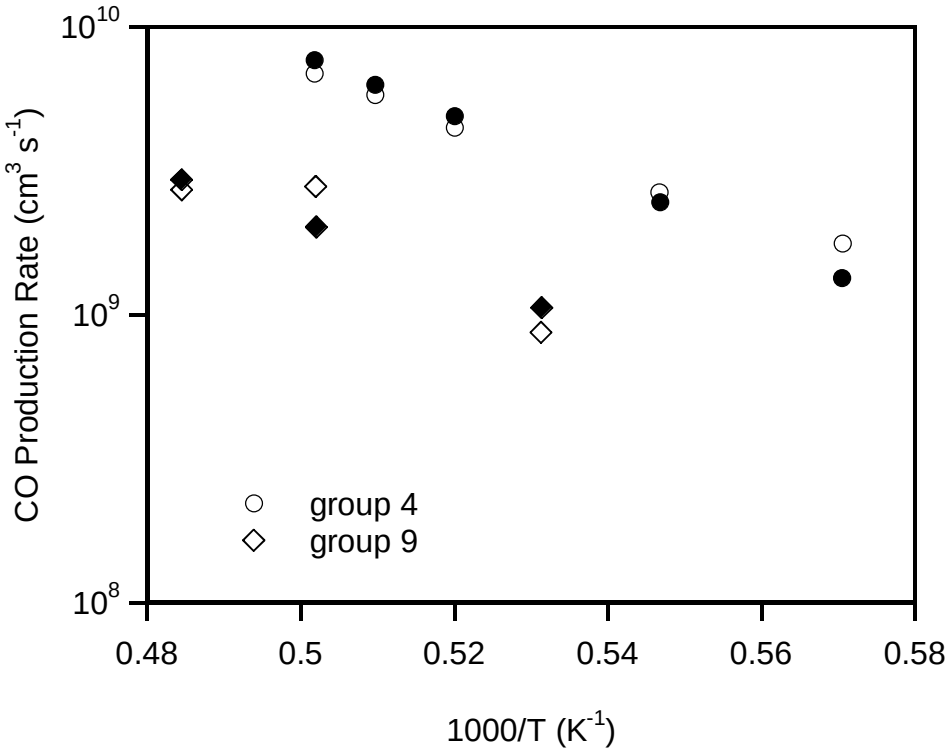

Figure 17 CO production rate during CH_2O pyrolysis in a shock tube. Initial conditions of group 4 are 1.3% CH_2O with balance Ar at 0.6 ~ 0.8 atm. Initial conditions of group 9 are 0.05% CH_2O with balance Ar at 3.2 ~ 3.5 atm. Open symbols represent the experimental data of Buxton and Simpson [126], and solid symbols represent predictions of the present CH_2O/O_2 mechanism.

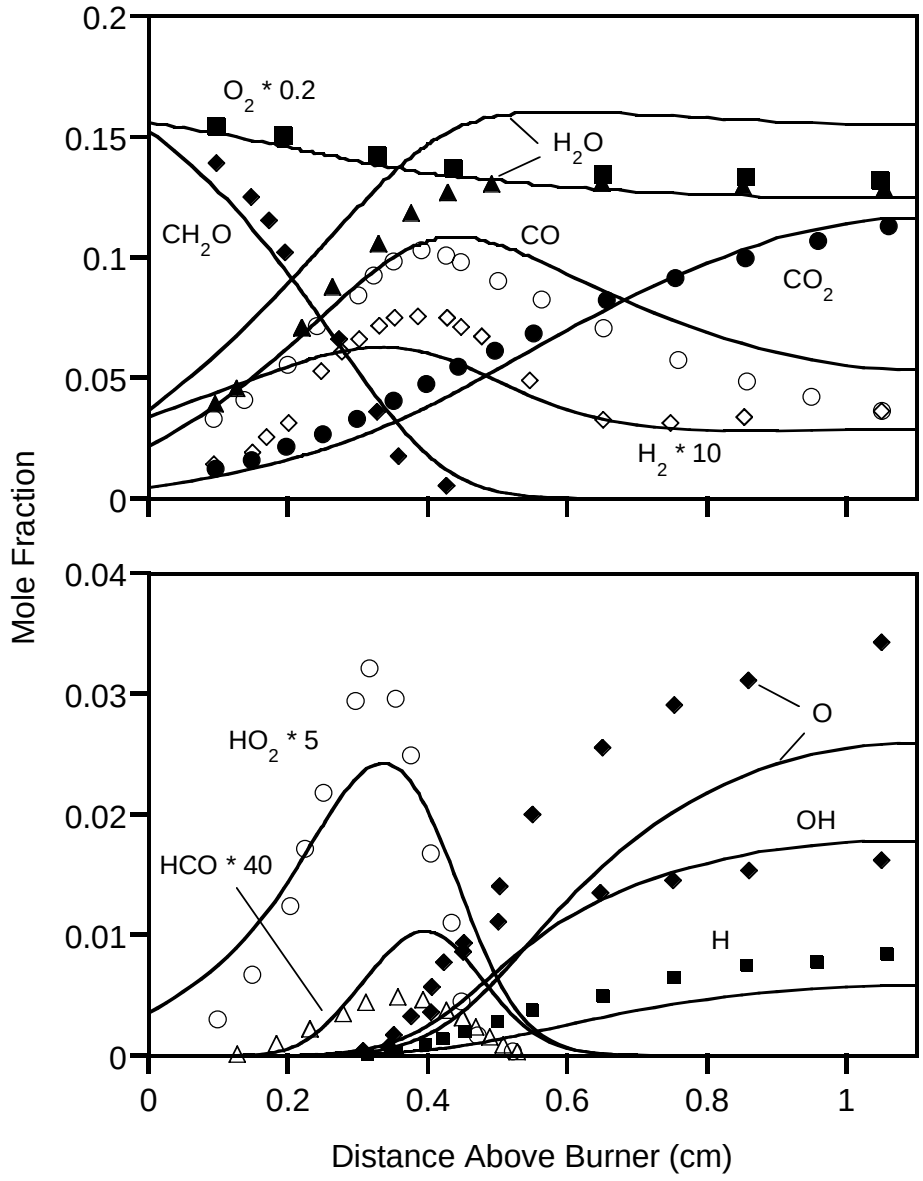

Figure 18 Species profiles in a CH_2O/O_2 burner-stabilized flame. Initial conditions are 17.9% CH_2O with 82.1% O_2 at 300 K and 0.03 atm. Symbols represent the experimental data of Vandooren et al. [127], and lines represent predictions of the present CH_2O/O_2 mechanism. The predictions are shifted by – 0.1 cm to match the fuel profile data.

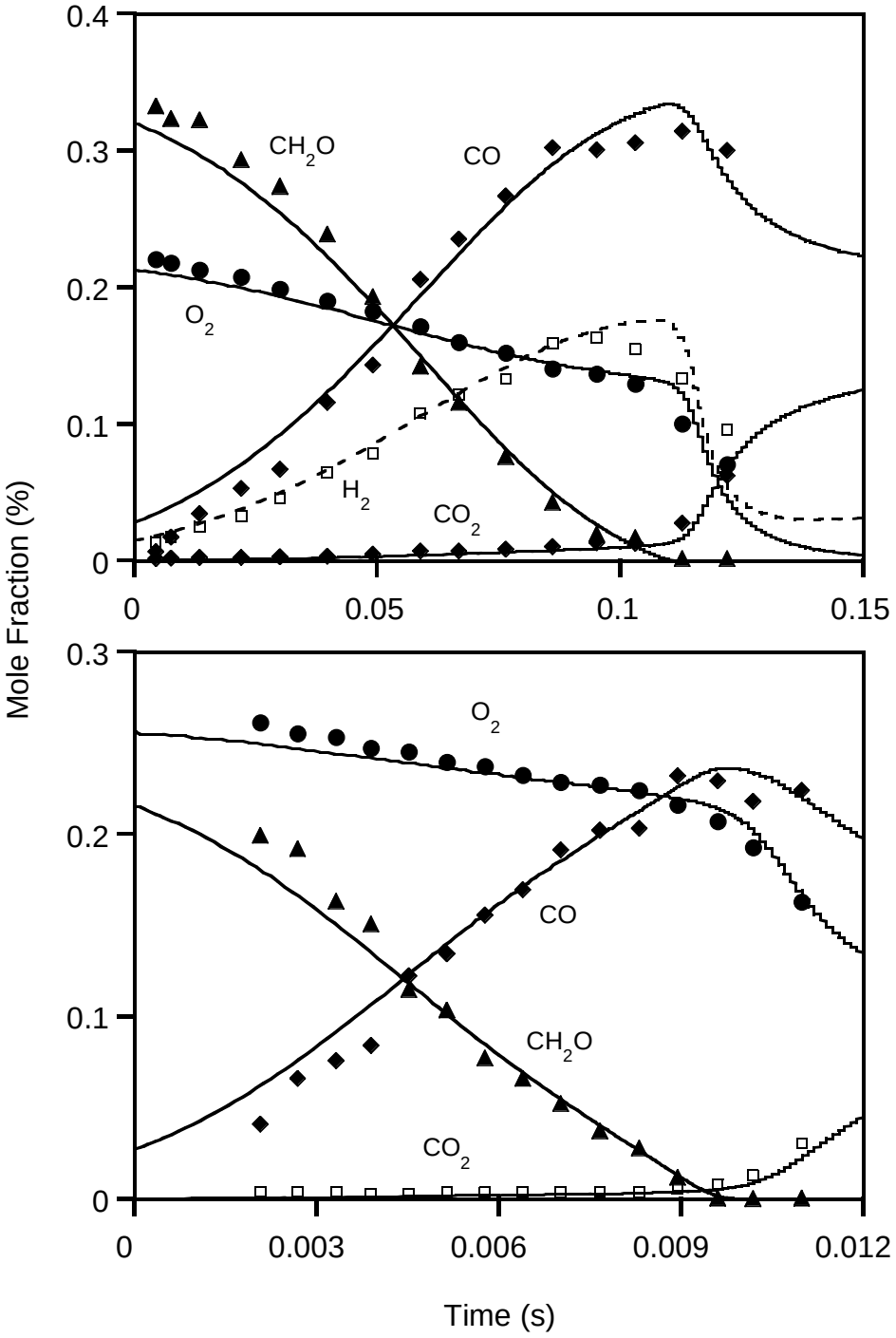

Figure 19 Reaction profiles of $CH_2O/O_2/N_2$ mixtures in an atmospheric flow reactor. Initial conditions: CH_2O = 0.348%, O_2 = 0.223% with balance N_2 at 945 K (top); CH_2O = 0.243%, O_2 = 0.261% with balance N_2 at 1095 K (bottom). Symbols represent the experimental data of Hochgreb and Dryer [13], and lines are predictions of the present CH_2O/O_2 mechanism. Model predictions are time shifted to match the 50% fuel consumption point.

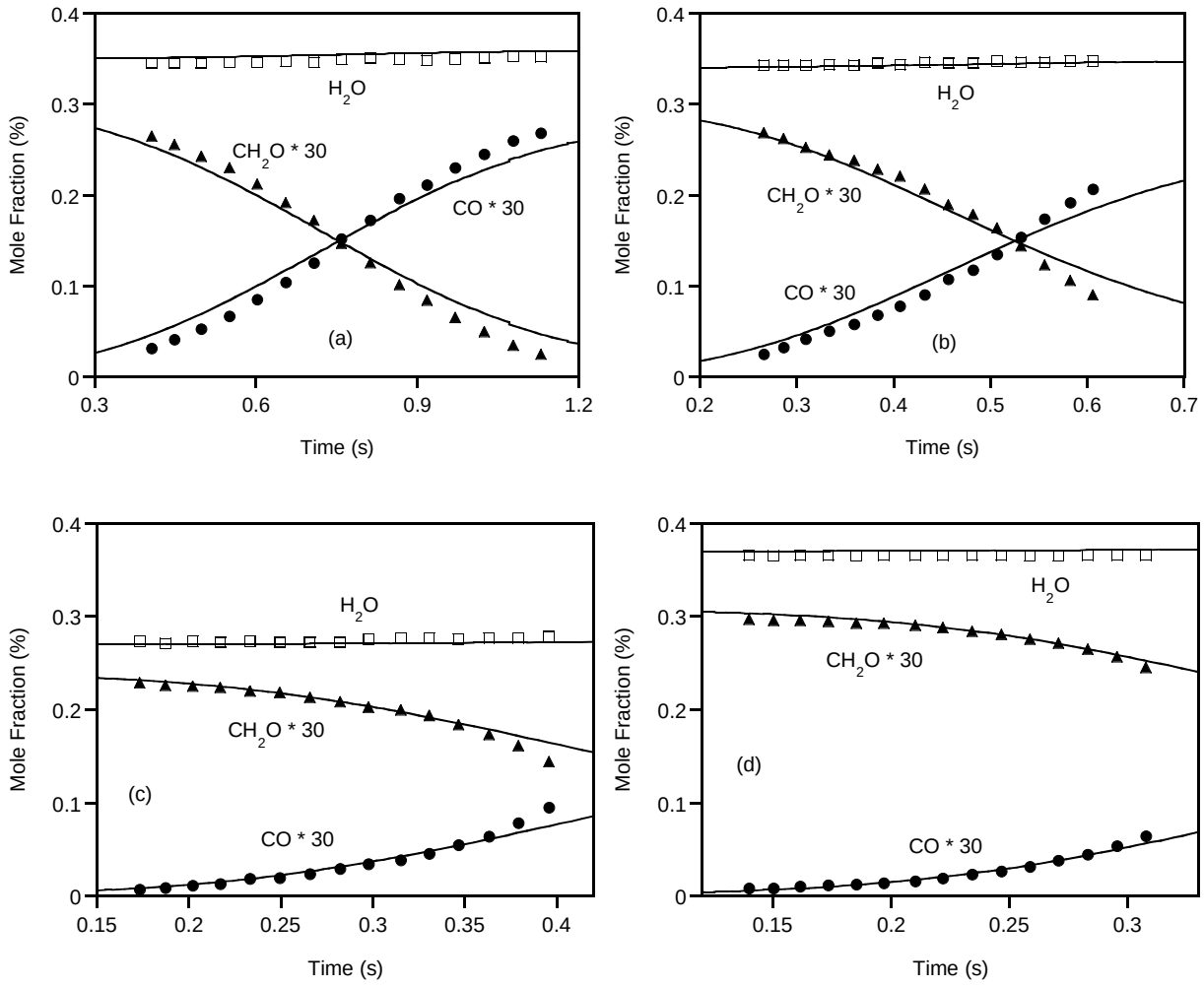

Figure 20 Reaction profiles of $CH_2O/H_2O/O_2/N_2$ mixtures in a flow reactor. Initial conditions are (a) CH_2O 100 ppm, O_2 1.5%, H_2O 0.35% with balance N_2 at 852 K and 6.0 atm; (b) CH_2O 100 ppm, O_2 2.0%, H_2O 0.34% with balance N_2 at 902 K and 3.0 atm; (c) CH_2O 80 ppm, O_2 1.8%, H_2O 0.27% with balance N_2 at 924 K and 2.5 atm; (d) CH_2O 103 ppm, O_2 2.0%, H_2O 0.37% with balance N_2 at 948 K and 1.5 atm. Symbols represent the present experimental data, and lines are predictions of the present CH_2O/O_2 mechanism. Model predictions are time shifted to match the 50% ((a) and (b)) or 90% ((c) and (d)) fuel consumption point.

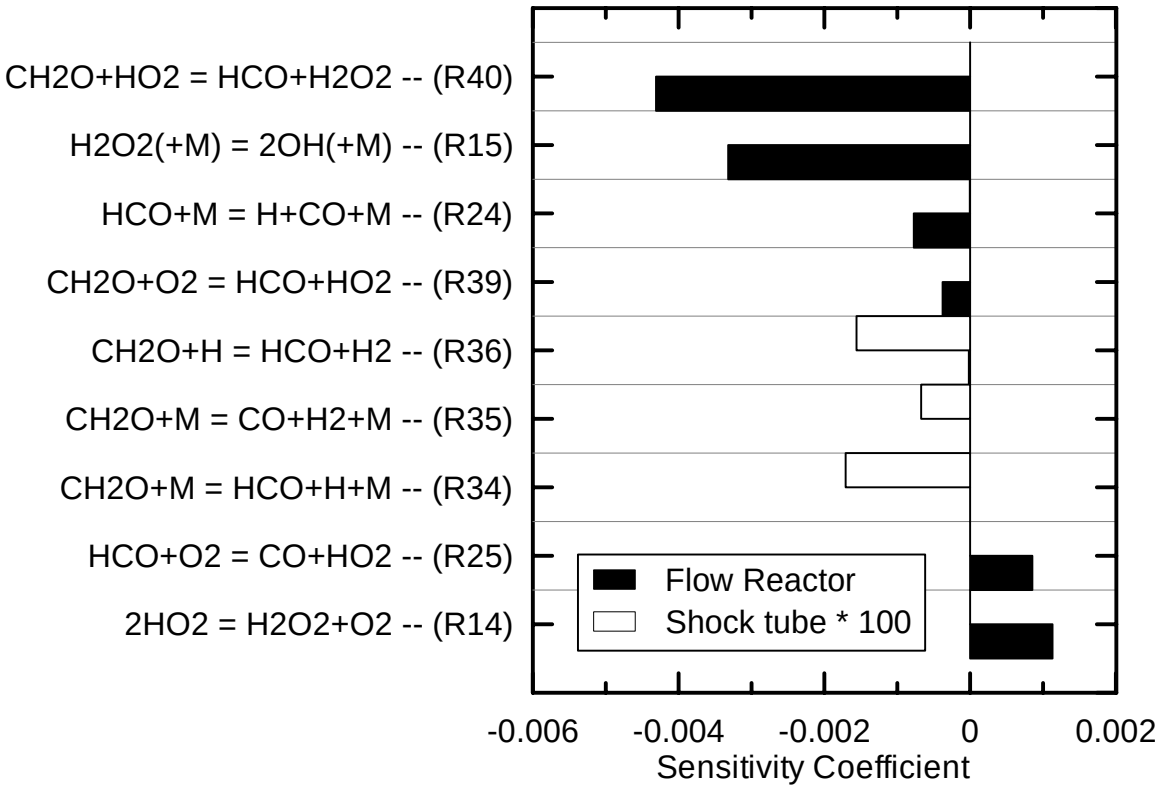

Figure 21 Sensitivity coefficients for flow reactor [13] and shock tube [22] cases. Initial conditions: 0.348% CH_2O, 0.223% O_2 with balance N_2 at 1 atm and 945 K [13]; 100 ppm CH_2O with balance Ar at 2.64 atm and 1907 K [22]. The sensitivity coefficient is calculated by using the present CH_2O/O_2 mechanism, and taken at the time when 50% CH_2O has been consumed. The sensitivity coefficient for shock tube case has been multiplied by 100.

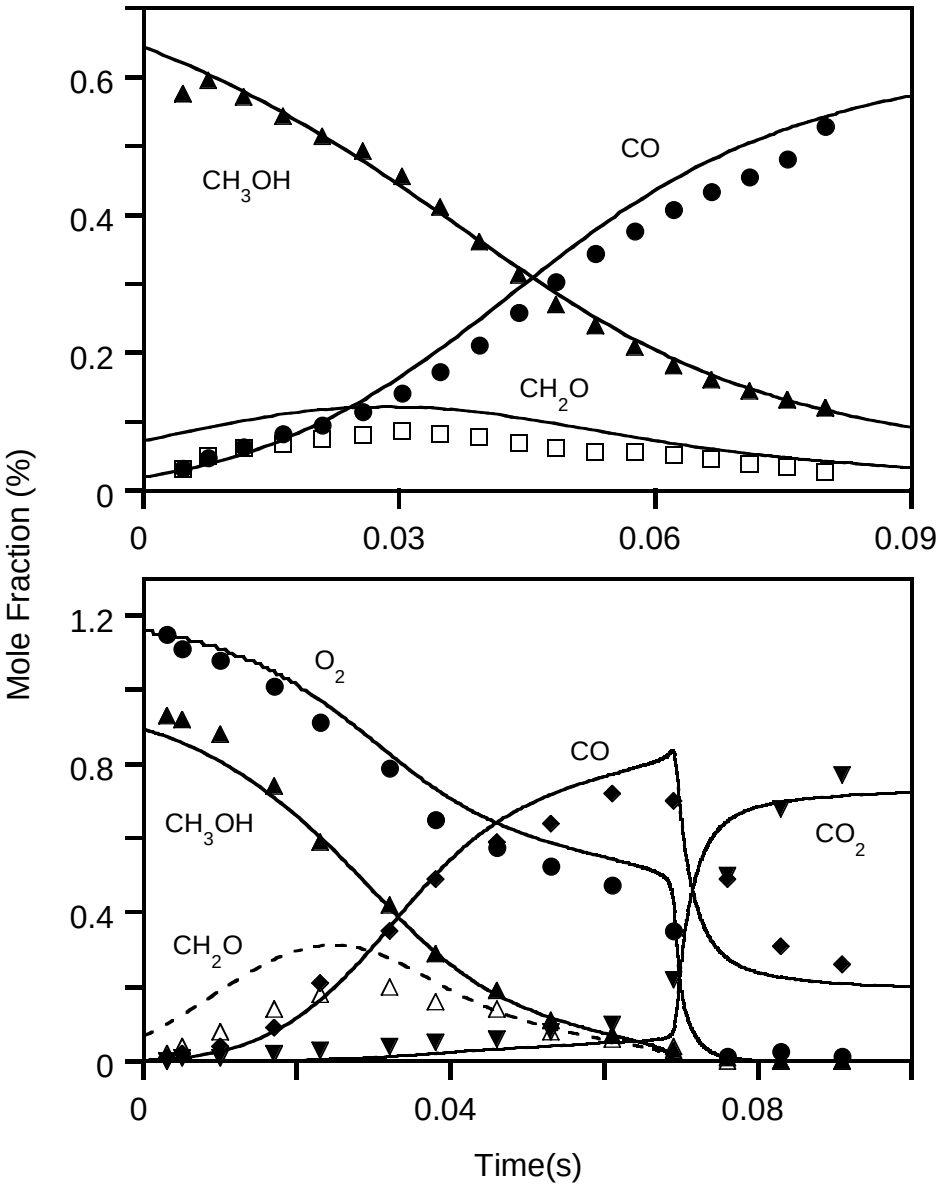

Figure 22 Reaction profiles of $CH_3OH/O_2/N_2$ mixtures in an atmospheric flow reactor. Initial conditions: CH_3OH = 0.735%, O_2 = 0.649% with balance N_2 at 1000 K (top); CH_3OH = 0.93%, O_2 = 1.18% with balance N_2 at 1031 K (bottom). Symbols represent the experimental data of Aronowitz et al. [128] (top) and Norton and Dryer [129] (bottom). Lines are predictions of the present CH_3OH/O_2 mechanism. Model predictions are time shifted to match the 50% fuel consumption point.

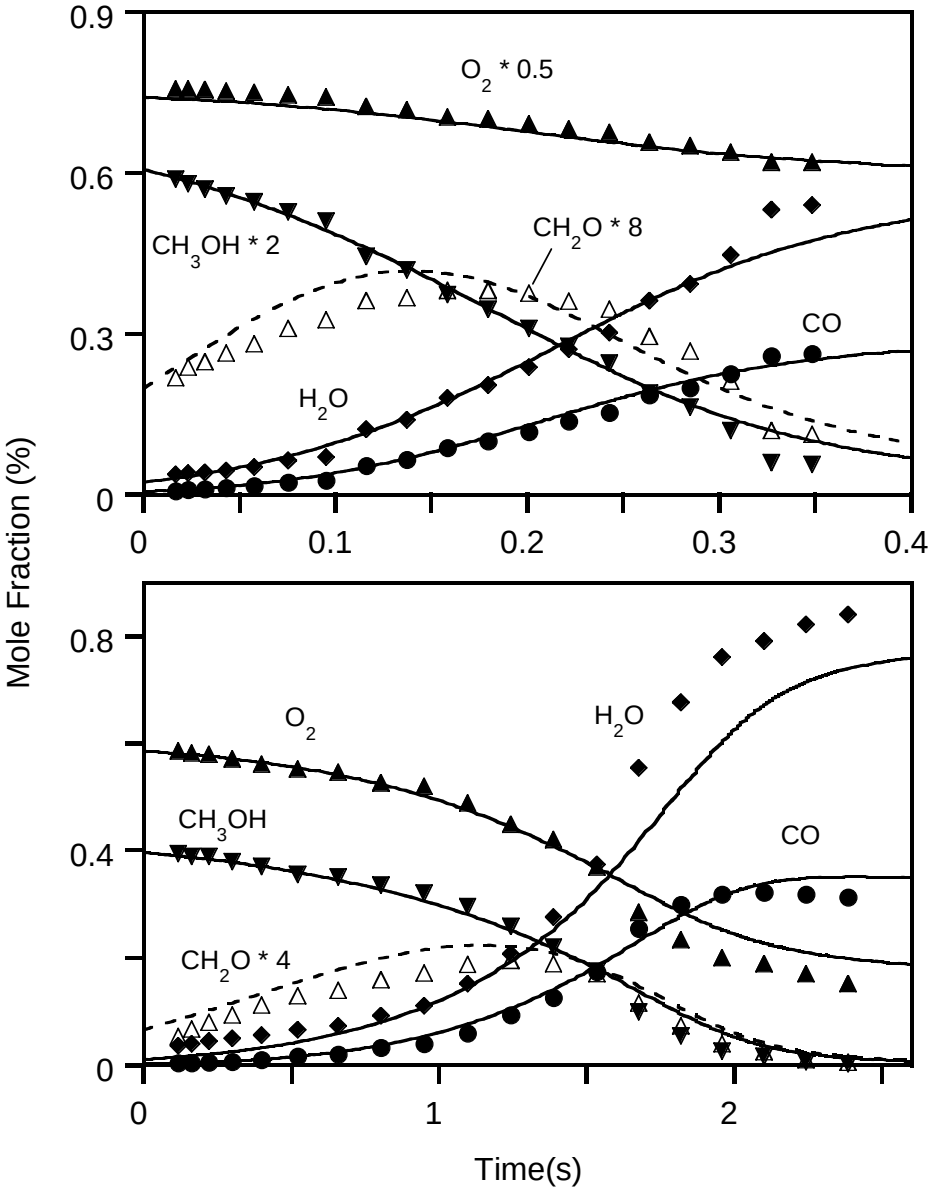

Figure 23 Reaction profiles of $CH_3OH/O_2/N_2$ mixtures in a flow reactor. Initial conditions: CH_3OH = 0.333%, O_2 = 1.5% with balance N_2 at 970 K and 2.5 atm (top); CH_3OH = 0.415%, O_2 = 0.6% with balance N_2 at 783 K and 15.0 atm (bottom). Symbols represent the experimental data of Held [29]. Lines are predictions of the present CH_3OH/O_2 mechanism. Model predictions are time shifted to match the 50% fuel consumption point.

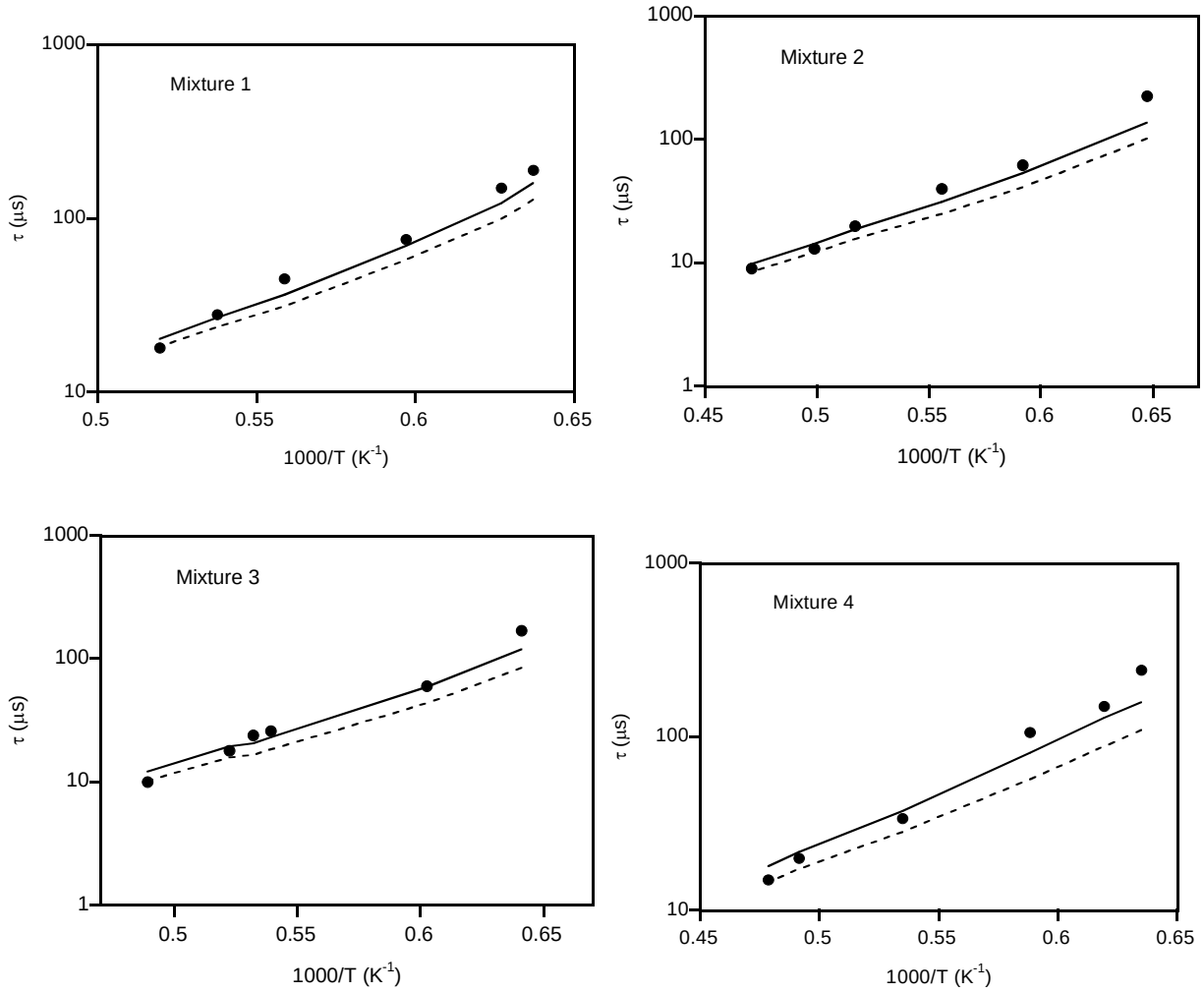

Figure 24 Ignition delay times of CH_3OH/O_2/Ar mixtures in a shock tube. Initial conditions for Mixture 1 are 2.0% CH_3OH, 4.0% O_2 with balance Ar at 1.2 ~ 1.7 atm; for Mixture 2, 1.0% CH_3OH, 2.0% O_2 with balance Ar at 2.9 ~ 3.6 atm; for Mixture 3, 0.75% CH_3OH, 1.5% O_2 with balance Ar at 3.8 ~ 4.5 atm; for Mixture 4, 1.0% CH_3OH, 1.0% O_2 with balance Ar at 2.9 ~ 3.3 atm. τ is defined as the time when the product of CO and O concentrations reaches its maximum value. Symbols represent the experimental data of Bowman [130], solid lines represent predictions of the present CH_3OH/O_2 mechanism, and dashed lines the predictions of Held and Dryer [8].

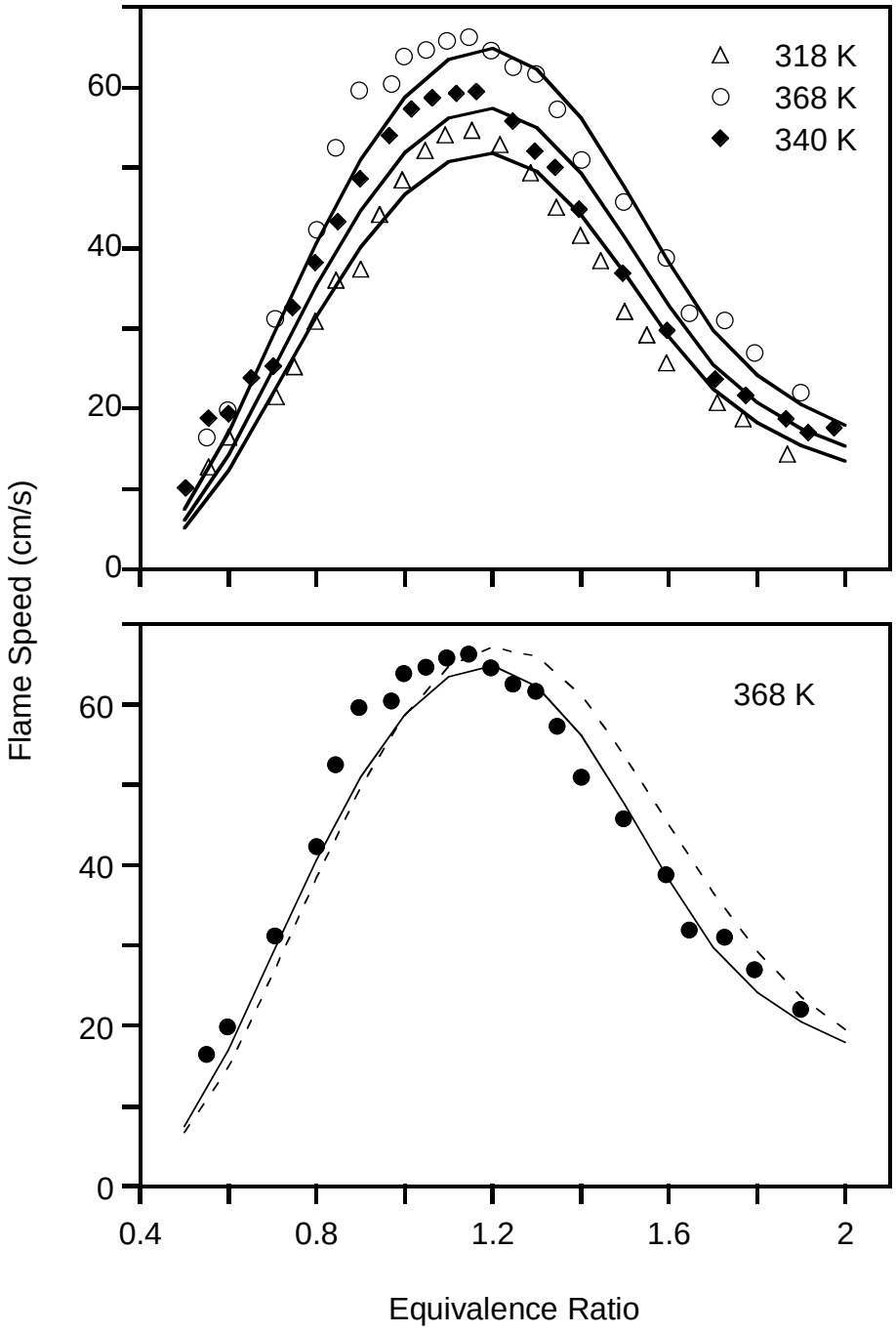

Figure 25 Atmospheric laminar flame speeds of CH_3OH/air mixtures at different initial temperatures (318, 340, and 368 K). Symbols represent the experimental data of Egolfopoulos et al. [131], solid lines are predictions of present CH_3OH/O_2 mechanism, and the dashed line in the bottom figure shows the predictions of Held and Dryer [8].

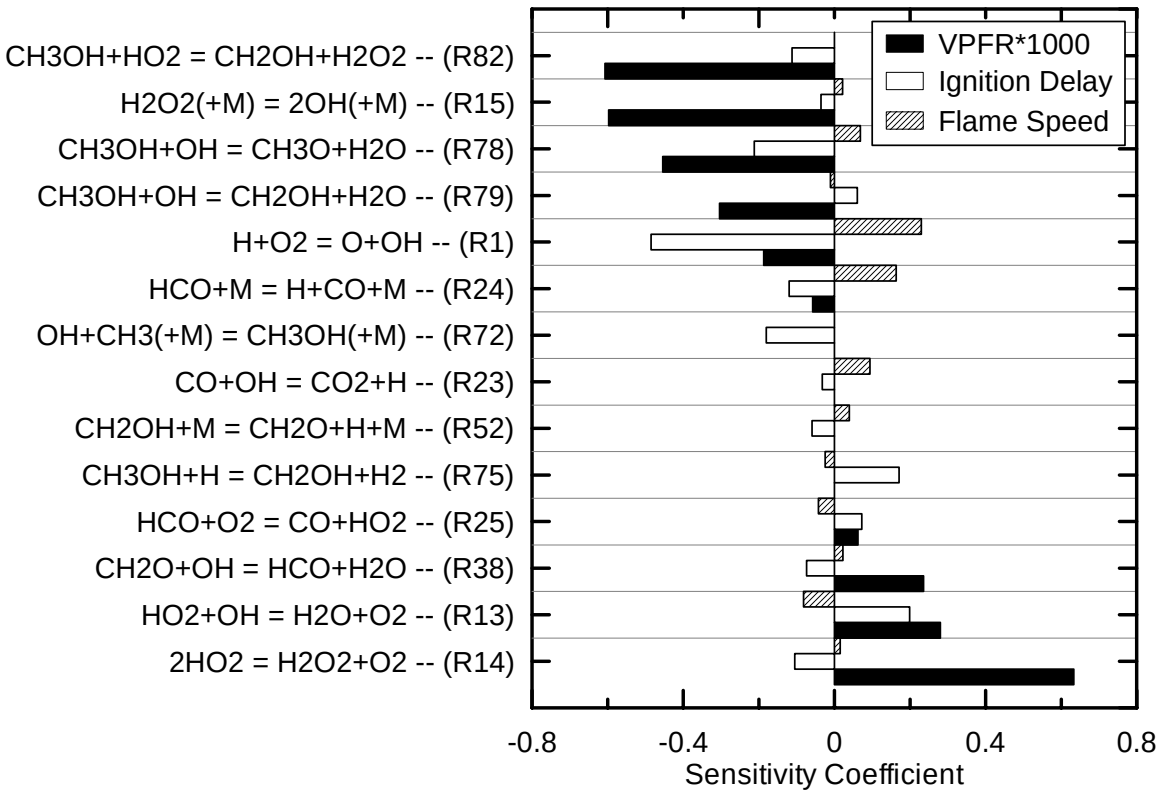

Figure 26 Sensitivity coefficients for flow reactor [29], shock tube [130], and laminar premixed flame [131] cases. Initial conditions are 0.333% CH_3OH, 1.5% O_2 with balance N_2 at 970 K and 2.5 atm [29]; 0.75% CH_3OH, 1.5% O_2 with balance Ar at 4.1 atm and 1660 K [130]; and CH_3OH/air mixture with equivalence ratio of 1.1 at 1.0 atm and 340 K [131]. The sensitivity coefficient for the flow reactor case is taken at the time when 50% CH_3OH has been consumed, and has been multiplied by 1000, except that multiplied by 250 for reactions H_2O_2 (+M) = 2OH (+M) (R15) and CH_3OH+HO_2 = $CH_2OH+H_2O_2$ (R82). The shock tube ignition delay time is defined as the time when the product of CO and O concentrations reaches its maximum.

Appendix B

Published in:
Combustion and Flame, vol. 152, iss. 1-2, 2008, 293-299.

Ignition of syngas/air and hydrogen/air mixtures at low temperatures and high pressures: Experimental data interpretation and kinetic modeling implications

Frederick L. Dryer* and Marcos Chaos

Department of Mechanical and Aerospace Engineering
Princeton University
Princeton, NJ 08544-5263

***Corresponding author:** Prof. Frederick L. Dryer
Department of Mechanical and Aerospace Engineering
Princeton University
Princeton, New Jersey 08544-5263
Fax: (609) 258-6109
Email: fldryer@princeton.edu

Type of article: Short Communication

Ignition of syngas/air and hydrogen/air mixtures at low temperatures and high pressures: Experimental data interpretation and kinetic modeling implications

Frederick L. Dryer[4] and Marcos Chaos

Department of Mechanical and Aerospace Engineering
Princeton University
Princeton, NJ 08544-5263

1. Introduction

An important aspect of minimizing pollutant emissions from industrial gas turbines operating on natural gas has been the implementation of lean, premixed combustion. A similar approach in terms of designing turbines for operating on syngas and pure hydrogen has led to a renewed interest in their combustion dynamics, and experiments have been recently reported from a variety of venues [1-10] under conditions relevant to industrial turbine mixing systems (i.e. lower temperatures and higher pressures; $T < 1000$ K, $10 < P < 30$ atm).

In a recent Short Communication in this journal [1], Petersen et al. reported new data on ignition delay for syngas-air mixtures in a high pressure shock tube and a flow reactor. Experiments were performed at lean conditions ($\phi \sim 0.5$) and for pressure/temperature ranges of 16-29 atm/940-1150 K (shock tube) and 5 atm/760-785 K (flow reactor). These new data were summarized in an Arrhenius-type plot (Fig. 1) along with other recently published data from the rapid compression studies of Walton et al [6] and from an earlier high pressure flow reactor study described in an Electric Power Research Institute report [8]. For comparison purposes, all of the ignition delay data were normalized to conditions of 20 atm pressure [1]. At temperatures lower than about 1050 K, experimental observations of syngas ignition delay, determined by

[4] Corresponding author. *Fax*: (609) 258-6109. *Email*: fldryer@princeton.edu

various criteria, were shown to substantially depart from homogeneous gas phase predictions utilizing any of the recently published H_2/CO detailed kinetic models.

Petersen et al. [1] note "a clear and disturbing disagreement between experiment and model under conditions of direct interest to power generation gas turbines operating on syngas." Through their observations that the disparity is similar across a wide range of experimental venues and in measurements made by a number of independent investigators, Petersen et al. [1] infer that missing gas phase kinetic paths and/or uncertainties in kinetic/thermo-chemical parameters are the most likely sources of the disparity. This inference is further supported by the authors' position that the disagreement between experiment and model "may not be surprising, since few data have existed at the temperature and pressure ranges of the present study to which the (previously) published models could be calibrated." Additional insights as to the source(s) of the disagreement are stated to be beyond the scope of their Short Communication [1].

We are in complete agreement with Petersen et al. [1] that the noted departures of the experimental observations of syngas ignition delay measurements from homogenous gas phase kinetic predictions at temperatures lower than about 1050 K are real and that the reported measurements impose limitations on gas turbine designs for lean premixing of syngas compositions with air. This is likely the most important message that should be taken from [1] and this Short Communication.

In contrast with the suggestion [1] that kinetic model inadequacies may exist since there have been no data to test models in the regime of interest, we argue that: 1) the principal underlying sources of the disparities noted for syngas ignition delays predictions in [1] have been evident in many hydrogen oxidation studies since the 1960's; 2) the disparities between measured and predicted syngas ignition delays are mostly a result of the failure of homogeneous

gas phase predictions to capture perturbations of chemical induction processes in the mild ignition regime by one or more phenomena.

Experiments and analyses of hydrogen-oxygen ignition delay measurements in the "mild" ignition regime show high sensitivity to perturbations by the presence of contaminants in the reactants or on experimental surfaces, compressible fluid dynamic effects, inhomogeneous mixing, and catalysis from particles or surface materials. In any combination, these perturbations can lead to repeatable reductions of the predicted chemical induction time scales in the mild ignition regime by as much as several orders of magnitude. The reactions $CO+HO_2 = CO_2+OH$ and $CO+O+M = CO_2+M$ also modify syngas chemical induction times from those observed for hydrogen-oxygen systems [11], but these modifications are small in comparison to those produced by the perturbation sources listed above.

The opinions presented herein were first offered along with supporting materials at a recent workshop sponsored by the U.S. Department of Energy and the Electric Power Research Institute [12]. The disparities reported in [1] were among several subjects discussed that impact development of new industrial gas turbine systems for operation on hydrogen. The purpose of this Short Communication is to bring these issues to the broader audience of readers of [1]. Moreover, we wish to remind the modeling community that ignition delay measurements in the mild ignition regime are strongly susceptible to perturbations and that model predictions of ignition delays that do not account for these perturbations can be significantly misleading. Finally, as a result of the fact that these sources of perturbations, in any combination, produce within a factor of ten or less the same reduction in chemical induction times in all of the venues discussed in [1], we show here that a simple zero-dimensional representation of their effects as homogenous catalytic processes that promote H_2O_2 production and decomposition to hydroxyl

radicals provides reasonable engineering estimates of the perturbed ignition delay in the mild ignition regime, without modification of homogenous ignition delay predictions at other conditions. A more detailed discussion of the oxidation kinetics of syngas mixtures and hydrogen, including the points summarized in this Short Communication appears elsewhere [13].

2. Discussion

It is historically well known that carbon monoxide oxidation is strongly influenced by the presence of even small amounts of hydrogen-containing species, including moisture, hydrocarbons, and, most importantly, hydrogen itself (e.g. [14-16]). However, the discussions in Ref. 1 do not reflect upon the similarity in ignition delay behavior for syngas-oxygen in shock tubes and other experimental venues with those found in the literature for pure hydrogen-oxygen mixtures. .

For example, disparities between hydrogen-air shock tube ignition delay experiments and homogenous predictions have been reported, analyzed, and discussed in the literature since the 1960's, see for example [17-32]. Above about 1200 K, the so called "strong" or "sharp" ignition is observed [18], with reaction initiation starting at a single locus point in the reflected region near the end-wall and quickly transitioning to a uniform detonation wave. At lower temperatures, a "mild" or "weak" ignition occurs, characterized by the appearance of random flame kernels, with eventual transition to a combusting front. The work of Meyer and Oppenheim [23], later reviewed by Oppenheim [26], also showed that mild ignition is a *multidimensional* process [25], with initial random flame kernels first appearing close to the shock tube walls and stagnant corners [28]. Chemical induction times in the mild ignition regime were also found to be very sensitive to temperature variations behind reflected shock waves. These results have been

confirmed by the extensive numerical work of Oran and coworkers [33-35] as well as in the early work of Gardiner and Wakefield [24]. The recent shock tube studies of hydrogen oxidation by Blumenthal et al. [27, 29], Wang et al. [30], and Martynenko et al. [31] add further experimental detail. Blumenthal et al. [27, 29] performed temporal measurements of the appearance and transition of the first flame kernel to a detonation in the mild ignition regime. Martynenko et al. [31] showed that during mild ignition, OH emission first occurs in the peripheral regions of the shock tube, close to the walls.

Fig. 1 reproduces the syngas data presented by Petersen et al. [1] along with representative results from the H_2/air shock tube study of Blumenthal et al. [27] and homogenous model predictions for both syngas-air and hydrogen-air ignition delays using the mechanism of Li et al. [11]. Conditions for the Blumenthal data [27] ($\phi = 0.42$) are similar to those reported for syngas [1] ($\phi \sim 0.5$). For comparison purposes, experimental data are normalized under the same assumptions used in [1] to 20 atm; modeling predictions were calculated directly at this pressure. The near identical experimental trends of ignition delays for the syngas-air and hydrogen-air mixtures considered in [1, 27] are striking. To be noted as well, is that the model predictions for both are also essentially identical, confirming that the influence of the CO sub-mechanism ($CO+OH = CO_2+OH$, $CO+O+M = CO_2+M$, $CO+HO_2 = CO+OH$) on ignition delay predictions is small in comparison to the influence of the hydrogen-oxygen subset. We have shown elsewhere [11] that the reaction $CO+HO_2 = CO+OH$, which has historically had a large uncertainty in its rate constant, has influence on chemical induction times through its competition with $H_2+HO_2 = H_2O_2+H$, but is insignificant in influencing post-induction chemistry [11]. We agree with Petersen et al. [1] that uncertainties in this reaction are not responsible for the disparities in experiments and predictions discussed in [1].

Blumenthal et al. [27] experimentally identified the onset of strong and weak ignitions experimentally using Schlieren imaging. In Fig. 1, the hydrogen strong ignition cases (filled circles) are modeled reasonably well by homogenous kinetic calculations, whereas weak ignition data (open circles) differ from predictions by up to three orders of magnitude, similar to the comparison of observations and predictions for syngas mixtures. The onset of weak ignition occurs for approximately $T < 1000$ K and it is noted from Fig. 1 that this point also corresponds to the temperature range at which order-of-magnitude discrepancies are observed for syngas ignition comparisons [1].

Through combined sensitivity/stability analysis methods, Yetter et al. [36] provide criteria to delineate mild and strong ignition processes kinetically as functions of initial reaction conditions. The transition temperatures noted in [27] are consistent qualitatively with those associated with these kinetic definitions. Yetter et al [36] show sources of the strong sensitivity of mild ignition and chemical induction times to perturbations and delineate the most important reactions associated with mild and strong ignition phenomena.

Blumenthal et al. [27, 29] note that inhomogeneities in temperature and concentration caused by compressible fluid dynamic effects related to shock reflection and bifurcations in the shock tube end-wall corners may not be large enough to entirely explain the discrepancies in gas phase kinetic predictions and experimental observations of ignition. Oran et al. [33] showed that small temperature perturbations of 10 K lead to variations in induction times predicted by their numerical scheme of a factor of two. We estimate that by themselves, temperature variations on the order of 150 K would be required to bring homogenous kinetic predictions into line with experimental observations in [27]. It has also been hypothesized that catalytic effects due to the presence of small particles in the gas [27, 37, 38] could be important in some observations. We

also add to this hypothesis that catalytic surface effects may occur in reflected shock experiments in the mild ignition regime, since end-wall/corner tube surfaces can be estimated to have fast transient heating times [39] in comparison to the experimentally measured chemical ignition delays, for example, under the conditions studied in [27].

Further work is clearly necessary to establish quantitative contributions of each type of perturbation that results in near-elimination of chemical induction times (in comparison to overall ignition delay times) under mild ignition conditions. Without question, however, these measurements should not be expected to be predicted by zero-dimensional (e.g., SENKIN [40]) modeling calculations, as ignition takes place *inhomogeneously* [23-31] especially in high energy density mixtures [31]. Unfortunately, the computational complexity of modeling the multi-dimensional phenomena and their coupling with detailed chemical kinetics has, to date, hampered comprehensive model studies to quantitatively determine the relative importance of the perturbing effects that might be present in shock tube ignition delay observations [41].

An intriguing point raised in [1] is that data collected in flow reactors [1, 8] and in recent rapid compression experiments in the University of Michigan Rapid Compression Facility (UM-RCF) [6] for high pressure, high energy density syngas-oxygen mixtures apparently "line up" with the "disparate" shock tube experimental ignition delay measurements. Fig. 1 shows that these data also share a parallelism in behavior with those for hydrogen-oxygen in shock tubes.

Addressing the flow reactor measurements first, work not discussed in [1] show that the shortening of ignition delays in flow reactors is not related solely to the energy density of the reacting mixtures studied. Very dilute flow reactor studies of hydrogen-oxygen [42-45] and carbon-monoxide-hydrogen-water-oxygen kinetics [15, 16, 46, 47] at Princeton have shown disparities with ignition delay predictions similar to those for the high energy density flow

reactor results summarized in [1]. Swigart [42] studied highly diluted hydrogen-oxygen kinetics at atmospheric pressure and at temperatures of 920-980 K in stainless steel reactor tubes of 2.54, 5.08, and 7.62 cm diameter. A distinct increase in the overall rate of the reaction with decreasing reactor diameter was observed and attributed to catalytic activity on the stainless steel walls. Additional measurements in silica reactor tubes [43] showed similar behavior for tube diameters smaller than 10 cm. No ignition delay measurements could be extracted in any of these experiments, as the reaction actually began during mixing.

Vermeersch [44] was able to perform ignition delay as well as post induction kinetic measurements for highly diluted $H_2/O_2/N_2$ mixtures in a 10 cm diameter silica-walled flow reactor tube at pressures from 1 to 9 atm. While the gas phase reaction rates of hydrogen-oxygen mixtures *after* mixing and chemical induction occurred were found to agree with homogenous kinetic predictions, the measured ignition delays reported in [44] were several orders of magnitude shorter than predicted, similar to what is observed in Fig 1. The shortened ignition delays were attributed to mixing and catalytic effects occurring in the mixing region. It should also be noted that Vermeersch [44] showed that catalytic surface effects were absent in the post induction oxidation as a result of the large reactor diameter used (10 cm). This same flow reactor was later employed in the post-induction kinetic studies of Mueller et al. [45, 47].

Similar results in terms of perturbations of chemical induction times were observed in the Princeton flow reactor studies of Yetter [15, 16] and Mueller et al. [45, 47]. These results are consistent with other research performed on the moist carbon monoxide oxidation system. In analyzing and modeling this work, we showed that kinetic perturbations in the mixing region can have significant effects on chemical induction processes (chemical “ignition delay times”), but do not significantly affect the observed post induction chemistry [48].

It is clear from these results that the differences in experimental observations and homogenous kinetic predictions of chemical induction times are present even at atmospheric pressure and in highly diluted mixtures of hydrogen-oxygen and carbon-monoxide-oxygen systems in the presence of hydrogen containing species. We have avoided using flow reactor ignition delay measurements for kinetic interpretation purposes because of the observed perturbations in the mixing region and the difficulty in interpreting multi-dimensional mixing and catalytic wall interactions. It is on the basis of these observations that our group adopted reaction "time shifting" as a means of comparing experimental observations of post induction oxidation kinetics with homogenous plug flow kinetic predictions [16].

The UM-RCF data [6] reported in [1] also appear to follow the same trends of other data discussed there, even though the data appear to exhibit considerable scatter. The regression analysis of Walton et al. [6] (considering pressure, temperature, equivalence ratio, and oxygen mole fraction as key parameters) yields a goodness of fit R^2-value of only 0.57. This statistical value, however, is consistent with other syngas flow reactor and shock tube studies shown in Fig. 1 at low temperatures. The low correlation of these data is a strong indication that other dependencies exist which are not represented by the chosen correlation parameters.

Drawing upon the similarities between hydrogen and syngas systems discussed above, the UM-RCF data [6] can also be compared against hydrogen ignition data collected in rapid compression machines (RCMs) [3, 49]. Walton et al. [6] point out that their measurements agree (on the order of magnitude of delay times measured) with the RCM data of Lee and Hochgreb [49] (at high temperatures) and indicate that a more quantitative comparison is complicated since different mixtures were used (i.e. hydrogen-oxygen-argon [49]). However, when properly scaled, a quantitative comparison can be performed between the two studies [13]. Whereas the two sets

of data [6, 49] are very similar at temperatures above 1000 K, the UM-RCF experiments result in significantly shorter ignition delays at lower temperatures. The overall activation energy (temperature dependence) of the data of Walton et al. [6] is considerably different from RCM hydrogen ignition studies [3, 49] (~12.5 kcal/mole versus ~75 kcal/mole), which more closely approximate that exhibited by homogenous gas phase kinetic predictions [13]. The temperature dependence of [6] is heavily weighted by the short ignition delays measured at lower temperatures. Walton et al. [6] attribute the difference in activation energies between model and data to the uncertainty of the reaction $CO+HO_2 = CO+OH$; this has since been clearly shown not to be the case [1, 13].

As discussed above, chemical induction processes are strongly influenced by various experimental perturbations and they appear to be quite different in the UM-RCF and other RCM devices. Types of perturbations on ignition delay measurements for rapid compression experiments discussed in the literature include surface contamination, particles as catalytic centers, and impurities [37, 38]. On the other hand, Walton et al. [6, 50] report the presence of pre-ignition reaction fronts as well as particles in the reaction chamber. All can have significant influence in the mild ignition regime.

A sensitivity analysis of what controls ignition delay times under mild ignition conditions at high pressures [13, 36] shows that the most important, controlling reactions are those that lead to generation of reactive radical species from hydroperoxyl radicals, namely $H_2+HO_2 = H_2O_2+H$ and $H_2O_2+M = OH+OH$. If radial diffusion time scales to/from walls are assumed to be sufficiently rapid in comparison to the observed ignition delay times in the experimental configurations considered, surface catalysis may remove the rate-limiting behavior of these gas phase reactions, significantly shorten chemical induction times, and therefore measured ignition

delays. We approximated this effect here as homogeneous gas phase processes with modified rate constants. Modeling of the syngas conditions shown in Fig. 1 using the mechanism of Li et al [11] including catalytically accelerated rates for only the above reactions (using rates adopted from Deutschmann et al. [51]; more details can be found in [13]) results in the dash-dotted curve shown in the figure, in reasonable agreement with observations. Localized radical production from catalytically accelerated peroxide formation/decomposition between the third and extended second limits leads to an overall straight chain kinetic conversion to H atoms and OH radicals and the exothermic reaction of OH with hydrogen to produce water and H rapidly drives the reacting systems across the extended second limit.

Clearly additional effort is needed to experimentally confirm the relevance of catalytic processes as a perturbing factor in each of the above experimental venues. Noting the sensitivity of chemical induction times to the hydrogen peroxide intermediate chemistry in the mild ignition regime, the hypothesis that surfaces can promote chemical induction processes, leading to further reaction and crossing of the extended second explosion limit is a hypothesis entirely consistent with all of the experimental observations. An equally important point stressed above is that the combination of several types of perturbations can lead to the same order of magnitude reduction in the chemical induction time scales. The simple approximating assumption that the perturbation is derived solely by homogenous catalysis of the two above reactions leads to an empirical modeling result that can be fitted to the experimental observations reported in Petersen et al. [1]. Moreover, at temperatures above the mild ignition regime, as well as at very low reaction temperatures, predictions return to those observed without homogenous catalysis of these reactions. The empirically fitted approximation can serve as an important engineering tool for conservative computational predictions in designing gas turbine mixing systems.

3. Conclusion

In summary, we note that the magnitude of ignition delay observations and homogenous kinetic calculations discussed in Petersen et al. [1] are a result in large measure to departures of the experimental configurations from behavior dominated solely by homogeneous gas phase kinetics alone. In the regime of interest (higher pressures, lower temperatures) the hydrogen-oxygen chemical induction processes can be significantly perturbed by several non-homogeneous effects, which include catalytic aberrations. The multiple perturbations that can significantly affect induction chemistry are very difficult to remove in research experiments and nearly impossible to control in engineering applications. The implications for developing lean premixing schemes for advanced syngas gas turbine applications are that designs must consider the inherent presence of these perturbations on ignition delay as well as those that might occur from potential particle contamination of the air stream exiting the compressor, if stimulated flashback into the mixing region is to be precluded.

We acknowledge that improvements in kinetic parameters for gas phase reactions in the H_2/CO system can be made that may influence predicted ignition delays by factors, but not by orders of magnitude in the mild ignition regime. Compressible flow, physical mixing, and/or catalytic surface processes occurring in the mild ignition regime are the main sources of the departure of experimentally observed ignition delays from homogenous gas phase kinetic predictions. The departures first described decades ago for hydrogen-air systems are evident in syngas-air observations recently reported [1].

Finally, we wish to point out that two stage ignition phenomena observed in many hydrocarbon-air systems display many multi-dimensional characteristics similar to those found

for hydrogen-air (i.e. local ignition kernels, coalescence into reaction fronts; single ignition kernels, development into detonations, e.g., see [52]). The "hot ignition" phenomena observed in these systems are controlled by the decomposition of hydrogen peroxide [53]. Catalytic processes that might potentially yield radicals from hydrogen peroxide at lower temperatures need to be carefully considered in ignition delay measurements of hydrocarbon-air systems at high pressures

Acknowledgements

We wish to acknowledge helpful discussions with Prof. R.A. Yetter of Pennsylvania State University. This work was supported by the U.S Department of Energy under Grant Number DE-FG02-86ER13503 from the Chemical Sciences, Geosciences and Biosciences Division, Office of Basic Energy Sciences, Office of Science and by the Pittsburgh-National Energy Technology Laboratories under Grant Number DE-FG26-05NT42544.

References

1. E.L. Petersen, D.M. Kalitan, A.B. Barrett, S.C. Reehal, J.D. Mertens, D.J. Beerer, R.L. Hack, V.G. McDonell, Combust. Flame 1-2 (2007) 244-247.
2. C.G. Fotache, Y. Tan, C.-J. Sung, C.K. Law, Combust. Flame 120 (2000) 417-426.
3. G. Mittal, C.-J. Sung, R.A. Yetter, Int. J. Chem. Kinet. 38 (2006) 516-529.
4. D.M. Kalitan, E.L. Petersen, J.D. Mertens, M.W. Crofton, ASME Paper GT2006-90488 (2006).
5. H. Sun, S.I. Yang, G. Jomaas, C.K. Law, Proc. Combust. Inst. 31 (2007) 439-446.

6. S.M. Walton, X. He, B.T. Zigler, M.H. Wooldridge, Proc. Combust. Inst. 31 (2007) 3147-3154.
7. M.P. Burke, X. Qin, Y. Ju, F.L. Dryer, Fifth U.S. Combustion Meeting, San Diego, CA (2007), paper A16.
8. W.T. Peschke, L.J. Spadaccini, Electric Power Research Institute, Report No. EPRI AP-4291 (1985).
9. J.H. Chen, V.J. Jermakian, G.S. Samuelsen, V.G. McDonell, University Turbine Systems Research, Report No. SR084 (2003); http://www.clemson.edu/scies/utsr/FinalSR084.pdf.
10. D.J. Beerer, M.U. Greene, G.S. Samuelsen, V.G. McDonell, University Turbine Systems Research, Report No. SR112 (2006).
11. J. Li, Z. Zhao, A. Kazakov, M. Chaos, F.L. Dryer, J.J. Scire, Int. J. Chem. Kinet. 39 (2007) 109-136.
12. F.L. Dryer, M. Chaos, Workshop on Hydrogen Combustion in Gas Turbines, EPRI Washington, March 22, 2007.
13. M. Chaos, F.L. Dryer, Special Issue on Syngas Combustion, Combust. Sci. Tech. (To Appear).
14. T.A. Brabbs, F.E. Belles, R.S. Brokaw, Proc. Combust. Inst. 13 (1971) 129-136.
15. R.A. Yetter, F.L. Dryer, H. Rabitz, Combust. Sci. Technol. 79 (1991) 97-128.
16. R.A. Yetter, F.L. Dryer, H. Rabitz, Combust. Sci. Technol. 79 (1991) 129-140
17. G.L. Schott, J.L. Kinsey, J. Chem. Phys. 29 (1958) 1177-1182.
18. R.A. Strehlow, A. Cohen, Phys. Fluids 5 (1962) 97-101.
19. H. Miyama, T. Takeyama, J. Chem. Phys. 41 (1964) 2287-2290.
20. G.B. Skinner, G.H. Ringrose, J. Chem. Phys. 42 (1965) 2190-2192.

21. V.V. Voevodsky, R.I. Soloukhin, Proc. Combust. Inst. 10 (1965) 279-283.

22. C.B. Wakefield, D.L. Ripley, W.C. Gardiner, J. Chem. Phys. 50 (1969) 325-332.

23. J.W. Meyer, A.K. Oppenheim, Proc. Combust. Symp. 13 (1970) 1153-1164.

24. W.C. Gardiner, C.B. Wakefield, Astro. Acta 15 (1970) 399-409.

25. K. Terao, Jap. J. Appl. Phys. 16 (1977) 29-38.

26. A.K. Oppenheim, Phil, Trans. R. Soc. Lond. A 315 (1985) 471-508.

27. R. Blumenthal, K. Fieweger, K.H. Komp, G. Adomeit, B.E. Gelfand, Proc. of the 20th Int. Symp. on Shock Waves (1995) 935-940.

28. R. Blumenthal, G. Adomeit, 3rd Workshop on Modelling of Chemical Reaction Systems, Heidelberg, Germany (1996); http://www.iwr.uni-heidelberg.de/groups/reaflow/user/crs96/Program/Contrib/a37ad.htm

29. R. Blumenthal, K. Fieweger, K.H. Komp, G. Adomeit, Combust. Sci. Tech. 113-114 (1996) 137-166.

30. B.L. Wang, H. Olivier, H. Grönig, Combust. Flame 133 (2003) 93-106.

31. V.V. Martynenko, O.G. Penyaz'kov, K.A. Ragotner, S.I. Shabunya, J. Eng. Phys. Thermophys. 77 (2004) 785-793.

32. P. Sabia, E. Schieβwohl, M.R. de Joannon, and A. Cavaliere, *Turkish J. Eng Env. Sci.* 30, (2006) 127-134.

33. E.S. Oran, T.R. Young, J.P. Boris, A. Cohen, Combust. Flame 48 (1982) 135-148.

34. E.S. Oran, J.P. Boris, Combust. Flame 48 (1982) 149-162.

35. E.S. Oran, V.M. Gamezo, Combust. Flame 148 (2007) 4-47.

36. R.A. Yetter, H. Rabitz, R. M. Hedges, Int. J. Chem. Kinet. 23 (1991) 251-278.

37. J.E. EIsworth, W.W. Haskell, I.A. Read, Combust. Flame 13 (1969) 437-438.

38. W.W. Haskell, SAE Paper 700059 (1970).

39. P.P. Andreev, Y.M. Tsirkunov, J. Eng. Phys. Thermophys. 51 (1986) 909-914.

40. A.E. Lutz, R.J. Kee, J.A. Miller, Technical Report SAND87-8248, Sandia National Laboratories (1987).

41. E.S. Oran, personal communication.

42. R. Swigart, M.S.E. Thesis, “A Study of the Kinetics of the Hydrogen-Oxygen Reaction in a New Flow Reactor,” Aerospace and Mechanical Sciences, Princeton University, Princeton, NJ (1958), Report No. 432.

43. R.F. Sawyer, Ph.D. dissertation, “The Homogeneous Gas Phase Kinetics of Reactions in the Hydrazine - Nitrogen Tetroxide Propellant System," Aerospace and Mechanical Sciences, Princeton University, Princeton, NJ (1965), Report No. 761.

44. M.L. Vermeersch, Ph.D. dissertation, "A Variable Pressure Flow Reactor for Chemical Kinetics Studies: Hydrogen, Methane and Butane Oxidation at 1 to 10 Atmospheres and 880 to 1,040 K,” Department of Mechanical and Aerospace Engineering, Princeton University, Princeton, NJ (1991), Number 1916-T.

45. M.A. Mueller, T.J. Kim, R.A. Yetter, F.L. Dryer, Int. J. Chem. Kinet. 31 (1999) 113-125.

46. R.A. Yetter, Ph.D. dissertation, “An Experimental/Numerical Study of Carbon Monoxide-Hydrogen-Oxygen Kinetics with Applications of Gradient Sensitivity Analysis,” Department of Mechanical and Aerospace Engineering, Princeton University, Princeton, NJ, 1985. MAE Report No. 1703-T

47. M.A. Mueller, R.A. Yetter, F.L. Dryer, Int. J. Chem. Kinet. 31 (1999) 705-724.

48. R.A. Yetter, F.L. Dryer, H. Rabitz, Combust. Flame 59 (1985) 107-133.

49. D. Lee, S. Hochgreb, Int. J. Chem. Kinet. 30 (1998) 385-406.

50. S.M. Walton, X. He, B.T. Zigler, M.S. Wooldridge, Combust. Flame 150 (2007) 246-262.

51. O. Deutschmann, R. Schmidt, F. Behrendt, J. Warnatz, Proc. Combust. Inst. 26 (1998) 1747-1754.

52. K. Fieweger, R. Blumenthal, G. Adomeit, Combust. Flame 109 (1997) 599-619.

53. A. Kazakov, M. Chaos, Z. Zhao, F.L. Dryer, J. Phys. Chem. A 110 (2006) 7003-7009.

FIGURE CAPTIONS

Fig. 1. Ignition delay times of syngas [1, 6, 8] and hydrogen mixtures [27]. Conditions: 38.6% H_2 + 51.1% CO + 10.3% CO_2 + Air; $\phi = 0.5$, $16.5 < P < 28.9$ atm [1, shock tube]; $\phi = 0.5$, $11.9 < P < 23$ atm [8]; 50% H_2 + 50% CO + Air, $0.33 < \phi < 0.6$, $5.0 < P < 5.3$ atm [1, flow reactor]; $6.7 < H_2 < 13.6\% + 4.5 < CO < 9.1\% + 16.2 < O_2 < 18.7\% + 44.1 < N_2 < 63.2\%$ in balance CO_2, $0.3 < \phi < 0.7$, $12 < P < 23.5$ atm [6]; 15% H_2 in air, $35 < P < 47$ bar [27]. Filled and open circles correspond to strong and weak ignition events, respectively [27]. All experimental data have been normalized to 20 atm assuming proportionality to P^{-1} [1]. Lines correspond to ignition delay calculations performed using the mechanism of Li et al. [11] at 20 atm; the solid line corresponds to the syngas mixture used in the shock tube experiments [1], the dashed line to the conditions of Blumenthal et al. [27], and the dash-dot line are predictions obtained for syngas ignition by catalyzing reactions involved in the formation and decomposition of H_2O_2 (see text). To improve clarity, modeled results are not shown for times greater than 1 s although it is noted that predictions can reach values of approximately 1000 s for the lowest temperatures ($T \sim 630$ K).

FIGURES

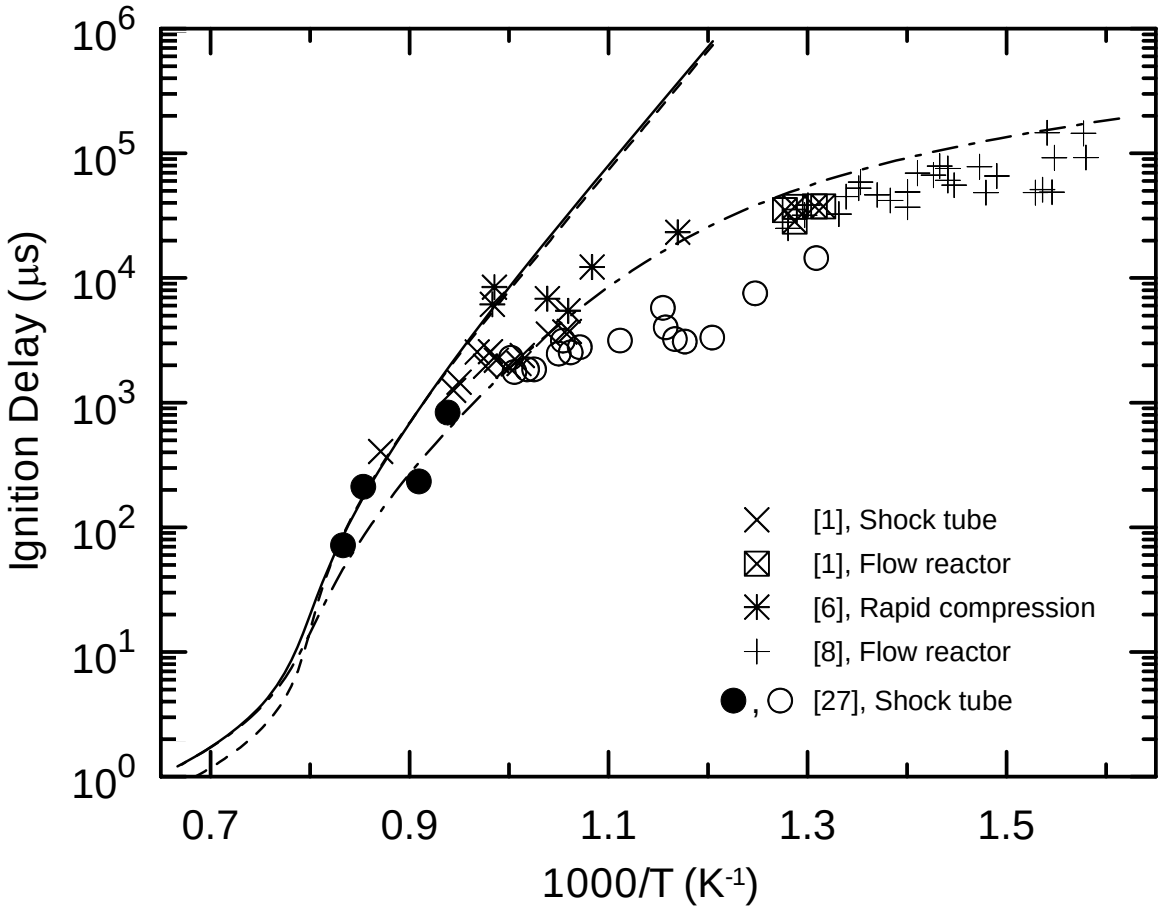

Figure 1

Appendix C

Accepted for publication in:
Combustion Science and Technology, on November 2007.

Syngas Combustion Kinetics and Applications

Marcos Chaos and Frederick L. Dryer
Department of Mechanical and Aerospace Engineering
Princeton University
Princeton, NJ 08544

Corresponding author: Dr. Marcos Chaos
Department of Mechanical and Aerospace Engineering
Princeton University
Princeton, New Jersey 08544-5263
Fax: (609) 258-6109
Email: mchaos@princeton.edu

Submitted for publication in the
syngas combustion special issue of
Combustion Science and Technology

Syngas Combustion Kinetics and Applications

Marcos Chaos and Frederick L. Dryer
Department of Mechanical and Aerospace Engineering
Princeton University
Princeton, NJ 08544

Abstract

Strong interest in the use of coal-derived syngas in gas turbines has led to recent experimental studies that highlight the important features of H_2/CO combustion at high pressures and relatively low temperatures. In the present study these investigations are reviewed, evaluated, and chemical kinetic updates based on these new results are discussed. Disparities observed between experimental measurements and kinetic model predictions of high pressure ignition delay and burning velocity are noted and the effect that surfaces, trace impurities, and contaminants may have on the H_2/CO kinetic system are elucidated. In particular, the impurity coupling with NO_x is discussed in relation to energy conversion processes involving hydrogen as a fuel component. An example of its importance to pre-ignition in reciprocating engine applications is also demonstrated.

***Keywords*:** hydrogen, carbon monoxide, kinetics, ignition, flame speeds, pressure, impurities, iron pentacarbonyl, nitrogen oxides.

INTRODUCTION

As world energy demands and environmental concerns continue to grow, combustion of reformed fuels is getting more attention due to a desire for greater fuel supply flexibility and security. Among these fuels, "syngas" fuels (synthesis gases containing varying amounts of carbon monoxide and hydrogen as the fuel components) are expected to play an important role in future energy production. Syngas mixtures can be produced from a wide variety of sources including coal, biomass, organic waste, and refinery residuals. Because of the large coal resources available worldwide (especially in the U.S., Europe, and Asia), there is renewed interest in coal-based integrated gasification combined cycle (IGCC) power generation. In these and other modern high-efficiency/low-emission combined cycle power plants, syngas is produced by partial oxidation of coal in pure oxygen and steam in high pressure gasifiers. Gas turbine engines are used as topping cycles that take advantage of the high temperature combustion products from the gasification process to improve the overall efficiency of the power plant. Most of the harmful and corroding contaminants (e.g. SO_x, H_2S, NO_x, particulates) can be removed in the post-gasification process prior to entering the turbine. Water-gas shift technologies can also be used to generate pure hydrogen from syngas. Furthermore, syngas mixtures can be used to produce liquid fuels through Fischer Tropsch conversion (Dry, 2002; Wilhelm et al., 2001). The implementation of carbon capture and storage (Chiesa et al., 2005) has the potential for "greening" fossil fuel energy resources, particularly when fuel production, electrical power generation, and chemical production processes are integrated along with carbon capture and storage. This article will principally consider syngas combustion properties relevant to gas turbine applications.

Combustors used in gas turbines operating on syngas and/or hydrogen must be "fuel flexible" as syngas composition can vary greatly. Although syngas is mostly composed of hydrogen and carbon monoxide, potential variables to be considered in the direct combustion of syngas mixtures include the carbon/hydrogen ratio, varying levels of carbon dioxide and water, as well as the presence of other trace species that can have a pronounced effect on combustion processes (Glarborg, 2007). Moreover, the flame temperatures of stoichiometric syngas combustion are sufficiently high to result in substantial NO_x emissions. An important aspect of minimizing pollutant emissions from industrial gas turbines operating on natural gas has been the implementation of lean, premixed combustion. A similar approach for turbines operating on syngas and hydrogen has led to a renewed interest in their combustion dynamics under conditions relevant to industrial turbine mixing systems (i.e. lower temperatures and higher pressures; $T < 1{,}000$ K, $10 < P < 30$ atm). This requires robust fluid dynamic as well as chemical kinetic modeling tools, thoroughly validated against experiments spanning a wide range of operating conditions (i.e. pressure, temperature, mixture composition, equivalence ratio).

$CO/H_2/O_2$ kinetic models are the fundamental hierarchical systems upon which understanding of all hydrocarbon combustion chemistry is dependent. Historically, the $CO/H_2/O_2$ system has been studied in detail (Dixon-Lewis and Williams, 1977; Gardiner and Olson, 1980; Westbrook and Dryer, 1984; Yetter et al., 1991a) and thought to be reasonably well established and understood. Comprehensive kinetic models for the oxidation of H_2/CO mixtures (Davis et al., 2005; Kim et al., 1994; Li et al., 2007; Sun et al., 2007; Yetter et al., 1991a) need to be continually tested and/or updated as new experimental, kinetic, and thermochemical data appear in the literature. Recently, as a result of interest in gas turbine syngas combustion, experiments have been reported in a variety of venues (Beerer and McDonell, 2007; Bradley et

al., 2007; Burke et al., 2007; Kalitan et al., 2006; Mittal et al., 2006; Natarajan et al., 2007; Petersen et al., 2007; Sivaramakrishnan et al., 2007; Sun et al., 2007; Walton et al., 2007a) for conditions that are sufficiently removed from the range of previous model validations. Considering the above discussion, the purpose of the present paper is to review and elaborate upon proposed H_2/CO kinetic changes based on these recent experimental observations and associated theoretical work. We discuss the need for careful analysis of data collected at high pressures and the implications that experimental anomalies, known to be present at these conditions, may have on interpreting these data as homogenous chemical kinetic observations.

As mentioned above, small amounts of impurities (e.g. NO_x) may also be present in syngas combustion systems, and their influence on and interactions with the kinetic behavior of H_2/CO mixtures are also addressed. A general overview of the H_2/CO kinetic system and its key reactions appears in another contribution to this special issue (Sung and Law, 2007) and provides substantial background for the present discussion.

RECENT AND PROPOSED UPDATES TO THE H_2/CO KINETIC MODEL

Recently, Li et al. (2004, 2007) performed an exhaustive study aimed at revising and updating prior work to produce an improved "C_1" model for prediction of CO, CH_2O, and CH_3OH kinetic behavior. The investigation was driven by the availability of new chemical kinetic rate and thermochemical information, as well as new validation data.

First, Li et al. (2004) updated the detailed H_2/O_2 model of Mueller et al. (1999a). The updates included a revision in the rate correlations used for the branching reaction $H+O_2=O+OH$ (R1), taken from Hessler (1998), and for the low pressure of the competing reaction $H+O_2(+M)=HO_2(+M)$ (R2), adopted from Michael et al. (2002) (Table 1 presents a list of

relevant reactions discussed herein). A major constraint in selecting these two correlations was that their ratio (which determines the second explosion limit behavior of the H_2/O_2 system) in the temperature range between 800K and 900K replicated the ratio experimentally determined by Mueller et al. (1998). Based on sensitivity analyses, Li et al. (2004) increased the rate of $H+OH+M=H_2O+M$ (R3) (within known uncertainty) to improve predictions of high pressure flame speed data (Tse et al., 2000). The enthalpy of formation of the hydroxyl radical was also updated to that recommended by Ruscic et al. (2002), and it should be noted that the heat of formation for HO_2 used by Li et al. (2004, 2007) is now recognized to be within the uncertainties of the recent evaluation of Ruscic et al. (2006).

Experimental measurements and theoretical studies continue to appear in the literature for both (R1) and (R2) (Hahn et al., 2004; Hwang et al., 2005; Troe, 2000; Troe and Ushakov 2001) to further reduce uncertainties in predicted rates, particularly at temperatures below 1000 K. For example, Fig. 1 compares recent correlations for the low pressure rate of reaction (R2) with Ar as the collisional partner. Although some uncertainties remain, (e.g., see Hwang et al., 2005), all of them lie within 20% of each other and within the uncertainty estimates derived from the exhaustive literature review of Baulch et al. (2005). Further refinements in the collisional efficiencies of species such as water and carbon dioxide in (R2) remain important.

Reaction (R4), $CO+OH=CO_2+H$, is of critical importance in the oxidation of $H_2/CO/O_2$ as well as moist CO mixtures (e.g., see Yetter et al., 1991a). As a result of temperature-dependent sensitivity analyses of laminar burning rates for CO/H_2 mixtures (Zhao et al., 2005), Li et al. (2007) developed and employed in their C_1 model a weighted empirical fit of the entire body of experimentally measured rate constants for (R4). Other updates relevant to the H_2/CO system included a similarly motivated, weighted empirical fit of rate data for the reaction

HCO+M=H+CO+M (R5) as well as associated adjustments for the rate constant of $HCO+O_2=HO_2+CO$ (R6). The resulting C_1 model was validated against a wide range of data for H_2/O_2 and $CO/H_2O/H_2/O_2$ experiments in various venues, and the sub-models were also utilized in additional validations against a wide range of data involving formaldehyde and methanol as fuels. Although Li et al. (2007) discuss the high pressure syngas experiments of Mittal et al. (2006), and early, high pressure shock tube results from Sivaramakrishnan et al. (2005), these targets were not included in the validation of the published C_1 mechanism (the reader is referred to Li et al. (2007) for further details.)

All of the new data relating to syngas gas turbine applications referenced above represent validation targets that place emphasis on reactions involving the hydroperoxyl radical (HO_2) as well as hydrogen peroxide (H_2O_2). In these publications, updates to important reactions involving HO_2 chemistry have been proposed (Mittal et al., 2006, 2007; Sivaramakrishnan et al., 2007), the most significant being the rate correlations for $CO+HO_2=CO_2+OH$ (R7) and $HO_2+OH=H_2O+O_2$ (R8). These reactions and their suggested updates are discussed further below, including kinetic predictions using a modified version of the C_1 model (Li et al., 2007).

$CO+HO_2=CO_2+OH$ (R7)

Mittal et al. (2006) investigated the ignition of $H_2/CO/O_2/N_2/Ar$ mixtures in a Rapid Compression Machine (RCM) at pressure and temperature ranges of 15-50 bar and 950-1100 K, respectively. They noted that the reproduction of their experimental data required rate values for $CO+HO_2=CO_2+OH$ (R7) that were up to a factor of four smaller than those used in current H_2/CO models (Davis et al., 2005; Li et al., 2007). The rate used by Li et al. (2007) was recommended by Mueller et al. (1999b), who argued even lower values might be justified upon

further evaluation. In a follow-up study to their RCM measurements, Mittal et al. (2007) used Monte Carlo and "Morris-one-at-a-time" uncertainty analyses in evaluating predictions based upon the model of Davis et al. (2005). The results pointed to a rate value for (R7) that could be up to a factor of ten lower with respect to that of Baulch et al. (1973), consistent with the findings of Mittal et al. (2006).

Until recently, (R7) had not received as much attention theoretically as other reactions in the H_2/CO system. As reviewed by You et al. (2007), the few theoretical studies available (Allen et al., 1996; Sun et al., 2007) did not adequately treat critical geometries as well as hindered internal rotations in the *trans*-HOOC•O adduct through which (R7) proceeds. Furthermore, the complexity of the potential energy surface due to the *trans*- and *cis*- conformers and their mutual isomerization were not considered. Consequently, You et al. (2007) performed an improved theoretical treatment of (R7) and showed that this reaction is pressure independent for conditions relevant to combustion applications with a temperature dependence of:

$$k_{R7}\left(\mathrm{cm^3/mol/s}\right) = 1.6\times10^{5} T^{2.18} \exp\left(\frac{-9030}{T}\right) \qquad (1)$$

Figure 2 shows the results of You et al. (2007) plotted against other theoretical predictions (Mittal et al., 2007; Sun et al., 2007) as well as recommended correlations commonly used for (R7) (Mueller et al., 1999b; Tsang and Hampson, 1987). S.J. Klippenstein employed transition state theory and a two barrier model to produce the correlation recommended in Mittal et al., 2007). Figure 2 clearly indicates that results from high-level quantum chemistry calculations support the need for a much lower rate for (R7).

Adopting the rate expression for (R7) derived by You et al. (2007) into the model of Li et al. (2007) considerably improves its predictions of RCM ignition delay at high pressures (Fig. 3). Li et al. (2007) detailed why reaction (R7) impacts observations under the RCM conditions of

Mittal et al. (2006) by performing computational singular perturbation (CSP) analyses. Unlike previous implementations of CSP, Li et al. (2007) used a recent formulation of the methodology (Kazakov et al., 2006) that included temperature as one of the state variables so that factors controlling ignition could be unambiguously determined. Modifications were also made in the methodology to accommodate systems with time-varying volume, as Mittal et al. (2006) report a time-varying volume correction to incorporate heat loss effects on their RCM observations.

Figure 4 shows the relative importance of selected elementary reactions (in terms of the participation index, see Kazakov et al., 2006) that most significantly affect the heat release rate (reaction temperature) under the RCM conditions of Mittal et al. (2006) at specific reaction times following the end of the compression stroke. It is apparent that reaction (R7) is only important during the chemical induction period, principally through its impact on the initial build-up of HO_2. After chemical ignition occurs, which is associated with the decomposition of hydrogen peroxide and transition to chemical branching through (R1), reaction (R7) no longer contributes significantly to the system behavior (i.e. the rate of heat release). Subsequent to ignition and at all pressures, the system dramatically shifts to one dominated by reactions involving the OH radical. As a result, in combustion applications where radical back-mixing or heterogeneous processes result in chemical reaction initiation, reaction (R7) does not significantly impact predictions.

HO_2+OH=H_2O+O_2 (R8)

Reaction (R8) carries significant importance in the HO_x cycle of atmospheric chemistry. Thus, (R8) has been extensively studied and is well characterized at low temperatures (e.g. see database evaluations such as http://kinetics.nist.gov). Early measurements near room

temperature showed a scatter of over a factor of two and suggested a possible pressure dependence (Burrows et al., 1981; DeMore, 1982; Rozenshtein et al., 1984; Sridharan et al., 1984). Keyser (1988) demonstrated that inconsistencies in earlier measurements were due to the presence of small amounts of H and O radicals. By adding NO_2 to remove these radical species, Keyser (1988) showed that (R8) exhibits no pressure dependence at pressures up to 1000 Torr. Recent high temperature measurements (Hippler et al. 1995; Kappel et al., 2002) show that (R8) exhibits an uncommon and highly non-Arrhenius behavior, indicative of the formation of an activated complex. There is an unusually narrow and deep minimum in the rate at about 1000-1200 K with a rapid increase below and above the minimum (see Fig. 5). In an earlier study (Roesler et al., 1994), high temperature moist CO oxidation was also found to be sensitive to reaction (R8) at lean conditions. The lack of experimental data at intermediate temperatures (400-900 K) makes finding an expression that accurately captures the observed temperature dependence challenging.

Stimulated by the failure of simulations using a H_2/CO kinetic model (Davis et al., 2005) to predict their high pressure experimental data (up to 450 atm), Sivaramakrishnan et al. (2007) recently proposed a new parameterization for the rate of (R8). Sivaramakrishnan et al. (2007) fitted experimental data from a number of studies (DeMore, 1982; Goodings and Hayhurst, 1988; Hippler et al., 1995; Hippler and Troe, 1992; Kappel et al., 2002; Keyser, 1988; Lii et al., 1980; Peters and Mahnen, 1973) by the following expression:

$$\begin{aligned} k_{R8}\left(\mathrm{cm^3/mol/s}\right) = {} & 1.41\times10^{18}T^{-1.76}\exp\left(\frac{-30}{T}\right) + 1.12\times10^{85}T^{-22.3}\exp\left(\frac{-13538}{T}\right) \\ & + 5.37\times10^{70}T^{-16.72}\exp\left(\frac{-16558}{T}\right) + 1.00\times10^{136}T^{-40.0}\exp\left(\frac{-17514}{T}\right) \\ & + 2.51\times10^{12}T^{2.0}\exp\left(\frac{-20131}{T}\right) \end{aligned} \qquad (2)$$

Equation 2 is plotted in Fig. 5 along with available experimental data. It can be seen that the proposed rate coefficient captures the sudden decrease in rate at around 1000 K. However, the fit gives larger weight to the data of Hippler et al. (1995) rather than to the more recent, and arguably more reliable, measurements of Kappel et al. (2002). Nevertheless, the use of the proposed rate expression appears to considerably improve H_2/CO oxidation predictions of the high pressure experiments (Sivaramakrishnan et al., 2007). It should be noted, however, that the rate predicted by Eqn. 2 increases for T > 1400 K (Fig. 5), quickly reaching values that exceed the collision limit.

It is more likely that (R8) will reach a limiting value at high temperatures, similar to the observations of Hippler et al. (1995) for the reaction H_2O_2+OH=HO_2+H_2O (R9). In fact, the studies of Goodings and Hayhurst (1988) and Srinivisan et al. (2006) show very little temperature dependence of the rate for (R8) for temperatures greater than about 1300 K. Here we report new least-squares analyses of available experimental data to obtain rate expressions constrained by a high temperature limiting value. First, we assumed that up to 800 K the rate of (R8) follows the temperature dependence proposed by Keyser (1988). We then generated two different rate expressions, one using the measurements of Hippler et al. (1995), who measured a rate minimum near 1240 K, and a second using the data of Kappel et al. (2002), who located the rate minimum near 1010 K. These expressions appear below as Eqns. 3 and 4, respectively (plotted in Fig. 5):

$$k_{R8}\left(\mathrm{cm^3/mol/s}\right) = 1.467\times10^{11}T^{0.73}\exp\left(\frac{587}{T}\right) + 1.105\times10^{37}T^{-6.35}\exp\left(\frac{-13297}{T}\right) - 8.976\times10^{163}T^{-42.44}\exp\left(\frac{-54377}{T}\right) \quad (3)$$

$$k_{R8}\left(\mathrm{cm^3/mol/s}\right) = 1.410\times10^{12}T^{0.46}\exp\left(\frac{316}{T}\right) + 1.225\times10^{21}T^{-3.20}\exp\left(\frac{-95}{T}\right) - 2.911\times10^{110}T^{-28.19}\exp\left(\frac{-28400}{T}\right) \quad (4)$$

Kappel et al (2002) argued that their more direct and accurate measurement of initial reactant concentrations probably made their measurements more reliable than those of Hippler et al. (1995), although the methods applied in the deriving the rate data had associated uncertainties. As noted below, however, reasonable predictions of the high pressure oxidation data of Sivaramakrishnan et al. (2007) can be obtained using values of the rate for (R8) predicted by Eqn 3, but not by Eqn. 4. Clearly additional studies of (R8) are required but at present Eqn 3 is preferable to Eqn 2 in that rate values that exceed the collisional limit are avoided.

In the study of Li et al. (2007) CSP analyses were also applied to the conditions of Sivaramakrishnan et al. (2007). The results from these analyses are reproduced in Fig. 6 for a representative condition. Due to the highly dilute mixtures studied, there is no well defined ignition criteria present in the pressure history of the experiment, although there is obvious evidence of an induction period. While (R7) is only important during chemical induction, (R8), on the other hand, becomes more dominant in importance as the reacting system evolves. An oxygen flux path analysis for two pressure conditions, 43 and 435 atm, provides insights to this result (Fig. 7) and is further elaborated below.

Figure 8 shows model comparisons against the entire data set of Sivaramakrishnan et al. (2007). This figure also shows the effect of adopting the changes discussed above for reaction (R8) (Eqn. 3) as well as for (R7) (Eqn. 1). It is clear that these changes only affect results at high pressures (Figs. 8c and 8d). On the basis of the above discussion and considering Fig. 7, one can see that as pressure increases, reaction (R8) strongly competes with HO_2+H=2OH (R10) for HO_2 radicals. Reaction (R10) is one of the major direct sources of OH at high pressures, thus

determining the amount of OH available to react with CO. Hydroxyl radical formation (relative to HO_2 formation) is greatly diminished at higher pressures. In fact, the maximum HO_2 concentration at 435 atm is nearly an order of magnitude higher than that of OH, whereas the opposite is true at 43 atm (see Fig. 9). The results displayed in Figs. 7 and 9 show that reactions involving HO_2 that compete for and generate OH radicals (such as reactions R8 and R10) become more important at high pressures in the H_2/CO system since the availability of OH determines the rate of CO oxidation through reaction (R4). Sivaramakrishnan et al. (2007) noted that their data could be reconciled by increasing the rate of (R7), which is consistent with the above argument, as (R7) both consumes CO and releases OH; however increasing this rate degrades model predictions against flow reactor data (Kim et al., 1994) and, as discussed above, recent studies support a much lower rate for (R7). The update proposed by Sivaramakrishnan et al. (2007) (Eqn. 2) as well as the present authors (Eqn. 3) essentially lowers the rate of (R8) over the temperature range of interest (see Fig. 5), therefore slowing a termination path for both HO_2 and OH. In fact, additional calculations that we performed using literature values for (R8) (Kappel et al., 2002; Kim et al., 1994; Srinivasan et al., 2006) that are lower than that employed in the model of Li et al. (2007) yielded results similar to those shown in Fig. 8. While marked improvement occurs for pressures of approximately 250 atm, the correlation of Eqn. 3 (as well as Eqn. 2) leads to only moderate improvements at higher pressures (Fig. 8d). At higher pressures, the flux of HO_2 to form H_2O_2 (Fig. 7) is considerably larger than through reaction (R8), and at high temperatures, H_2O_2 decomposes rapidly to yield OH, removing the significance of reaction (R8).

In closing this section we conclude that interest in gas turbine syngas combustion has led to new kinetic studies that show important uncertainties remain for several reactions in the

HO_2/H_2O_2 subsystem. The updates put forth by Mittal et al. (2006) and You et al. (2007) for $CO+HO_2=CO_2+OH$ (R7) can be readily absorbed into current kinetic models without affecting the quality of their predictions against validation targets that are insensitive to induction chemistry. Moreover, induction chemistry is typically of less importance in control of ignition in applications where convective and diffusive processes contribute to initial radical concentration evolution. The analyses presented here suggest that the study of Sivaramakrishnan et al. (2007) only supports the likelihood of a lower rate for reaction (R8) over $1200 < T < 1400$ K consistent with the measurements of Hippler et al. (1995). The complex expression given by Eqn. 2, appears to marginally impact predictions of the experimental measurements of Sivaramakrishnan et al. (2007) at the highest pressures and should be used with caution for high temperature applications. Eqn. 3, developed here, yields similar quantitative results to those obtained with Eqn. 2 at temperatures below 1400 K, while providing a reasonable rate prediction for (R8) at higher temperatures.

HIGH-PRESSURE/LOW-TEMPERATURE SYNGAS IGNITION AND KINETIC IMPLICATIONS

Ignition of H_2/CO mixtures has traditionally been studied at relatively low pressures and high temperatures (e.g. Dean et al., 1978). Petersen et al. (2007) recently reported new ignition delay data for syngas/air mixtures in a high pressure shock tube and a flow reactor at conditions relevant to gas turbine combustion. These new data are summarized in Fig. 10 along with other recently published data from the rapid compression studies of Walton et al (2007a) and from an earlier high pressure flow reactor study described in an Electric Power Research Institute report (Peschke and Spadaccini, 1985). All of the ignition delay data have been normalized to conditions of 20 atm pressure. Petersen et al. (2007) noted that at reaction temperatures lower

than about 1050 K, experimental observations of ignition delay (determined by various criteria) all begin to substantially depart from zero-dimensional, homogeneous gas phase predictions based upon any of the recently published H_2/CO kinetic models (see Fig. 10).

The views expressed by Petersen et al. (2007) should raise considerable concern, as they bring into question the predominant kinetic understanding of gas phase oxidation phenomena for the H_2/CO system shared by numerous researchers, including the present authors. Hydrogen and carbon monoxide oxidation are the fundamental basis for all hydrocarbon combustion chemistry and severe deficiencies in reactions, rate and/or thermochemistry sufficient to be the cause of the noted disparity would be far reaching. We believe, along with Petersen et al. (2007), that the noted departures of syngas ignition delay experimental results from homogenous gas phase kinetic predictions are real and impose limitations to lean premixed schemes in gas turbine designs using syngas. However, we argue that the majority of these differences are not a result of missing gas phase kinetic paths or kinetic/thermo-chemical parameter uncertainties. It is our opinion that the disparities result from the fact that in each of the experimental venues discussed in Petersen et al (2007), the relevant homogenous gas phase kinetics are not only dominated by those of the hydrogen-oxygen system at reaction temperatures between the extended second and third explosion limits, but that key limiting processes are perturbed by one or more phenomena that significantly enhance the overall rate of reaction typical of pure homogenous gas phase chemistry. These views have been briefly summarized in the literature recently (Dryer and Chaos, 2007) and the supporting details that led us to the expressed opinions are presented below.

Carbon monoxide oxidation is strongly influenced by the presence of small amounts of hydrogen-containing species, including moisture, hydrocarbons, and, most importantly, hydrogen itself (e.g. Yetter et al., 1991a). Subsequently, it should not at all be unexpected that

ignition phenomena for syngas/air mixtures will be similar in character to those for hydrogen/air mixtures themselves. For example, both low and high pressure shock tube measurements of syngas ignition delay (Kalitan et al., 2006; Kalitan and Petersen, 2005) exhibit the well known explosion limit behavior typical of hydrogen oxidation (Lewis and von Elbe, 1987). Moreover, the inconsistencies observed between modeled and measured syngas ignition times (Petersen et al., 2007) for the pressures of interest occur at temperatures between the extended second limit (Mueller et al., 1999a) and the classical third explosion limit for the hydrogen/oxygen system, where disparities are well known to exist for experimental measurements of hydrogen/oxygen ignition delay and homogenous gas phase predictions.

While many researchers have approached these problems as though there might be something missing in the current understanding of homogenous gas phase kinetics for hydrogen/air or carbon monoxide/air systems, the experimental data have seldom been scrutinized as to their representation of homogeneous gas phase kinetic phenomena. For hydrogen shock tube ignition delay results, similar disparities between predictions and observations have been frequently discussed in the published literature since the early 1960's. For example, Wakefield et al. (1969) showed that analytic solutions using a linearized hydrogen oxidation model could not reconcile shock tube ignition data observations (Miyama and Takeyama, 1964; Skinner and Ringrose; 1965; Voevodsky and Soloukhin, 1965) below approximately 1100 K. Maas and Warnatz (1988) developed a hydrogen reaction scheme, using the data of Skinner and Ringrose (1965) and Schott and Kinsey (1958) as validation targets. Order-of-magnitude differences were evident between predictions and experimental ignition delay observations close to the second explosion limit, but were not elaborated upon by the authors (Maas and Warnatz, 1988). More recently, the studies of Blumenthal et al. (1995), Wang

et al. (2003), and Martynenko et al. (2004) further show results similar to those mentioned above. Figure 11 compares and summarizes ignition delay predictions obtained from the model of Li et al. (2007) against the early and more recent H_2/O_2 shock tube studies. One should note remarkable similarity between Fig. 11 and results reported by Petersen et al. (2007) for syngas (Fig. 10).

As first identified by Strehlow and Cohen (1962), ignition of reactive hydrogen/oxygen mixtures behind reflected shocks can exhibit substantially differing transient behavior. At sufficiently high reflected shock temperatures, the so called "strong" or "sharp" ignition is observed, and reaction initiation starts at a single locus point in the reflected region near the end-wall, quickly transitioning to a uniform detonation wave. At lower reflected shock temperatures (of interest in the studies considered here), "mild" or "weak" ignition occurs. Random flame kernels are initially formed, eventually merging and transitioning to a contiguous combustion front. Figures 12 and 13 show evidence of these two distinct processes, as observed in the studies of Blumenthal et al. (1996) and Wang et al. (2003). The work of Meyer and Oppenheim (1970), as later reviewed by Oppenheim (1985), showed that mild ignition is a *multidimensional* process where the initial random flame kernels start close to the shock tube walls and stagnant corners. Meyer and Oppenheim (1970) also explained that induction times in the mild ignition regime are very sensitive to temperature variations behind the reflected shock wave. This result has been confirmed by the extensive numerical work of Oran and coworkers (Oran and Boris, 1982; Oran and Gamezo, 2007; Oran et al., 1982) as well as in the early work of Gardiner and Wakefield (1970). Indeed, Yetter et al. (1991c) identify distinct kinetic regimes associated with "weak" and "strong" ignition through combined sensitivity/stability analyses of the hydrogen/oxygen kinetic system.

In more recent H_2/air shock tube studies, Blumenthal et al. (1995) were able to identify and perform temporal measurements on the appearance of the first flame kernel and subsequent transition to detonation in the mild ignition regime. Martynenko et al. (2004) also showed that during mild ignitions, OH emission first occurs in the peripheral regions of the shock tube, close to the walls. It is noted that all of the major discrepancies observed between homogeneous kinetic model predictions and measured shock-tube ignition delays occur in this mild ignition regime for both H_2 (Blumenthal et al., 1995; Maas and Warnatz, 1988; Martynenko et al., 2004; Miyama and Takeyama, 1964; Schott and Kinsey, 1958; Skinner and Ringrose, 1965; Voevodsky and Soloukhin, 1965; Wakefield et al., 1969; Wang et al., 2003) and syngas (Petersen et al., 2007) systems. For these referenced works, it is clear that the hydrogen-oxygen ignition occurs *inhomogeneously* (Terao, 1977) and that observations are not representative of zero-dimensional phenomena (see Figs. 12a and 13a), especially in high energy density mixtures (Martynenko et al., 2004). Utilizing zero-dimensional modeling calculations, e.g. SENKIN (Lutz et al., 1987), to represent these events is inappropriate. It is generally believed that chemical kinetics and gas dynamics behind the reflected shock wave and in the vicinity of the endwall are strongly coupled, and gas state changes are, at least in part, responsible for the observed behavior, especially for the relatively long ignition delay times measured in the mild regime. These observations are universal over the wide range of shock tube diameters (Blumenthal et al., 1995) and configurations utilized in the various studies. Thus far, no multidimensional modeling of these phenomena with detailed kinetics has appeared to further elucidate observations.

Figure 10 reproduces the syngas data presented by Petersen et al. (2007) along with representative results from the H_2/air shock tube study of Blumenthal et al. (1995) and

calculations using the model of Li et al. (2007). Data are those for lean mixtures ($\phi \sim 0.5$, Petersen et al., 2007; $\phi = 0.42$, Blumenthal et al., 1995) and similar oxygen concentrations (~ 17 %) and are normalized to 20 atm under the same assumptions used by Petersen et al. (2007). Model results show near identical trends for the different syngas/air and hydrogen/air mixtures considered, indicating that under the conditions studied, kinetics specific to hydrogen, rather than to CO are controlling. The data of Blumenthal et al. (1995) are especially relevant since the onset of strong and weak ignitions are definitively differentiated by direct photographic records of the ignition process, similar to those shown in Figs. 12 and 13. It is seen in Fig. 10 that strong ignition cases (filled circles) are predicted reasonably well by homogenous kinetic calculations, based upon computed reflected shock temperatures and measured pressures. However mild ignition observations (open circles) differ from similarly predicted results by up to three orders of magnitude. Mild ignition events occur at temperatures below about 1100 K, as do order-of-magnitude differences for syngas ignition data and homogenous gas phase predictions (Fig. 10).

Blumenthal et al. (1995) note that inhomogeneities in temperature and concentration known to be present in the mild ignition regime may not be large enough to entirely explain the discrepancies between gas phase kinetic predictions and experimental observations of ignition. Calculations performed by the present authors indicate that local temperature hot spots exceeding calculated reflected shock temperatures by up to 150 K would be needed to reduce predicted homogeneous gas phase ignition delays to the corresponding experimental values in the mild regime shown in Fig. 10. Moreover, it has been hypothesized that catalytic effects due to the presence of small particles in the gas (Blumenthal et al., 1995; Elsworth et al., 1969; Haskell, 1970) could also have been important in some of the observations. In summary of the above shock tube discussions, observations of ignition delay for hydrogen/air mixtures at temperatures

below 1100 K are well known to disagree with homogenous gas phase predictions, and it is universally observed that the ignition phenomena is multi-dimensional and inhomogenous.

One of the more intriguing points raised by data in Fig. 10 (for both syngas/air and hydrogen/air systems) is that data collected in flow reactors (Peschke and Spadaccini, 1985; Petersen et al., 2007) apparently follow the trend established by the shock tube data in the mild ignition regime. Petersen et al. (2007) also suggest that recent syngas ignition data generated in the University of Michigan Rapid Compression Facility (UM-RCF), Walton et al. (2007a), similarly "line up" with flow reactor and shock tube measurements. Here we note, however, as shown in Fig. 14, that the data of Walton et al. (2007a) exhibit considerable scatter, even when the data are normalized. A regression analysis of the data (considering pressure, temperature, equivalence ratio, and oxygen mole fraction as key parameters) yields a goodness of fit R^2-value of only 0.57 (Fig. 14). The low data correlation is common to these as well as other data shown in Fig. 10 for flow reactor and shock tube studies at low temperatures, indicating that some unaccounted factors exist in correlating the observations.

The similarities of hydrogen and syngas shock tube observations noted above, can also be shown when comparing the syngas data of Walton et al (2007a) and other rapid compression machine (RCM) hydrogen-oxygen ignition data present in the literature. Upon further inspection of Fig. 14, it is appears that two distinct "regimes" can be identified for the UM-RCF syngas ignition data (Walton et al., 2007a). The circled data in Fig. 14 have different temperature dependence than the data at lower temperatures. We have further analyzed these data (which are for temperatures above about 1,000 K) by performing regression analyses considering pressure, equivalence ratio, oxygen mole fraction, as well as CO content. Walton et al. (2007a) did not include the CO content in their regression analyses, though Mittal et al. (2006) showed that CO

had a marked (exponential) effect on their RCM ignition delay observations. The regression thus obtained is:

$$\tau(\mu s) = 1.0325\times10^{-13}\, P^{-0.20}\phi^{-1.34}\exp(9.19\chi_{CO})\chi_{O_2}{}^{-4.11}\exp\left(\frac{61{,}335\ \text{cal/mol}}{RT}\right) \qquad (5)$$

where P is the pressure in atm, ϕ the equivalence ratio of the H_2/CO mixture, R the universal gas constant (in cal/mol/K), and χ_{O2} and χ_{CO} the mole fractions of oxygen and carbon monoxide, respectively. Based on the results of Mittal et al. (2006), an exponential CO concentration dependence has been assumed in Eqn. 5. There are two important features to note about Eqn. 5. First, the correlation R^2-value is approximately 0.9; second, the activation energy of the correlation is consistent with those determined in the RCM studies of Lee and Hochgreb (1998) and Mittal et al. (2006): 76,000 and 74,000 cal/mol, respectively. A similar activation energy can be derived from direct measurements in a flow reactor (Mueller et al., 1999a).

The RCM hydrogen data of Lee and Hochgreb (1998) were collected over similar pressure and temperature as in the syngas study of Walton et al. (2007a). However, Lee and Hochgreb (1998) used stoichiometric mixtures, while Walton et al. (2007a) studied mostly lean conditions. The data of Walton et al. (2007a) span a sufficiently wide range of stoichiometries and H_2/CO concentrations such that Eqn. 5 can be used to normalize the syngas data to compare with the pure hydrogen observations of Lee and Hochgreb (1998). Figure 15 presents the data of Lee and Hochgreb (1998) along with the syngas data of Walton et al. (2007a) normalized to 15 atm (an average value in both studies),

12.5% O_2 concentration (similar to Lee and Hochgreb, 1998), and stoichiometric conditions in the absence of CO (i.e. "pure" hydrogen). In Fig. 15, it is clear that the data selected to generate Eqn. 5 (see Fig. 14) are in excellent agreement with the data of Lee and Hochgreb (1998). The remaining data (open circles in Fig. 15) significantly deviate from those of Lee and Hochgreb (1998) at lower temperatures. For example, at approximately 960 K there is a difference of nearly a factor of seven between the two data sets.

The syngas data of Walton et al., 2007a can also be compared with the recent RCM hydrogen ignition observations of Mittal et al. (2006). Mittal et al. (2006) studied much lower oxygen concentrations (in the order of 6% as opposed to 13-20%) than those investigated by Walton et al, and thus Eqn 5 is not appropriate for normalization (Chaos et al., 2007). Instead, we scaled the normalized data shown in Fig. 15 linearly with oxygen concentration (i.e. 0.125×15 atm× $(RT)^{-1}$) along with the data of Mittal et al. (2006). Figure 16 shows the results of this scaling; very good agreement is observed between the two sets of data (in terms of absolute values and activation energies) at higher temperatures. However, the data of Walton et al. (2007a) considerably deviate from the Mittal et al. (2006) data trend at lower temperatures. The presence of reaction fronts, as noted and explained by Walton et al. (2007b), may have influenced these cases. However, photographic image sequences shown in the studies of Walton et al. (2007a, 2007b) also indicate the presence of particles in the test volume. Particles have been

observed to considerably affect the ignition process in rapid compression machine studies (Elsworth et al., 1969; Haskell, 1970). In summary, while one cannot identify why there are such substantial differences of the Walton et al data from other rapid compression machine results at lower temperatures, it is clear that some rapid compression machine measurements do not follow the trend of results presented in Fig. 10 and are in reasonable agreement with homogenous kinetic predictions even at temperatures below 1000 K.

Finally, we comment on the flow reactor results presented in Fig. 10. Our laboratory has a long history involving the use of flow reactors and the study of hydrogen-oxygen and carbon monoxide-hydrogen-oxygen kinetics which shed some additional light on the flow reactor ignition delay measurements. Highly diluted hydrogen-oxygen kinetics at atmospheric pressure and at temperatures 920-980 K were first studied at Princeton by Swigart (1958) in stainless steel tube reactors of 2.54, 5.08, and 7.62 cm diameter. A distinct increase in the overall rate of the reaction with decreasing reactor diameter was observed and was attributed to catalytic activity on the stainless steel walls. Similar measurements were made by Sawyer (1965) in silica reactor tubes, also suggesting that catalytic wall reactions were present in the mixing region as well as downstream. In more recent work, this laboratory performed experiments on hydrogen/oxygen/carbon monoxide systems that traversed the extended second explosion limit condition (Vermeersch, 1991; Yetter et al., 1991a, 1991b). Vermeersch (1991) performed ignition delay as well as kinetic measurements in highly diluted $H_2/O_2/N_2$ mixtures in silica-walled flow reactor tubes (the current Princeton Variable Pressure Flow Reactor) at pressures up to 9 atm. While the gas phase reaction of hydrogen after ignition occurred was found to agree

with homogenous kinetic predictions, the measured ignition delays were several orders of magnitude shorter than predicted, similar to what is observed in Fig 10. Equivalence ratio variations within and catalytic interactions on the mixing region surfaces were speculated to affect the chemical induction kinetics, significantly reducing the time required to establish the exothermic reaction (post induction chemistry) region downstream.

Vermeersch (1991) showed that because of the large reactor tube diameter (10 cm) used, catalytic aberrations of the kinetic rate observations along the centerline of the reactor tube and downstream of the mixing region (after ignition occurred) were negligible. These results are consistent with earlier experiments and analyses performed on the moist carbon monoxide oxidation system (Yetter et al., 1991a, 1991b). In analyzing and modeling this work, it was shown that kinetic perturbations in the mixing region can have significant effects on the chemical induction processes. Chemical initiation processes were shown to strongly influence "ignition delay times" but to have little effect on the observed rates of reaction thereafter (Yetter et al., 1985). Indeed it was on the basis of this early work that reaction "time shifting" was introduced as a means of comparing experimental observations of post induction oxidation kinetics of carbon monoxide and hydrogen oxidation data with homogenous plug flow kinetic predictions (Yetter et al., 1991b; Zhao et al. 2008). We have avoided making flow reactor ignition delay measurements of hydrogen/carbon monoxide systems because of the observed sensitivity to perturbations in the mixing region and the difficulty in interpreting multi-dimensional mixing and catalytic wall interactions. However, it is clear from these studies that the differences in experimental observations and homogenous kinetic predictions of chemical induction times are present even at atmospheric pressure and in highly diluted mixtures of hydrogen-oxygen and carbon-monoxide-oxygen systems in the presence of hydrogen containing species.

The fact that anomalous ignition delays are observed even in highly diluted systems argues against the likelihood that some (previously neglected) homogenous initiation reaction involving molecular hydrogen and oxygen could be responsible for the differences between experimental and predicted observations in high energy density mixtures. Additionally, sensitivity analyses of syngas ignition delay times under conditions shown in Fig. 10 do not appear to support missing initiation processes (Fig. 17). As expected, at temperatures near the explosion limit, the rate of reaction is determined by reactions (R1) and (R2). However, at lower temperatures, in the region between the extended second limit and third limit where discrepancies are observed, the most important reactions are those that lead to generation of reactive radical species from hydroperoxyl radicals, namely $H_2O_2+M=OH+OH$ (R11) and $H_2+HO_2=H_2O_2+H$ (R12). Ignition is also sensitive to reaction (R7) at lower temperatures; however, the sensitivity of this reaction is essentially temperature independent. Furthermore, adjusting the rate of (R7) to the value recommended by You et al. (2007) (see discussion in previous section) cannot account for the discrepancies seen in Fig. 10. Chemical initiation reactions do not appear amongst the most sensitive processes. We conclude through our own analyses that no reasonable updates to the present homogenous kinetic understanding of H_2/CO systems can reconcile the large differences seen in Fig. 10 between model predictions and experiments. This result is consistent with the claim of Petersen et al. (2007) and with the observations of Sabia et al. (2006) who performed extensive analyses of hydrogen/oxygen kinetic behavior to show that only with unreasonable assumptions regarding rate constants as well as third body efficiencies of reactants can homogenous kinetic predictions even crudely approach experimental observations in high pressure shock tube studies of hydrogen/air ignition.

It is important to note that mixing, fluid dynamic, and catalytic issues affecting experimental observations were not considered as potential problems in any of the analyses presented by Petersen et al. (2007), or in their supporting references. The results shown in Fig. 10 further induce us to raise concerns about catalytic effects from the fact that the overall activation energy of the data (including shock tube, rapid compression, and flow reactor measurements) in the region where big differences exist with model results is approximately 8 kcal/mole, much lower than typical gas-phase, kinetically-controlled processes. As noted above, induction processes in the mild ignition regime are extremely sensitive to any type of perturbation (Yetter et al, 1991c), catalytic or otherwise. Perturbations that remove the rate limiting nature of reactions such as (R11) and (R12), considerably shorten induction and, therefore, ignition delay time. Assuming diffusive time scales are sufficiently rapid in comparison to reaction time scales, catalytic effects can be approximated as homogenous gas phase processes with modified rate constants. Syngas ignition delay predictions under the conditions shown in Fig. 10 using the model of Li et al. (2007) including catalytically accelerated rates, similar to those used by Deutschmann et al. (1996), for only (R11) and (R12) result in the dash-dotted curve shown in the figure, which is in reasonable agreement with observations. The catalytic reactions used in the modeling depend on the presence of catalytic "centers". The amount of these centers was adjusted in the model to obtain the curve shown in Fig. 10. An initial level of only a few ppm was needed, consistent with what might be present (in terms of impurities) in any experimental venue. The required concentration of centers is sufficiently small such that after crossing the explosion limit (i.e. at higher temperatures) the catalytic enhancement of the rates for (R11) and (R12) have no effect on ignition delay predictions. Localized radical production rates from catalytically accelerated H_2O_2

formation/decomposition between the third and extended second limit leads to an overall straight chain kinetic conversion to H atoms and OH radicals ($HO_2+H_2 \rightarrow H_2O_2+H \rightarrow OH+OH+H$) and the exothermic reaction of OH with hydrogen to produce water and H rapidly drives the reacting systems across the extended second limit.

Clearly additional effort is needed to experimentally investigate what processes may be present in each of the noted experimental configurations that augment the reaction rate above that consistent with homogenous kinetics at (estimated) experimental conditions (pressure, temperature, etc.). The hypothesis that surfaces can promote chemical induction is entirely consistent with all of the experimental observations and their departure from homogenous predictions. It is further noted that catalytic wall effects may even be present in reflected shock experiments since end-wall/corner tube surfaces have fast transient heating times (Andreev and Tsirkunov, 1985) in comparison to chemical induction kinetic times at conditions where the disparities are noted.

In summary, we note that the large differences observed between high-pressure/low-temperature syngas ignition delay measurements and homogenous kinetic calculations are similar to those for hydrogen/air systems first described decades ago. These discrepancies are a result in large measure to departures of the experimental configurations from behavior dominated by homogeneous gas phase kinetics alone, and to aberrations of homogenous gas phase chemistry of the hydrogen-oxygen kinetic systems by multi-dimensional, surface-coupled effects. The congruous nature of the experimental data shown in Fig. 10 is interesting and suggests that whatever the perturbation may be, the reduction in chemical induction times are of the same order of magnitude in all of the experimental devices considered. In Fig. 10 a band of possible ignition times obtained by multiplying and dividing the catalytic enhancement terms described

above by a factor of ten is also shown. The relative level of catalytic enhancement certainly changes the overall ignition delay significantly (up to an order of magnitude at any temperature). However, in all cases the predicted ignition delays remain significantly shorter than those derived from the unperturbed homogenous gas phase model at all temperatures below 1100 K and orders of magnitude shorter than the homogenous values for T< 900 K.

Although we acknowledge that improvements in kinetic parameters for gas phase reactions can certainly be made, there is no reasonable change in the rates of any elementary kinetic step (or third body efficiencies) involved in the oxidation of H_2/CO or H_2 mixtures that can reconcile the large disparity of the data and homogeneous kinetic predictions shown in Fig. 10. An approximating assumption, that the perturbation is derived solely by homogeneous catalysis of reactions (R11) and (R12), provides a good empirical modeling tool that can be used in engineering designs to fit experimental observations, irrespective of the source of the chemical induction perturbations.

EFFECT OF IMPURITIES ON THE H_2/CO SYSTEM

Iron Pentacarbonyl – $Fe(CO)_5$

Williams and Shaddix (2007) have recently reported observing wall deposits formed when operating a swirl-stabilized combustor running on simulated syngas-air mixtures. The deposits were analyzed and found to be composed mostly of iron oxides and, to a lesser extent, nickel oxides. It was concluded that the source of the metal contaminants was the CO used. For laboratory combustion experiments, many researchers use CO stored in high pressure carbon-steel cylinders. CO can readily react at high pressure with metals present in steel to form carbonyls; especially iron pentacarbonyl, $Fe(CO)_5$. Depending on handling, steel CO cylinders

obtained from commercial suppliers with, initially, little or no contaminants are prone to contamination by $Fe(CO)_5$ over time. For example, Tepe et al. (1999), measured levels of up to 200 ppm $Fe(CO)_5$ in CO steel cylinders stored over a nine month period. Over this period it was observed that $Fe(CO)_5$ levels increased by a factor of as much as seven. This was attributed to the pressure in the cylinder (~ 120 atm) as pressure greatly affects the rate of iron pentacarbonyl formation.

Metallic compounds have been shown to have strong flame inhibition effects (Lask and Wagner, 1960; Reinelt and Linteris, 1996; Rumminger and Linteris, 2000, 2002; Rumminger et al., 1999; Vanpee and Shirodkar, 1978). When present in premixed flames, iron pentacarbonyl can reduce the burning velocity considerably (Lask and Wagner, 1960; Reinelt and Linteris, 1996; Rumminger and Linteris, 2000). Of relevance to the present discussion is the work of Rumminger and Linteris (2000) who studied stoichiometric $H_2/CO/O_2/N_2$ premixed flames with hydrogen contents of up to 1.5%. It was shown that reductions in burning velocity of 30% were attained for $Fe(CO)_5$ concentrations on the order of 150 ppm as a result of a catalytic inhibition cycle that removes H and O atoms. At higher iron pentacarbonyl loadings, it was observed that the inhibition effectiveness decreased due to saturation of the catalytic cycle, and perhaps particle condensation (Rumminger and Linteris, 2000).

The above discussions led us to further analyze recent measurements of syngas laminar burning velocities at both atmospheric and elevated pressures. As shown in Fig. 18 there exists considerable scatter in available atmospheric pressure measurements (Burke et al., 2007; Hassan et al., 1997; McLean et al., 1994; Sun et al., 2007), especially at rich conditions. A similar trend is also observed for high pressure H_2/CO flame conditions (Burke et al., 2007; Sun et al., 2007), see Fig. 19. Even though inconsistencies may be due in part to data processing methodology to

obtain laminar burning velocities (e.g. Burke et al., 2007), unintentional addition of iron pentacarbonyl from the CO source used in these studies (generally unreported) might contribute to the observed differences.

Rumminger et al (1999) developed a submechanism for $FeCO_5$ interactions in flames that reasonably reproduced their experimental data at low $Fe(CO)_5$ loadings (< 100 ppm). For the conditions we investigated, the CO source was assumed to contain 200 ppm of $Fe(CO)_5$ so that the overall maximum iron pentacarbonyl mixture concentrations for a wide range of equivalence ratio were always less than 75 ppm, approximately. To further investigate the effects of $Fe(CO)_5$ contamination on CO burning velocities, the $Fe(CO)_5$ submechanism, kinetic rate correlations, and transport properties developed by Rumminger et al. (1999) were added to the model of Li et al. (2007). Figs. 18 and 19 compare the predicted burning velocities for pure fuel (solid lines) and for mixtures using CO contaminated by 200 ppm of $Fe(CO)_5$ (dashed lines) with experimental data.

Figures 18 and 19 confirm that $Fe(CO)_5$ has a very noticeable effect on rich flames, in qualitative agreement with the onset of the experimental disparities found in the literature. A sensitivity analysis of burning velocity on kinetic rates (Fig. 20) shows that iron containing species become important at rich conditions. Burning velocity inhibition of rich flames is due to a chemical catalytic cycle that removes reactive H radicals (i.e. the "H-atom" cycle, Rumminger et al., 1999). A chemical flux analysis for a 20 atm, $\phi = 3$, flame (Fig. 21) reveals that hydrogen atoms are removed through reactions involving iron oxide and hydroxide species (i.e. the cycle $FeO \rightarrow Fe(OH)_2 \rightarrow FeOH \rightarrow FeO$). The "O-atom" cycle (Rumminger and Linteris, 2000) involving the path $Fe \rightarrow FeO_2 \rightarrow FeO \rightarrow Fe$ is not active in the cases studied here since the present flames have considerable amounts of hydrogen as opposed to the case studied by

Rumminger and Linteris (2000). Figure 20, however, shows that iron oxide hydroxide – FeO(OH) – is also an important species as it interacts with the main H-atom cycle (not noted in prior work).

The previous discussion raises concern regarding recent updating of kinetic models to reproduce fuel-rich burning velocity data. Sun et al. (2007) proposed model revisions based primarily on high pressure H_2/CO/He burning velocity measurements (up to 40 atm). Revisions were motivated by the fact that predictions using other published models (Davis et al, 2005; Li et al., 2007) deviated from their experimental measurements at rich conditions. A revised model was developed to better predict these high pressure H_2/CO burning velocity predictions. Sun et al. (2007) also report favorable comparisons against other H_2 as well as H_2/CO targets (Dean et al., 1978; Fotache et al., 2000; Mueller et al., 1999b; Yetter et al, 1991b), claiming the model to be the most comprehensively tested of those present in the literature.

However, Fig. 22 compares predictions using the model of Sun et al. (2007) against experimental burning velocities for high pressure pure hydrogen flames (Tse et al., 2000). Unfortunately, the model updates presented by Sun et al. (2007) seriously degrade agreement with these experimental data at rich conditions. The differences between the measurements of Burke et al. (2007)and Sun et al. (2007) cannot be satisfactorily explained; however further experimental measurements in our laboratory confirm the results of Burke et al. (2007) are free of $Fe(CO)_5$ contaminant effects (Burke, personal communication). The uncertainties in fuel rich burning rate data remain disconcerting, and additional experimental work that includes consideration of iron carbonyl effects is needed.

We also investigated numerically the effects of $Fe(CO)_5$ on counterflow diffusion flame ignition (Fotache et al., 2000) as well as homogeneous ignition delay (Dean et al., 1978) of

H_2/CO systems, again assuming 200 ppm $Fe(CO)_5$ concentration in the CO source. No substantial differences were found between predictions with or without iron pentacarbonyl in the fuel source for the counterflow configuration. The flame initiation (Fotache et al., 2000) occurs on the air side, and due to the low diffusivity of iron-containing species, results are not affected by the presence of $Fe(CO)_5$ in the fuel stream. When 100 ppm of $Fe(CO)_5$ was added to the air stream, however, ignition temperatures increased considerably. For example, for 5% H_2 / 95% CO flames at 1 atm and a strain of 100 s^{-1} Fotache et al. (2000) report an ignition temperature of approximately 956 K, in close agreement with model predictions. Adding 100 ppm $Fe(CO)_5$ to the air side increases the modeled ignition temperature to approximately 1030 K. The presence of iron pentacarbonyl in the fuel source may, therefore, affect counterflow observations for flames that reside on the fuel side.

Oxidation of carbon monoxide in shock tubes has been shown to be accelerated in the presence of chromium, nickel, and iron carbonyls (Izod et al., 1972; Matsuda, 1972a; Matsuda, 1972b). Here, we performed ignition delay calculations under the conditions used in the shock tube study of Petersen et al. (2007). At these conditions and by assuming a CO source contaminated by 200 ppm of $Fe(CO)_5$ an overall mixture concentration of iron pentacarbonyl of approximately 10 ppm was obtained. Over a temperature range of 850-2000 K, computations showed moderate ignition delay reductions on the order of 3% to 30%. Recently, Linteris (2007) attributed this reduction to early build-up of H and OH radicals through reactions of iron compounds with H_2 and O_2. At higher $Fe(CO)_5$ loadings, the radical scavenging cycles shown in Fig. 21 will reduce radical concentrations leading to ignition delay inhibition (Linteris, 2007). Such high concentrations (on the order of a few hundred ppm), however, cannot occur given the estimated iron pentacarbonyl contamination levels of CO cylinder sources.

The radical scavenging cycles described above would also be expected to affect flow reactor measurements. The presence of iron pentacarbonyl, even in trace amounts at flow reactor conditions, alter measurements near the explosion limit of H_2/O_2 as well as $H_2/CO/O_2$ mixtures as shown in Fig. 23. Figure 23 plots the characteristic reaction times of stoichiometric H_2/CO mixtures defined as the initial (H_2+CO) mole fraction divided by the maximum rate of (H_2+CO) consumption. $Fe(CO)_5$ shifts the temperature at which the explosion limit is reached but its effect is not as pronounced at temperatures above and below the explosion limit and as pressure increases. The moist CO oxidation experiments of Mueller et al. (1999b) were performed at conditions near the explosion limit, but typically at pressures and equivalence ratios where the effects of iron pentacarbonyl are small. We cannot unequivocally state that none was present, but perturbations, if they exist, are likely within experimental uncertainties of kinetic measurements for pure mixtures. Moreover, the decomposition of iron pentacarbonyl occurs at temperatures above 475 K (Dewar and Jones, 1905). In flow reactor experiments, fuel supply lines are well above these temperatures, approaching the reaction temperature, yielding free iron that would immediately be fully oxidized upon entry into the reaction zone.

In this section we have shown that carbon monoxide sources used in research should be carefully scrutinized in terms of metallic impurities. The presence of these impurities under syngas generation from coal gasification and its downstream purification will be intimately tied to the process design and material construction Thus, the commercial implications of metal carbonyl contamination are unknown, but deserve attention. For research purposes, carbonyl-free carbon monoxide sources supplied in pressurized aluminum cylinders with brass fittings should be used. The above discussion supports the need for further experimental investigation of

carbonyl effects, especially on burning rate measurements of syngas mixtures to be used for model validation.

Nitrogen Oxides (NO_X)

Generation of syngas (through coal gasification, for example) for gas turbine applications can lead to the presence of small hydrocarbons (e.g., methane) and other combustion gas components (e.g. NO_x) in these systems, particularly in mixing regions of entering fuel and air. These contaminants can have significant influence on the underlying H_2/O_2 sub-model behavior. For example, as shown by Ashmore and Tyler (1962) and more recently by Mueller et al. (1998, 1999b) the presence of small quantities of NO_x can drastically modify the relative influence of HO_2 chemistry at conditions near the extended second explosion limit of the H_2/O_2 system. NO_x provides an alternate consumption route for HO_2 radicals via $NO+HO_2=NO_2+OH$ (R13). The NO_2 so formed can then react with H atoms via $NO_2+H=NO+OH$ (R14) to give back NO and thereby reactions (R13) and (R14) establish a catalytic cycle which consumes H_2 at temperatures well below the explosion limits of the unperturbed system. This coupling results in two very important effects. In the temperature range where this catalytic cycle is active, small amounts of NO_x significantly affect the overall chemical reaction rate, principally through substantial reductions in the chemical induction time leading to establishing critical branching. At very low NO_x concentrations (sub-ppm), essentially all the NO is oxidized to NO_2 without significant consequence. However, increasing the NO_x concentration beyond a threshold value (which is very low) leads to sufficient NO_2 concentrations that enable reaction (R14) to compete effectively with reaction (R2) for H atoms. In this case, not only is the extended second explosion limit behavior modified, but the overall rate of reaction (defined by the fuel

concentration reacted over the characteristic reaction time) is significantly altered. At higher concentrations of NO_x, the reaction NO+OH=HONO (R15) rapidly comes to partial equilibrium, and the addition of further amounts of NO leads to chemical inhibition by removal of OH radicals.

Figure 24 shows the effects of the addition of small amounts of NO on the constant pressure oxidation of H_2/CO mixtures at pressures from 0.5 to 40 atm. This figure plots the numerically predicted characteristic reaction times (using the model of Li et al., 2007 with NO_x kinetic reactions adopted from Mueller et al., 1999b), similarly defined as for Fig. 23. For low pressures and at temperatures below the explosion limit (clearly evident in Fig. 24), HO_2 radicals are the primary chain carriers and the addition of even small quantities of NO can reduce the characteristic reaction times by orders of magnitude This result can have significant consequences on the autoignition characteristics of hydrogen-oxygen and carbon monoxide-hydrogen-oxygen reactions if small amounts of combustion exhaust gases become back-mixed into entering reactants.

Note from Fig. 24 that there is a non-linear effect in terms of the amount of added NO, and further that the effect is also a function of both reaction temperature and pressure. Addition of an appropriate amount of NO causes the overall activation energy of the reaction to be nearly the same above and below the explosion limit condition. The difference in overall oxidation rate above and below the explosion limit eventually is decreased (due to the increased rate of reactions involving HO_2), and the explosion limit becomes described by essentially the same overall temperature dependence. It is this function that is most important in defining the engineering parameters over which mixing can be accomplished without flashback or pre-ignition in gas turbine systems.

The effect of NO_x on ignition under back-mixing conditions in gas turbines has not been studied previously and is beyond the scope of the present discussion. However, a recent consideration of residual gas effects in reciprocating spark ignition combustion of hydrogen provides an interesting example of this important coupling. Hydrogen has received considerable attention from several automotive manufacturers for use in hydrogen-fueled internal combustion engines (H_2ICEs) (Tang et al., 2002) as well as an additive to improve performance, efficiency, and emissions of homogeneous charge compression ignition (HCCI) engines. The inherent hydrogen characteristics allow H_2ICEs to operate at very lean conditions with good stability as well as high compression ratios and thermal efficiencies (White et al., 2006).

To investigate the importance of NO_x contamination as a result of in-cylinder residual gas, we numerically studied the autoignition of hydrogen/air mixtures with added trace amounts of NO under HCCI conditions. Simulations were performed during a single compression/expansion cycle utilizing the geometric parameters of the Scania-D12-based single cylinder engine (parameter values can be found in the work of Andrae et al., 2005). This engine has been the subject of recent experimental testing as part of the "Green Car" project involving Volvo, Scania CV, Shell, and the Swedish government (Hultqvist et al., 2002; Nygren et al., 2002). Stoichiometric H_2/air homogeneous mixtures were considered with trace amounts of NO ranging from 10 to 1000 ppm. Modeling was performed utilizing a single zone approach (i.e. no crevices or charge inhomogeneities) and neglecting heat transfer to the cylinder wall (i.e. adiabatic case). This approach is useful for comparative purposes as it provides an estimate of ignition delay as a function of the thermodynamic conditions in the combustion chamber. Simulations employed a modified Perfectly Stirred Reactor code (Glarborg et al., 1986) coupled with CHEMKIN II libraries (Kee et al., 1989). The kinetics and thermochemistry used for these calculations were

derived by combining the Li et al., 2007 model with the nitrogen sub-model components found in Mueller et al. (1999b). Calculations were performed as a function of crank angle degrees (CAD) with a resolution of 0.1 degrees. Operating conditions were chosen based on reported experiments (Andrae et al., 2005; Hultqvist et al., 2002; Nygren et al., 2002). Namely, two engine speeds were selected (900, 1200 RPM) at two inlet temperatures (100^{o}C, 140^{o}C) with no intake boost (i.e. intake pressure = 1 atm).

Based on the results shown in Fig. 25, the presence of NO is observed to significantly affect the autoignition time of the mixture present in the cylinder, especially at concentration levels above 100 ppm. The preliminary results indicate that at "low" intake temperatures, the ignition advance due to the NO present in the mixture increases for increasing engine speed whereas this effect appears to be suppressed as the intake temperature increases. While additional studies at other intake temperatures and engine speeds as well as different intake boost pressures are needed to better determine engine effects, the present results point to the need to consider NO coupling through EGR utilization in hydrogen engine operation. Exhaust gas analyses of H_2ICEs (White et al., 2006) have shown NO_x levels of nearly 10000 ppm at near stoichiometric conditions (with no after treatment). In-cylinder, residual levels will be much lower, depending on the internal exhaust gas recirculation operating condition, but certainly could be in the range of concentrations utilized in the above calculations.

CONCLUSION

Recent interest in gas turbine syngas combustion has inspired an extension of the existing experimental validation resources to considerably higher pressures and lower temperatures that are sufficient for testing the comprehensive nature of existing detailed chemical kinetic models.

The present paper has reviewed these experimental efforts and the proposed kinetic changes suggested for improving predictions of the new data have been discussed. The higher pressure, lower temperature conditions encountered in gas turbines points to the importance and the need of further theoretical as well as experimental studies of elementary reactions involving HO_2 and H_2O_2. We note that recent re-evaluations of the reaction rate for $CO+HO_2=CO_2+OH$ (R7) are primarily important to ignition delay measurements at high pressures due to modifications of induction chemistry and have little influence on post induction observations. It appears that modifications in the reaction of $HO_2+OH=H_2O+O_2$ (R8) improve comparisons of predictions with high pressure oxidation, but recommended rate correlations for this reaction should be modified to avoid exceeding collisional rates at high temperatures.

We show that recent investigations of high pressure ignition and flame propagation of H_2/CO mixtures should be cautiously evaluated prior to implementing any changes to improve the agreement of predictions from chemical kinetic models. H_2/CO ignition measurements in shock tubes, rapid compression machines, and flow reactors can exhibit aberrations at low temperature and high pressures that cause observations to differ from homogenous gas phase predictions. Although phenomena characterized as mild ignition in hydrogen-oxygen shock tube experiments are historically well known and can even be kinetically differentiated from strong ignition observations, the source(s) of chemical induction perturbations that lead to their manifestation are not understood in quantitative detail. We show here that similar behavior of syngas mixtures is derived almost entirely as a result of perturbations of hydrogen-oxygen chemical induction kinetics, with only minor differences from the presence of carbon monoxide. Numerous processes can affect induction chemistry (i.e. compressible flow, physical mixing, and/or catalytic surface coupling), and it is likely that no one cause is universally responsible for

the mild ignition observations in shock tubes. Moreover, that multiple sources of chemical induction perturbations can all lead to similar magnitudes of reduction in ignition delay in the mild ignition regime is the reason that observations in shock tube venues, are "correlated" with experimental observations in other venues (flow reactors, rapid compression machine experiments). From comparing several rapid compression machine data sets, it appears that in some cases perturbing sources and effects may differ. However, it is unlikely that in real systems, perturbations can be controlled to an extent such that homogenous kinetic predictions provide limiting, realistic design criteria. We show here that by approximating these perturbation effects as homogenous catalytic enhancements of the limiting kinetic rates of only two reactions, the order of magnitude discrepancies of pure homogenous kinetic ignition delay predictions and perturbed experimental observations can be reasonably reproduced. While the exact nature and relative importance of each perturbing source in the various experimental venues remains to be determined, this simple approach can yield valuable engineering approximation for the safe design of lean premixing systems for gas turbines, based upon fundamental experimental data.

Carbon monoxide stored in high-pressure carbon-steel cylinders is commonly used in laboratory research. These sources are prone to contamination by metal carbonyls and it has been shown through computations that these contaminants, especially iron pentacarbonyl, can considerably affect fuel rich H_2/CO laminar burning velocities. The potential effect of this contaminant in applied conditions is unknown, but it is important that fuel-rich burning rate measurements used for validation of kinetic models should be carefully scrutinized for contaminant effects. Quantitative experimental validation of carbonyl effects remain to be

completed. The importance of other trace contaminants, i.e. NO_x, on the kinetic behavior of H_2 and H_2/CO oxidation at gas turbine as well as engine conditions has also been discussed.

ACKNOWLEDGEMENTS

This work was supported by the U.S Department of Energy under Grant Number DE-FG02-86ER13503 from the Chemical Sciences, Geosciences and Biosciences Division, Office of Basic Energy Sciences, Office of Science and by the Pittsburgh National Energy Technology Laboratories under Grant Number DE-FG26-05NT42544. The authors would like to thank Dr. Gregory Linteris for providing an electronic version of the iron pentacarbonyl kinetic model developed at NIST.

REFERENCES

Allen, T.L., Fink, W.H., and Volman, D.H. (1996) Theoretical Studies of the Mechanism of the Gas Phase Reaction of the Hydroperoxo Radical with Carbon Monoxide to Form Hydroxyl Radical and Carbon Dioxide. *J. Phys. Chem.*, 100, 5299-5302.

Andrae, J., Johansson, D., Björnbom, P., Risberg, and P., Kalghatgi, G. (2005) Co-Oxidation in the Auto-Ignition of Primary Reference Fuels and *n*-Heptane/Toluene Blends. *Combust. Flame*, 140, 267-286.

Andreev, P.P. and Tsirkunov, Y.M. (1986) Conjugate Heat Exchange in the Initial Stage of Reflection of a Viscous Shock Wave from a Wall. *J. Eng. Phys. Thermophys.*, 51, 909-914.

Ashmore, P.G. and Tyler, B.J. (1962) Reaction of Hydrogen Atoms with Nitrogen Dioxide. *Trans. Farad. Soc.*, 58, 1108-1116.

Baulch, D.L., Bowman, C.T., Cobos, C.J., Cox, R.A., Just, T., Kerr, J.A., Pilling, M.J., Stocker, D., Troe, J., Tsang, W., and Walker, R.W. (2005) Evaluated Kinetic Data for Combustion Modeling: Supplement II. *J. Phys. Chem. Ref. Data*, 34, 757-1397.

Baulch, D.L., Cobos, C.J., Cox, R.A., Frank, P., Hayman, G., Just, T., Kerr, J.A., Murrells, T., Pilling, M.J., Troe, J., Walker, R.W., and Warnatz J. (1994) Evaluated Kinetic Data for Combustion Modeling: Supplement I. *J. Phys. Chem. Ref. Data*, 23, 847-1033.

Baulch, D.L., Drysdale, D.D., Duxbury, J., and Grant, S. (1973) *Evaluated Kinetic Data for High Temperature Reactions*. Vol. 3, Butterworths, London.

Beerer, D.J. and McDonell, V.G. (2007) Experimental Study of Ignition Delay for Application to Hydrogen and Syn-gas Fired Lean Premixed Gas Turbine Engines. *Proceedings of the Fifth U.S. Combustion Meeting*, San Diego, CA, paper E01.

Blumenthal, R., Fieweger, K., Komp, K.H., Adomeit, G., and Gelfand B.E. (1995) Self-Ignition of H_2-Air Mixtures at High Pressure and Low Temperature. *Proc. of the 20th Int. Symp. on Shock Waves*, 935-940.

Blumenthal, R., Fieweger, K., Komp, K.H., and Adomeit, G. (1996) Gas Dynamic Features of Self Ignition of Non Diluted Fuel/Air Mixtures at High Pressure. *Comb. Sci. Tech.*, 113-114, 137-166.

Bradley, D., Lawes, M., Liu, K., Verhelst, S., and Woolley, R. (2007) Laminar Burning Velocities of Lean Hydrogen–Air Mixtures at Pressures up to 1.0 MPa. *Combust. Flame*, 149, 162-172.

Braun M., Hofzumahaus, A., and Stuhl F. (1982) VUV Flash-Photolysis Study of the Reaction of HO with HO_2 at 1 Atm and 298 K. *Ber. Bunsenges. Phys. Chem.*, 86, 597-602.

Burke. M.P., Qin, X., Ju, Y., and Dryer, F.L. (2007) Measurements of Hydrogen Syngas Flame Speeds at Elevated Pressures. *Proceedings of the Fifth U.S. Combustion Meeting*, San Diego, CA, paper A16.

Burrows, J.P., Cox, R.A., and Derwent, R.G. (1981) Modulated Photolysis of the Ozone-Water Vapour System: Kinetics of the Reaction of OH with HO_2. *J. Photochem.*, 16, 147-168.

Chaos, M., Kazakov, A., Zhao, Z., and Dryer, F.L. (2007) A High-Temperature Chemical Kinetic Model for Primary Reference Fuels. *Int. J. Chem. Kinet.*, 39, 399-414.

Chiesa, P., Consonni, S., Kreutz, T., and Williams R.H. (2005) Co-production of Hydrogen, Electricity and CO_2 from Coal with Commercially Ready Technology. Part A: Performance and Emissions. *Int. J. Hydrogen Energ.*, 30, 747-767.

Cox, R.A., Burrows, J.P., and Wallington, T.J. (1981) Rate Coefficient for the Reaction OH + HO_2 = H_2O + O_2 at 1 Atmosphere Pressure and 308 K. *Chem. Phys. Lett.*, 84, 217-221.

Craig, R.R. (1966) A Shock Tube Study of the Ignition Delay of Hydrogen-Air Mixtures Near the Second Explosion Limit. Report AFAPL-TR-66-74, Air Force Aeropropulsion Lab, Wright-Patterson.

Davis, S.G., Joshi, A.V., Wang, H., and Egolfopoulos, F. (2005) An Optimized Kinetic Model of H_2/CO Combustion. *Proc. Combust. Inst.*, 30, 1283-1292.

Dean, A.M., Steiner, D.C., and Wang, E.E. (1978) A Shock Tube Study of the $H_2/O_2/CO/Ar$ and $H_2/N_2O/CO/Ar$ Systems: Measurement of the Rate Constant for $H + N_2O = N_2 + OH$. *Combust. Flame*, 32, 73-84.

Demore, W.B. (1979) Reaction of HO_2 with O_3 and the Effect of Water Vapor on HO_2 Kinetics. *J. Phys. Chem.*, 83, 1113-1118.

DeMore, W.B. (1982) Rate Constant and Possible Pressure Dependence of the Reaction Hydroxyl + Hydroperoxo. *J. Phys. Chem.*, 86, 121-126.

Deutschmann, O., Schmidt, R., Behrendt, F., and Warnatz, J. (1996) Numerical Modeling of Catalytic Ignition. *Proc. Combust. Inst.*, 26, 1747-1754.

Dewar, J. and Jones H.O. (1905) The Physical and Chemical Properties of Iron Carbonyl. *Proc. Roy. Soc. Lond. A*, 76, 558-577.

Dixon-Lewis, G. and Williams, D.J. (1977) The Oxidation of Hydrogen and Carbon Monoxide. In Branford, C.H. and Tipper, C.F.H. (eds.) *Comprehensive Chemical Kinetics*, Elsevier, Amsterdam, vol. 17, pp. 1-248.

Dry, M.E. (2002) The Fischer-Tropsch Process: 1950-2000. *Catal. Today*, 71, 227-241.

Dryer, F.L. and Chaos, M. (2007) Ignition of Syngas/Air and Hydrogen/Air Mixtures at Low Temperatures and High Pressures: Experimental Data Interpretation and Kinetic Modeling Implications. *Combust Flame*, doi:10.1016/j.combustflame.2007.08.005.

EIsworth, J.E., Haskell, W.W., and Read, I.A. (1969) Non-Uniform Ignition Processes in Rapid-Compression Machines. *Combust. Flame*, 13, 437-438.

Fotache, C.G., Tan, Y., Sung, C.J., and Law, C.K. (2000) Ignition of CO/H2/N2 versus Heated Air in Counterflow: Experimental and Modeling Results. *Combust. Flame*, 120, 417–426.

Fujimoto, S. (1963) Chemical Reaction In A Shock Wave I: The Ignition Delay of a Hydrogen-Oxygen Mixture in a Shock Tube. *Bull. Chem. Soc. Japan*, 36, 1233-1236.

Gardiner, Jr., W.C. and Olson, D.B. (1980) Chemical Kinetics of High Temperature Combustion. *Ann. Rev. Phys. Chem.*, 31, 377-399.

Gardiner, W.C. and Wakefield, C.B. (1970) Influence of Gasdynamic Processes on the Chemical Kinetics of the Hydrogen-Oxygen Explosion at Temperatures near 1000^{o}K and Pressures of Several Atmospheres. *Astro. Acta*, 15, 399-409.

Glarborg, P. (2007) Hidden Interactions - Trace Species Governing Combustion and Emissions. *Proc. Combust. Inst.*, 31, 77-98.

Glarborg, P., Kee, R.J., Grcar, J.F., and Miller, J.A. (1986) PSR: A Fortran Program for Modeling Well-Stirred Reactors. Technical Report SAND86-8209, Sandia National Laboratories.

Goodings, J.M. and Hayhurst, A.N. (1988) Heat Release and Radical Recombination in Premixed Fuel-Lean Flames of $H_2 + O_2 + N_2$ - Rate Constants for $H + OH + M \rightarrow H_2O + M$ And $HO_2 + OH \rightarrow H_2O + O_2$. *J. Chem. Soc. Faraday Trans. 2*, 84, 745-762.

Hahn, J., Krasnoperov, L., Luther, K., and Troe, J. (2004) Pressure Dependence of the Reaction $H + O_2$ (+Ar) $\rightarrow HO_2$ (+Ar) in the Range 1-900 bar and 300-700 K. *Phys. Chem. Chem. Phys.*, 6, 1997-1999.

Hassan, M.I., Aung, K.T., Faeth, G.M. (1996) Markstein Numbers and Unstretched Laminar Burning Velocities of Wet Carbon Monoxide Flames. AIAA Paper 96-0912.

Haskell, W.W. (1970) Fuel Ignition in a Rapid Compression Machine: Sensitivity to Flame Ignition by Particles. SAE Paper 700059.

Hessler, J.P. (1998) Calculation of Reactive Cross Sections and Microcanonical Rates from Kinetic and Thermochemical Data. *J. Phys. Chem. A*, 102, 4517-4526.

Hippler, H. and Troe, J. (1992) Rate Constants of the Reaction HO + H_2O_2 → HO_2 + H_2O at T ≥ 1000 K. *Chem. Phys. Lett.*, 192, 333-337

Hippler, H., Troe, J., and Willner, J. (1990) Shock Wave Study of the Reaction HO_2 + HO_2 → H_2O_2 + O_2: Confirmation of a Rate Constant Minimum near 700 K. *J. Chem. Phys.*, 93, 1755-1760.

Hippler, H., Neubauer, H., and Troe, J. (1995) Shock Wave Studies of the Reactions HO + H_2O_2 → H_2O + HO_2 and HO + HO_2 → H_2O + O_2 between 930 and 1680 K. *J. Chem. Phys.*, 103, 3510-3516.

Hultqvist, A., Christensen, M., Johansson, B., Richter, M., Nygren, J., Hult, J., and Aldén, M. (2002) The HCCI Combustion Process in a Single Cycle-High-Speed Fuel Tracer LIF and Chemiluminescence Imaging. SAE paper 2002-01-0424.

Hwang S.M., Ryu, S.-O., De Witt, K.J., and Rabinowitz, M.J. (2005) High Temperature Rate Coefficient Measurements of H + O_2 Chain-Branching and Chain-Terminating Reaction. *Chem. Phys. Lett.*, 408, 107-111.

Izod, T.P.J, Kistiakowsky, G.B., and Matsuda, S. (1972) Mechanism of Oxidationof Carbon Monoxide in the Presence of Chromium Carbonyl. *J. Chem. Phys.*, 56, 1083-1090.

Kalitan, D.M. and Petersen, E.L. (2005) Ignition and Oxidation of Lean CO/H_2 Fuel Blends in Air. AIAA Paper 2005-3767.

Kalitan, D.M., Petersen, E.L., Mertens, J.D., and Crofton, M.W. (2006) Ignition of Lean CO/H_2/Air Mixtures at Elevated Pressures. ASME Paper GT2006-90488.

Kappel, Ch., Luther, K., and Troe, J. (2002) Shock Wave Study of the Unimolecular Dissociation of H_2O_2 in its Falloff Range and of its Secondary Reactions. *Phys. Chem. Chem. Phys.*, 4, 4392-4398.

Kazakov, A., Chaos, M., Zhao, Z., and Dryer, F.L. (2006) Computational Singular Perturbation Analysis of Two-Stage Ignition of Large Hydrocarbons. *J. Phys. Chem. A*, 110, 7003-7009.

Kee, R.J., Rupley, F.M., and Miller, J.A. (1989) CHEMKIN II: A Fortran Chemical Kinetics Package for the Analysis of Gas Phase Chemical Kinetics. Technical Report SAND89-8009, Sandia National Laboratories.

Keyser, L.F. (1988) Kinetics of the Reaction $OH + HO_2 \rightarrow H_2O + O_2$ From 254 K to 382 K. *J. Phys. Chem.*, 92, 1193-1200.

Kim, T.J., Yetter, R.A., and Dryer, F.L. (1994) New Results on Moist CO Oxidation: High Pressure, High Temperature Experiments and Comprehensive Kinetic Modeling. *Proc. Combust. Inst.*, 25, 759-766.

Kurylo, M.J., Klais, O., and Laufer, A.H. (1981) Mechanistic Investigation of the $HO + HO_2$ Reaction. *J. Phys. Chem.*, 85, 3674-3678.

Lask, G. and Wagner, H.Gg. (1960) Influence of Additives on the Velocity of Laminar Flames. *Proc. Combust. Inst.*, 8, 432-438.

Lee, D. and Hochgreb, S. (1998) Hydrogen Autoignition at Pressures above the Second Explosion Limit (0.6–4.0 MPa). *Int. J. Chem. Kinet.*, 30, 385-406.

Lewis, B. and von Elbe, G. (1987) *Combustion, Flames and Explosion of Gases*. 3rd Ed., Academic Press, Inc., Orlando.

Li, J., Zhao, Z., Kazakov, A., and Dryer, F.L. (2004) An Updated Comprehensive Kinetic Model of Hydrogen Combustion. *Int. J. Chem. Kinet.*, 36, 566-575.

Li, J., Zhao, Z., Kazakov, A., Chaos, M., Dryer, F.L., and Scire, Jr., J.J. (2007) A Comprehensive Kinetic Mechanism for CO, CH_2O, and CH_3OH Combustion. *Int. J. Chem. Kinet.*, 39, 109-136.

Lii, R.-R., Corse, R.A., Sauer, M.C., and Gordon, S. (1980) Temperature Dependence of the Gas-Phase Self-Reaction of Hydroperoxo Radicals In The Presence Of Ammonia. *J. Phys. Chem.*, 84, 813-817.

Linteris, G.T. (2007) Promotion of Hydrogen-Air Ignition by Iron Compounds. *Fall Technical Meeting of the Eastern States Section of the Combustion Institute*, Charlottesville, VA, paper C06.

Lutz, A.E., Kee, R.J., and Miller, J.A. (1987) SENKIN: A Fortran Program for Predicting. Homogeneous Gas Phase Chemical Kinetics with Sensitivity Analysis. Technical Report SAND87-8248, Sandia National Laboratories.

Maas, U. and Warnatz, J. (1988) Ignition Processes in Hydrogen Oxygen Mixtures. *Combust. Flame*, 74, 53-69.

Martynenko, V.V., Penyaz'kov, O.G., Ragotner, K.A., and Shabunya, S.I. (2004) High-Temperature Ignition of Hydrogen and Air at High Pressures Downstream of the Reflected Shock Wave. *J. Eng. Phys. Thermophys.*, 77, 785-793.

Matsuda, S. (1972a) Gas Phase Homogeneous Catalysis in Shock Waves. II. The Oxidation of Carbon Monoxide by Oxygen in the Presence of Iron Pentacarbonyl. *J. Chem. Phys.*, 57, 807-812.

Matsuda, S. (1972b) Gas Phase Homogeneous Catalysis in Shock Waves. III. The Oxidation of Carbon Monoxide by Oxygen in the Presence of Nickel Carbonyl. *J. Phys. Chem.*, 76, 2833-2838.

McLean, I.C., Smith, D.B., and Taylor, S.C. (1994) The Use of Carbon Monoxide/Hydrogen Burning Velocities to Examine the Rate of the CO + OH Reaction. *Proc. Combust. Inst.*, 25, 749-757.

Meyer, J.W. and Oppenheim, A.K. (1970) On the Shock Induced Ignition of Explosive Gases. *Proc. Combust. Symp.*, 13, 1153-1164.

Michael, J.V., Su, M.C., Sutherland, J.W., Carroll, J.J., and Wagner, A.F. (2002) Rate Constants for $H+O_2+M \rightarrow HO_2+M$ in Seven Bath Gases. *J. Phys. Chem. A*, 106, 5297-5313.

Mittal, G., Sung, C.J., and Yetter, R.A. (2006) Autoignition of H_2/CO at Elevated Pressures in a Rapid Compression Machine. *Int. J. Chem. Kinet.*, 38, 516–529.

Mittal, G., Sung, C.J., Fairweather, M., Tomlin, A.S., Griffiths, J.F., and Hughes, K.J. (2007) Significance of the HO_2+CO Reaction during the Combustion of CO+H_2 Mixtures at High Pressures. *Proc. Combust. Inst.*, 31, 419-428.

Miyama, H. and Takeyama, T. (1964) Kinetics of Hydrogen-Oxygen Reaction in Shock Waves. *J. Chem. Phys.*, 41, 2287-2290

Mueller, M.A., Kim, T.J., Yetter, R.A., and Dryer, F.L. (1999a) Flow Reactor Studies and Kinetic Modeling of the H_2/O_2 Reaction. *Int. J. Chem. Kinet.*, 31, 113-125.

Mueller, M.A., Yetter, R.A., and Dryer, F.L. (1998) Measurement of the Rate Constant for H + O_2 + M $\rightarrow$ HO_2 + M (M = N_2, Ar) Using Kinetic Modeling of the High-Pressure $H_2/O_2/NO_x$ Reaction. *Proc. Combust. Inst.*, 27, 177-184.

Mueller, M.A., Yetter, R.A., and Dryer, F.L. (1999b) Flow reactor studies and kinetic modeling of the $H_2/O_2/NO_x$ and $CO/H_2O/O_2/NO_x$ reactions. *Int. J. Chem. Kinet.*, 31, 705-724.

Natarajan, J., Lieuwen, T., and Seitzman, J. (2007) Laminar Flame Speeds of H_2/CO Mixtures: Effect of CO_2 Dilution, Preheat Temperature, and Pressure. *Combust. Flame*, 151, 104-119.

Nygren, J., Hult, J., Richter, M., Aldén, M., Christensen, M., Hultqvist, A., and Johansson, B. (2002) Three-Dimensional Laser Induced Fluorescence of Fuel Distributions in an HCCI Engine. *Proc. Combust. Inst.*, 29, 679-685.

Oppenheim, A.K. (1985) Dynamic Features of Combustion. *Phil, Trans. R. Soc. Lond. A*, 315, 471-508.

Oran, E.S. and Boris, J.P. (1982) Weak and Strong Ignition. II. Sensitivity of the Hydrogen-Oxygen System. *Combust. Flame*, 48, 149-162.

Oran, E.S. and Gamezo, V.M. (2007) Origins of the Deflagration-to-Detonation Transition in Gas-Phase Combustion. *Combust. Flame*, 148, 4-47.

Oran, E.S., Young, T.R., Boris, J.P., and Cohen, A. (1982) Weak and Strong Ignition. I. Numerical Simulation of Shock Tube Experiments. *Combust. Flame*, 48, 135-148.

Peeters, J. and Mahnen, G. (1973) Reaction Mechanisms and Rate Constants of Elementary Steps in Methane-Oxygen Flames. *Proc. Combust. Inst.*, 14, 133-146.

Peschke, W.T. and Spadaccini, L.J. (1985) Determination of Autoignition and Flame Speed Characteristics of Coal Gases having Medium Heating Values. Electric Power Research Institute, Report EPRI AP-4291.

Petersen, E.L., Kalitan, D.M., Barrett, A.B., Reehal, S.C., Mertens, J.D., Beerer, D.J., Hack, R.L., and McDonell, V.G. (2007) New Syngas/Air Ignition Data at Lower Temperature and Elevated Pressure and Comparison to Current Kinetics Models. *Combust. Flame*, 149, 244-247.

Reinelt, D. and Linteris, G.T. (1996) Experimental Study of the Inhibition of Premixed and Diffusion Flames by Iron Pentacarbonyl. *Proc. Combust. Inst.*, 26, 1421-1428.

Roesler, J.F., Yetter, R.A., and Dryer, F.L. (1994) On the Dependence of the Rate of Moist CO Oxidation on O_2 Concentration at Atmospheric Pressure. *Combust. Sci. Tech.*, 95, 161-171.

Rozenshtein, V.B., Gershenzon, Yu.M., Il'in, S.D., and Kishkovjtch, O.P. (1984) Reactions of HO_2 with NO, OH and HO_2 Studied by EPR/LMR Spectroscopy. *Chem. Phys. Lett.*, 112, 473-478.

Rumminger, M.D. and Linteris, G.T. (2000) Inhibition of Premixed Carbon Monoxide-Hydrogen-Oxygen-Nitrogen Flames by Iron Pentacarbonyl. *Combust. Flame*, 120, 451-464.

Rumminger, M.D. and Linteris, G.T. (2002) The Role of Particles in the Inhibition of Counterflow Diffusion Flames by Iron Pentacarbonyl. *Combust. Flame*, 128, 145-164.

Rumminger, M.D., Reinelt, D., Babushok, V., and Linteris, G.T. (1999) Numerical Study of the Inhibition of Premixed and DiffusionFlames by Iron Pentacarbonyl. *Combust. Flame*, 116, 207-219.

Ruscic, B., Pinzon, R.E., Morton, M.L., Srinivasan, N.K., Su, M.-C., Sutherland, J.W., Michael, J.V. (2006) Active Thermochemical Tables: Accurate Enthalpy of Formation of Hydroperoxyl Radical, HO_2. *J. Phys. Chem. A*, 110, 6592-6601.

Ruscic, B., Wagner, A.F., Harding, L.B., Asher, R.L., Feller, D., Dixon, D.A., Peterson, K.A., Song, Y., Qian, X., Ng, C.-Y., Liu, J., Chen, W., and Schwenke, D.W. (2002) On the

Enthalpy of Formation of Hydroxyl Radical and Gas-Phase Bond Dissociation Energies of Water and Hydroxyl. *J. Phys. Chem. A*, 106, 2727-2747.

Sabia, P., Schießwohl, E., de Joannon, M.R., and Cavaliere, A. (2006) Numerical Analysis of Hydrogen Mild Combustion. *Turk. J. Eng. Env. Sci.*, 30, 127-134.

Sawyer, R.F. (1965) The Homogeneous Gas Phase Kinetics of Reactions in the Hydrazine - Nitrogen Tetroxide Propellant System. Ph.D. dissertation. Report No. 761, Aerospace and Mechanical Sciences, Princeton University, Princeton, NJ.

Schott, G.L. and Kinsey, J.L. (1958) Kinetic Studies of Hydroxyl Radicals in Shock Waves. 2. Induction Times in the Hydrogen-Oxygen Reaction. *J. Chem. Phys.*, 29, 1177-1182.

Sivaramakrishnan, R., Comandini, A., Tranter, R. S., and Brezinsky, K. 6th International Conference on Chemical Kinetics, Gaithersburg, MD, July 25–29, 2005.

Sivaramakrishnan, R., Comandini, A., Tranter, R.S., Brezinsky, K., Davis, S.G., and Wang, H. (2007) Combustion of CO/H_2 Mixtures at Elevated Pressures. *Proc. Combust. Inst.*, 31, 429-437.

Skinner, G.B. and Ringrose, G.H. (1965) Ignition Delays of Hydrogen-Oxygen-Argon Mixture at Relatively Low Temperatures. *J. Chem. Phys.*, 42, 2190-2192.

Slack, M.W. (1977) Rate Coefficient for $H + O_2 + M = HO_2 + M$ Evaluated from Shock Tube Measurements of Induction Times. *Combust. Flame*, 28, 241-249.

Snyder, A.D., Robertson, J., Zanders, D.L., and Skinner, G.B. (1965) Shock Tube Studies of Fuel-Air Ignition Characteristics. Report AFAPL-TR-65-93, Air Force Aeropropulsion Lab, Wright-Patterson.

Sridharan, U.C., Qiu, L.X., and Kaufman, F. (1984) Rate Constant of the $OH + HO_2$ Reaction from 252 to 420 K. *J. Phys. Chem.*, 88, 1281-1282.

Srinivasan, N.K., Su, M.-C, Sutherland, J.W., Michael, J.V., and Ruscic, B. (2006) Reflected Shock Tube Studies of High-Temperature Rate Constants for OH + $NO_2 \rightarrow HO_2$ + NO and OH + $HO_2 \rightarrow H_2O + O_2$. *J. Phys. Chem. A*, 110, 6602-6607.

Strehlow, R.A. and Cohen, A. (1962) Initiation of detonation. *Phys. Fluids*, 5, 97-101.

Sun, H.Y., Yang, S.I., Jomaas, G., and Law, C.K. (2007) High-Pressure Laminar Flame Speeds and Kinetic Modeling of Carbon Monoxide/Hydrogen Combustion. *Proc. Combust. Inst.*, 31, 439-446.

Sung, C.-J. and Law, C.K. (2007) Fundamental Combustion Properties of H_2/CO Mixtures: Ignition and Flame Propagation at Elevated Pressures. *Combust. Sci. Tech.*, this issue.

Swigart, R. (1958) A Study of the Kinetics of the Hydrogen-Oxygen Reaction in a New Flow Reactor. M.S.E. Thesis. Report No. 432, Aerospace and Mechanical Sciences, Princeton University, Princeton, NJ.

Tang, X., Kabat, D.M., Natkin, R.J., Stockhausen, W.F., and Heffel, J.W. (2002) Ford P2000 Hydrogen Engine Dynamometer Development. SAE Paper 2002-01-0242.

Tepe, R.K., Vassallo, D., Jacksier, T., and Barnes, R.M. (1999) Iron Pentacarbonyl Determination in Carbon Monoxide. *Spectrochim. Acta B*, 54, 1861, 1868.

Terao, K. (1977) Explosion Limits of Hydrogen-Oxygen Mixtures as a Stochastic Phenomenon. *Jap. J. Appl. Phys.*, 16, 29-38.

Troe J. and Ushakov, V.G. (2001) Theoretical Studies of the HO + O $\leftrightarrow$ HO_2 $\leftrightarrow$ H + O_2 Reaction. II. Classical Trajectory Calculations on an Ab Initio Potential for Temperatures Between 300 and 5000 K. *J. Chem. Phys.*, 115, 3621-3628.

Troe, J. (2000) Detailed Modeling of the Temperature and Pressure Dependence of the Reaction H + O_2 (+M) $\rightarrow$ HO_2 (+M). *Proc. Combust. Inst.*, 28, 1463-1469.

Tsang, W and Hampson, R.F. (1987) Chemical Kinetic Database for Combustion Chemistry. 1. Methane and Related-Compounds. *J. Phys. Chem. Ref. Data*, 15, 1087-1279.

Tse, S.D., Zhu, D.L., and Law, C.K. (2000) Morphology and Burning Fluxes of Expanding Spherical Flames in H2/O2/Inert Mixtures up to 60 Atmospheres. *Proc. Combust. Inst.*, 28, 1793–1800.

Vanpee, M. and Shirodkar, P.P. (1978) Study of Flame Inhibition by Metal Compounds. *Proc. Combust. Inst.*, 17, 787-795.

Vermeersch, M.L. (1991) A Variable Pressure Flow Reactor for Chemical Kinetics Studies: Hydrogen, Methane and Butane Oxidation at 1 to 10 Atmospheres and 880 to 1,040 K. Ph.D. dissertation. Number 1916-T, Department of Mechanical and Aerospace Engineering, Princeton University, Princeton, NJ.

Voevodsky, V.V. and Soloukhin, R.I. (1965) On the Mechanism and Explosion Limits of Hydrogen-Oxygen Chain Self-Ignition in Shock Waves. *Proc. Combust. Inst.*, 10, 279-283.

Wakefield, C.B., Ripley, D.L., and Gardiner, W.C. (1969) Chemical Kinetics of the Shock-Initiated Combustion of Hydrogen at High Pressure and Low Temperatures. *J. Chem. Phys.*, 50, 325-332.

Walton, S.M., He, X., Zigler, B.T., and Wooldridge, M.S. (2007a) An Experimental Investigation of the Ignition Properties of Hydrogen and Carbon Monoxide Mixtures for Syngas Turbine Applications. *Proc. Combust. Inst.*, 31, 3147-3154.

Walton, S.M., He, X., Zigler, B.T., and Wooldridge, M.S. (2007b) An Experimental Investigation of Iso-octane Ignition Phenomena. *Combust. Flame*, 150, 246-262.

Wang, B.L., Olivier, H., and Grönig, H. (2003) Ignition of Shock-Heated H_2-Air-Steam Mixtures. *Combust. Flame*, 133, 93-106.

Westbrook, C.K. and Dryer, F.L. (1984) Chemical Kinetics Modeling of Hydrocarbon Combustion. *Prog. Energ. Combust. Sci.*, 10, 1-57.

White, C., Oefelein, J., and Siebers, D. (2006) Sandia Hydrogen-Fueled Internal Combustion Engine Program. National Science Foundation Workshop on Research Frontiers for Combustion in the Hydrogen Economy, Arlington, VA, March 9-10.

Wilhelm, D.J., Simbeck, D.R., Karp, A.D., and Dickenson R.L. (2001) Syngas Production for Gas-to-Liquids Applications: Technologies, Issues and Outlook. *Fuel Process. Technol.*, 71, 139-148.

Williams, T.C. and Shaddix, C.R. (2007) Contamination of Carbon Monoxide with Metal Carbonyls: Implications for Combustion Research. *Combust. Sci. Tech.*, 175, 1225-1230.

Yetter, R.A., Dryer, F.L., and Rabitz, H. (1985) Some Interpretive Aspects of Elementary Sensitivity Gradients in Combustion Kinetics Modeling. *Combust Flame*, 59, 107-133.

Yetter, R.A., Dryer, F.L., and Rabitz, H. (1991a) A Comprehensive Reaction Mechanism for Carbon Monoxide/Hydrogen/Oxygen Kinetics. *Combust. Sci. Tech.*, 79, 97-128.

Yetter, R.A., Dryer, F.L., and Rabitz, H. (1991b) Flow Reactor Studies of Carbon Monoxide/Hydrogen/Oxygen Kinetics. *Combust. Sci. Tech.*, 79, 129-140.

Yetter, R.A., Rabitz, H., and Hedges, R.M. (1991c) A Combined Stability-Sensitivity Analysis of Weak and Strong Reactions of Hydrogen/Oxygen Mixtures. *Int. J. Chem. Kinet.*, 23, 251-278.

You, X., Wang, H., Goos, E., Sung, C.J., and Klippenstein, S.J. (2007) Reaction Kinetics of CO + HO_2 → Products: Ab Initio Transition State Theory Study with Master Equation Modeling. *J. Phys. Chem. A*, 111, 4031-4042.

Zhao, Z., Chaos, M., Kazakov, A., and Dryer, F.L. (2008) Thermal Decomposition Reaction and a Comprehensive Kinetic Model of Dimethyl Ether. *Int. J. Chem. Kinet.*, 40, 1-18.

Zhao, Z., Li, J., Kazakov, A., and Dryer, F.L. (2005) Temperature-Dependent Feature Sensitivity Analysis for Combustion Modeling. *Int. J. Chem. Kinet.*, 37, 282-295.

TABLES

Table 1. List of reactions discussed in the text.

Label	*Reaction*
(R1)	$H + O_2 = O + OH$
(R2)	$H + O_2 (+M) = HO_2 (+M)$
(R3)	$H + OH + M = H_2O + M$
(R4)	$CO + OH = CO_2 + H$
(R5)	$HCO + M = H + CO + M$
(R6)	$HCO + O_2 = HO_2 + CO$
(R7)	$CO + HO_2 = CO_2 + OH$
(R8)	$HO_2 + OH = H_2O + O_2$
(R9)	$H_2O_2 + OH = HO_2 + H_2O$
(R10)	$HO_2 + H = 2OH$
(R11)	$H_2O_2 + M = OH + OH$
(R12)	$H_2 + HO_2 = H_2O_2 + H$
(R13)	$NO + HO_2 = NO_2 + OH$
(R14)	$NO_2 + H = NO + OH$
(R15)	$NO + OH = HONO$

FIGURE CAPTIONS

Figure 1. Temperature dependence of the low-pressure limit reaction rate of $H+O_2(+M)\rightarrow HO_2(+M)$ for M = Ar. The recent evaluation of Baulch et al. (2005) is also plotted with associated uncertainties.

Figure 2. Rate coefficient for reaction $CO+HO_2=CO_2+OH$ obtained from a number of empirical and theoretical studies.

Figure 3. Comparison between measured (Mittal et al., 2006) and predicted RCM ignition delay times for a $(H_2+CO)/O_2/N_2/Ar$ – 12.5/6.25/18.125/63.125 (molar) mixture. R_{CO} is the fraction of CO in (H_2+CO). Compressed conditions are 50 bar and 1044 K. Lines show the difference in the quality of model predictions when the rate of You et al. (2007) for (R7) (Eqn. 1) is used in the model of Li et al. (2007).

Figure 4. Reactions participating in the thermal evolution of a $H_2/CO/O_2/N_2$ kinetic system (molar composition 6.25/6.25/6.25/18.125 % in balance Ar) under rapid compression machine conditions of 30 bar and 1011 K (Mittal et al., 2006) obtained from CSP analysis. Analyses were performed after the compression stroke at the selected points shown in the top figure.

Figure 5. Rate constants for $HO_2+OH=H_2O+O_2$; – Peeters and Mahnen (1973); – DeMore (1979); – Lii et al. (1980); – Cox et al. (1981); – Kurylo et al (1981); – Braun et al. (1982); – DeMore (1982); – Goodings and Hayhurst (1988); – Keyser (1988); – Hippler and Troe (1992) (reevaluation of data from Hippler et al., 1990); – Hippler et al. (1995); – Kappel et al. (2002); – Srinivasan et al. (2006); dashed line – rate expression of Sivaramakrishnan et al. (2007) (Eqn. 2); solid line – present fit (Eqn. 3) considering the rate minimum measured by Hippler et al. (1995); dash-dot line – present fit

(Eqn. 4) considering the rate minimum measured by Kappel et al. (2002). The figure insert provides details of data and rate fits at high temperatures.

Figure 6. CSP analysis of the induction period during H_2/CO oxidation under the shock tube conditions of Sivaramakrishnan et al. (2007); H_2/CO/O_2 = 160/450/320 ppm in balance Ar at 300 bar and 1355 K. The top figure shows the temporal pressure profile along with the points chosen for CSP analysis. Note that the participation indices of reactions (R1) and (R2) have been reduced by one third to better display the spectrum of other reactions involved in the system.

Figure 7. Oxygen flux paths for dilute H_2/CO/O_2/Ar mixtures in a shock tube. Conditions are (from Sivaramakrishnan et al., 2007): a) 163/408/300 ppm H_2/CO/O_2 in Ar at 42.5 atm, 1386 K, and 13.9 ms residence time; b) 176/475/325 ppm H_2/CO/O_2 in Ar at 435.5 atm, 1392 K, and 11.5 ms residence time. The thickness of the arrows is proportional to the reaction rate of progress (in mol/cm^3/s) of reactions involving the connected species integrated over the residence time and has been normalized in each case by the flux of $O_2 \rightarrow HO_2$. The table below the figure lists reactions involved in the paths shown along with their percent contribution to the *destruction* of a given species.

Figure 8. Species profiles during the oxidation of stoichiometric CO/H_2/O2/Ar mixtures in a shock tube. Initial conditions can be found in Sivaramakrishnan et al. (2007), average pressures are (a) 24 atm; (b) 43 atm; (c) 256 atm; (d) 450 atm. - O_2; - CO; - CO_2, experiments. - O_2; - CO; - CO_2, base model (Li et al., 2007). - O_2; - CO; - CO_2, base model with updates for reactions (R7) and (R8) (see text).

Figure 9. Calculated HO_2 and OH concentrations as a function of time for the conditions listed in Fig. 7. Solid and dashed lines are HO_2 and OH profiles, respectively. Gray and black lines are results for the 42.5 and 435.5 atm cases, respectively.

Figure 10. Ignition delay times of syngas/air (Peschke and Spadaccini, 1985; Petersen et al., 2007; Walton et al., 2007a) and hydrogen/air mixtures (Blumenthal et al., 1995). Conditions: 38.6% H_2 + 51.1% CO + 10.3% CO_2 + Air, ϕ = 0.5, 16.5 < P < 28.9 atm (Petersen et al, 2007; shock tube), 11.9 < P < 23 atm (Peschke and Spadaccini, 1985); 50% H_2 + 50% CO + Air, 0.33 < ϕ < 0.6, 5.0 < P < 5.3 atm (Petersen et al., 2007; flow reactor); (6.7 < H_2 < 13.6%) + (4.5 < CO < 9.1%) + (16.2 < O_2 < 18.6%) + (44.1 < N_2 < 63.2%), 0.3 < ϕ < 0.7, 12 < P < 23.5 atm (Walton et al., 2007a); 15% H_2 in air, 35 < P < 47 bar (Blumenthal et al., 1995). Filled and open circles correspond to strong and weak ignition events, respectively (Blumenthal et al., 1995). All experimental data have been normalized to 20 atm assuming proportionality to P^{-1}. Lines correspond to ignition delay calculations performed using the model of Li et al. (2007) at 20 atm; the solid line corresponds to the syngas mixture used in the shock tube experiments of Petersen et al. (2007), the dashed line to the conditions of Blumenthal et al. (1995), and the dash-dot line are predictions obtained for syngas ignition by catalyzing reactions involved in the formation and decomposition of H_2O_2 (R11 and R12, see text). The grey area denotes the range of ignition delays that are obtained when multiplying or dividing the catalytic rates by a factor of 10. To improve clarity, modeled results are not shown for times greater than 1 s although it is noted that predictions can reach values of approximately 1000 s for the lowest temperatures (T ~ 630 K).

Figure 11. Hydrogen shock tube ignition delays (symbols) from a number of experimental studies compared against chemical kinetic predictions (lines) using the model of Li et al. (2007).

Figure 12. Shadowgraphs of the ignition process of 15% H_2 + 85 % air mixtures in a shock tube. a) Mild ignition: 7.7 atm, 977 K, 100 μs separation between frames; b) Strong ignition: 3.4 atm, 1096 K, 40 μs separation between frames. Images adopted from Blumenthal et al. (1996).

Figure 13. Schlieren records of the ignition process of 15% H_2 + 85 % air mixtures in a shock tube. a) Mild ignition: 3.65 atm, 1030 K, 300 μs separation between frames; b) Strong ignition: 4.5 atm, 1156 K, 8 μs separation between frames. Images adopted from Wang et al. (2003).

Figure 14. Experimental H_2/CO ignition delay data (Walton et al., 2007a) normalized to the conditions shown using the expression developed by Walton et al. (2007a) (also shown). The circled data have been used here to perform regression analyses (Eqn. 5).

Figure 15. Comparison of syngas (Walton et al., 2007a) and hydrogen (Lee and Hochgreb, 1998) rapid compression ignition data. The data of Lee and Hochgreb (1998) have been normalized to 15 atm using $P^{-0.96}$, as found in their study; the syngas data of Walton et al. (2007a) are normalized to the conditions shown using the parameters of Eqn. 5. Solid circles are the data chosen for regression (see Fig. 14).

Figure 16. Comparison of rapid compression ignition delay times (Lee and Hochgreb, 1998; Mittal et al., 2006; Walton et al., 2007a) scaled with oxygen concentration.

Figure 17. Syngas ignition delay sensitivity to reaction rates for a mixture of 38.6% H_2 + 51.1% CO + 10.3% CO_2 + Air, $\phi = 0.5$ at 20 atm.

Figure 18. Laminar burning velocities of H_2:CO mixtures (1:1) in air at 1 atm. Symbols are experimental measurements. The solid line shows the predictions of the model of Li et al. (2007); the dashed line are results assuming a $Fe(CO)_5$ content of 200 ppm in the CO (using the kinetic subset of Rumminger et al., 1999).

Figure 19. Laminar burning velocities of H_2:CO (1:3) + O_2:He (1:7) mixtures at high pressure. Symbols are experimental measurements. The solid line shows the predictions of the model of Li et al. (2007); the dashed line are results assuming a $Fe(CO)_5$ content of 200 ppm in the CO (using the kinetic subset of Rumminger et al., 1999).

Figure 20. Burning velocity sensitivity to iron pentacarbonyl reaction rates for H_2:CO (1:3) + O_2:He (1:7) premixed flames at 20 atm. For relative comparison the most sensitive rate is that of reaction (R1) with a coefficient of 0.45.

Figure 21. Iron pentacarbonyl reaction pathways for a H_2:CO (1:3) + O_2:He (1:7) premixed flame at 20 atm and $\phi = 3$. It is assumed that the CO contains 200 ppm of $Fe(CO)_5$. The width of the arrows is proportional to the integrated species flux; the numbers in parenthesis denote the percentage contribution to the destruction of the species connected to the arrow tails. The integration domain was chosen to be from the cold boundary to the location of maximum H radical concentration.

Figure 22. Measured and calculated unstretched laminar mass burning rates for H_2 + (O2:He – 1:11.5) flames at 10, 15, and 20 atm. Symbols are experimental data (Tse et al., 2000); solid lines are predictions using the model of Sun et al. (2007); dashed lines are predictions using the model of Li et al. (2007).

Figure 23. Characteristic reaction times of stoichiometric H_2/CO mixtures at flow reactor conditions (0.5% H_2/0.5% CO/0.5% O_2/ in balance N_2). Predictions using the model of Li

et al. (2007) are shown for pure CO (solid lines) and CO contaminated with 200 ppm of $Fe(CO)_5$.

Figure 24. Characteristic reaction times of H_2/CO mixtures as a function of temperature at various pressures and initial NO concentrations. For illustration purposes mixture compositions similar to those of Mittal et al. (2006) are chosen (H_2/CO/O_2/N_2/Ar – 6.25/6.25/6.25/18.125/63.125 %). Reaction times were determined assuming isobaric systems.

Figure 25. Calculated pressure traces as a function of crank angle for stoichiometric H_2/Air/NO mixtures (0, 10, 100, and 1000 ppm initial NO concentration) at different engine speeds for inlet temperatures of 100^{o}C (left panel) and 140^{o}C (right panel). Calculations start at inlet valve closing (-139 degrees ATDC, after top dead center). Only a region spanning 100 crank angle degrees (CAD) is shown to better illustrate the effect of NO.

FIGURES

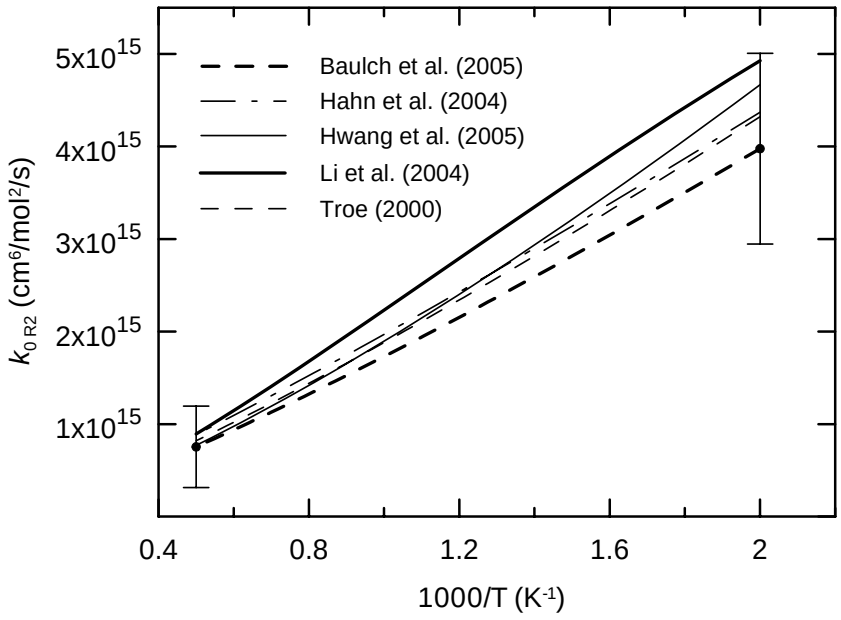

Figure 1

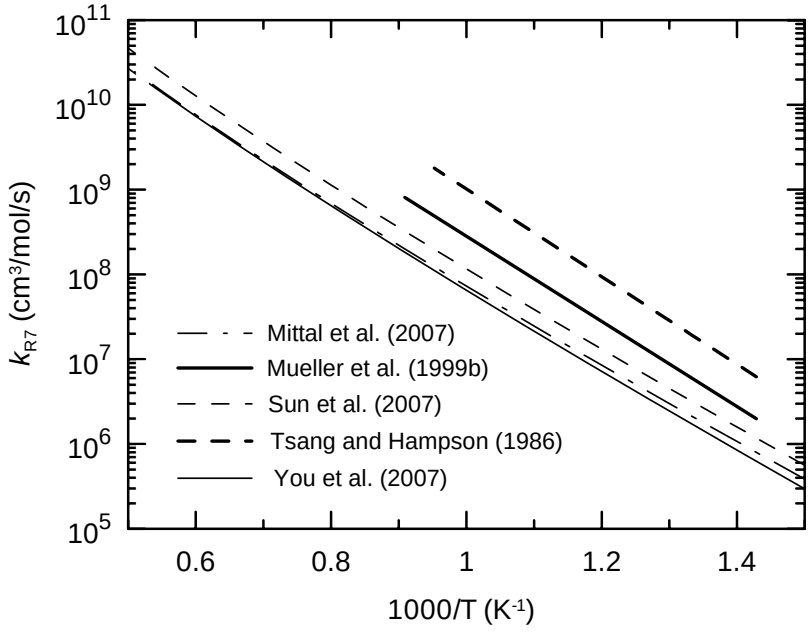
10^{11}
10^{10}
10^{9}
10^{8}
10^{7}
10^{6}
10^{5}
k_{R7} (cm³/mol/s)
Mittal et al. (2007)
Mueller et al. (1999b)
Sun et al. (2007)
Tsang and Hampson (1986)
You et al. (2007)
0.6
0.8
1
1.2
1.4
1000/T (K^{-1})

Figure 2

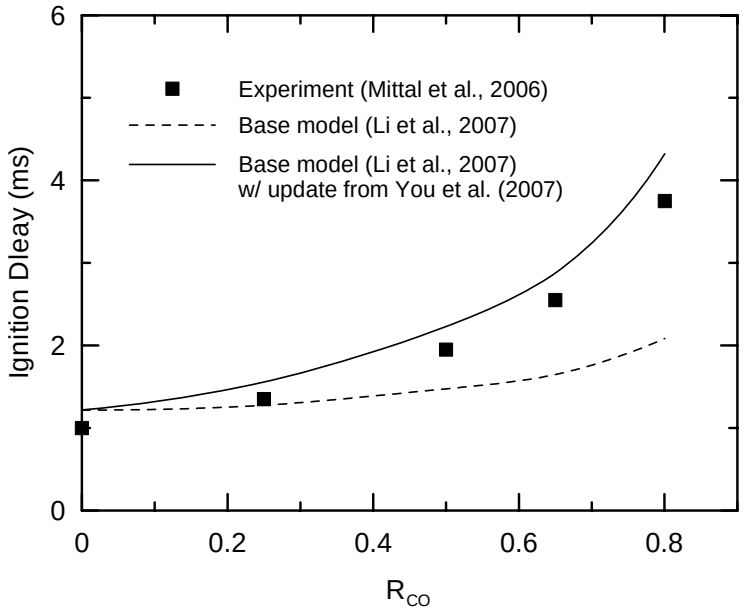
Experiment (Mittal et al., 2006)
Base model (Li et al., 2007)
Base model (Li et al., 2007)
w/ update from You et al. (2007)
Ignition Dleay (ms)
0
2
4
6
0
0.2
0.4
0.6
0.8
R_{CO}

Figure 3

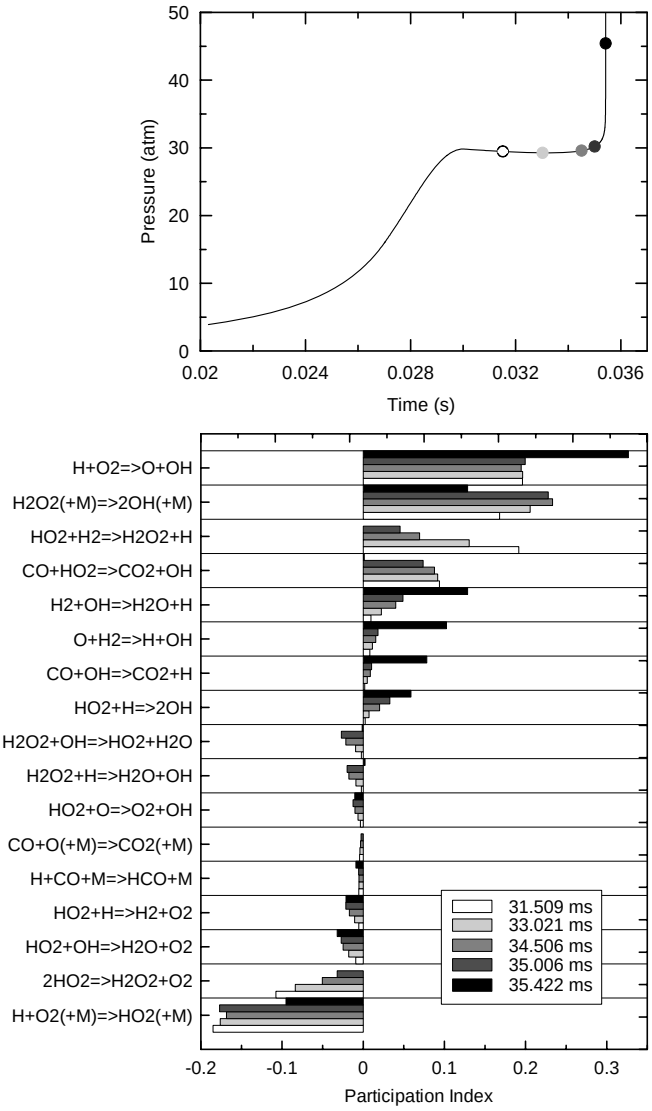
Pressure (atm)
Time (s)
H+O2=>O+OH
H2O2(+M)=>2OH(+M)
HO2+H2=>H2O2+H
CO+HO2=>CO2+OH
H2+OH=>H2O+H
O+H2=>H+OH
CO+OH=>CO2+H
HO2+H=>2OH
H2O2+OH=>HO2+H2O
H2O2+H=>H2O+OH
HO2+O=>O2+OH
CO+O(+M)=>CO2(+M)
H+CO+M=>HCO+M
HO2+H=>H2+O2
HO2+OH=>H2O+O2
2HO2=>H2O2+O2
H+O2(+M)=>HO2(+M)
31.509 ms
33.021 ms
34.506 ms
35.006 ms
35.422 ms
Participation Index

Figure 4

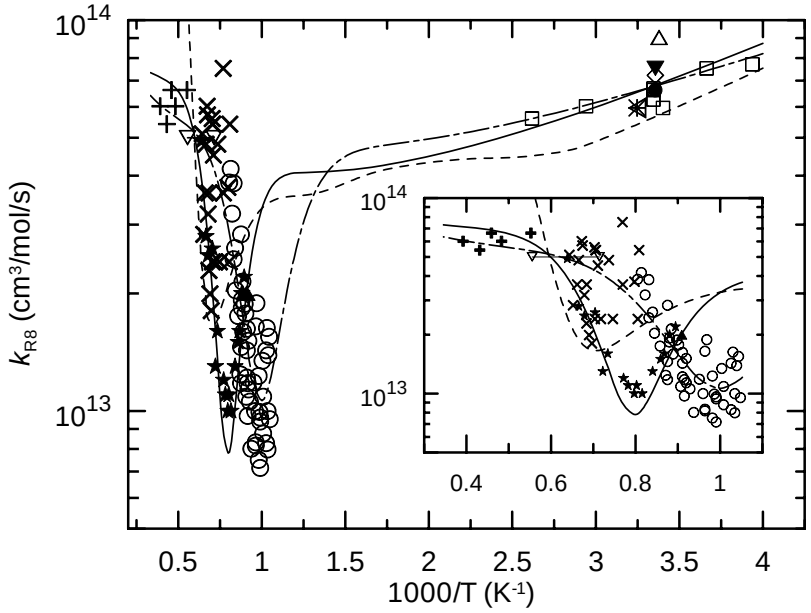
10^{14}
10^{13}
k_{R8} (cm³/mol/s)
0.5
1
1.5
2
2.5
3
3.5
4
1000/T (K⁻¹)
10^{14}
10^{13}
0.4
0.6
0.8
1

Figure 5

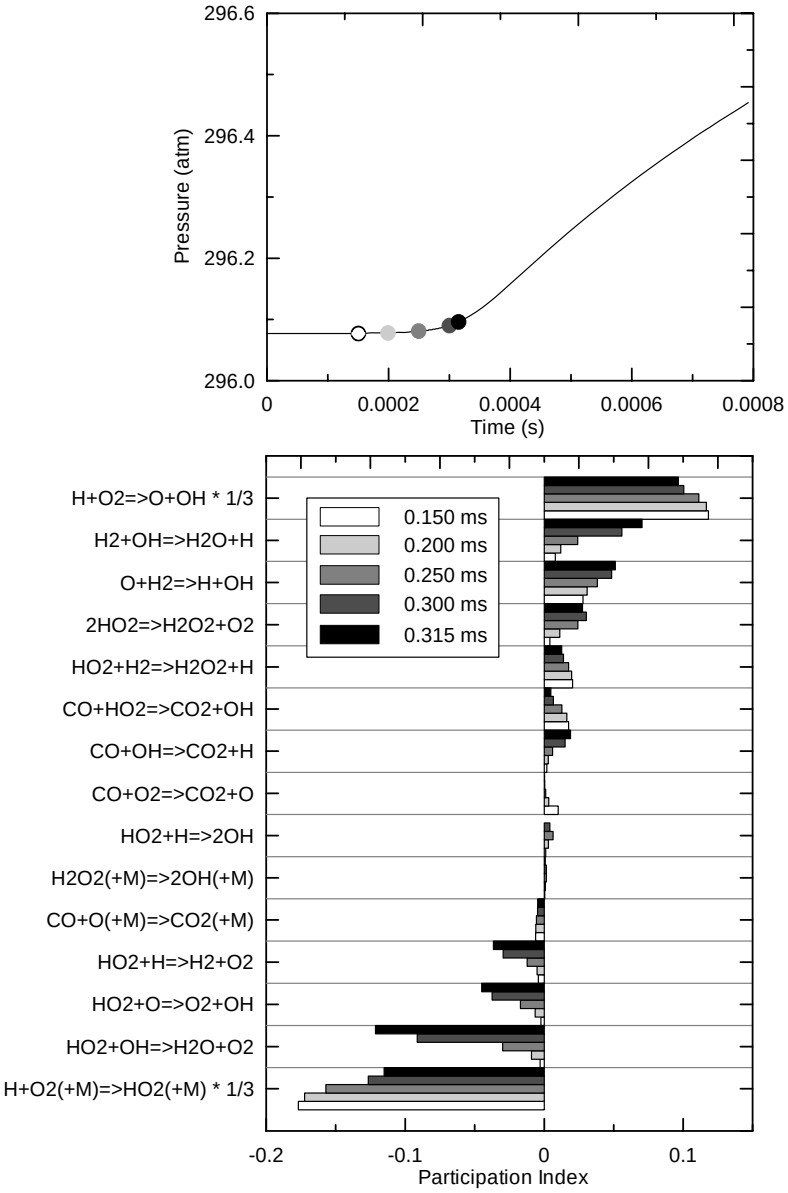
296.6
296.4
296.2
296.0
Pressure (atm)
0
0.0002
0.0004
0.0006
0.0008
Time (s)
H+O2=>O+OH * 1/3
H2+OH=>H2O+H
O+H2=>H+OH
2HO2=>H2O2+O2
HO2+H2=>H2O2+H
CO+HO2=>CO2+OH
CO+OH=>CO2+H
CO+O2=>CO2+O
HO2+H=>2OH
H2O2(+M)=>2OH(+M)
CO+O(+M)=>CO2(+M)
HO2+H=>H2+O2
HO2+O=>O2+OH
HO2+OH=>H2O+O2
H+O2(+M)=>HO2(+M) * 1/3
0.150 ms
0.200 ms
0.250 ms
0.300 ms
0.315 ms
-0.2
-0.1
0
0.1
Participation Index

Figure 6

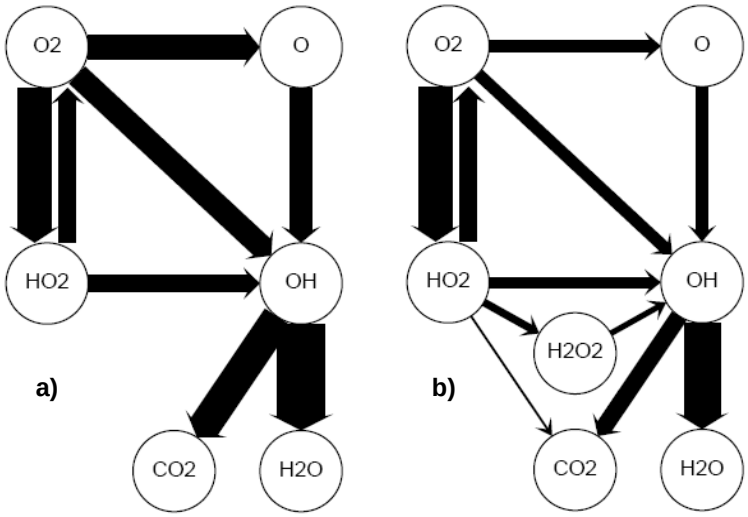

O_2

$H+O_2(+M)=HO_2(+M)$	57%
$H+O_2=O+OH$	43%

O

$O+H_2=H+OH$	58%
$HO_2+O=O_2+OH$	30%
$O+H+M=OH+M$	6%
$CO+O(+M)=CO_2(+M)$	3%
$O+H_2O=2OH$	3%

HO_2

$HO_2+H=2OH$	48%
$HO_2+O=O_2+OH$	21%
$HO_2+OH=H_2O+O_2$	20%
$HO_2+H=H_2+O_2$	10%
$2HO_2=H_2O_2+O_2$	1%

OH

$H_2+OH=H_2O+H$	46%
$CO+OH=CO_2+H$	41%
$HO_2+OH=H_2O+O_2$	8%
$H+OH+M=H_2+M$	5%

O_2

$H+O_2(+M)=HO_2(+M)$	81%
$H+O_2=O+OH$	19%

O

$O+H_2=H+OH$	68%
$HO_2+O=O_2+OH$	26%
$O+H_2O=2OH$	3%
$CO+O(+M)=CO_2(+M)$	2%
$O+H+M=OH+M$	1%

HO_2

$2HO_2=H_2O_2+O_2$	50%
$HO_2+H=2OH$	16%
$HO_2+OH=H_2O+O_2$	13%
$CO+HO_2=CO_2+OH$	11%
$HO_2+O=O_2+OH$	7%
$HO_2+H=H_2+O_2$	3%

OH

$H_2+OH=H_2O+H$	62%
$CO+OH=CO_2+H$	28%
$HO_2+OH=H_2O+O_2$	10%

H_2O_2

$H_2O_2(+M)=2OH(+M)$	100%

Figure 7

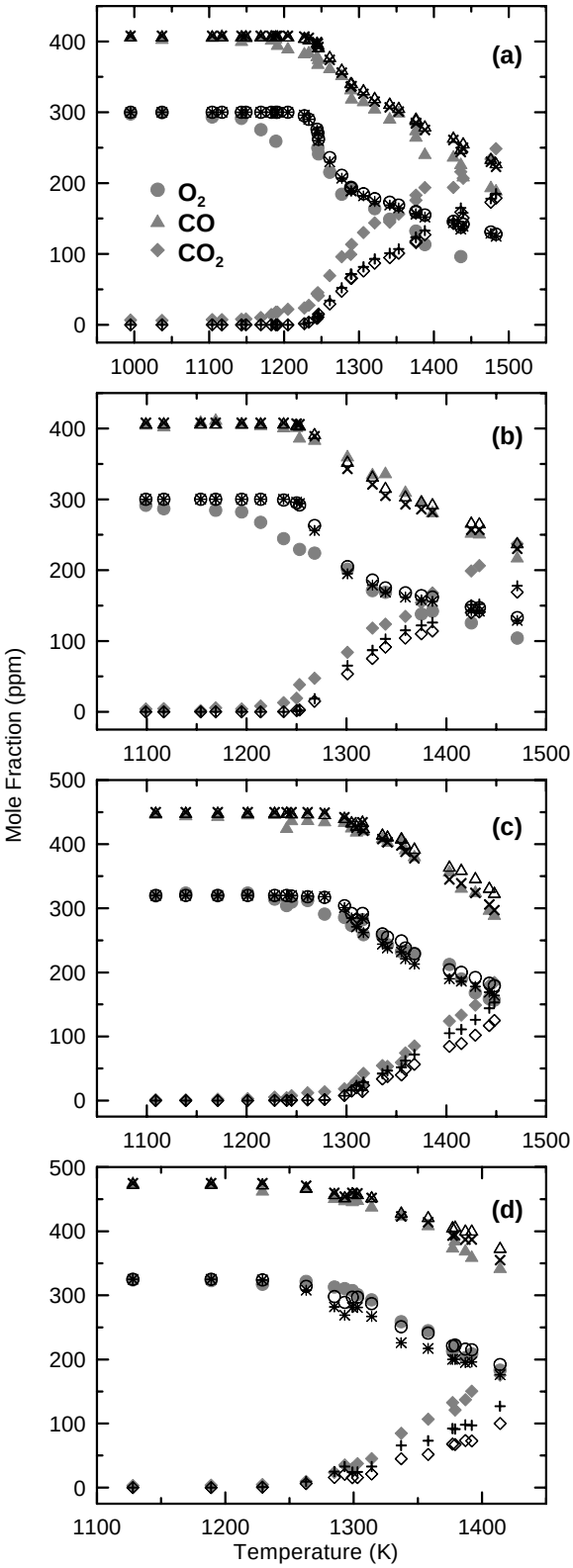

Figure 8

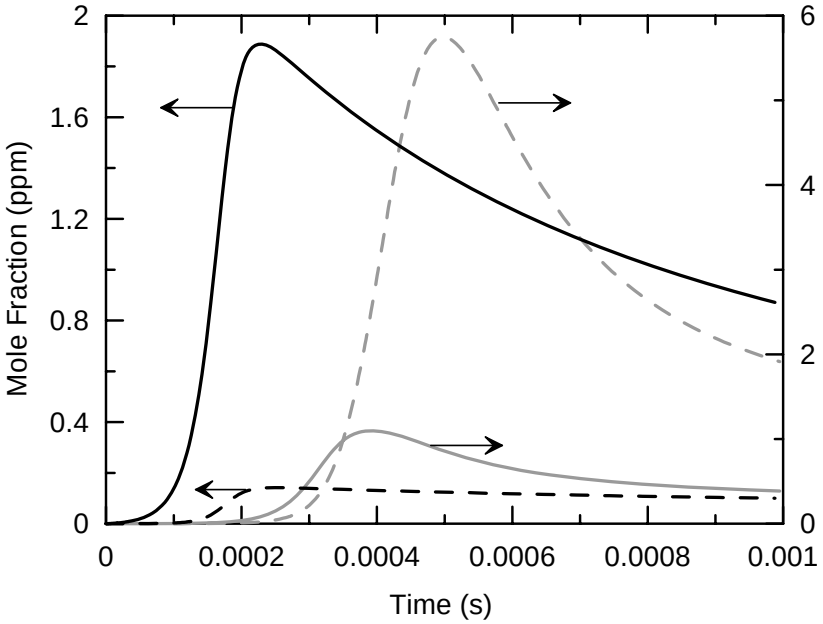
Mole Fraction (ppm)
Time (s)
0
0.4
0.8
1.2
1.6
2
0
2
4
6
0
0.0002
0.0004
0.0006
0.0008
0.001

Figure 9

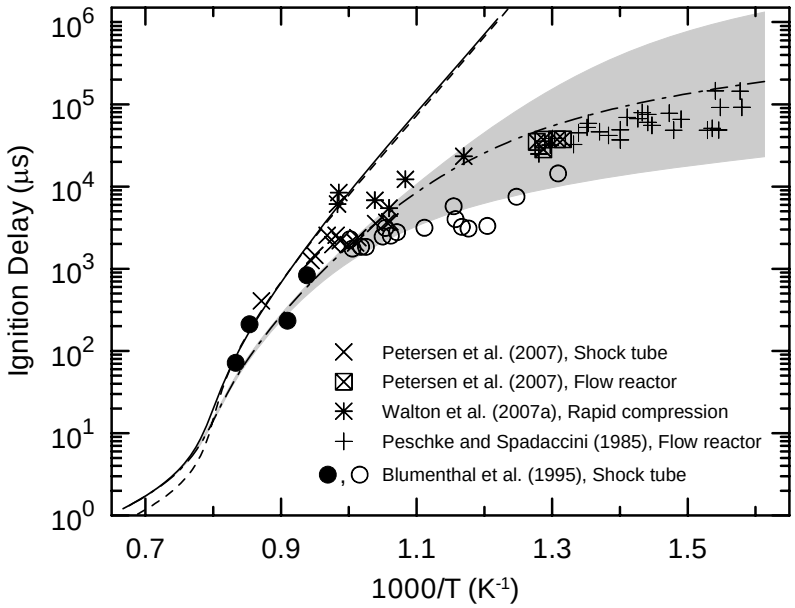
Ignition Delay (μs)
10^6
10^5
10^4
10^3
10^2
10^1
10^0
0.7
0.9
1.1
1.3
1.5
1000/T (K^-1)
Petersen et al. (2007), Shock tube
Petersen et al. (2007), Flow reactor
Walton et al. (2007a), Rapid compression
Peschke and Spadaccini (1985), Flow reactor
Blumenthal et al. (1995), Shock tube

Figure 10

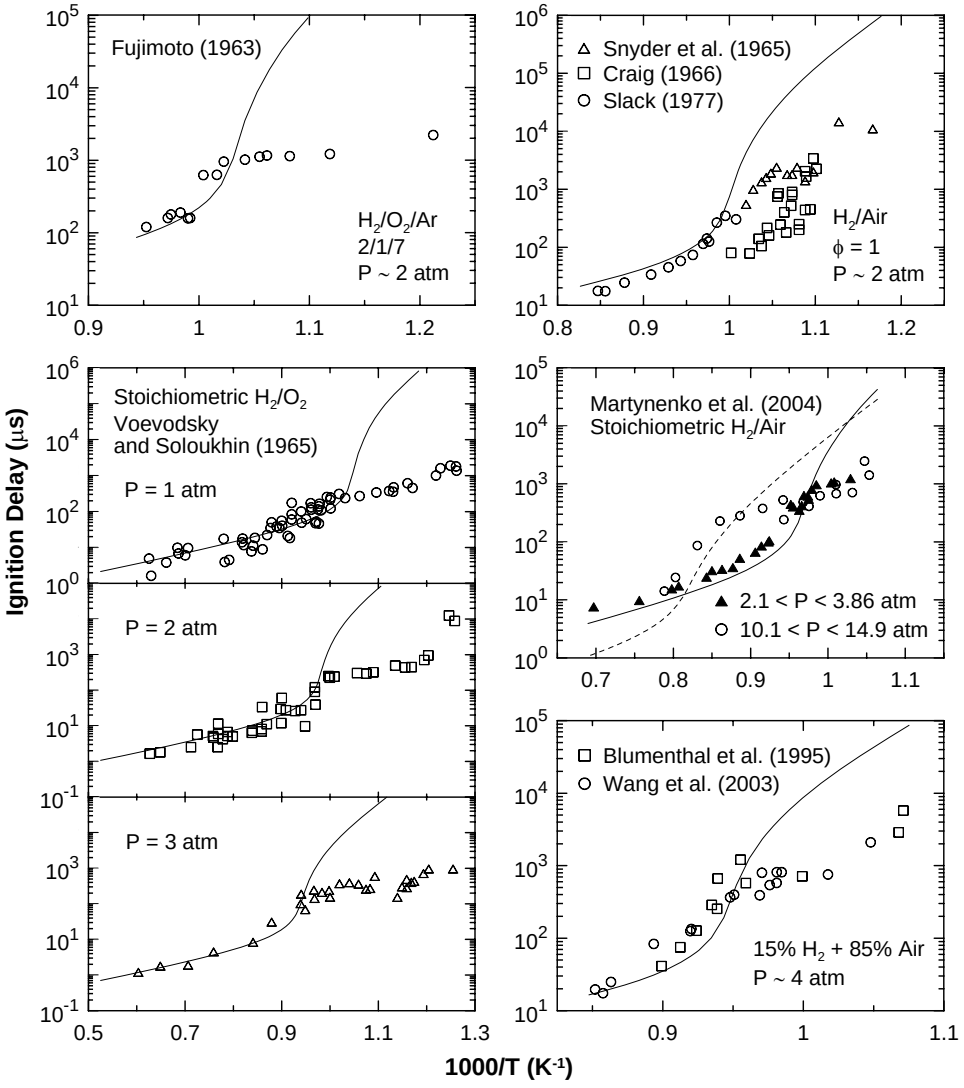
Fujimoto (1963)
H2/O2/Ar
2/1/7
P ~ 2 atm
Snyder et al. (1965)
Craig (1966)
Slack (1977)
H2/Air
ϕ = 1
P ~ 2 atm
Stoichiometric H2/O2
Voevodsky
and Soloukhin (1965)
P = 1 atm
P = 2 atm
P = 3 atm
Martynenko et al. (2004)
Stoichiometric H2/Air
2.1 < P < 3.86 atm
10.1 < P < 14.9 atm
Blumenthal et al. (1995)
Wang et al. (2003)
15% H2 + 85% Air
P ~ 4 atm
Ignition Delay (μs)
1000/T (K-1)

Figure 11

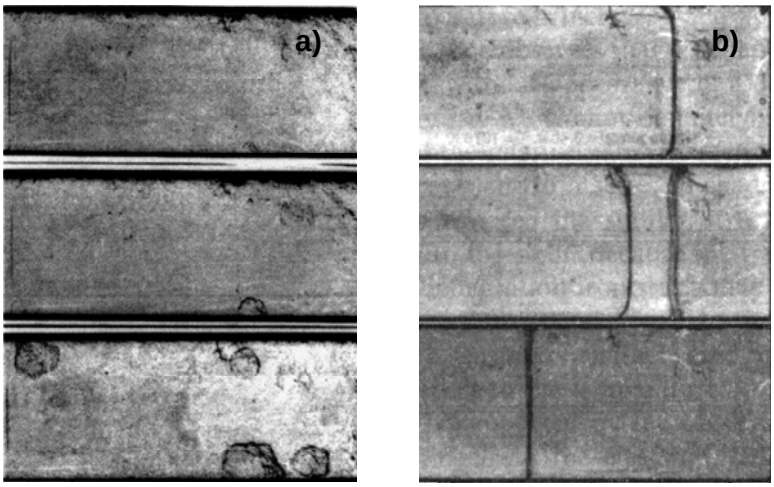

Figure 12

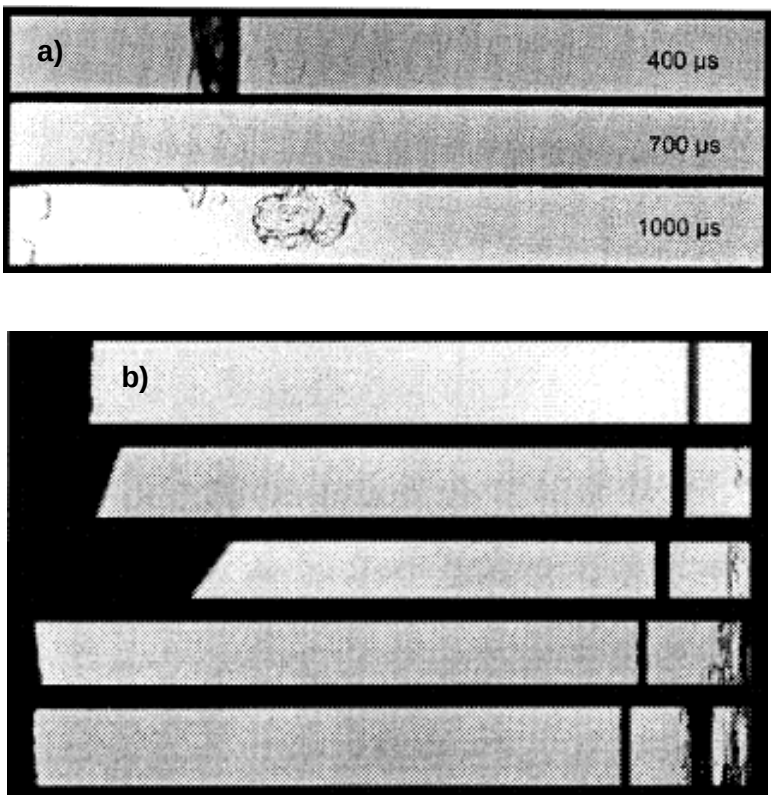

Figure 13

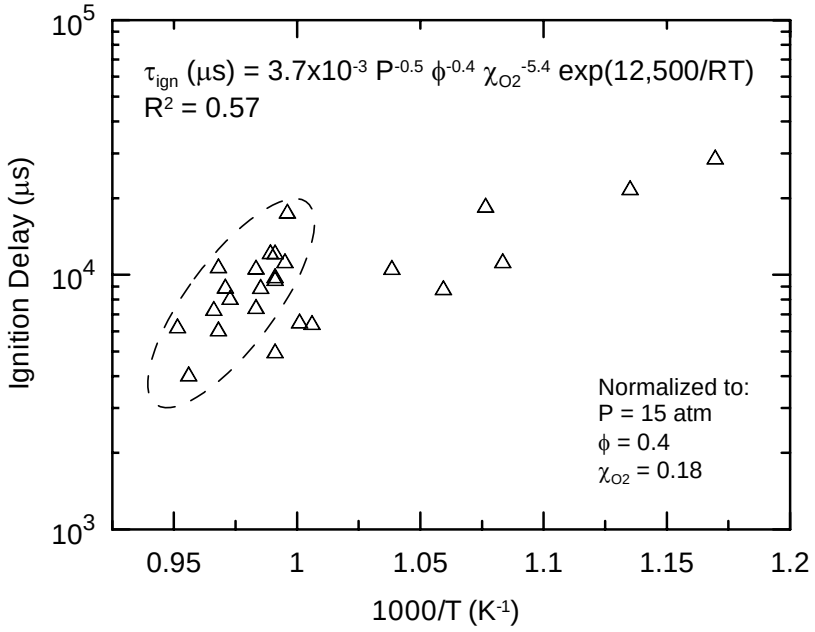
τ_{ign} (μs) = 3.7x10^{-3} P$^{-0.5}$ ϕ$^{-0.4}$ $\chi_{O2}^{-5.4}$ exp(12,500/RT)
R^2 = 0.57
Normalized to:
P = 15 atm
ϕ = 0.4
χ_{O2} = 0.18
Ignition Delay (μs)
1000/T (K^{-1})
10^5
10^4
10^3
0.95
1
1.05
1.1
1.15
1.2

Figure 14

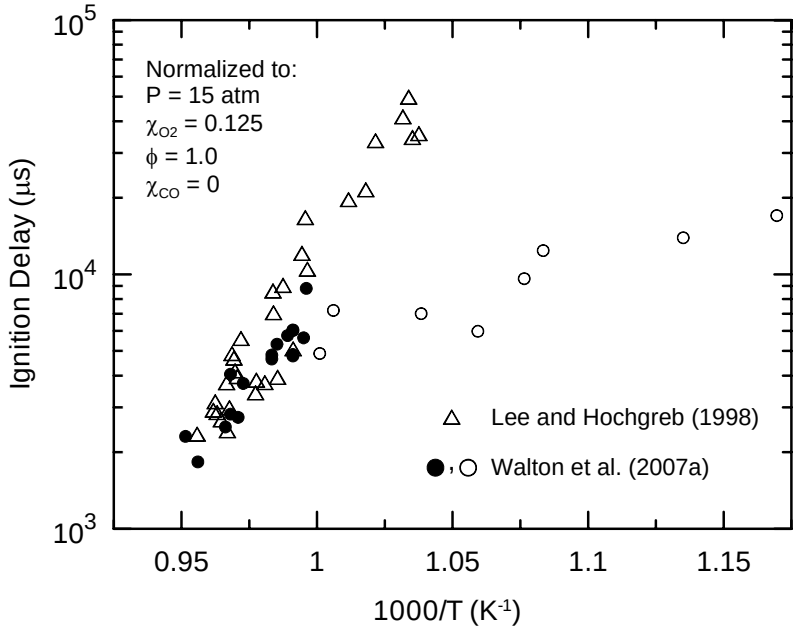
Normalized to:
P = 15 atm
χO2 = 0.125
ϕ = 1.0
χCO = 0
Ignition Delay (μs)
10^5
10^4
10^3
0.95
1
1.05
1.1
1.15
1000/T (K^-1)
Lee and Hochgreb (1998)
Walton et al. (2007a)

Figure 15

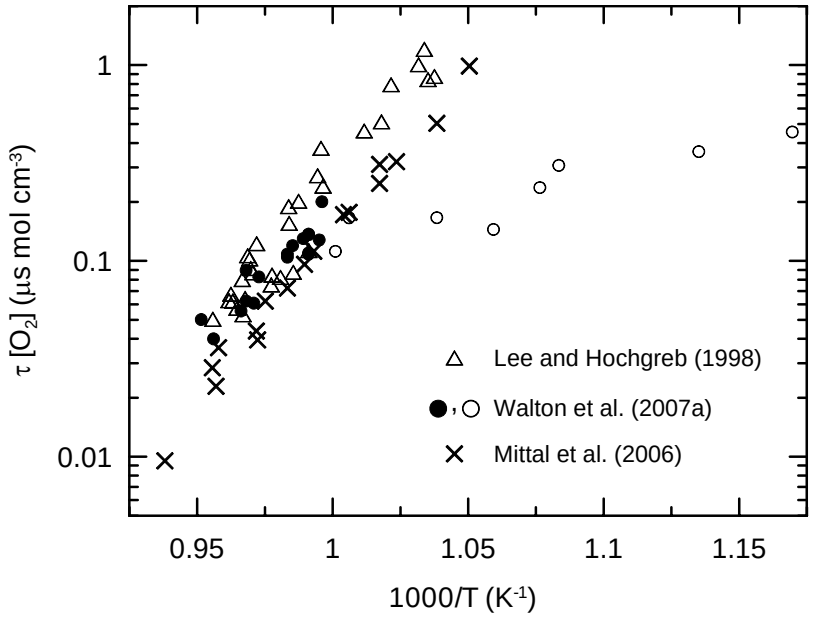
1
0.1
0.01
τ [O2] (μs mol cm-3)
0.95
1
1.05
1.1
1.15
1000/T (K-1)
Lee and Hochgreb (1998)
Walton et al. (2007a)
Mittal et al. (2006)

Figure 16

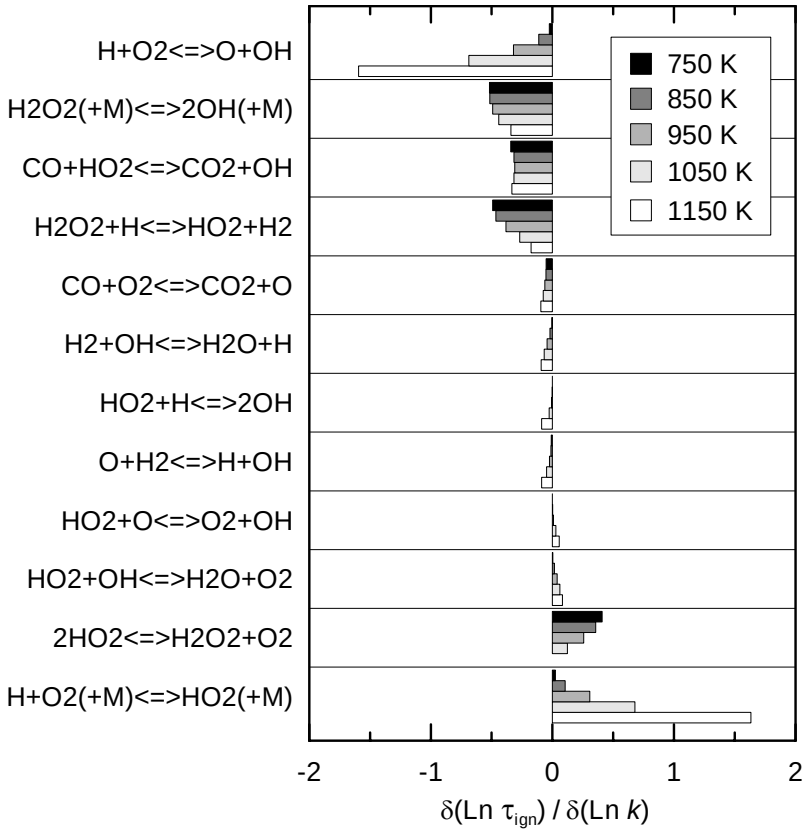
H+O2<=>O+OH
H2O2(+M)<=>2OH(+M)
CO+HO2<=>CO2+OH
H2O2+H<=>HO2+H2
CO+O2<=>CO2+O
H2+OH<=>H2O+H
HO2+H<=>2OH
O+H2<=>H+OH
HO2+O<=>O2+OH
HO2+OH<=>H2O+O2
2HO2<=>H2O2+O2
H+O2(+M)<=>HO2(+M)
750 K
850 K
950 K
1050 K
1150 K
-2
-1
0
1
2
δ(Ln τign) / δ(Ln k)

Figure 17

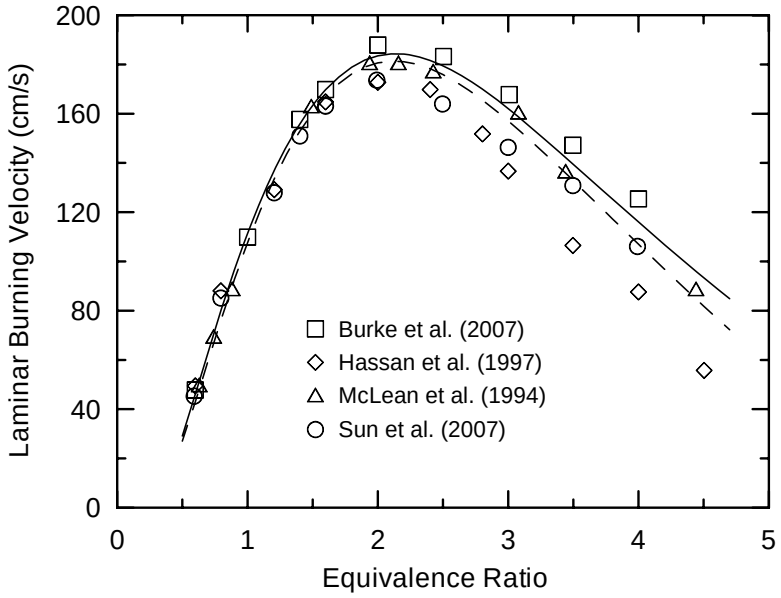
Laminar Burning Velocity (cm/s)
Equivalence Ratio
0
40
80
120
160
200
0
1
2
3
4
5
Burke et al. (2007)
Hassan et al. (1997)
McLean et al. (1994)
Sun et al. (2007)

Figure 18

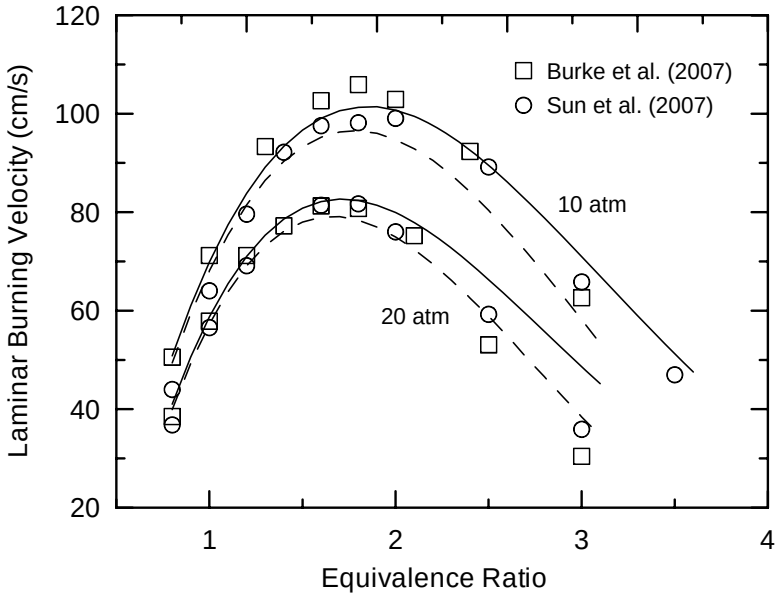
Laminar Burning Velocity (cm/s)
Equivalence Ratio
Burke et al. (2007)
Sun et al. (2007)
10 atm
20 atm
120
100
80
60
40
20
1
2
3
4

Figure 19

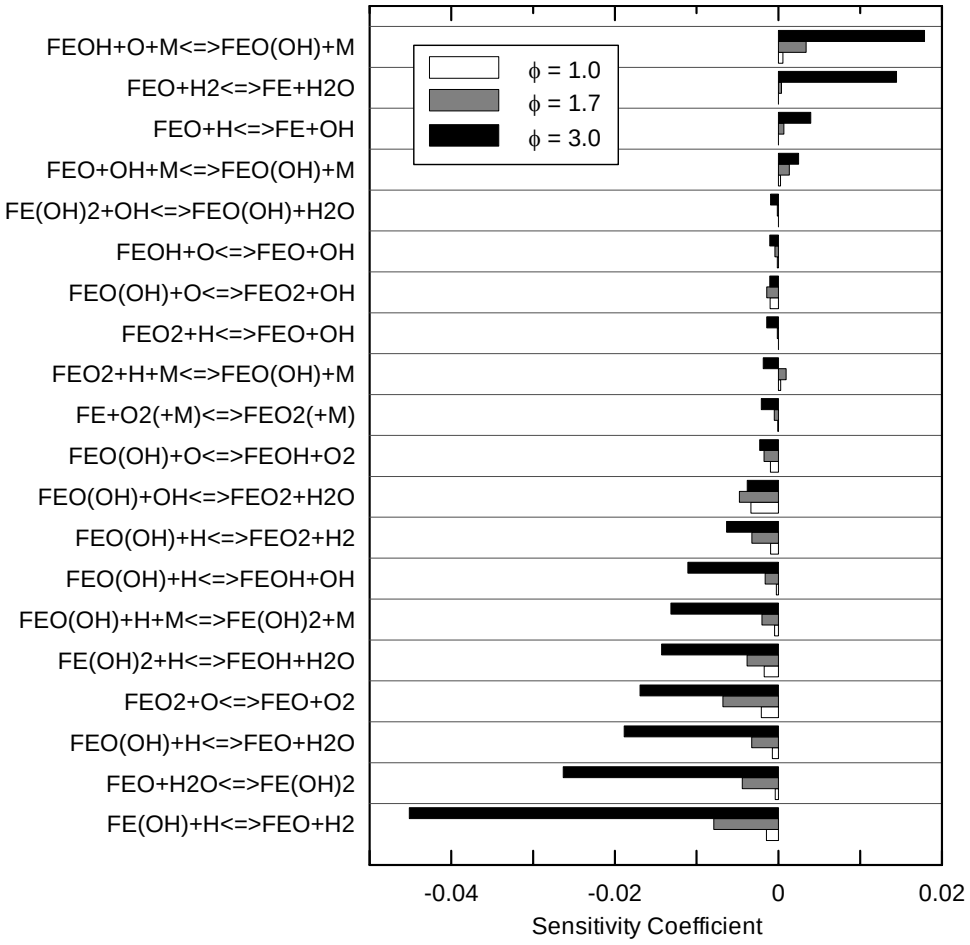
FEOH+O+M<=>FEO(OH)+M
FEO+H2<=>FE+H2O
FEO+H<=>FE+OH
FEO+OH+M<=>FEO(OH)+M
FE(OH)2+OH<=>FEO(OH)+H2O
FEOH+O<=>FEO+OH
FEO(OH)+O<=>FEO2+OH
FEO2+H<=>FEO+OH
FEO2+H+M<=>FEO(OH)+M
FE+O2(+M)<=>FEO2(+M)
FEO(OH)+O<=>FEOH+O2
FEO(OH)+OH<=>FEO2+H2O
FEO(OH)+H<=>FEO2+H2
FEO(OH)+H<=>FEOH+OH
FEO(OH)+H+M<=>FE(OH)2+M
FE(OH)2+H<=>FEOH+H2O
FEO2+O<=>FEO+O2
FEO(OH)+H<=>FEO+H2O
FEO+H2O<=>FE(OH)2
FE(OH)+H<=>FEO+H2
ϕ = 1.0
ϕ = 1.7
ϕ = 3.0
-0.04
-0.02
0
0.02
Sensitivity Coefficient

Figure 20

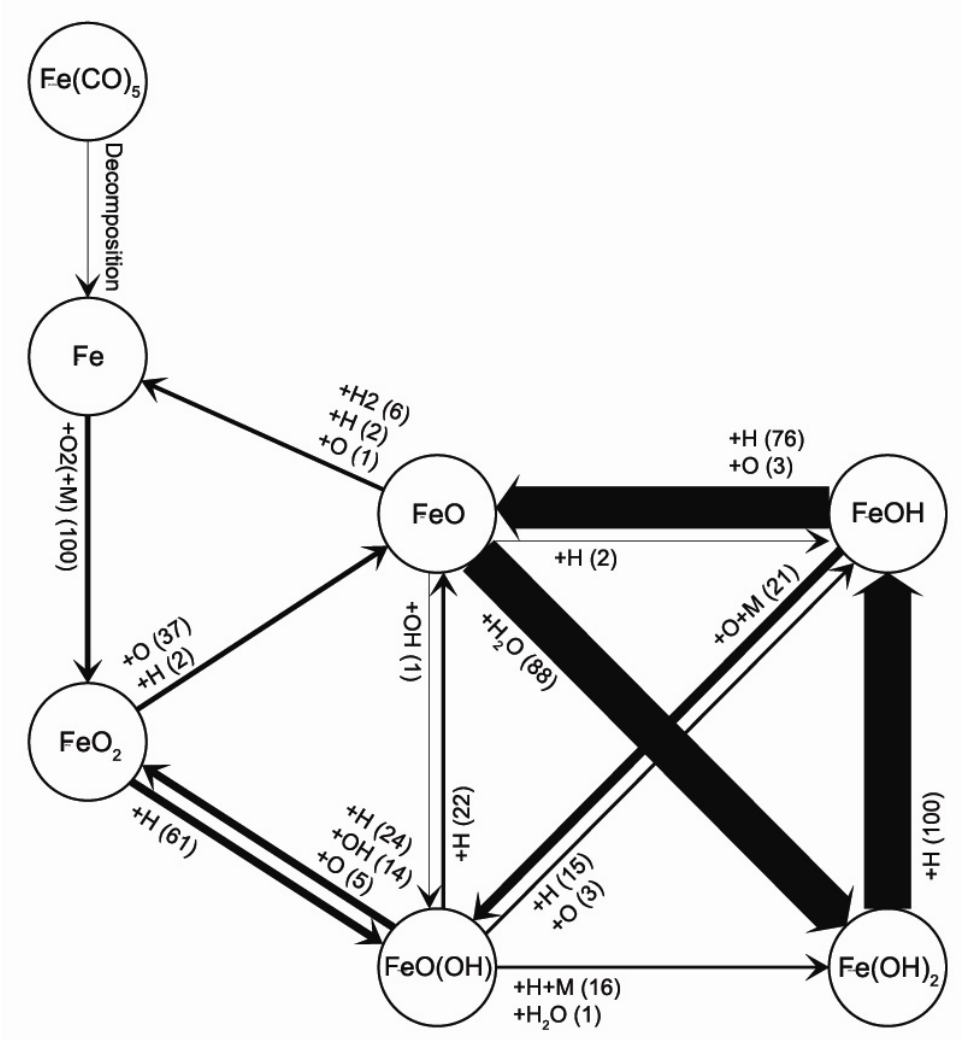
Fe(CO)5
Decomposition
Fe
+O2(+M) (100)
+H2 (6)
+H (2)
+O (1)
FeO
+H (76)
+O (3)
FeOH
+H (2)
+O (37)
+H (2)
+OH (1)
+H2O (88)
+O+M (21)
FeO2
+H (61)
+H (24)
+OH (14)
+O (5)
+H (22)
+H (15)
+O (3)
+H (100)
FeO(OH)
+H+M (16)
+H2O (1)
Fe(OH)2

Figure 21

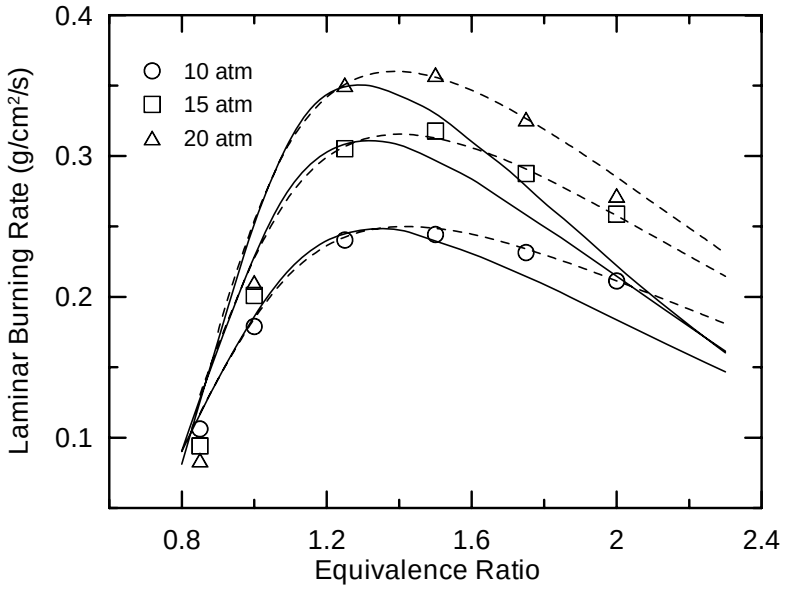
0.4
0.3
0.2
0.1
Laminar Burning Rate (g/cm²/s)
10 atm
15 atm
20 atm
0.8
1.2
1.6
2
2.4
Equivalence Ratio

Figure 22

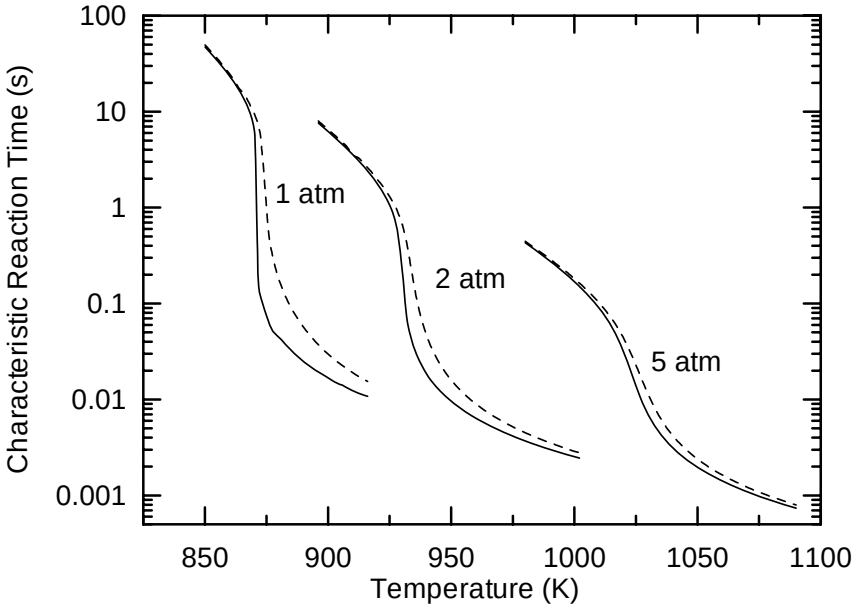
100
10
1
0.1
0.01
0.001
Characteristic Reaction Time (s)
1 atm
2 atm
5 atm
850
900
950
1000
1050
1100
Temperature (K)

Figure 23

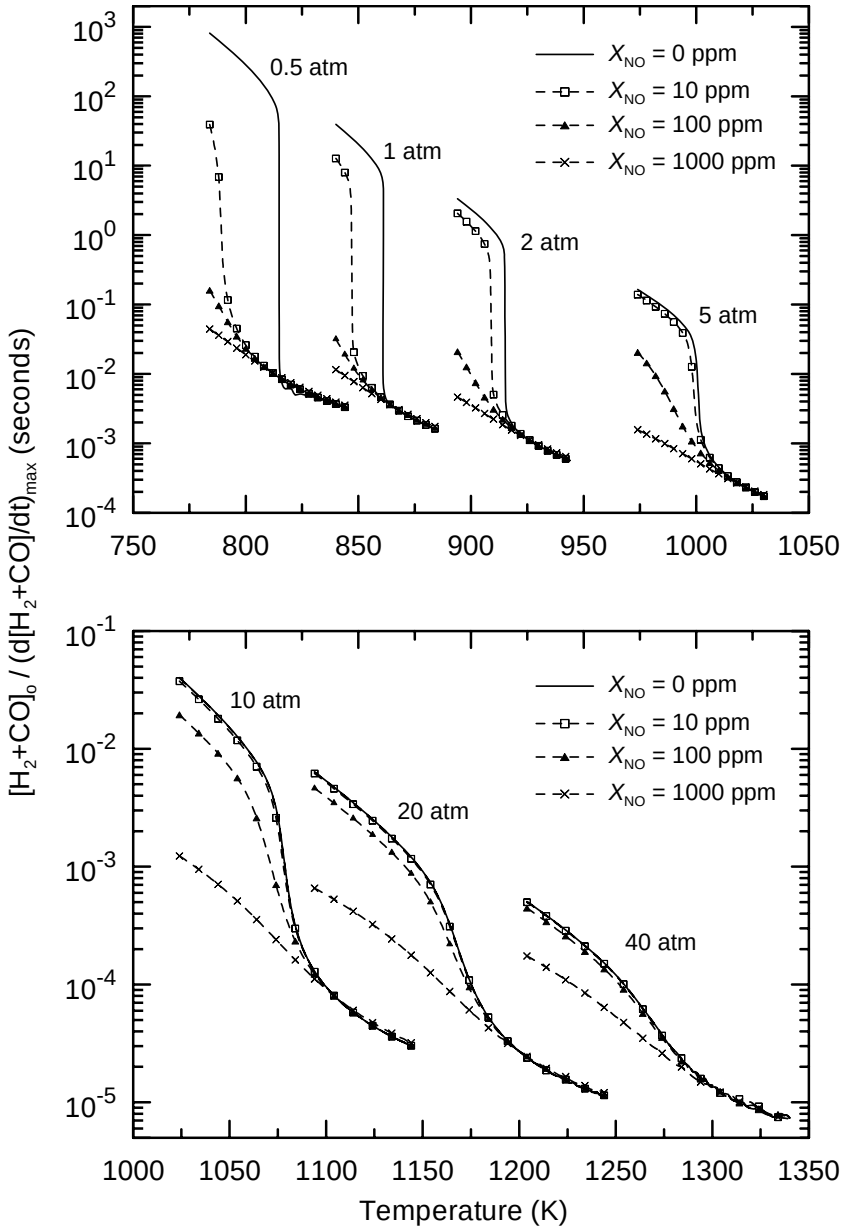
0.5 atm
1 atm
2 atm
5 atm
10 atm
20 atm
40 atm
X_{NO} = 0 ppm
X_{NO} = 10 ppm
X_{NO} = 100 ppm
X_{NO} = 1000 ppm
$[H_2+CO]_o$ / $(d[H_2+CO]/dt)_{max}$ (seconds)
Temperature (K)

Figure 24

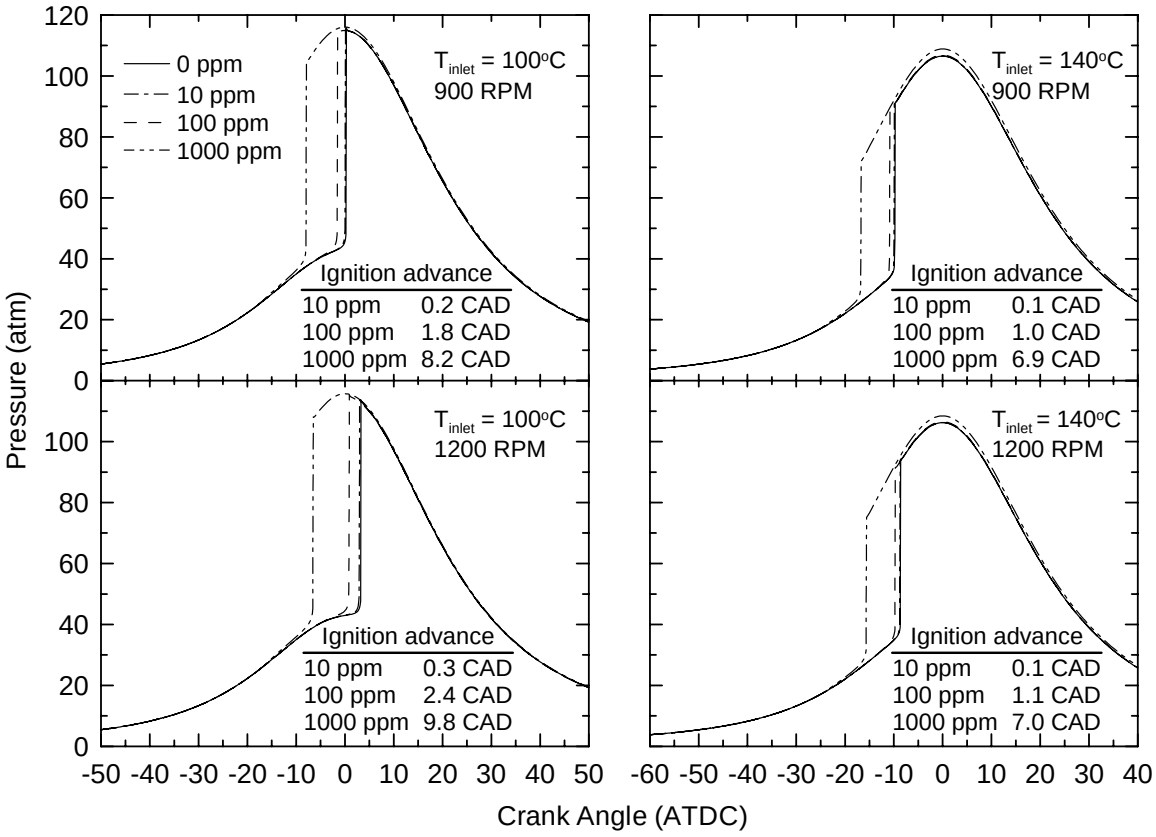
0 ppm
10 ppm
100 ppm
1000 ppm
T_inlet = 100°C
900 RPM
Ignition advance
10 ppm 0.2 CAD
100 ppm 1.8 CAD
1000 ppm 8.2 CAD
T_inlet = 140°C
900 RPM
Ignition advance
10 ppm 0.1 CAD
100 ppm 1.0 CAD
1000 ppm 6.9 CAD
T_inlet = 100°C
1200 RPM
Ignition advance
10 ppm 0.3 CAD
100 ppm 2.4 CAD
1000 ppm 9.8 CAD
T_inlet = 140°C
1200 RPM
Ignition advance
10 ppm 0.1 CAD
100 ppm 1.1 CAD
1000 ppm 7.0 CAD
Pressure (atm)
Crank Angle (ATDC)

Figure 25